A MULTI-YEAR COMPARISON OF VEGETATION PHENOLOGY BETWEEN MILITARY TRAINING LANDS AND NATIVE TALLGRASS PRAIRIE USING TIMESAT AND MODERATE-RESOLUTION SATELLITE IMAGERY

by

BRYANNA RAE POCKRANDT

B.A., Kansas State University, 2012

A THESIS

submitted in partial fulfillment of the requirements for the degree

MASTER OF ARTS

Department of Geography
College of Arts and Sciences

KANSAS STATE UNIVERSITY
Manhattan, Kansas

2014

Approved by:

Major Professor
Dr. J.M. Shawn Hutchinson

Abstract

Time series of normalized difference vegetation index (NDVI) data from satellite spectral measurements can be used to characterize and quantify changes in vegetation phenology and explore the role of natural and anthropogenic activities in causing those changes. Several programs and methods exist to process phenometric data from remotely-sensed imagery, including TIMESAT, which extracts seasonality parameters from time-series image data by fitting a smooth function to the series. This smoothing function, however, is dependent upon user-defined input parameter settings which have an unknown amount of influence in shaping the final phenometric estimates. To test this, a sensitivity analysis was conducted using MODIS maximum value composite NDVI time-series data acquired for Fort Riley, Kansas during the period 2001-2012. The phenometric data generated from the different input setting files were compared against that from a base scenario using Pearson and Lin's Concordance Correlation Analyses. Findings show that small changes to parameter settings results in insignificant differences in phenometric estimates, with the exception of end of season data and growing season length.

Next, a time-series analysis of the same MODIS NDVI data for Fort Riley and nearby Konza Prairie Biological Station (KPBS) was conducted to determine if significant differences existed in selected vegetation phenometrics. Phenometrics of interest were estimated using TIMESAT and based on a Savitzky-Golay filter with parameter settings found optimal in the previous study. The phenometrics *start of season*, *end of season*, *length of season*, *maximum value*, and *small seasonal integral* were compared using Kolmogorov-Smirnov (K-S) and showed significant differences existed for all phenometrics in the comparison of Fort Riley training areas and KPBS, as well as low- versus high-training intensity areas within Fort Riley.

Fort Riley and high-intensity training areas have earlier dates for the start and end of the growing season, shorter growing season lengths, lower maximum NDVI values, and lower small seasonal integrals compared to KPBS and low-intensity training areas, respectively. Evidence was found that establishes a link between military land uses and/or land management practices and observed phenometric differences.
KEYWORDS: NDVI, TIMESAT, phenology, phenometrics, Fort Riley, Konza Prairie

Table of Contents

List of Figures

List of Tables

Acknowledgements

I thank my major advisor, Dr. Shawn Hutchinson for his guidance, comments and patience during my master's program. I also want to thank him, as well as graduate student Phil Denker for contributing their expert knowledge of Fort Riley military training practices. I thank my supervisory committee members, Dr. Douglas Goodin, and Dr. Stacy Hutchinson, for their valuable comments and suggestions on how to improve my research. I also thank Dr. Leigh Murray and graduate student Nicholas Bloedow, for their substantial assistance and guidance with the statistical techniques used in this study.

Chapter 1 - Introduction

Research Background

Time-series analysis of remotely sensed imagery has seen an increase in use across a number of environmental studies. Using vegetation indices from satellite spectral measurements, valuable information on vegetation life cycles, or phenology, may be obtained (Reed *et al.,* 1994; Wardlow 2005). Given its spectral, spatial, and temporal resolution, the study of time series datasets of normalized difference vegetation index (NDVI) images captured by the Moderate Resolution Imaging Spectrometer (MODIS) sensor has been shown to be a very cost-effective means to assess phenology trends (Ahl *et al.,* 2006, Jacquin *et al.,* 2009; Verbesselt *et al.,* 2009; Wardlow 2005; Zhang *et al.,* 2003).

The well-known NDVI is calculated as the ratio of the difference between the near-infrared (841-876 nm) and red bands (620-670 nm) over the sum of these same two bands of the electromagnetic spectrum (Eidenshink and Faundeen 1994; Rouse *et al.*, 1973; Wardlow 2005). Because spectral response in the red and near-infrared bands is related to chlorophyll content and cell structure respectively, changes in NDVI values over time is a good measure of the annual cycle of vegetation growth and development. It is also a relative measure of the amount of photosynthetic biomass and total primary production and often correlates well with biophysical measures such as green leaf biomass, the ratio of green vegetation cover, fraction of photosynthetically active radiation (FPAR), and leaf area index (LAI) (Asrar *et al.*, 1989; Baret and Guyot 1991; Tucker 1991; Wardlow 2005; An 2009).

Phenology has emerged as an important focus in ecological research because of its importance in addressing issues and questions in global modeling, monitoring, and climate change. Phenology is the timing of seasonal activities for vegetation (Parmesan 2006) and the study of how it is affected by interannual and seasonal variations in factors such as weather conditions and soil variables (Schwartz 1998; Cleland *et al.,* 2007). Usually measured in Julian dates, or days since December 31, phenology can be described using satellite imagery and phenometric data extracted from vegetation index data such as that acquired by the MODIS sensor (Ahas *et al*., 2002; An 2009). The spectral-temporal information obtained from time-series NDVI data can be used to characterize and quantify changes in vegetation phenology (Reed *et al.,* 1994; Wardlow 2005) and to explore the potential role of different natural and anthropogenic activities in causing those changes (Jacquin *et al.,* 2009).

Phenometrics such start and end of growing season, growing season length, and maximum greenness value may be extracted from a time series of NDVI data by fitting a function to the original data, which often incorporates use of a filter, or smoothing function, to remove atmospheric and sensor calibration noise (Chen *et al*., 2004; Eklundh and Jönsson 2010; Jönsson *et al*., 2010). A number of software packages and methods exist to facilitate data smoothing and extraction of fitted functions, including the TIMESAT software package (Eklundh and Jönsson 2010). However, smoothing typically requires a number of user-defined parameter settings to optimize a given curve-fitting function to the raw satellite data. For example, the Savitzky-Golay filter available in TIMESAT requires values for important parameters such as start and end of season threshold, window size, and number of envelope iterations (Eklundh and Jönsson 2010). While general guidelines are available for selecting the proper values for these parameters, it remains unclear as to what impact adoption of TIMESAT "default" parameter setting might have on extracted phenometrics.

Research Goals

This study investigates differences in phenology between Fort Riley, Kansas, a U.S. Army military installation, and Konza Prairie Biological Station (KPBS), a natural tallgrass prairie preserve. The overarching goal was to determine if a long time series of course-resolution satellite imagery, such as that acquired by the MODIS sensor, is capable of detecting differences in selected phenometrics caused by dominant landuses between the two nearby sites. Assuming differences would be detected, further analyses of Fort Riley only would follow to determine whether the same imagery could be used to assess the impact of varying levels of military training intensity on vegetation growth and dynamics.

To achieve the overarching goal, two distinct studies were conducted using the TIMESAT program to (1) smooth a time series of MODIS 16-day maximum value NDVI composite images for the period 2001-2012 and then (2) extract key phenometric values and dates. The first study (Chapter 4) presents a sensitivity analysis of selected parameters required by the TIMESAT Savitzky-Golay filter using as input the complete MODIS NDVI time series for Fort Riley. Phenometric data from the time series was extracted using different Savitzky-Golay filters created from unique user-defined parameter settings. Ordered pairs of extracted phenometrics obtained from the different filter parameter settings were compared at the pixel level using Pearson and Lin's Concordance Correlation tests (Lin 1989; McGrew and Monroe 2000). This analysis allowed for specification of an "optimal" Savitzky-Golay filter parameter settings file for the Fort Riley and KPBS study areas based on the vegetation characteristics of the Flint Hills ecoregion.

Following this sensitivity analysis, a second study (Chapter 5) was conducted to extract and compare selected phenometrics from the Fort Riley and KPBS study sites using the same 2001-2012 time series of MODIS 16-day maximum value NDVI composite images. Of interest here was whether the dominant landuse of each site (e.g., military training versus natural grassland) would result in measurable differences in phenometrics when using NDVI information derived from course-resolution satellite images. Again, TIMESAT was used to pre-process the NDVI time series and also to extract phenometric data for KPBS and three different spatial configurations of Fort Riley, including (1) all military training areas (excluding developed areas), (2) high-intensity military training areas only, and (3) low-intensity military training areas only. TIMESAT-generated phenometrics for each of the four study areas were compared using the non-parametric Kolmogorov-Smirnov test to determine if significant differences existed. In addition, a "normal" vegetation phenology curve was developed for KPBS and the three Fort Riley study sites.

Chapter 2 - Literature Review

Remote Sensing of the Environment

In the early 1980's, the United States National Oceanic and Atmospheric Administration (NOAA) satellites began collecting course spatial resolution reflectance data for large areas of the Earth's surface on a daily basis (Schwartz 1998). Satellite remote sensing presents a practical means to obtain data vital to the understanding of vegetation processes. Data collection is completed without direct physical contact to the land, as remote sensors record electromagnetic radiation (EMR). Once detected, changes in the amount and properties of EMR become a valuable data source for interpreting important properties of the Earth's surface, including vegetation processes (Suits 1975). Specific advantages of remote sensing include a large areal extent, high spatial and temporal dynamics, and the ability to detect vegetation condition (Cihlar *et al.,* 1991). It combines comprehensive ground coverage and regularly repeated observations, which allows for both intensive and extensive phenological monitoring (Cleland *et al.,* 2007).

Remote sensing technology has proven to be a valuable tool for analyzing, observing, differentiating, and mapping changes across constantly changing landscapes. Such tools include spaceborne sensors that provide both synoptic and recurring coverage of the Earth's surface. The Moderate Resolution Imaging Spectroradiometer (MODIS) is carried on NASA's Terra and Aqua platforms and acquires high quality image data with global coverage at a high temporal resolution (Justice and Townshend 2002). The MODIS sensor was designed to capture images at a 250 meter spatial resolution to assist in identifying human-induced land cover changes (Justice *et al.,* 1988).

MODIS incorporates seven spectral bands that encompass the visible through middle infrared regions of the electromagnetic spectrum. Each band is narrowed to avoid atmospheric absorption while retaining the ability to record spectral features of terrestrial objects. To help reduce atmospheric contamination, MODIS is equipped with several atmosphere-related bands that measure cloud properties, aerosols, and water vapor for post-processing accurate surface reflectance values (Justice *et al.*, 1998). Further, the MODIS platform is very stable with a highly precise external orientation, resulting in subpixel geolocational accuracy (~50-m at nadir) (Wolfe *et al.,* 2002).

Remote sensing of the environment involves recording and interpreting images produced by radiant flux from a source area or target to a sensor, such as a satellite. Discrete measurements made within the visible and near infrared (NIR) regions of the electromagnetic spectrum are used to create spectral reflectance curves (Jensen 1983). These “spectral signatures” are not constant for a given feature and depend on the spectral distribution of the incident radiant flux onto a target, on geometric interactions between the sensor angle-of-view of the satellite sensor and the exiting energy from the Earth’s surface, on atmospheric properties, and on the physical characteristics of the target feature (Slater 1980).

Chlorophyll in plant tissue absorbs visible energy for photosynthesis most effectively in the blue and red regions of the electromagnetic spectrum (An 2009). The red region is highly chlorophyll absorptive and dependent on chlorophyll content (Figure 2.1) and is therefore sensitive to green, or photosynthetically active, vegetation (Tucker 1979; Tucker *et al.,* 1991; Wardlow 2005).

Figure 2-1 Spectral reflectance curve for healthy, green vegetation at the 0.35-2.6 µm wavelengths of the electromagnetic spectrum, including the dominant factors regulating leaf reflectance and absorption (from Jensen 1983).

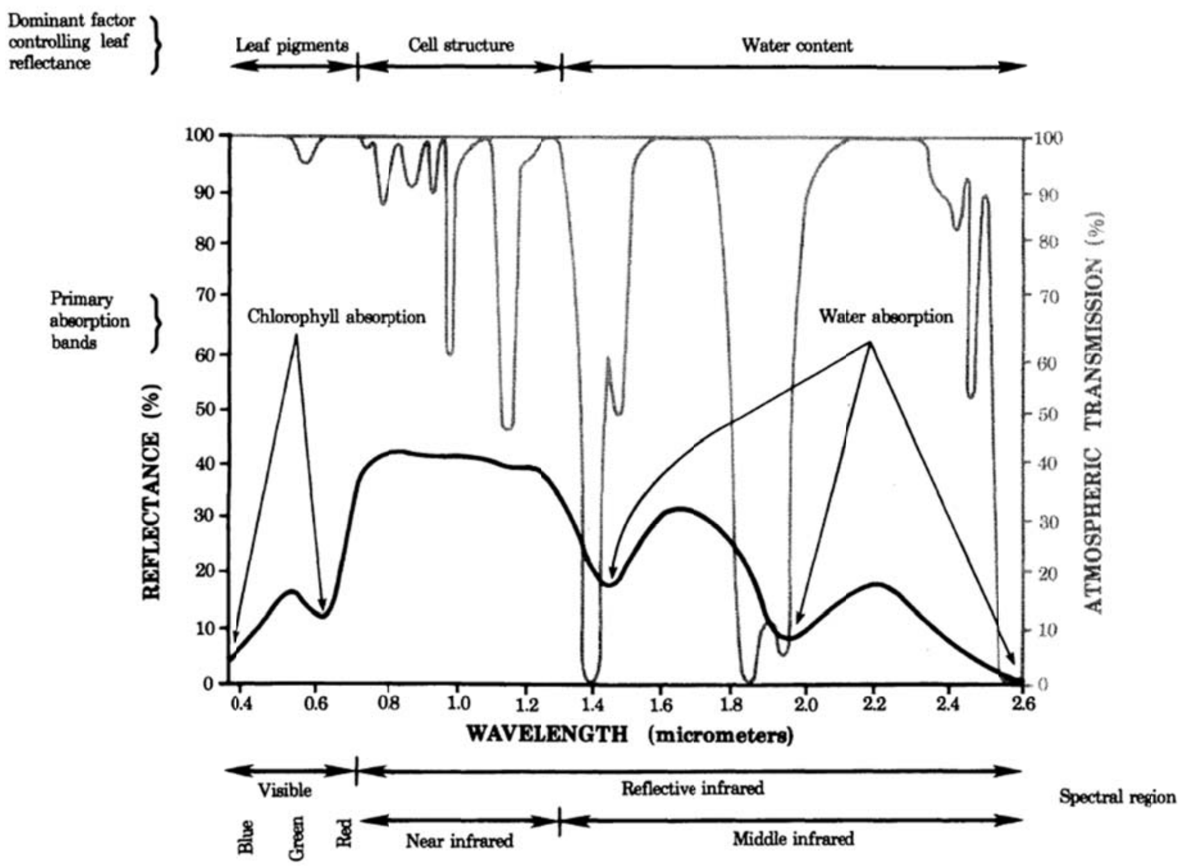

The optimum NIR spectral region for direct estimation of vegetation biomass is between 0.74-.90 µm (Tucker 1979). Reflectance in the NIR portion of the electromagnetic spectrum responds is controlled primarily by the spongy mesophyll cells in vegetation which contain intercellular airspaces below the palisade layers and is highly dependent on plant water content (Jensen 1983). Energy in NIR is not absorbed by plant pigments but travels through most of the leaf and interacts with the mesophyll cells. In healthy plants with a sufficient water supply, and characterized by dense canopies, more NIR energy will be reflected than transmitted. In general, the relationship between biomass and NIR reflectance is linear and positive (Jensen 1983) with the amount of reflectance dependent upon plant developmental stage.

Satellite remote sensing has been used to assess regional environmental change by post-classification analysis of land cover change to document separate, abrupt anthropogenic impacts on the land surface such as deforestation and urbanization. However, a variety of spectral vegetation indices, such as the normalized difference vegetation index (NDVI), can also be calculated from satellite image data in order to quantify the spatial and temporal variation in vegetation growth and activity (Linderholm 2006). Indices such as NDVI have also been successfully used to assess vegetation phenology (Wright *et al.,* 2012).

Vegetation Indices

Vegetation indices are mathematical combinations of surface reflectance at two or more wavelengths that are designed to emphasize particular vegetation properties. Derivation of vegetation indices are based on the reflectance properties of plant foliage, such as leaves, needles, and other green materials which vary greatly in chemical composition. Vegetation indices often correlate well with several biophysical parameters such as leaf area index (LAI), fraction of photosynthetically active radiation (FPAR), and green aboveground biomass (Asrar *et al.*, 1989; Baret and Guyot 1991; Wardlow 2005). The most significant components that affect leaf spectral response are pigments, water, carbon and nitrogen (ENVI Online Help 2005). By understanding the basic composition of leaves and how they change under different environmental conditions, vegetation indices can be used to determine the general condition of vegetation, biomass, and land cover, in order to estimate net productivity (Cihlar *et al.,* 1991; Tucker *et al.,* 1991; An 2009).

Several studies have been conducted using different spectral band combinations to assess and monitor vegetation biomass, physiological status, and properties of plant canopies (Colwell 1973, Colwell 1974; Tucker 1979; Jensen 1983). Several combinations can accurately estimate biomass, monitor crops and rangelands, and detect changes in agricultural crop development while also accounting for soil background reflectance variations. Additionally, several different combinations of spectral bands have been proven effective in capturing phenological dynamics while monitoring different types of vegetation (Colwell 1973, Colwell 1974; Tucker 1979).

Vegetation biomass discrimination is highly dependent on the ratio of soil surface-vegetation spectral reflectance, or radiance contrast, making particular wavelengths better to use over others (Colwell 1974). The ideal vegetation index for this purpose is one that would be highly sensitive to vegetation, insensitive to background soils, and minimally influenced by atmospheric path radiance. Examples of frequently used vegetation indexes include the IR/red ratio (Colwell 1973, Colwell 1974), the soil-adjusted vegetation index (SAVI) (Huete 1988), the transformed SAVI (TSAVI) (Baret *et al.,* 1989), the perpendicular vegetation index (PVI) (Richardson and Weigand 1977), the Kauth-Thomas transformation (tasseled cap or K-T) (Kauth and Thomas 1976), the enhanced vegetation index (EVI) (Huete *et al.,* 2002), and the normalized difference vegetation index (NDVI) (Rouse *et al.,* 1973).

Equation 2.1 shows NDVI as the ratio of the difference between the near-infrared band (.75 to 1.10 μm) and the red band (.58 to .68 μm) and the sum of these two bands (Rouse *et al*., 1973, Eidenshink and Faundeen 1994, Wardlow 2005):

NDVI = (NIR – red) / (NIR + red) **Equation 2.1**

where:
NDVI = Normalized difference vegetation index
NIR = reflectance in the near-infrared spectrum
red = reflectance in the red spectrum

NDVI is a measure of greenness that correlates well with total primary production (Tucker *et al.,* 1991; Wardlow 2005; An 2009), and the amount of photosynthetic biomass (Cihlar *et al.,* 1991; Zhou *et al.,* 2001), which dominates both photosynthesis and transpiration processes. Typically, NDVI increases rapidly in the spring and then levels off until the end of August (Cihlar *et al.,* 1991). Therefore, changes in NDVI translate into changes in vegetation conditions that coincide with the absorption of photosynthetically active radiation (Sellers 1985). Healthier vegetation conditions, and overall density and intensity of active vegetation, are associated with higher NDVI values, while degraded vegetation tends to result in lower NDVI values.

Though NDVI has been proven to be very useful, limitations exist. Because NDVI is ratio-based, it is essentially non-linear, meaning lower ratio values tend to be enhanced and higher ratio values condensed causing values to saturate over high biomass conditions. This "ratio predicament" may cause areas with high biomass density to have much larger NDVI values than areas with lower densities, even if the vegetation health conditions were identical.

Since electromagnetic radiation in the visible and NIR bands of the spectrum cannot penetrate cloud cover, satellite images suffering from cloud contamination yield significantly lower NDVI values that do not correctly reflect actual surface conditions unless preprocessing filtering and smoothing is applied to the raw data. Additionally, the NIR band includes a strong water absorption region, which can reduce the reliability of NDVI calculations (Wardlow 2005). Other limitations associated with most vegetation indices include atmospheric path radiance, satellite drift, calibration uncertainties, inter-satellite sensor differences, bidirectional and atmospheric effects, and even volcanic eruptions (Zhou *et al.,* 2001).

Phenology and Phenometrics

Phenology has emerged as an important focus in ecological research for its use in vegetation monitoring/modeling and addressing issues related to climate change. Phenology is the timing of seasonal vegetation activities (Parmesan 2006) and the study of how vegetation growth may be affected by interannual and seasonal variations in meteorological conditions, soil characteristics, and photoperiod (Schwartz 1998; Cleland *et al.,* 2007). It can be used to predict the fitness and probability of species occurrence under certain conditions (Cleland *et al.,* 2007), making it one of the most efficient ways of following species response to changing ecosystem conditions (Walther *et al.,* 2002). Through the use of remote sensing, the study of phenology provides additional insights into the natural and anthropogenic processes impacting vegetation life cycles.

Phenophases represent a particular stage of development such as plant emergence or green-up, growth rate, blooming period and senescence (Price *et al.,* 2004; Yu *et al.,* 2004; Cleland *et al.,* 2007). Usually measured in Julian dates, or days since December 31 (Ahas *et al.,* 2002; An 2009), different phenology metrics, or phenometrics, can be described using satellite imagery and monitoring NDVI values during the course of a growing season.

A multitemporal index profile will illustrate the relative phenological characteristics of vegetation (*e.g.,* timing of greenup, peak greenness, senescence) if the satellite imagery used to generate the profile has sufficient spatial, spectral, and temporal resolution (Wardlow 2005). A typical NDVI profile, or phenology curve, illustrates the onset of greenness or when the vegetation begins to green-up, the maximum NDVI value illustrating the highest relative photosynthetic biomass, the rate of senescence or decay, the end of greenness date, and the growing and brown days (days of senescence) of a year accumulating to the season length of the year (Figure 2.2). The area beneath this phenology curve represents the accumulated NDVI or an indication of relative photosynthetic biomass, which is dependent upon all other phenometric data.

Figure 2-2 A typical vegetation phenology curve, and associated phenometrics, derived from time series NDVI values (from Jacquin *et al.,* 2009).

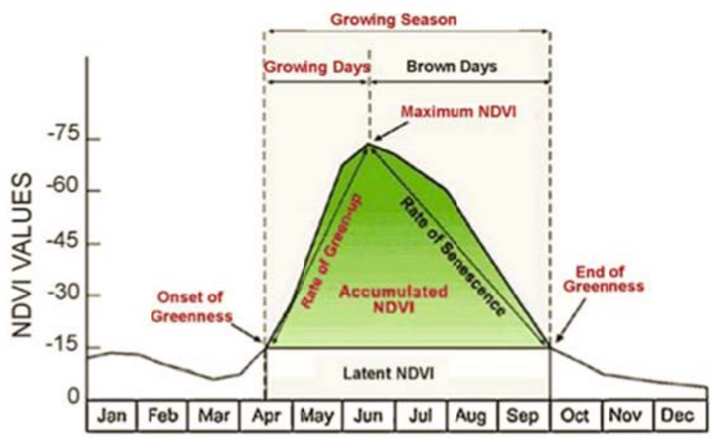

Time Series Analysis

A time series is defined as an ordered sequence of variable values at equally-spaced time intervals and time series analysis methods can be used to determine if data has an internal structure such as autocorrelation, trend, or seasonal variation (NIST/SEMATECH 2003). A time series of satellite imagery compares images of the same quantity for consecutive years, and when the time series consists of vegetation index (VI) imagery, shifts in vegetation cover due to dynamic events may be revealed (Eklundh and Olsson 2003, Heumann *et al*., 2007; Eklundh and Jönsson 2010). Spectral-temporal information extracted from time-series vegetation index data has been used successfully to characterize vegetation phenology and assist with forecasting/monitoring vegetation density and health (Reed *et al.,* 1994; Wardlow 2005; Jacquin *et al.,* 2009).

Time series of MODIS-derived NDVI datasets have been used to assess vegetation activity and measure vegetation dynamics (Zhang *et al.,* 2003; Ahl *et al.,* 2006), including spatiotemporal changes in vegetation condition and biomass (Huete *et al.,* 2002). Specifically, 16-day MODIS maximum value NDVI composite images (MOD13Q1) with a 250 meter spatial resolution have been shown successful in measuring important phenometrics and detecting possible human-induced land cover changes (Wardlow 2005; Jacquin *et al.,* 2009; Verbesselt *et al.,* 2009). Variations in phenometric values associated with different land cover regions, land use practices, climatic conditions, as well as planting dates for crops, may be determined (Wardlow 2005).

An observed time series can be decomposed into three components: the trend (long term direction), the seasonal (systematic, calendar related movements) and the irregular (unsystematic, short term fluctuations) (Cleveland *et al.,* 1990; Australian Bureau of Statistics 2005; Verbesselt *et al.,* 2009). The seasonal component represents the phenology for an area of interest, illustrating the timing and signal magnitude of the vegetation growing season. Year-to-year variations in the seasonal component of a time series suggest difference in weather conditions or changes in land cover type (Verbesselt *et al.,* 2009). The trend component, often expressed as a linear trend from the beginning to end of a time series, provides an indication of the direction and magnitude of vegetation change (i.e., positive or negative) (Jacquin *et al.,* 2009). The remainder, or irregular component, is essentially treated as signal noise caused by external factors.

Signal decomposition is usually performed in order to discriminate the time series signal from its associated noise. Raw data from remote sensors must first be processed through a series of filtering, compositing, smoothing or screening procedures in order to isolate the signal from the noise. This preprocessing is often based on a smoothing of distinct sequences of temporally adjacent data points and may mask some abrupt phenological changes taking place on the ground (Cleland *et al.,* 2007).

There are many different types of time series analysis techniques used to filter raw NDVI data and the extract phenometrics, including the seasonal Kendall (SK) trend test (Hirsch and Slack 1984; de Beurs and Henebry 2004, de Beurs and Henebry 2005; de Beurs *et al.,* 2009;), principal component analysis (PCA) (Crist and Cicone 1984), pixel-above-threshold technique (PAT) (Cleland *et al.,* 2007), wavelet decomposition (Anyamba and Eastman 1996), change vector analysis (CVA) (Lambin and Strahler 1994), and Fourier analysis (Azzali and Menenti 2000). In addition, the TIMESAT software program provides several filtering options to smooth raw vegetation index data and extract key phenometric data (Eklundh and Jönsson 2010).

The TIMESAT program was created to smooth and extract phenometrics from remotely-sensed time series data. In previous studies, TIMESAT has been used to study vegetation phenology (Eklundh and Jönsson 2003), map phenological and environmental changes (Eklundh and Olsson 2003; Hickler *et al.,* 2005; Olsson *et al.,* 2005; Seaquist *et al.,* 2006; Heumann *et al.,* 2007; Seaquist *et al.,* 2009), examine high-latitude forest phenology (Beck *et al.,* 2007), assess satellite and climate data-derived indices of fire risk (Verbesselt *et al.,* 2006), monitor human impacts of fire seasons (Le Page *et al.,* 2009), and evaluate relationships between coniferous forest NDVI and models of conifer photosynthetic activity (Eklundh and Jönsson 2010).

Chapter 3 - Study Areas

Fort Riley

Background

Fort Riley is a United States military base located in northeastern Kansas (39.18°N, 96.57°W), on the Kansas River, between Junction City and Manhattan and within Geary, Riley, and Clay counties (Figure 3.1). The total installation area is 41,141 ha and is located within the Flint Hills ecoregion (Omernik 1987; Bailey *et al.,* 1994). The Flint Hills ecoregion spans 1.6 million ha and is the largest untilled tallgrass prairie in North America (Omernik 1987; Dickson *et al.,* 2008).

Figure 3-1 Fort Riley study area, located in parts of Clay, Geary, and Riley counties in northeastern Kansas.

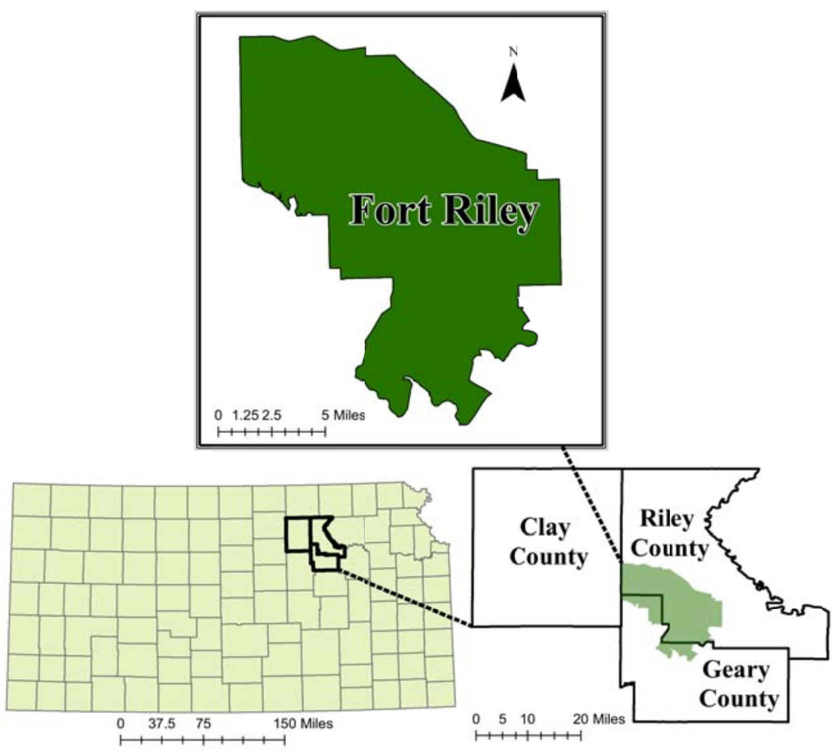

Fort Riley's climate is generally considered temperate continental. Weather is highly variable but can be characterized as having hot summers, cold, dry winters, moderate winds, low humidity, and a pronounced peak in rainfall late in the spring and in the first half of summer. Average monthly temperatures range from approximately -3°C in January to 26°C in July (PRISM Climate Group 2012). Mean annual precipitation is approximately 843 mm, but extremely variable from year to year, with 75% of precipitation occurring during the growing season (Figure 3.2). The source of much precipitation is thunderstorms, which typically have intense rainfall rates of approximately 60 mm/hr and occur approximately 55 days each year in this area (U.S. Department of Agriculture Soil Conservation Service 1975; Knapp 1998).

Figure 3-2 Average annual precipitation (inches) in Kansas (from NRCS 2007).

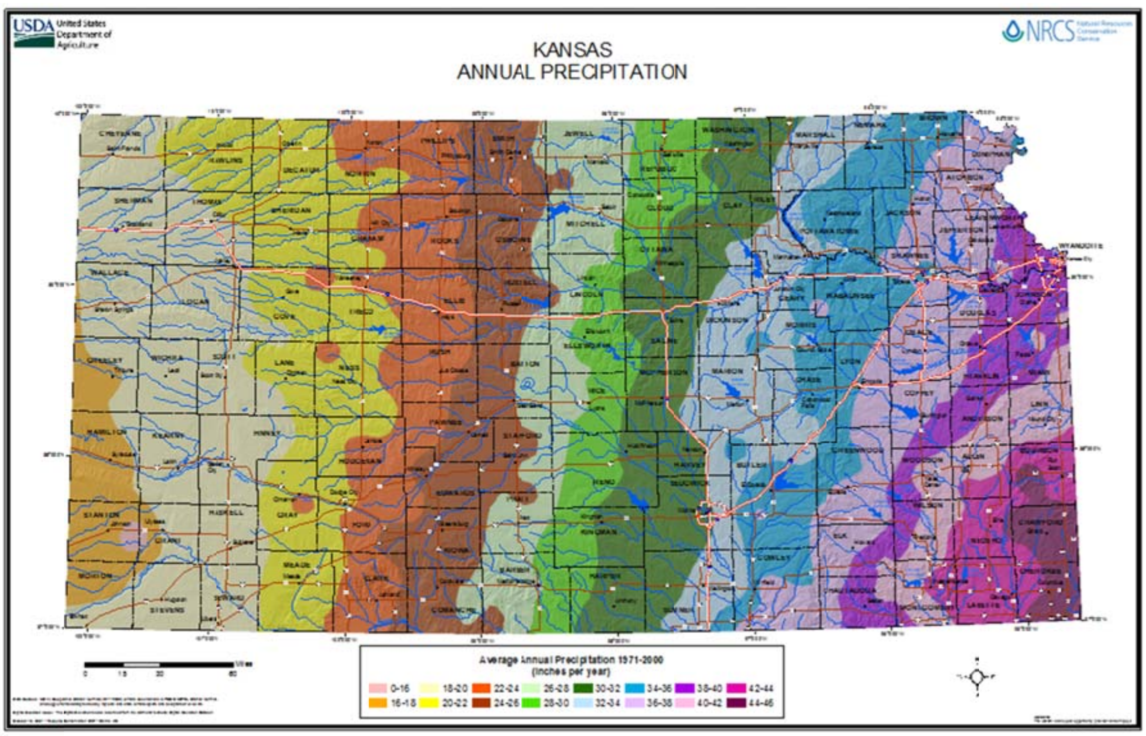

Fort Riley consists of three physiographic types: High upland prairies, alluvial bottomland flood plains, and broken and hilly transition zones (U.S. Department of Agriculture

Soil Conservation Service 1975). Elevations range from 312 to 420 meters above mean sea level with the highest elevations located along a north-south axis through the center of the installation and generally decreasing towards the southwest and southeast directions. The average slope is 4.1% with the highest slope values found in the south and east, mainly near the alluvial bottomlands.

Most Fort Riley soils are friable, overlying nearly impervious clays and were developed residually from parent materials and/or from other materials carried by water or wind and deposited on the base. Simplified soil classifications show that the majority of the soil is a clay upland that is combined with loamy uplands, limy soils, and loamy lowlands. Soil permeability varies from excessively drained sandy lowland soils to tight clays with very slow permeability (U.S. Department of Agriculture Natural Resources Conservation Service 2012).

The vegetation of Fort Riley is a mix of native prairie and introduced vegetation consisting of C4 grasses (46%), forbs (32%), legumes (11%), and C3 grasses (11%) (Dickson *et al.,* 2008). According to Althoff *et al.,* (2006), the installation is comprised of three major vegetation communities, including grasslands (32,200 ha), shrublands (1,600 ha), and woodlands (6,000 ha). The eastern portion of Fort Riley shares many of the characteristics to the Flint Hills, with vegetation dominated by warm-season highly productive C4 grasses and a mixture of annual and perennial forbs. The western portion of Fort Riley represents a plant community undergoing succession back to native prairie from past cultivation in the 1960s (Quist *et al.,* 2003).

Fort Riley grasslands are dominated by big bluestem (*Andropogon gerardii*), Indiangrass (*Sorghastrum nutans*), switchgrass (*Panicum virgatum*), and little bluestem (*Schizachyrium scoparium*). Other grasses and forbs are also present at lower abundances. Shrublands consist primarily of buckbrush (*Symphoricarpos orbiculatas*), smooth sumac (*Rhus glabra*), and rough-leaved dogwood (*Cornus drummondii).* Additionally, there is a mixture of grasses and forbs that occur along the edges of woodlands and in solitary patches of grassland areas. Typically located along riparian lowlands, woodlands are dominated by chinquapin oak (*Quercus muhlenbergii*), bur oak (*Quercus macrocarpa*), American elm (*Ulmus americana*), hackberry (*Celtis occidentalis*), and black walnut (*Juglans nigra).*

The majority (80%) of the forb community, most common within Fort Riley grasslands, is dominated by white heath aster (*Symphyotrichum ericoides*), the common sunflower (*Helianthus annuus*), whorled milkweed (*Asclepias verticillata*), and common milkweed (*Asclepias syriaca*). Common sunflower abundance and distribution is closely linked to disturbance caused by tracked military vehicles during maneuvers (Althoff *et al.,* 2006). Various introductions of non-native invasive species have resulted in shifts in species composition and productivity (Quist *et al.,* 2003), similar to that experienced throughout the Great Plains region.

Military Training and Environmental Impacts

Fort Riley serves as a combat training ground for mortar and artillery fire, small arms fire, aircraft flights, field maneuvers, tanks, and mechanized infantry units (Quist *et al.,* 2003; Althoff *et al.,* 2006). Since the 1980's, military units have engaged in continuous maneuver-based training across the entire installation (U.S. Army 1994), though such activities are concentrated in the northern 75% portion of the installation (Quist *et al.,* 2003; Althoff *et al.,* 2006). This concentrated area of activity includes 17 of the 18 total training areas at Fort Riley (approximately 26,000 ha) which experiences significant disturbance from military vehicle traffic.

High intensity military training associated with mechanized military maneuvers has been cited as the cause of increased bare soil, reduced plant cover, compacted soil conditions, and compositional shifts in plant communities (Shaw and Diersing 1990; Trumbell *et al*., 1994; Whitecotton *et al*., 2000; Quist *et al.,* 2003; Guretzky *et al.,* 2006). Military training alters vegetation composition by decreasing the basal cover of perennial warm-season grasses and increasing the cover of perennial cool season grasses and annual warm-season forbs (Wilson 1988; Shaw and Diersing 1990; Milchunas *et al.,* 1999; Dickson *et al.,* 2008). Mechanized military maneuvers increase the populations of non-native species, weeds, forbs, and annuals (Milchunas *et al.,* 2000), while reducing the cover provided by native perennial grasses and forbs (Quist *et al.,* 2003; Guretzky *et al.,* 2006; Dickson *et al.,* 2008). Roughly 25-35% of the surface area of military training grounds is heavily damaged by military operations. Changes in the proportion of bare ground, litter, vegetative basal cover, as well as the churning of soil surface from military vehicle traffic increases the potential for invasion by undesirable species (Milchunas *et al.,* 1999) as bare ground is essential for weed development (Wilson 1988). Smaller annual species tend to replace large perennials (Dickson *et al.,* 2008) and short-lived perennials tend to replace long-lived perennials (Milchunas *et al.,* 1999).

Introduced non-native species, such as broad-leaved forbs, are extremely vulnerable to military disturbance as compared to native prairie vegetation communities. Graminoids, such as the native tall grasses of Fort Riley, show higher resistance and resilience to military disturbance due to their deeper root systems (Dickson *et al.,* 2008). The native grasses of Fort Riley are matrix-forming, meaning they consume the majority of available resources and have dense root systems that give them the ability to reduce surface erosion. However, when stripped or replaced of such characteristics, military training areas become highly susceptible to soil erosion (Quist *et* *al.,* 2003) and suffer from significant decreases in plant species richness and diversity (Milchunas *et al.,* 2000; Quist *et al.,* 2003). In 2001, 50% of the grassland areas at Fort Riley were characterized as bare ground, which may have been due to increased off-road training by wheeled and tracked vehicles during this time (Althoff *et al.,* 2006).

Sustainable Management of U.S. Army Military Training Lands

Since passage of the National Environmental Policy Act of 1969 (NEPA) and publication of U.S. Army Regulation 200-2 (Department of the Army 1988), the U.S. Army has challenged itself to consider environmental effects and costs identified through decision-making based upon "a systematic, interdisciplinary approach that ensures integrated use of the natural and social sciences, planning, and the environmental design arts." To help achieve this requirement, U.S. Army Regulation 350-19 mandates the critical goal of "maximizing the capability, availability, and accessibility of ranges and training lands to support doctrinal requirements, mobilization, and deployments" (Department of the Army, 2005). This same regulation established the Integrated Training Area Management (ITAM) program at the installation level whose objective is to establish the "policies and procedures to achieve optimum, sustainable use of training and testing lands" through implementation of "a uniform land management program." A key term used in U.S. Army Regulation 350-19 is "sustainable use" which helps ITAM personnel develop a local philosophy for training land management, as well as identifying specific methods and approaches for managing and maintaining training lands to support military mission readiness at the installation level.

The Range and Training Land Assessment (RTLA) component of the Integrated Training Area Management (ITAM) program was created by the U.S. Army to support the ITAM mission by monitoring training lands for environmental degradation, including trends in plant communities. This monitoring information helps military land managers maintain valuable training lands for present and future generations without losing ecological diversity (Althoff *et al.,* 2006). The Land Condition Trend Analysis (LTCA) denotes a standard methodology for the collection, analysis, and documentation of vegetation conditions on installations (Tazik *et al*., 1992; Althoff *et al.,* 2006). Through the use of GIS and remote sensing techniques, RTLA personnel can effectively monitor training land impacts, and their subsequent recovery, over long time periods at low cost.

Konza Prairie Biological Station

Konza Prairie Biological Station (KPBS) is located on 3,487-hectares of protected land south of Manhattan, Kansas (39.09°N, 96.57°W), in Northeastern Kansas (Figure 3.3). The KPBS is owned by the Nature Conservancy (http://www.nature.org) and operated by the Division of Biology at Kansas State University (http://kpbs.konza.ksu.edu). One of the National Science Foundation's Long-term Ecological Research Sites, KPBS has similar vegetation, soils, prescribed burning practices, and climate due to its close proximity (less than 10 kilometers) to Fort Riley.

KPBS is dominated by native tallgrass prairie of the Flint Hills ecoregion, part of the same largest continuous tallgrass prairie in North America. Because of the steep slopes and underlying limestone soils, KPBS proves unsuitable for cultivation and has remained unplowed, retaining its native characteristics. Elevation range from approximately 318 to 445 m above sea level and average 397 m across the site (Knapp *et al.,* 1998; Briggs 2012;). On average, KPBS experiences 34-36 inches of precipitation, usually from April to October (Hayden 1998), with average monthly air temperature ranging from -3°C in January to 27°C in July and soil temperatures tend to range from 1.6°C in January to 29.3°C in July (Blair 1997).

Figure 3-3 Konza Prairie Biological Station study area showing experimental watersheds but excluding agricultural and developed areas.

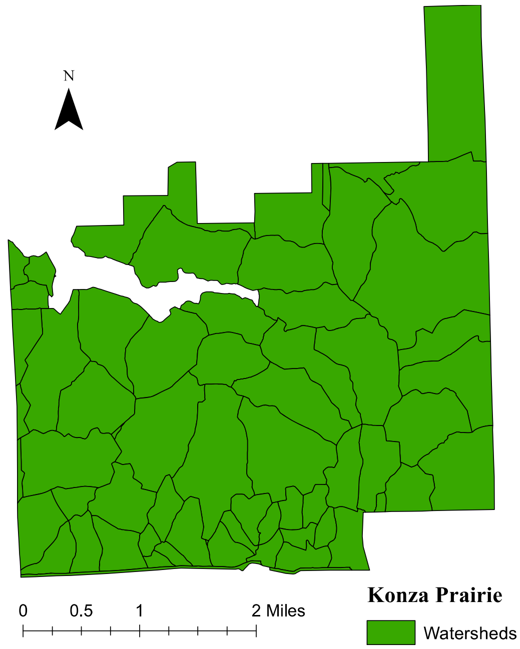

An experimental plan established in 1971 assigned KPBS watersheds to different treatments of prescribed burning, ranging from annual burns to long-term (*e.g.,* 20 years) unburned. In October 1987, bison were introduced to Konza to examine the effects of grazing on the prairie ecosystem and, as of 1992, 1,100 ha were being actively grazed. Cattle also graze in selected watersheds.

The flora of KPBS results from both regional climatic influences as well as local-scale factors such as soils, burning regime, and grazing. Over five hundred species of vascular plants have been reported on Konza Prairie since 1975 (Freeman 1998). The ten most species-rich families account for nearly 60% of all species identified at KPBS and are comparable to those found throughout the Flint Hills ecoregion (Kuchler 1974). Perennial plants comprise 65% of all the species at Konza, with annuals representing most of the remaining species.

KPBS shares a similar grassland species composition mix with Fort Riley, being dominated by native warm-season C4 grasses such as big bluestem (*Andropogon gerardii*), little bluestem (*Schizachyrium scoparium*), indiangrass (*Sorghastrum nutans*), and switchgrass (*Panicum virgatum*). In addition to grasses, forbs are commonly found throughout the site. Common species on mesic sites include white aster (*Aster ericoides*), daisy fleabane (*Erigeron strigosus*), and wild alfalfa (*Psoralea tenuiflora*). Species on more xeric areas include western ragweed (*Ambrosia psilostachya*), white sage (*Artemisia ludoviciana*), and aromatic aster (*Aster oblongifolius*) (Freeman and Hulbert 1985; Freeman 1998).

Chapter 4 - Sensitivity of TIMESAT-derived Phenometrics to Adaptive Savitzky-Golay Filters Applied to MODIS Time Series Data

Abstract

Time series of normalized difference vegetation index (NDVI) data from satellite spectral measurements can be used to characterize and quantify changes in vegetation phenology and explore the role of natural and anthropogenic activities in causing those changes. Several programs and methods exist to process phenometric data from remotely-sensed imagery, including TIMESAT, which extracts seasonality parameters from time-series image data by fitting a smooth function to the series. This smoothing function, however, is dependent upon user-defined input parameter settings which have an unknown amount of influence in shaping the final phenometric estimates. To test this, a sensitivity analysis was conducted using MODIS maximum value composite NDVI time-series data acquired for Fort Riley, Kansas during the period 2001-2012. A total of three parameter settings were changed to create 7 TIMESAT input setting files. The 7 extracted phenometric data extracted by TIMESAT using the different input settings files were compared against that from a base scenario using Pearson and Lin's Concordance Correlation Analyses. Findings showed that small changes to parameter settings result in insignificant differences in phenometric estimates, with the exception of end of season data and growing season length. Phenometric results are dependent upon user-defined input settings and an optimal input settings file may differ based on distinctive study areas. For Fort Riley, the optimal settings file included a start and end of season threshold value of 25%, a window size of 4, and envelope iteration value of 2.

Introduction

Phenology has emerged as an important focus in ecological research for its use in vegetation monitoring/modeling and addressing issues related to climate change. Phenology is the timing of seasonal vegetation activities (Parmesan 2006) and the study of how vegetation growth may be affected by interannual and seasonal variations in meteorological conditions, soil characteristics, and photoperiod (Schwartz 1998; Cleland *et al.,* 2007). It can be used to predict the fitness and probability of species occurrence under certain conditions (Cleland *et al.,* 2007), making it one of the most efficient ways of following species response to changing ecosystem conditions (Walther *et al.,* 2002). Through the use of remote sensing, the study of phenology provides additional insights into the natural and anthropogenic processes impacting vegetation life cycles.

Usually measured in Julian dates, or days since December 31, phenology can be measured by using satellite imagery and extracting phenometric data from vegetation index data such as that acquired by the MODIS sensor (Ahas *et al*., 2002; An 2009). The spectral-temporal information obtained from time-series NDVI data can be used to characterize and quantify changes in vegetation phenology (Reed *et al.,* 1994; Wardlow 2005) and to explore the potential role of different natural and anthropogenic activities in causing those changes (Jacquin *et al.,* 2009).

Phenometrics such as start and end of growing season, growing season length, and maximum greenness value may be extracted from a time series of NDVI data by fitting a function to the original data, which often incorporates use of a filter, or smoothing function, to remove atmospheric and sensor calibration noise (Chen *et al*., 2004; Eklundh and Jönsson 2010; Jönsson *et al*., 2010). A number of software packages and methods exist to facilitate data smoothing and extraction of fitted functions, including the TIMESAT software package

(Eklundh and Jönsson 2010). However, smoothing typically requires a number of user-defined parameter settings to optimize a given curve-fitting function to the raw satellite data. For example, the Savitzky-Golay filter available in TIMESAT requires values for important parameters such as start and end of season threshold, window size, and number of envelope iterations (TIMESAT MANUAL). While general guidelines are available for selecting the proper values for these parameters, it remains unclear as to what impact adoption of TIMESAT "default" parameter settings might have on extracted phenometrics.

Past Work

A typical NDVI profile, or phenology curve, illustrates the onset of greenness or when the vegetation begins to green-up, the maximum NDVI value illustrating the highest relative photosynthetic biomass, the rate of senescence or decay, the end of greenness date, and the growing and brown days (days of senescence) of a year accumulating to the season length of the year (Figure 4.1). The area beneath this phenology curve represents the accumulated NDVI or an indication of relative photosynthetic biomass, which is dependent upon all other phenometric data.

Spectral-temporal information extracted from time-series vegetation index data has been used successfully to characterize vegetation phenology and assist with forecasting/monitoring vegetation density and health (Reed *et al.,* 1994; Wardlow 2005; Jacquin *et al.,* 2009). Time series of satellite-derived NDVI datasets have been used to assess vegetation activity and measure vegetation dynamics (Zhang *et al.,* 2003; Ahl *et al.,* 2006), including spatiotemporal changes in vegetation condition and biomass (Huete *et al.,* 2002). Specifically, 16-day MODIS maximum value NDVI composite images (MOD13Q1) with a 250 meter spatial resolution have been shown successful in measuring important phenometrics and detecting possible human-induced land cover changes (Wardlow 2005; Jacquin *et al.,* 2009; Verbesselt *et al.,* 2009). Variations in phenometric values associated with different land cover regions, land use practices, climatic conditions, as well as planting dates for crops, may be determined (Wardlow 2005).

Figure 4-1 A typical vegetation phenology curve, and associated phenometrics, derived from time series NDVI values (from Jacquin *et al.,* 2009).

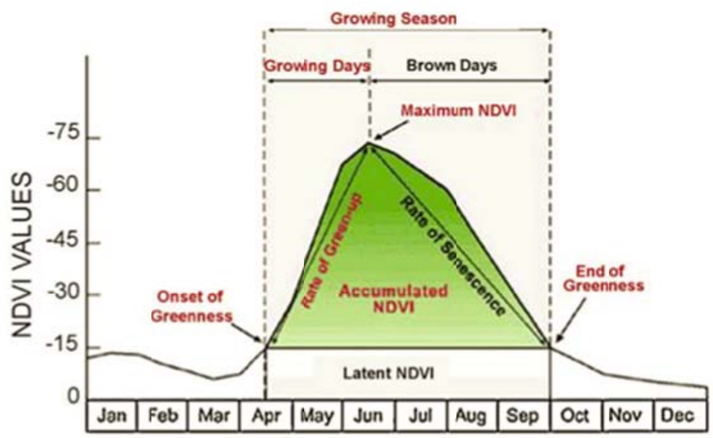

Raw data from remote sensors must first be processed through a series of filtering, compositing, smoothing or screening procedures in order to isolate the desired phenometric signals from noise. There are many different types of time series analysis techniques used to filter raw NDVI data and then extract phenometrics, including the seasonal Kendall (SK) trend test (Hirsch and Slack 1984; de Beurs and Henebry 2004, de Beurs and Henebry 2005; de Beurs *et al.,* 2009;), principal component analysis (PCA) (Crist and Cicone 1984), pixel-above-threshold technique (PAT) (Cleland *et al.,* 2007), wavelet decomposition (Anyamba and Eastman 1996), change vector analysis (CVA) (Lambin and Strahler 1994), and Fourier analysis (Azzali and Menenti 2000).

In addition, the TIMESAT software program provides several filtering options to smooth raw vegetation index data and extract key phenometric data (Eklundh and Jönsson 2010). In previous studies, TIMESAT has been used to study vegetation phenology (Eklundh and Jönsson 2003), map phenological and environmental changes (Eklundh and Olsson 2003; Hickler *et al.,* 2005; Olsson *et al.,* 2005; Seaquist *et al.,* 2006; Heumann *et al.,* 2007; Seaquist *et al.,* 2009), examine high-latitude forest phenology (Beck *et al.,* 2007), assess satellite and climate data-derived indices of fire risk (Verbesselt *et al.,* 2006), monitor human impacts of fire seasons (Le Page *et al.,* 2009), and evaluate relationships between coniferous forest NDVI and models of conifer photosynthetic activity (Eklundh and Jönsson 2010).

As pointed out in the TIMESAT manual, optimal curve fitting during smoothing is "more of an art than a science" and some trial and error may be necessary to arrive at a final set of parameter settings (Eklundh and Jönsson 2010). This study reports the results of a sensitivity analysis of phenometrics to selected parameters required by the TIMESAT Savitzky-Golay filter using as input a 2001-2012 time series of MOD13Q1 images for Fort Riley, Kansas. Phenometric data from the time series was extracted using different Savitzky-Golay filters created from unique user-defined parameter settings. Ordered pairs of extracted phenometrics obtained from the different filter parameter settings were compared at the pixel level using Pearson and Lin's Concordance Correlation tests (Lin 1989; McGrew and Monroe 2000). This analysis allowed for specification of an "optimal" Savitzky-Golay filter parameter settings file and, ultimately, more confidence in the validity of extracted phenometrics for the Fort Riley study area.

Study Area

Fort Riley is a United States Army base located in northeastern Kansas (39°11'N, 96°48'W), on the Kansas River, between Junction City and Manhattan and within Geary, Riley, and Clay counties (Figure 4.2). The total installation area is 41,141 ha and is located within the Flint Hills ecoregion (Omernik 1987, Bailey *et al.,* 1994).

Figure 4-2 Fort Riley study area, located in parts of Clay, Geary, and Riley counties in northeastern Kansas.

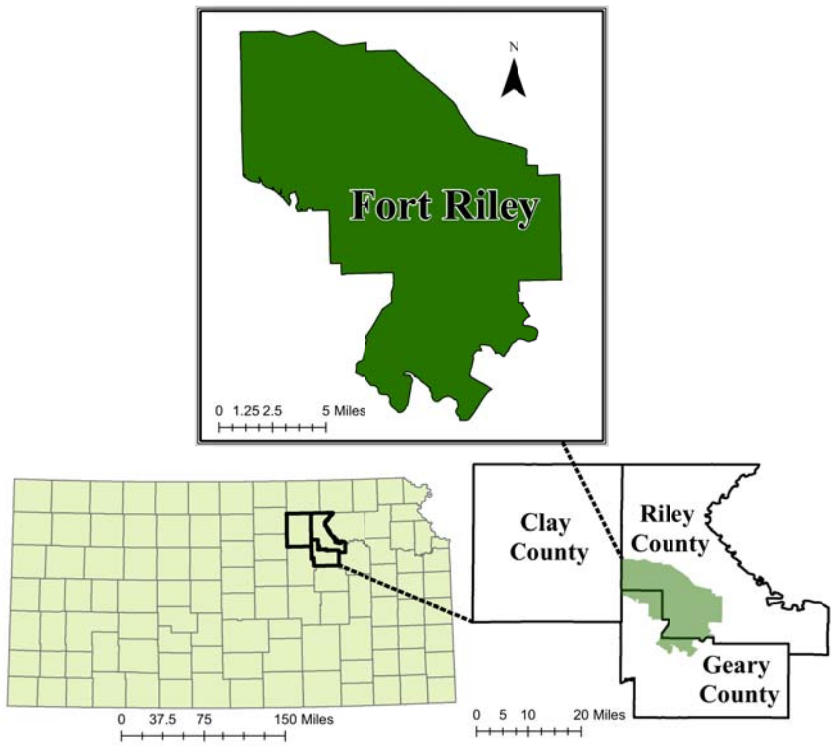

The installation serves as a combat training ground for mortar and artillery fire, small arms fire, aircraft flights, field maneuvers, tanks, and mechanized infantry units (Quist *et al.,* 2003; Althoff *et al.,* 2006). Since the 1980's, military units have engaged in continuous maneuver-based training across the entire installation (U.S. Army 1994), though such activities are concentrated in the northern 75% portion of the installation (Quist *et al.,* 2003; Althoff *et al.,* 2006).

High intensity military training associated with mechanized military maneuvers has been cited as the cause of increased bare soil, reduced plant cover, compacted soil conditions, and compositional shifts in plant communities (Shaw and Diersing 1990; Trumbell *et al*., 1994; Whitecotton *et al*., 2000; Quist *et al.,* 2003; Guretzky *et al.,* 2006). Military training alters vegetation composition by decreasing the basal cover of perennial warm-season grasses and increasing the cover of perennial cool season grasses and annual warm-season forbs (Wilson 1988; Shaw and Diersing 1990; Milchunas *et al.,* 1999; Dickson *et al.,* 2008). Mechanized military maneuvers increase the populations of non-native species, weeds, forbs, and annuals (Milchunas *et al.,* 2000), while reducing the cover provided by native perennial grasses and forbs (Quist *et al.,* 2003; Guretzky *et al.,* 2006; Dickson *et al.,* 2008).

Fort Riley's climate is generally considered temperate continental. Weather is highly variable but can be characterized as having hot summers, cold, dry winters, moderate winds, low humidity, and a pronounced peak in rainfall late in the spring and in the first half of summer. Average monthly temperatures range from approximately -3°C in January to 26°C in July (PRISM Climate Group 2012). Mean annual precipitation is approximately 843 mm, but extremely variable from year to year, with 75% of precipitation occurring during the growing season. The source of much precipitation is thunderstorms, which typically have intense rainfall rates of approximately 60 mm/hr and occur approximately 55 days each year in this area (U.S. Department of Agriculture Soil Conservation Service 1975; Knapp 1998).

The vegetation of Fort Riley is a mix of native prairie and introduced vegetation consisting of C4 grasses (46%), forbs (32%), legumes (11%), and C3 grasses (11%) (Dickson *et al.,* 2008). The installation is comprised of three major vegetation communities, including grasslands (32,200 ha), shrublands (1,600 ha), and woodlands (6,000 ha) (Althoff *et al.,* 2006)

The eastern portion of Fort Riley shares many of the characteristics to the Flint Hills, with vegetation dominated by warm-season highly productive C4 grasses and a mixture of annual and perennial forbs. The western portion of Fort Riley represents a plant community undergoing succession back to native prairie from past cultivation in the 1960s (Quist *et al.,* 2003).

Fort Riley grasslands are dominated by big bluestem (*Andropogon gerardii*), Indiangrass (*Sorghastrum nutans*), switchgrass (*Panicum virgatum*), and little bluestem (*Schizachyrium scoparium*). Other grasses and forbs are also present at lower abundances. Shrublands consist primarily of buckbrush (*Symphoricarpos orbiculatas*), smooth sumac (*Rhus glabra*), and rough-leaved dogwood (*Cornus drummondii).* Additionally, there is a mixture of grasses and forbs that occur along the edges of woodlands and in solitary patches of grassland areas. Typically located along riparian lowlands, woodlands are dominated by chinquapin oak (*Quercus muhlenbergii*), bur oak (*Quercus macrocarpa*), American elm (*Ulmus americana*), hackberry (*Celtis occidentalis*), and black walnut (*Juglans nigra).*

The majority (80%) of the forb community, most common within Fort Riley grasslands, is dominated by white heath aster (*Symphyotrichum ericoides*), the common sunflower (*Helianthus annuus*), whorled milkweed (*Asclepias verticillata*), and common milkweed (*Asclepias syriaca*). Common sunflower abundance and distribution is closely linked to disturbance caused by tracked military vehicles during maneuvers (Althoff *et al.,* 2006).

Data and Methods

Data Acquisition

The image data used in this analysis was the MODIS MOD13Q1 product, a 16-day maximum value NDVI composite with a 250 meter spatial resolution. A gridded level-3 product delivered in a sinusoidal projection, MODIS radiance counts are calibrated and geolocated based on grid and angular data, masked from cloud, land/water, perceptible water and aerosol products, incorporate spectral reflectance, and undergo quality assurance flags associated with atmospheric correction products (Huete *et al.,* 1999).

Imagery data was downloaded from the Earth Observing System Data and Information System (EOSDIS 2009) and saved as an 8-bit unsigned integer grid. At the latitude of the study area, cell resolution was 213.705 meters. Images were reprojected into the North American Datum of 1927, Universal Transverse Mercator Zone 14 North projection, clipped to the extent of the study area (106 columns by 128 rows), and resaved as a single band IMAGINE file. This format meets the TIMESAT input requirement of a headerless binary file. Saved images were placed in the same file directory for later processing in TIMESAT (Figure 4.3).

Figure 4-3 MODIS MOD13Q1 NDVI images of Fort Riley, Kansas from May 9, 2005 (image 106, left) and September 30, 2010 (image 224, right) as viewed in TIMESAT. Red and light blue represent areas with high and low NDVI values, respectively. Note that areas outside of the Fort Riley boundary were assigned values of 0.

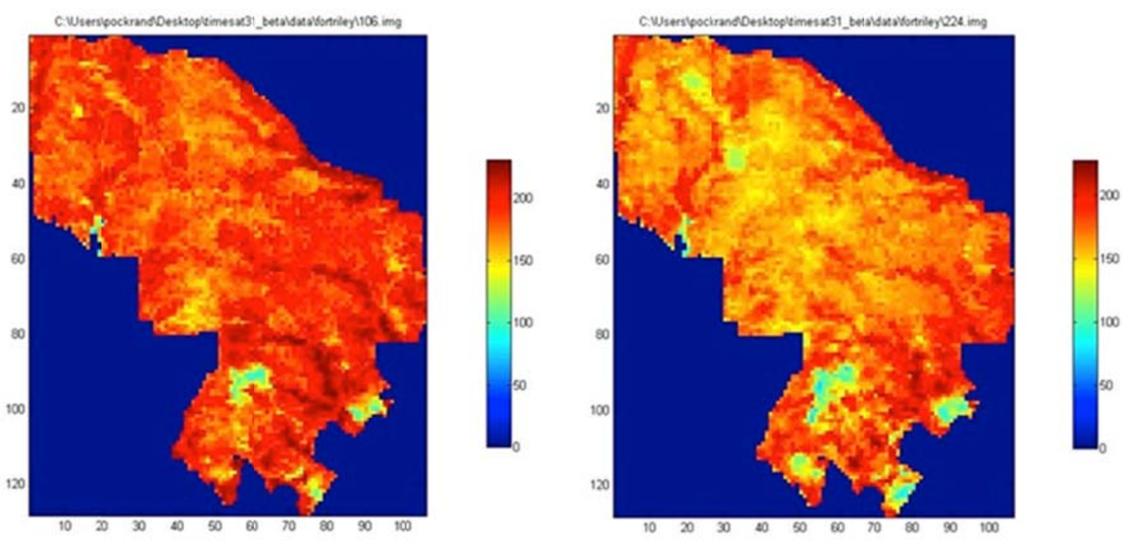

Collected images spanned the period from January 2001 through December 2012 (n = 12 years). Because TIMESAT only analyzes for the n – 1 centermost seasons, the results presented here will be based on 11 years and exclude 2012 (Eklundh and Jönsson 2010). Each calendar year includes 23 total MOD13Q1 images with this study incorporating 276 total images (23 x 12).

Data Processing in TIMESAT

After data acquisition and preprocessing was complete, a text file was prepared to serve as the input for TIMESAT processing (see Appendix A for the complete text file used in this study). The first row of the input text file included the number of images to be used in the analysis (*i.e.,* 276) followed in the second row by the full path and filename of the first MOD13Q1 image. Each subsequent row lists the next image, including the full path and filename.

After reading the input file and initial lines for each of the images, TIMESAT reads each image file comprising the time series image (and any optional quality indicators incorporated), preprocesses the images using optional quality indicators, smooth's the time series data using a number of possible filter types and user-defined parameter settings, and extracts seasonality parameters (*i.e.,* phenometrics) to a file based on the selected smoothing function.

The TIMESAT graphical user interface (GUI) presents the controls for selecting the smoothing function and parameter settings, and provides a graphical view of the raw and smoothed curves for one pixel, along with the resulting phenometrics (Figure 4.4). The critical steps of selecting a smoothing function and related parameter settings are organized in three subsections within the TIMESAT interface and include data plotting, common settings, and class-specific settings. A brief discussion of each subsection follows.

Figure 4-4 The TIMESAT graphical user interface showing the raw (blue) and fitted (brown) phenology curves for one MODIS image cell during the study period. The blue line represents the raw NDVI data of one MODIS imagery cell. Brown points on the fitted curve represent the SOS (left) and EOS (right) phenometrics for each season.

Data Plotting

Three different filters, or smoothing functions, are available for selection in TIMESAT, including Gaussian, logistic, and Savitzky-Golay. The Gaussian approach is an asymmetric function fitting method that determines the position of the maximum or the minimum value in the time series while considering the independent time variable (Jönsson and Eklundh 2002). A disadvantage to selecting this function is in the difficulty associated with identifying a reasonable and consistent set of maxima and minima which, in turn, determine the local functions used to fit to the raw data (Jönsson and Eklundh 2002; Chen *et al.,* 2004). It may be difficult to discriminate between the maxima and minima that may be due to seasonal variation, and that which may be due to noise or disturbances (Jönsson and Eklundh 2002). The double logistic function included with TIMESAT has been found to preserve NDVI signal integrity (Hird and McDermid 2009) but result in no major differences with the Savitzky-Golay method (Jönsson *et al.,*2010).

First proposed in 1964, the Savitzky-Golay filter is a simplified least-squares-fit convolution for extracting derivatives and smoothing a spectrum of consecutive values. It is essentially a weighted moving average filter based on a polynomial where the polynomial order dictates the convolution. When the weight coefficients are applied to a signal, a polynomial least squares fit will be applied to the filter window. Such a procedure is intended to maintain peak times within the data and reduce introduced bias noise from the data (Chen *et al.,* 2004; Eklundh and Jönsson 2010). It is intended to preserve the area and mean position of a seasonal peak, but alter both the width and height. This method is sensitive to local variations in vegetation index values, proving useful when comparing against different regions (Jönsson *et al.,* 2010). The end result is a smoothed curve adapted to the upper envelope (peak values) of the values in a time-series. More information on the mathematics behind this procedure and its coefficients may be found in Savitzky and Golay (1964), Steinier *et al.,* (1972), and Press *et al.,* (1996).

As Figure 4.4 indicates, Fort Riley experiences growing season transitions during green-up and senescence phases. An optimal smoothing filter for this situation would utilize a narrow moving window approach. The Savitzky-Golay filter has the option of modifying the width of the moving window that is used to filter the raw data. A large window will have a higher degree of filtering, flatten sharp peaks and hamper the ability to detect rapid changes in the data. A smaller window will detect these rapid changes occurring on Fort Riley and preserve sharp peaks in the data.

Common Settings

Common settings in TIMESAT affect all pixels in the image time series. Similar to the data plotting options, TIMESAT makes available three different methods in common settings: *STL original*, *STL replace spike* method, and *median spike* method. The *STL* method (seasonal trend LOESS) provides seasonal smoothing and decomposes time series data by using a LOESS smoother (locally weighted regression smoother) based on a weight system (Verbesselt *et al.,* 2009). This decomposition takes the full time-series and partitions it into a seasonal and a trend component, and low weights are assigned to the values that do not fit these patterns (Cleveland *et al.,* 1990).

The *median spike* method was used in this analysis because, unlike the two STL options, it retains all raw data values. However, any values in the time series that are significantly different from their left- and right neighbors – and from the median in a window – are classified as outliers and are assigned zero weight (Eklundh and Jönsson 2010).

The median filter option also incorporates a spike value. The spike value is used to help determine significant differences in adjacent values in the time series. Data values that differ from the median by more than the product of the spike value and standard deviation of the time-series, and that are different from the left- and right neighbors are removed. The TIMESAT manual suggests that a normal setting for the spike value is 2 and warns that a lower value will remove more data values from the analysis (Eklundh and Jönsson 2010). Based on this recommendation, a spike value of 2 was used in this analysis.

Fixed Class-Specific Settings

Class-specific settings in TIMESAT apply to individual land classes (*i.e.,* different landuse/landcover categories). While only a single class is recognized when processing data through the TIMESAT GUI, multiple classes can be accommodated and analyzed separately through the TIMESAT *process* function. A total of eight different class-specific settings can be applied. The first four, and those which will not be examined by the sensitivity analysis, are briefly discussed below.

The *seasonal* parameter defines the number of growing seasons per year. A parameter value of 1, like that applied to the Fort Riley data, indicates a single season per year. For areas experiencing dual seasons, a parameter value of 0 should be used.

A second parameter, *start of season* method, offers two choices: Amplitude and absolute value. This parameter works with the season start and season stop values. When choosing amplitude as the method, the season start and stop values are entered as percentages of the growing season maximum value. For example, a season start value of 0.20 will identify the time when 20% of the maximum growing season amplitude is reached. Conversely, setting an absolute value for start of season method finds the time each season when that specific digital number value is reached.

Further fine-tuning of the impact of the *number of envelope iterations* (explained in the following section) can be made through adjustments to the third setting *adaptation strength*. Ranging from a minimum of 1 to a maximum of 10, normal adaptation values are typically 2 or 3 (Eklundh and Jönsson 2010). After reviewing the Fort Riley time series data in the TIMESAT GUI, and visually comparing differences in curve fits using typical adaptation strength values, a final setting of 2 was selected as the curve fit tended to honor the raw data values best.

The *force minimum* option (setting number 4), if active, essentially removes extremely low values in the time series (e.g., outliers) and replaces them with the new value entered. Using this option is helpful in eliminating unusually low NDVI values such as those recorded during the winter when snow covers the land surface. Forcing these low values into something approaching the mean winter minima helps preserve the true seasonal curves generated by the fitted function. Fort Riley does experience extended winter periods with snow on the ground, so this study implements a forced minimum value of 80.

Dynamic Class-Specific Settings

The second set of four class-specific settings, and those selected for participation in the sensitivity analysis, include the Savitzky-Golay *window size*, *number of envelope iterations*, *start of season* (SOS) and *end of season* (EOS). When previewed in the TIMESAT GUI, each of these settings appeared to exert considerable influence on the shape of the curve fitted to the NDVI time series, as well as the resulting phenometrics reported in the seasonality data window. Related literature does not provide definitive guidance on the most appropriate values for these settings. For example, *SOS* and *EOS* values (start of season method = amplitude) typically range between a setting of 10-25%.

The *window size* represents the width, or half-window, of the moving window used by the Savitzky-Golay filter during smoothing. The width of the moving window helps to determine the amount of smoothing that takes place and impacts the ability to capture rapid changes in the NDVI time series. Implementing a large window size may neglect important variations and flatten out sharp peaks in the data (Chen *et al.,* 2004). The TIMESAT manual suggests a starting window size value of *floor(noptsperyear/4)*. For the Fort Riley MOD13Q1 time series, this results in a base value of 5. Chen *et al.,* (2004) concluded that a *window size* of 4 was the optimal setting for their data as it provided the best fit.

The second dynamic class-specific setting in the sensitivity analysis is *number of envelope iterations*. The fit of the smoothing function previously selected can be made to approach the upper envelope of a time series using an iterative and multi-step procedure that can be repeated twice. Specifying a value of 1 for *number of envelope iterations* results in only one "fit" to the data and no adaptation. With values of 2 or 3, one or two additional fits are applied to force the fitted function towards the upper envelope (Eklundh and Jönsson 2010). Because the Savitzky-Golay filter is generally sensitive to the upper envelope of the smoothing function, *number of envelope iterations* is one of the parameters settings that will be examined with the sensitivity analysis. Selecting too large of a value may introduce error into the estimated beginning of season and end of season dates by over-fitting the curve. Values which are too small may cause errors by including in the fitted curve data related to atmospheric or calibration noise.

The final two dynamic settings are *SOS* and *EOS*, represented in the TIMESAT GUI as season start and season end, respectively. Assuming *amplitude* as the start of season method, values for *SOS* and *EOS* will range between 0 and 1. These values represent the proportion of the seasonal amplitude reached each season. For example, a *SOS* value of 0.20 establishes as the season start the date where the fitted curve reaches 20% of its maximum value each growing season. Though two separate settings, *SOS* and *EOS* are typically assigned the same values. Past researchers have used various values for *SOS/EOS* including 0.10 (White *et al.,* 1997; Jönsson and Eklundh 2002; Jones *et al.,* 2012) and 0.25 (Dragoni and Rahman 2012). Selecting low values for this setting may place *SOS/EOS* too early/late in the season in portions of the fitted curve dominated by atmospheric and calibration noise. High values may mistakenly label as the *SOS/EOS* date periods well inside the actual growing season instead of its true beginning/end. Table 4.1 offers a quick summary of the specific input values chosen for this analysis based both on recommendations from the TIMESAT manual and those in related literature.

Table 4.1 TIMESAT parameter settings and input values selected for this analysis.

Parameters	Suggested	Source	Used
Data Plotting			
Filters	Gaussian, logistic, Savitzky-Golay	Savitzky and Golay 1964; Jönsson and Eklundh 2002; Hird and McDermid 2009; Jönsson et al., 2010	Savitzky-Golay
Common Settings			
Spike Method	STL original; STL replace spike; median spike	Verbesselt *et al.,* 2009; Eklundh and Jönsson 2010	Median spike
Spike Value	2	Eklundh and Jönsson 2010	2
Fixed Class-Specific Settings			
Seasonal Parameter	1	Eklundh and Jönsson 2010	1
Start of Season Method	Amplitude, absolute value	Eklundh and Jönsson 2010	Amplitude
Adaptation Strength	2-3	Eklundh and Jönsson 2010	2
Force Minimum	N/A	N/A	80
Dynamic Class-Specific Settings			
Savitzky-Golay Window Size	5	Chen *et al.,* 2004; Eklundh and Jönsson 2010	3, 4, and 5
Number of Envelope Iterations	1, 2, 3	Eklundh and Jönsson 2010	1, 2, 3
SOS and EOS Threshold	10-25%	White et al., 1997; Jönsson and Eklundh 2002; Dragoni and Rahman 2012; Jones et al., 2012	10%, 20%, 25%, 30%

Phenometric Extraction

To assess the sensitivity of TIMESAT-derived phenometrics to the adaptive Savitzky-Golay filter, as applied to the MOD13Q1 NDVI time series of Fort Riley, phenometrics resulting from a base scenario of fixed and dynamic class-specific settings was compared. In TIMESAT, a parameter settings file was created using different combinations of the dynamic class-specific settings including *SOS/EOS* (4 settings), *window size* (3 settings), and *number of envelope iterations* (3 settings) (Table 4.2). The base scenario featured a *window size* of 4, *SOS/EOS* of 0.2, and 2 *envelope iterations*. The sensitivity analysis compared a subset of phenometrics estimated by TIMESAT using these base settings against those arrived at by different combinations of input settings (identified with a checkmark in Table 4.2). This resulted in 8 total parameter settings files.

Table 4.2 Matrix depicting the values of dynamic class-specific settings assessed when using a number of envelope iterations = 2 (left) and all combinations of settings analyzed for significant differences (right).

Start/End of Season Input

Window Size		0.1	0.2	0.25	0.3
	3		√		
	4	√	Base	√	√
	5		√		

Envelope Iteration 2

Test #	Envelope Iteration	Window Size	SOS EOS
Base	**2**	**4**	**0.20**
1	2	4	0.10
2	2	4	0.25
3	2	4	0.30
4	2	3	0.20
5	2	5	0.20
6	1	4	0.20
7	3	4	0.20

Once the parameter settings files were created, the MOD13Q1 time series data was processed using TIMESAT *TSF_process* (TIMESAT Fortran process) which applied unique Savitzky-Golay filters to the raw NDVI data. Seasonality data was extracted from the smoothed curves and output as a TPA file and processed by the TIMESAT *TSM_printseasons* routine to generate numerical phenometric data for further analysis. The TIMESAT seasonality files contain 11 total phenometrics estimated for each pixel in every NDVI image in the 11 season time series (Table 4.3).

Each individual NDVI image had 106 columns and 128 rows of pixels which results in more than 13,500 data values per phenometric per season. Five of these 11 phenometrics were selected for comparison, including *start of season*, *length of season*, *end of season*, *maximum value*, and *small season integral*. A graphic depiction of these 5 phenometrics is shown in Figure 4.5.

Table 4.3 List, definition, and biological significance of the phenometrics extracted using TIMESAT (Eklundh and Jönsson 2010). Rows highlighted in gray indicate phenometrics used in later analyses.

Phenometric	**Definition**	**Biological Significance**
Start of Season	Time at which the left edge has increased to a user-defined level measured from the left minimum value.	Time of initial vegetation green up
End of Season	Time at which the right edge has decreased to a user-defined level measured from the right minimum value	Time of initial vegetation senescence
Season Length	Time from start to end of season	Length of growing season from green up to senescence
Base Level	Average of the left and right minimum values	Baseline for the seasonal phenology curve
Middle of Season	Mean value of the times at which the left edge has increased to the 80% level and the right edge has decreased to the 80% level.	Time of the middle of the growing season.
Maximum Value	Largest data value for the fitted function during the season.	The highest NDVI value of the season.
Seasonal Amplitude	Difference between the maximum value and base level.	Used for referencing Start and End of Season thresholds.
Rate of Increase at Beginning of Season	Ratio of the difference between the left 20% and 80% levels and the corresponding time difference.	Rate of vegetation green up.
Rate of Decrease at End of Season	Absolute value of the ratio of the difference between the right 20% and 80% levels and the corresponding time difference.	Rate of vegetation senescence.
Large Seasonal Integral	Integral of the function describing the season from season start to season end.	Proxy for the relative amount of vegetation biomass without regarding minimum values.
Small Seasonal Integral	Integral of the difference between the function describing the season and the base level from season start to season end.	Proxy for the relative amount of vegetation biomass while regarding minimum values.

Figure 4-5 Graphic depiction of selected phenometrics used in the sensitivity analysis: Start of season (a), end of season (b), maximum value (e), season length (g), small seasonal integral (h) (from Eklundh and Jönsson 2010).

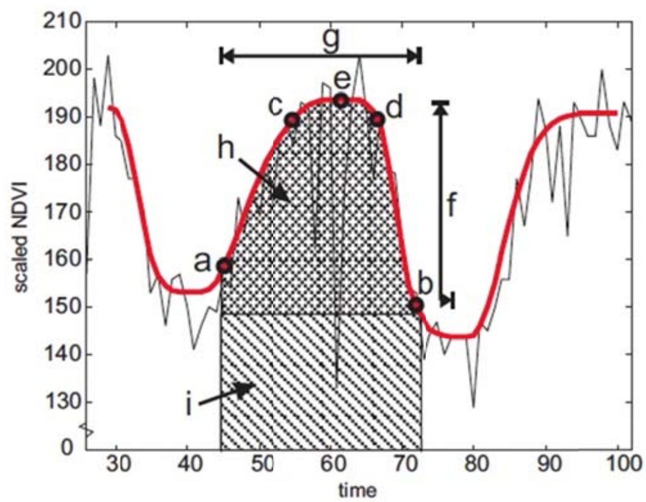

Statistical Analysis

The output generated from the 8 phenometric data files by *TSM_printseasons* were organized by sorting the phenometric data first by season, then row, and then by column which allowed later statistical analysis on the phenometric to be performed uniformly across the different parameter settings files (Figure 4.6). There is a total of 8 parameter settings files (n = 8) and 2 files will be compared against each other (r = 2), yield a total of 28 different paired combinations (nCr = 28) included in this analysis (Equation 4.1).

nCr = (n!) / (r! (n-r)!) **Equation 4.1**

where:
n = number of parameter settings
r = number of comparisons
nCr = number of paired combinations

Figure 4-6 Example of a portion of one phenometric data file created from a parameter settings file. The table includes the row and column of each image pixel, the season, and the 11 different phenometrics estimated by TIMESAT.

Row	Col.	Seas.	Beg.	End.	Length	Base	Mid-x	Max.	Amp.	L-der.	R-der.	L-integ.	S-integ.
1	1	1	5.2	24.3	19	105.5	9.9	196.7	91.2	26.8	3.9	3459.3	1243.8
1	1	2	28.9	45.5	16.6	108.4	33.4	177.2	68.8	13.9	4.3	2798.3	739.6
1	1	3	52.2	67.3	15	102.4	59.3	188.9	86.5	23.2	15.2	2788.3	1048.3
1	1	4	75.3	91	15.7	103.9	83.6	213.6	109.7	10.3	11	2878.3	1111.6
1	1	5	96.6	112.4	15.8	102.5	104.5	185.6	83.1	13.7	12.9	2877.9	1033.5
1	1	6	121.4	135.9	14.5	98.8	130.3	198.6	99.8	9	18.5	2621.8	1040.4
1	1	7	144.6	161.9	17.3	103.1	150.8	188.5	85.4	17.7	5.7	3001	1042.4
1	1	8	166.5	181.7	15.3	105.4	173.5	190.6	85.2	16.2	12.1	2800.3	1008.1
1	1	9	191.3	204.5	13.3	97.9	197.5	207.4	109.5	18.3	15	2530.4	1061.7
1	1	10	213.5	226.6	13.1	96.6	220.7	211	114.4	15.7	22.7	2574.4	1125
1	1	11	235.6	249.6	13.9	100.7	240.8	195.5	94.8	19.9	8.2	2577.9	966.8
1	2	1	5.8	23.6	17.8	96.6	12.6	201	104.4	25	9.1	3317.7	1385.6
1	2	2	29.1	44.5	15.4	100.7	36.3	179.3	78.6	17.9	10.8	2676	964.4
1	2	3	52.3	68.9	16.6	106.8	56.6	194.9	88.2	23.7	4.9	2957.7	1036
1	2	4	75.5	89.6	14.1	104.3	81.3	213.5	109.2	28.8	13.1	2838	1168.5
1	2	5	98.2	112.4	14.2	102.5	104.9	203.6	101.1	16.4	12.9	2716.5	1076.1
1	2	6	121.3	135.8	14.5	102	128.4	187	85.1	19.5	14.6	2624.5	993.1
1	2	7	144	160.4	16.4	101.4	151.1	190.1	88.7	16.4	8.8	2907.8	1082.8
1	2	8	167.5	181.8	14.3	102	174.3	197.1	95.1	17.9	14.2	2687.9	1055.9
1	2	9	191.1	204.5	13.5	98.2	196.9	214.8	116.6	24.1	14.9	2642.7	1169.8
1	2	10	213.3	226.8	13.5	98.4	219.1	204.1	105.7	29.2	13.6	2587.5	1111.1
1	2	11	237	250	13	102.4	242.1	200.7	98.3	27	10.4	2370	936.1
1	3	1	5.6	21.6	16.1	100.7	12.8	195	94.3	21.3	12	3023.7	1211
1	3	2	29.7	44.5	14.8	105.5	33.9	193.8	88.2	23.3	5.6	2744.4	950.4
1	3	3	52.4	68.8	16.4	109.5	56.7	203.8	94.3	23.9	5.3	3033.9	1062.8
1	3	4	75.3	89.1	13.9	107.2	81.7	205.9	98.8	21.1	13.9	2798.2	1083.4
1	3	5	98.3	112	13.7	104.4	105.1	204.2	99.7	15.6	14.5	2587.6	1021
1	3	6	121.3	136	14.7	103	127.9	190.4	87.3	21.1	12.8	2651.2	1002.4
1	3	7	143.9	160.5	16.6	100.8	151	194.1	93.4	16.3	9.2	3057.8	1143.5
1	3	8	168.1	181	12.9	102.9	174	208	105.1	24	15.9	2604.9	1062.1
1	3	9	190.9	204.4	13.5	100.4	196.5	206.5	106	23.3	13	2678	1070.9
1	3	10	213.3	227.1	13.8	99.3	219.2	206.7	107.4	22.7	12.4	2709.5	1121.2
1	3	11	237.1	250	12.9	102.1	242.8	198.7	96.6	24.8	12.8	2408.8	980
1	4	1	5.6	22	16.4	98.9	12.6	201.4	102.5	26.5	11	3060.1	1279.8
1	4	2	29.3	44.2	14.9	109.2	36.6	182.9	73.8	18.7	12.6	2738.3	882.2

A Pearson correlation analysis was conducted on the phenometrics from the 28 different combinations of parameter settings using SAS 9.3 (Equation 4.2). This method has been used successfully to compare green up dates and start of season values (Jones *et al.,* 2012).

$$r = \frac{n(\sum xy)-(\sum x)(\sum y)}{\sqrt{([n\sum x^2-(\sum x^2][n\sum y^2-(\sum y)^2])}}$$ **Equation 4.2**

where:
n = the number of pairs of scores
Σxy = the sum of the products of paired scores
Σx = the sum of x scores
Σy = the sum of y scores
Σx^2 = the sum of squared x scores
Σy^2 = the sum of squared y scores

This test is a measure of precision and describes how far each observation deviates from the best-fit line. A Pearson correlation coefficient will measure a linear relationship, but is unable to detect any deviation from a 45° line. This means that when the data is very scattered (*i.e.,* non-reproducible), the less likely it is that the null hypothesis will be rejected (Figure 4.7).

Figure 4-7 Examples where the Pearson correlation coefficient fails to detect non-reproducibility (from Lin 1989).

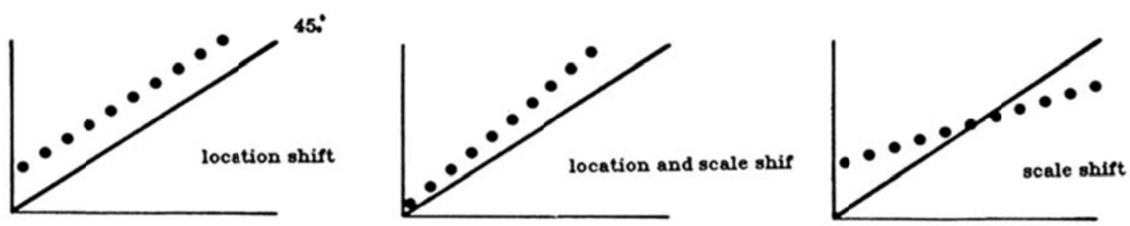

A Lin's Concordance Correlation test was also performed on the phenometrics from the combinations of parameter settings in order to measure the accuracy of the relationship and to determine the agreement between two compared settings files. The degree of concordance between two pairs of samples can be described as the expected value of the squared difference

(Equation 4.3). Unlike Pearson's, it incorporates the sample means (μ) and sample standard deviations (σ) in order to include a bias correction factor (C_b) in the analysis (Lin 1989).

$$E[(Y_1 - Y_2)^2] = (\mu_1 - \mu_2)^2 + (\sigma_1^2 + \sigma_2^2 - 2\sigma_{12}) \qquad \textbf{Equation 4.3}$$

$$= (\mu_1 - \mu_2)^2 + (\sigma_1 - \sigma_2)^2 + 2(1 - \rho)\,\sigma_1\sigma_2$$

The bias correction factor (Equation 4.4) must be greater than 0, but less than 1, and measures how far the best-fit line deviates from the 45°line (measure of accuracy). When $C_b = 1$, there is no deviation from the 45° line, and as C_b decreases, the deviation increases. Therefore, the Lin's concordance correlation coefficient contains both the measurements of accuracy (ρ_c) and precision (ρ) (Lin 1989).

$$\boldsymbol{\rho_c = 1 - \frac{E[(Y_1 - Y_2)^2]}{\sigma_1^2 + \sigma_2^2 + (\mu_1 - \mu_2)^2}} \qquad \textbf{Equation 4.4}$$

$$\rho_c = 1 - \frac{Expected\ Squared\ Perpendicular\ Deviation\ from\ 45^o line}{\begin{array}{c}Expected\ Squared\ Perpendicular\ Deviation\ from\ 45^o line\\ when\ Y_1 and\ Y_2 are\ uncorrelated\end{array}}$$

or,

$$\rho_c = \frac{2\sigma_{12}}{\sigma_1^2 + \sigma_2^2 + (\mu_1 - \mu_2)^2} = \boldsymbol{\rho C_b}$$

where:
$C_b = [(\upsilon + 1/\upsilon + u^2)/2]^{-1}$
$\upsilon = \sigma_1 / \sigma_2$ = scale shift
$u = (\mu_1 - \mu_2)/ (\sqrt{\sigma_1 \sigma_2})$ = location shift relative to the scale

In order to determine whether combinations of parameter settings yield significant similar phenometric results, a threshold value of 0.90 need to be met (or exceeded) for both the

Pearson's and Lin's coefficients. Generally, a Pearson's coefficient value above 0.55 is considered sufficient, with higher values indicating a stronger relationship (McGrew and Monroe 2000). A Lin's concordance coefficient value of >= 0.90 is considered moderate to almost perfect as the value increases (Lin 1989). Phenometrics were classified as 'unaffected' by a modification to an input parameter if the Pearson's and Lin's coefficients met the 0.90 threshold for every season assessed. Phenometrics labeled as 'slightly affected' did not meet the 0.90 threshold for four, or fewer, seasons. Those that were 'significantly affected' failed to meet the 0.90 threshold for eight or more seasons.

In addition to the 0.90 similarity threshold, examination of coefficient results allowed for additional insight regarding the sensitivity of phenometrics to different parameter settings. Of particular interest are coefficients whose difference values are below 0.05, but less than 0.10, and greater than 0.10. Difference values less than 0.05 suggest that paired values are nearly identical, and values between 0.05 and 0.10 are considered at the second level tier of similarity. Those exceeding 0.10 were considered insignificant. These threshold values provide a spectrum indicating how similar test combinations are to one another by determining how close coefficients were to the significance threshold.

Results

With all other parameter settings were held constant, the *SOS/EOS* and *window size* and the *envelope iteration number* coefficients had no effect on the **beginning of season** phenometric (Table 4.4). This means that TIMESAT is insensitive to this parameter.

Table 4.4 Summary of sensitivity analysis results for the beginning of season phenometric.

Phenometric	Input Setting	Input Value	Impact on Phenometric
Beginning of Season	SOS/EOS Threshold	0.1	Unaffected
		0.25	Unaffected
		0.3	Unaffected
	Window Size	3	Unaffected
		5	Unaffected
	Envelope Iteration	1	Unaffected
		3	Unaffected

The *SOS/EOS* and *window size* coefficient had a significant effect on the **end of season** phenometric data. The *envelope iteration number* significantly affected this phenometric only when the input value was 1 and only for 4 of the 11 seasons. These seasons did not reach the 0.90 significance threshold value and are generally characterized as having either growing seasons with less than normal average precipitation, a season that experienced a significant lack of precipitation during at least one month of the growing season, or growing season average temperatures much cooler than the normal average temperatures. Results were unaffected when using an *envelope iteration number* of 3 (Table 4.5). Therefore, the **end of season** phenometric data was highly sensitive to the threshold value for the *SOS* and *EOS* and *window size*, but only slightly sensitive to the *number envelope iterations*.

Table 4.5 Summary of sensitivity analysis results for the end of season phenometric.

Phenometric	Input Setting	Input Value	Impact on Phenometric
End of Season	SOS/EOS Threshold	0.1	Significantly Affected
		0.25	Significantly Affected
		0.3	Significantly Affected
	Window Size	3	Significantly Affected
		5	Significantly Affected
	Envelope Iteration	1	Slightly Affected
		3	Unaffected

The input settings impacted the **length of season** in a manner nearly identical to that of the **end of season** phenometric (Table 4.6). Because the **length of season** is dependent upon both the *SOS* and *EOS*, it makes sense why the length of season is sensitive to the same parameters impacting the EOS. An *envelope iteration number* of 1 was insensitive to an additional season, indicating the only difference in results between these parameters.

Table 4.6 Sensitivity analysis results for the length of season phenometric.

Phenometric	Input Setting	Input Value	Impact on Phenometric
Length of Season	SOS/EOS Threshold	0.1	Significantly Affected
		0.25	Significantly Affected
		0.3	Significantly Affected
	Window Size	3	Significantly Affected
		5	Significantly Affected
	Envelope Iteration	1	Slightly Affected
		3	Unaffected

The *SOS/EOS* threshold results for the **EOS** and **length of season** phenometrics indicated a smaller insignificance when the base setting was compared to the 30% threshold value versus the 10% threshold value. This would suggest eliminating the 10% threshold value as an optimal parameter setting for this study. After comparing 20%, 25%, and 30% against each other, it was determined that the larger the threshold value, the smaller the difference in phenometric results exhibiting the highest similarities.

The non-definitive results for these phenometrics may be due a number of reasons including the introduced noxious vegetation species that are commonly associated with military maneuvers in grassland vegetation communities (Quist *et al.,* 2003; Dickson *et al.,* 2008), vegetation species composition, soil composition, climatic variables, military training, or a cumulative effect of these variables.

The *SOS/EOS* and *window size* coefficients had no effect on the **maximum of season** phenometric data. The *envelope iteration number* only significantly affected this phenometric in 3 of the 11 seasons when the input value was 1, and in 4 of 11 seasons when the input value was 3 (Table 4.7). The results suggest a consistent maximum NDVI value, regardless of the threshold value for *SOS/EOS* and *window size*, but some seasons may be more sensitive to the *number of envelope iterations*.

Table 4.7 Sensitivity analysis results for the maximum of season phenometric.

Phenometric	Input Setting	Input Value	Impact on Phenometric
Maximum of Season	SOS/EOS Threshold	0.1	Unaffected
		0.25	Unaffected
		0.3	Unaffected
	Window Size	3	Unaffected
		5	Unaffected
	Envelope Iteration	1	Slightly Affected
		3	Slightly Affected

The *SOS/EOS* and *window size* and the *envelope iteration number* coefficients had no effect on the **small integral of season** phenometric data (Table 4.8). This model suggests that the small integral of season remains unaffected, regardless of the input settings for these parameters.

Table 4.8 Sensitivity analysis results for the small integral of season phenometric.

Phenometric	Input Setting	Input Value	Impact on Phenometric
Small Integral of Season	SOS/EOS Threshold	0.1	Unaffected
		0.25	Unaffected
		0.3	Unaffected
	Window Size	3	Unaffected
		5	Unaffected
	Envelope Iteration	1	Unaffected
		3	Unaffected

Conclusions and Discussion

This study defined an optimal Savitzky-Golay filter parameter settings file for Fort Riley, Kansas and other sites within the Flint Hills ecoregion. It is the first known attempt to understand the impact of changing parameter values of the TIMESAT curve fitting process on generated seasonality (phenometric) data. One benefit of this analysis is increased confidence in the phenometrics estimated from the MODIS MOD13Q1 time series data for the Fort Riley study area by better understanding the influence of curve-fitting parameters on the result.

The *SOS/EOS* parameter only impacted the phenometrics **EOS** and the **length of season**. When the threshold values were compared against one another, the phenometric results for **EOS** and the **length of season** were most similar when using a *SOS/EOS* threshold of 25% or 30%. By comparing the extracted phenometrics from the EOS using different SOS/EOS input values, the phenometric differences by season were smallest when comparing the 25% versus 30%. The length of season parameter had an identical relationship. Generally, higher *SOS/EOS* threshold values yield smaller differences in the **EOS** and **length of season** phenometrics. However, using 30% may be an unrealistic threshold value for the SOS and EOS for this data, because Fort Riley generally experiences a tall and narrow phenology curve, partially due to abrupt spring green up. As depicted in the input data and applied filter (Figure 4.8), it is obvious that the differences between phenometric outputs will decrease as the threshold value is set nearer the maximum seasonal value. For this reason, the 25% threshold would be considered an appropriate value for this input.

Figure 4-8: Raw time series NDVI data for Fort Riley prior to application of the Savitzky-Golay filter.

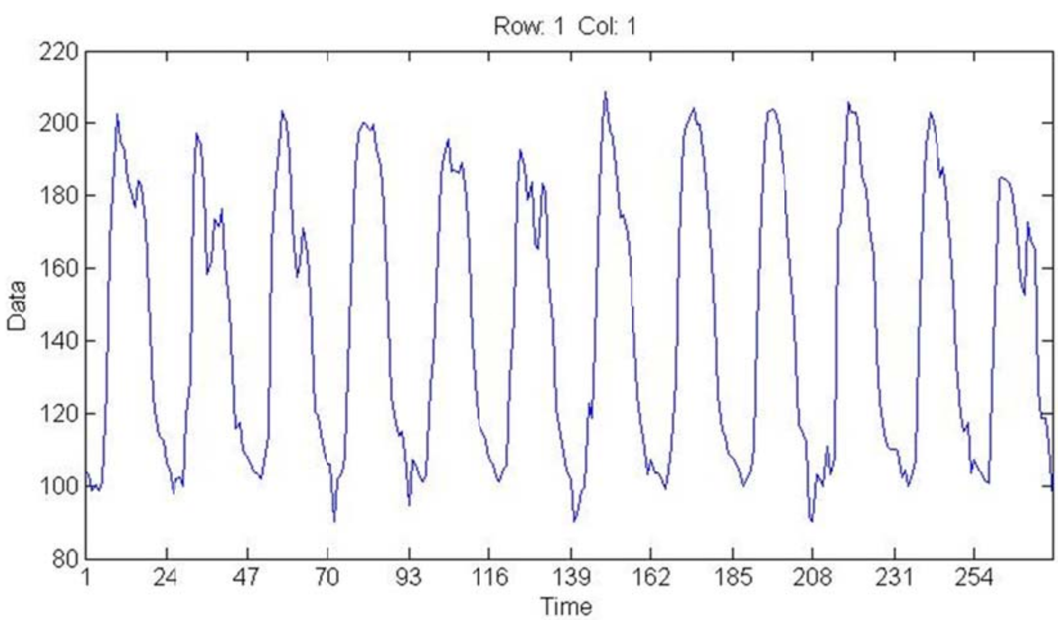

The *window size* parameter impacted only the **EOS** and **length of season** phenometrics. Therefore, a three-way comparison of the window sizes was conducted and evaluated for these particular phenometrics. By comparing the extracted phenometrics from the EOS using different window size input values, the phenometric differences by season were smallest when comparing 4 against 3 or 5. This is because the difference between 3 and 5 was significantly greater than the comparisons between 4 and 5, and the comparisons between 4 and 3. The length of season parameter had an identical relationship, and therefore, a window size of 4 was determined as the best input for this data.

For a majority of the phenometrics examined, the comparison between 2 and 3 envelope iterations was most analogous. The largest difference in phenometric results from this input value was the **maximum of season**. A three-way comparison of the envelope iteration numbers determined that 2 envelope iterations would be the best input for this data.

In summary, the optimal parameter input settings for the Fort Riley study area includes a *SOS/*EOS threshold value of 0.25, a window size of 4, and an envelope iteration number of 2. Figure 4.9 shows the TIMESAT-generated fitted curve for NDVI resulting from these parameters settings for the time period 2001-2012.

Though NDVI has been proven to be very useful, there are a few key issues that limit the effectiveness of using NDVI for biophysical calculations and vegetation monitoring. NDVI is ratio-based and responds in a non-linear manner to changing vegetation conditions, which often causes lower ratio values to be enhanced and higher ratio values tend to be condensed. This may cause results to be insensitive as values saturate over high biomass conditions. Though it may prove useful in sparse vegetation plots, NDVI is a poor discriminator of stress when that stress occurs at high values of green cover (Jackson *et al.,* 1983). Lastly, NDVI is more sensitive to early rain seasons and to canopy background noise such as soil or plant litter, which also introduces non-vegetation-related variations in the NDVI data (Huete 1988).

Figure 4-9 Fitted curve for the Fort Riley NDVI time series after the Savitzky-Golay filter with "optimal" parameter settings were applied.

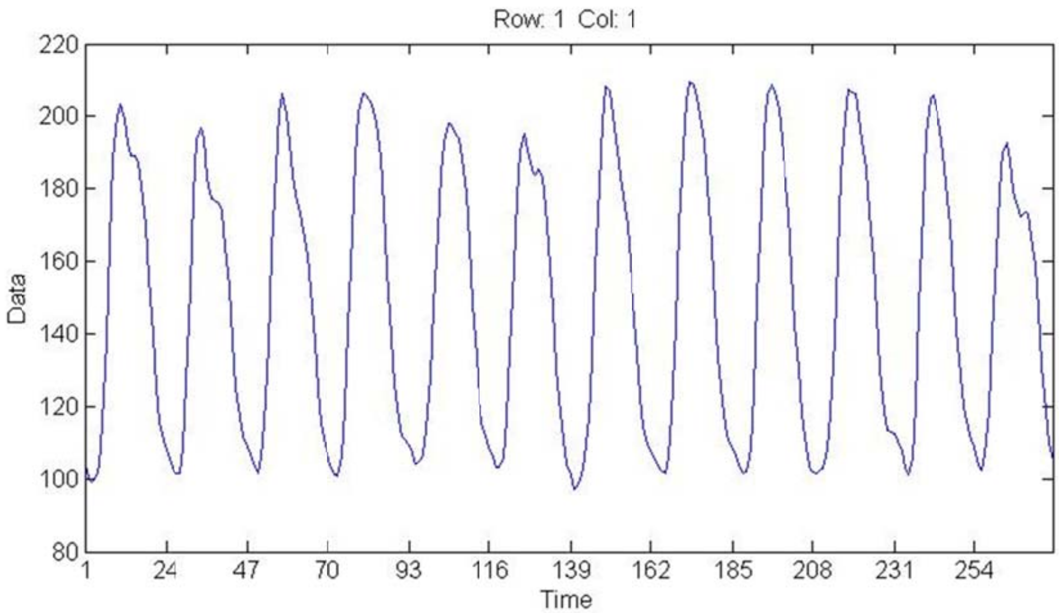

Any analysis including remote sensing must acknowledge the possibility of errors. As with most spectral reflectance combinations, atmospheric path radiance will reduce the normalized difference value. A number of other variables may impact resulting NDVI values, including satellite drift and volcanic eruption, calibration uncertainties, inter-satellite sensor differences, bidirectional and atmospheric effects (Zhou *et al.,* 2001).

Satellite imagery with daily temporal resolution is rarely used in time series analysis since short wavelength electromagnetic radiation cannot penetrate cloud cover. Though a time series with increased temporal resolution could enhance our ability to detect seasonal variations within vegetation, it may also negatively impact our ability to identify subtle variations and key differences in important vegetation phenometrics (*i.e.,* the beginning of season) due to higher noise levels associated with atmospheric interference (Zhang *et al.,* 2009). Therefore, a composited vegetation index product, such as the MODIS MOD13Q1 product, can use a constrained-view angle to limit residual cloud and atmospheric effects (Verbesselt *et al.,* 2009).

Imagery with greater spatial resolutions could potentially provide a more accurate spatial view of vegetation conditions across a study area as NDVI values would be averaged over smaller ground areas. This greater spatial resolution would, however, have a computational cost and increase the amount of time needed for analysis. Also, there are no satellite platforms able to capture "high spatial resolution" imagery at a temporal frequency comparable with that of the MODIS system.

TIMESAT requires the same number of images per year throughout the time series to perform an analysis. This certainly places limits on the selection of sensors if some captured images are cloudy or of poor quality, but there are ways users could work around this limitation. For example, a missing or corrupt image could be excluded from every year in the analysis. However, phenology results might be suspect given the introduction of a data "gap" in the time series. Alternatively, missing or corrupt images could be replaced in the time series with that which appears before/after it in the series. This option is likely to have less of an impact on estimation of phenometrics than excluding an entire date each year across the assessed seasons.

One direction for future phenology analysis at Fort Riley using TIMESAT would be to incorporate a landuse/landcover classification. This would allow for separate analyses on the impact of TIMESAT input parameter settings on the resulting phenometrics based on landuse/landcover type, and estimation of separate sets of phenometrics. For example, grassland areas would be expected to have a phenology curve different than that of woody vegetation. Additional work is also needed to determine if the sensitivity analysis results reported here are independent of location. Since phenology is dependent upon climate, soil properties, and species composition, it is possible that TIMESAT phenometrics for non-grassland sites would be better estimated using different input parameter settings.

Chapter 5 - Time Series Analysis of Vegetation Phenometrics for Military and Non-Military Lands using Moderate Resolution Satellite Imagery

Abstract

A time-series analysis of MODIS maximum value composite normalized difference vegetation index (NDVI) data for Fort Riley, Kansas and the nearby Konza Prairie Biological Station (KPBS) was conducted to determine if significant differences exist in selected vegetation phenometrics between the two sites. Additional comparisons were made using areas at Fort Riley that experience high and low training intensities. Phenometrics of interest were estimated from the time series satellite data using the program TIMESAT, which extracts seasonality parameters from remotely-sensed time series data by fitting a smooth function to the series. For this study, a Savitzky-Golay filter, with parameter settings found optimal for Fort Riley, was applied. The phenometrics *start of season*, *end of season*, *length of season*, *maximum value*, and *small seasonal integral* were compared using Kolmogorov-Smirnov (K-S) test for each of the four study sites and three seasons based on annual temperature and precipitation characteristics. Significant differences existed for all phenometrics in the comparison of Fort Riley training areas and KPBS, as well as low- versus high-training intensity areas within Fort Riley. Results show earlier dates for the start and end of the growing season, shorter growing season lengths, lower maximum NDVI values, and lower small seasonal integrals for both Fort Riley (in the Fort Riley-KPBS comparison) and high-intensity training areas (in the high- versus low-intensity training area comparison). No significant seasonal differences were detected between study sites for 97% of all comparisons, suggesting that phenometric differences were caused by varying land uses and/or land management practices rather than weather conditions. A detailed report of

the phenometric differences between the study areas is presented, and a normal phenology curve was determined for all study areas.

Introduction

Phenology has emerged as an important focus in ecological research for its use in vegetation monitoring/modeling and addressing issues related to climate change. Phenology is the timing of seasonal vegetation activities (Parmesan 2006) and the study of how vegetation growth may be affected by interannual and seasonal variations in meteorological conditions, soil characteristics, and photoperiod (Schwartz 1998; Cleland *et al.,* 2007). It can be used to predict the fitness and probability of species occurrence under certain conditions (Cleland *et al.,* 2007), making it one of the most efficient ways of following species response to changing ecosystem conditions (Walther *et al.,* 2002). Through the use of remote sensing, the study of phenology provides additional insights into the natural and anthropogenic processes impacting vegetation life cycles.

Usually measured in Julian dates, or days since December 31, phenology can be described using satellite imagery and phenometric data extracted from vegetation index data such as that acquired by the MODIS sensor (Ahas *et al*., 2002; An 2009). With sufficient spatial and temporal resolutions, the spectral-temporal information obtained from time-series NDVI data can be used to characterize and quantify changes in vegetation phenology across time and space (Reed *et al.,* 1994; Wardlow 2005) and to explore the potential role of different natural and anthropogenic activities in causing those changes (Jacquin *et al.,* 2009).

This study investigates differences in phenology between Fort Riley, Kansas, a U.S. Army military installation, and Konza Prairie Biological Station (KPBS), a natural tallgrass prairie preserve. Phenometrics for both study sites were estimated after using TIMESAT and a

Savitzky-Golay filter to smooth a time series of MODIS 16-day maximum value NDVI composite images for the period 2001-2012. Of interest here was whether the dominant landuse of each site (*e.g.,* military training versus natural grassland) would result in measurable differences in phenometrics when using NDVI information derived from course-resolution satellite images.

Select phenometrics for KPBS and three different spatial configurations of Fort Riley, including (1) all military training areas (excluding developed areas), (2) high-intensity military training areas only, and (3) low-intensity military training areas only were extracted and then compared using the non-parametric Kolmogorov-Smirnov test to determine if significant differences existed. In addition, a "normal" vegetation phenology curve was developed for KPBS and the three Fort Riley study sites.

Past Work

NDVI is calculated from a normalized transformation of the red and near-infrared (NIR) reflectance ratio (Tucker 1979). These bands of the electromagnetic spectrum are highly sensitive to vegetation compositions, making NDVI one of the most common measures of vegetation greenness and overall health (Cihlar *et al.,* 1991; Tucker *et al.,*1991; Wardlow 2005; An 2009). A typical NDVI profile, or phenology curve, illustrates the onset of greenness or when the vegetation begins to green-up, the maximum NDVI value illustrating the highest relative photosynthetic biomass, the rate of senescence or decay, the end of greenness date, and the growing and brown days (days of senescence) of a year accumulating to the season length of the year (Figure 5.1). The area beneath this phenology curve represents the accumulated NDVI and is an indication of relative photosynthetic biomass.

Figure 5-1 A typical vegetation phenology curve, and associated phenometrics, derived from time series NDVI values (from Jacquin *et al.,* 2009).

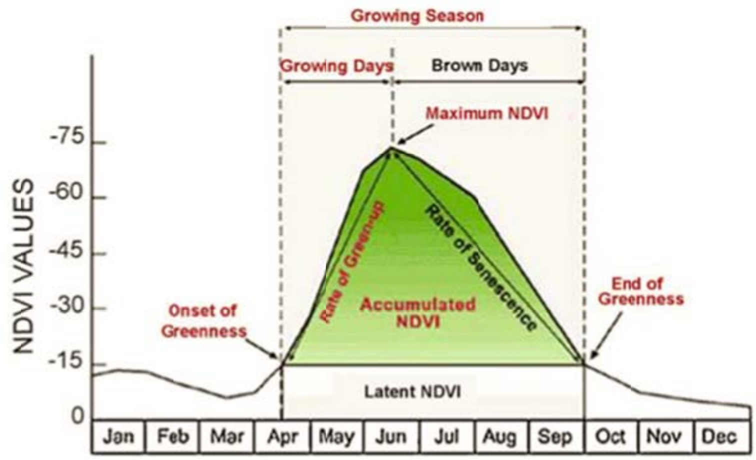

Spectral-temporal information extracted from time-series vegetation index data has been used successfully to characterize vegetation phenology and assist with forecasting/monitoring vegetation density and health (Reed *et al.,* 1994; Wardlow 2005; Jacquin *et al.,* 2009). Time series of satellite-derived NDVI datasets have been used to assess vegetation activity and measure vegetation dynamics (Zhang *et al.,* 2003; Ahl *et al.,* 2006), including spatiotemporal changes in vegetation condition and biomass (Huete *et al.,* 2002). Specifically, 16-day MODIS maximum value NDVI composite images with a 250 meter spatial resolution (MOD13Q1) have been shown successful in measuring important phenometrics and detecting possible human-induced land cover changes (Wardlow 2005; Jacquin *et al.,* 2009; Verbesselt *et al.,* 2009). Variations in phenometric values associated with different land cover regions, land use practices, climatic conditions, as well as planting dates for crops, may be determined (Wardlow 2005).

Raw data from remote sensors must first be processed through a series of filtering, compositing, smoothing and/or screening procedures in order to isolate the desired phenometric signal from noise. There are many different types of time series analysis techniques used to filter raw NDVI data and then extract phenometrics, including the seasonal Kendall (SK) trend test (Hirsch and Slack 1984; de Beurs and Henebry 2004, de Beurs and Henebry 2005; de Beurs *et al.,* 2009;), principal component analysis (PCA) (Crist and Cicone 1984), pixel-above-threshold technique (PAT) (Cleland *et al.,* 2007), wavelet decomposition (Anyamba and Eastman 1996), change vector analysis (CVA) (Lambin and Strahler 1994), and Fourier analysis (Azzali and Menenti 2000). In addition, the TIMESAT software program provides several filtering options to smooth raw vegetation index data and extract key phenometric data (Eklundh and Jönsson 2010).

In previous studies, TIMESAT has been used to study vegetation phenology (Eklundh and Jönsson 2003), map phenological and environmental changes (Eklundh and Olsson 2003; Hickler *et al.,* 2005; Olsson *et al.,* 2005; Seaquist *et al.,* 2006; Heumann *et al.,* 2007; Seaquist *et al.,* 2009), examine high-latitude forest phenology (Beck *et al.,* 2007), assess satellite and climate data-derived indices of fire risk (Verbesselt *et al.,* 2006), monitor human impacts of fire seasons (Le Page *et al.,* 2009), and evaluate relationships between coniferous forest NDVI and models of conifer photosynthetic activity (Eklundh and Jönsson 2010).

As pointed out in the TIMESAT manual, optimal curve fitting during smoothing is "more of an art than a science" and some trial and error may be necessary to arrive at a final set of parameter settings (Eklundh and Jönsson 2010). Previous work using TIMESAT at Fort Riley identified optimal values for a number of parameters required when applying a Savitzky-Golay filter to smooth MODIS NDVI (Chapter 4).

Study Area

Fort Riley is a United States Army base located in northeastern Kansas (39.18°N, 96.80°W), on the Kansas River, between Junction City and Manhattan and within Geary, Riley, and Clay counties (Figure 5.2). The total installation area is 41,141 ha and is located within the

Flint Hills ecoregion (Omernik 1987, Bailey *et al.,* 1994). It is part of the Flint Hills ecoregion, the largest untilled tallgrass prairie in North America that spans 1.6 million ha (Omernik 1987; Dickson *et al.,* 2008).

Figure 5-2 Fort Riley study area, located in parts of Clay, Geary, and Riley counties in northeastern Kansas.

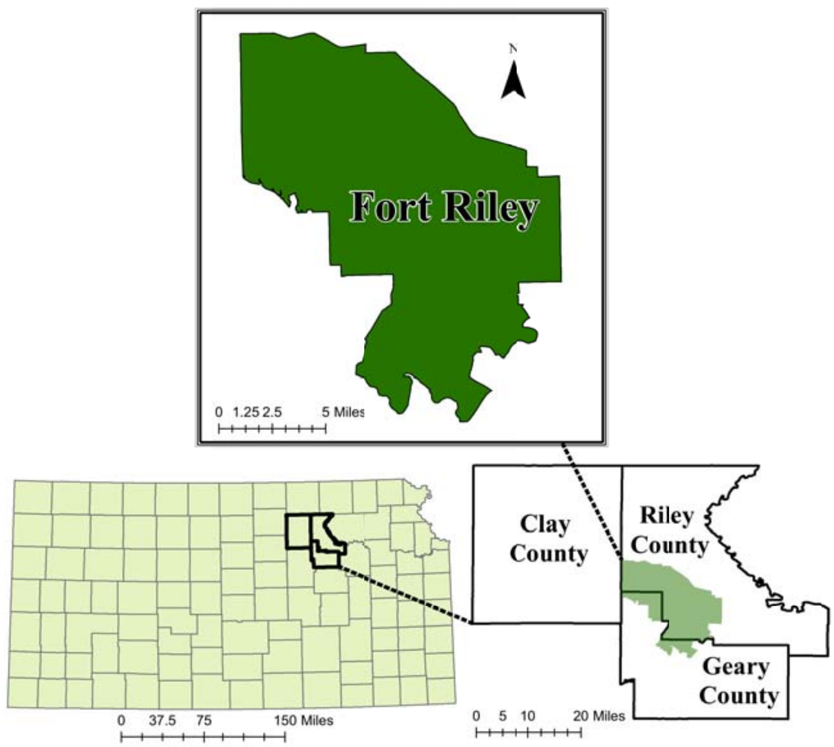

Fort Riley's climate is generally considered temperate continental. Weather is highly variable but can be characterized as having hot summers, cold, dry winters, moderate winds, low humidity, and a pronounced peak in rainfall late in the spring and in the first half of summer. Average monthly temperatures range from approximately -3°C in January to 26°C in July (PRISM Climate Group 2012). Mean annual precipitation is approximately 843 mm, but extremely variable from year to year, with 75% of precipitation occurring during the growing season. The source of much precipitation is thunderstorms, which typically have intense rainfall rates of approximately 60 mm/hr and occur approximately 55 days each year in this area (U.S. Department of Agriculture Soil Conservation Service 1975; Knapp 1998).

The vegetation of Fort Riley is a mix of native prairie and introduced vegetation consisting of C4 grasses (46%), forbs (32%), legumes (11%), and C3 grasses (11%) (Dickson *et al.,* 2008). The installation is comprised of three major vegetation communities, including grasslands (32,200 ha), shrublands (1,600 ha), and woodlands (6,000 ha) (Althoff *et al.,* 2006). The eastern portion of Fort Riley shares many of the characteristics to the Flint Hills, with vegetation dominated by warm-season highly productive C4 grasses and a mixture of annual and perennial forbs. The western portion of Fort Riley represents a plant community undergoing succession back to native prairie from past cultivation in the 1960s (Quist *et al.,* 2003).

Fort Riley grasslands are dominated by big bluestem (*Andropogon gerardii*), Indiangrass (*Sorghastrum nutans*), switchgrass (*Panicum virgatum*), and little bluestem (*Schizachyrium scoparium*). Other grasses and forbs are also present at lower abundances. Shrublands consist primarily of buckbrush (*Symphoricarpos orbiculatas*), smooth sumac (*Rhus glabra*), and rough-leaved dogwood (*Cornus drummondii).* Additionally, there is a mixture of grasses and forbs that occur along the edges of woodlands and in solitary patches of grassland areas. Typically located along riparian lowlands, woodlands are dominated by chinquapin oak (*Quercus muhlenbergii*), bur oak (*Quercus macrocarpa*), American elm (*Ulmus americana*), hackberry (*Celtis occidentalis*), and black walnut (*Juglans nigra).*

The installation serves as a combat training ground for mortar and artillery fire, small arms fire, aircraft flights, field maneuvers, tanks, and mechanized infantry units (Quist *et al.,* 2003; Althoff *et al.,* 2006). Since the 1980’s, military units have engaged in continuous maneuver-based training across the entire installation (U.S. Army 1994), though such activities are concentrated in the northern 75% portion of the installation (Quist *et al.,* 2003; Althoff *et al.,* 2006).

High intensity military training associated with mechanized military maneuvers has been cited as the cause of increased bare soil, reduced plant cover, compacted soil conditions, and compositional shifts in plant communities (Shaw and Diersing 1990; Trumbell *et al*., 1994; Whitecotton *et al*., 2000; Quist *et al.,* 2003; Guretzky *et al.,* 2006). Military training alters vegetation composition by decreasing the basal cover of perennial warm-season grasses and increasing the cover of perennial cool season grasses and annual warm-season forbs (Wilson 1988; Shaw and Diersing 1990; Milchunas *et al.,* 1999; Dickson *et al.,* 2008). Mechanized military maneuvers increase the populations of non-native species, weeds, forbs, and annuals (Milchunas *et al.,* 2000), while reducing the cover provided by native perennial grasses and forbs (Quist *et al.,* 2003; Guretzky *et al.,* 2006; Dickson *et al.,* 2008).

Konza Prairie Biological Station (KPBS) is located on 3,487-hectares of protected area south of Manhattan, KS (39.09°N, 96.57°W), in northeastern Kansas (Figure 5.3). The KPBS is owned by the Nature Conservancy (http://www.nature.org) and operated by the Division of Biology at Kansas State University (http://kpbs.konza.ksu.edu).

One of the National Science Foundation's Long-term Ecological Research Sites, KPBS has similar vegetation, soils, prescribed burning practices, and climate due to its close proximity (less than 10 kilometers) to Fort Riley. KPBS is dominated by native tallgrass prairie of the Flint Hills ecoregion, part of the same largest continuous tallgrass prairie in North America. Because of the steep slopes and underlying limestone soils, KPBS proves unsuitable for cultivation and has remained unplowed, retaining its native characteristics.

Figure 5-3 Konza Prairie Biological Station study area in Kansas depicting watersheds and excluding built up areas.

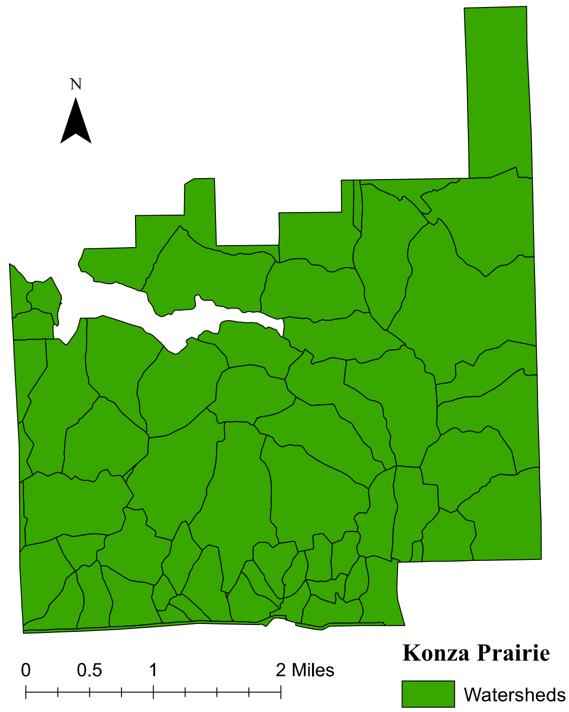

KPBS shares a similar grassland species composition mix with Fort Riley, being dominated by native warm-season C4 grasses such as big bluestem (*Andropogon gerardii*), little bluestem (*Schizachyrium scoparium*), indiangrass (*Sorghastrum nutans*), and switchgrass (*Panicum virgatum*). In addition to grasses, forbs are commonly found throughout the site. Common species on mesic sites include white aster (*Aster ericoides*), daisy fleabane (*Erigeron strigosus*), and wild alfalfa (*Psoralea tenuiflora*). Species on more xeric areas include western ragweed (*Ambrosia psilostachya*), white sage (*Artemisia ludoviciana*), and aromatic aster (*Aster oblongifolius*) (Freeman and Hulbert 1985; Freeman 1998).

Data and Methods

Data Acquisition

The image data used in this analysis was MODIS MOD13Q1 project, a 16-day maximum value NDVI composite with a 250-meter spatial resolution. A gridded level-3 product delivered in a sinusoidal projection, MODIS radiance counts are calibrated and geolocated based on grid and angular data, masked from cloud, land/water, perceptible water and aerosol products, incorporate spectral reflectance, and undergo quality assurance flags associated with atmospheric correction products (Huete *et al.,* 1999).

Imagery data was downloaded from the Earth Observing System Data and Information System (EOSDIS 2009) and saved as an 8-bit unsigned integer with a 213.705 meter spatial resolution for the latitude of these study area. Each image was reprojected into the North American Datum of 1927, Universal Transverse Mercator Zone 14 North projection clipped to the extent of the study area, and resaved as a single band IMAGINE file. This format meets the TIMESAT requirement of a headerless binary format. Saved images were placed in the same file directory for later processing in TIMESAT (Figure 5.4).

Collected images spanned the period from January 2001 through December 2012 (n = 12 years). Because TIMESAT only analyzes for the n – 1 centermost seasons, the results presented here will be based on 11 years and exclude 2012 (Eklundh and Jönsson 2010). Each calendar year includes 23 total MOD13Q1 images with this study incorporating 276 total images (23 x 12).

Figure 5-4 MODIS MOD13Q1 NDVI images of Fort Riley, Kansas from May 9, 2005 (image 106, left) and September 30, 2010 (image 224, right) as viewed in TIMESAT. Red and light blue represent areas with high and low NDVI values, respectively. Note that areas outside of the Fort Riley boundary were assigned values of 0

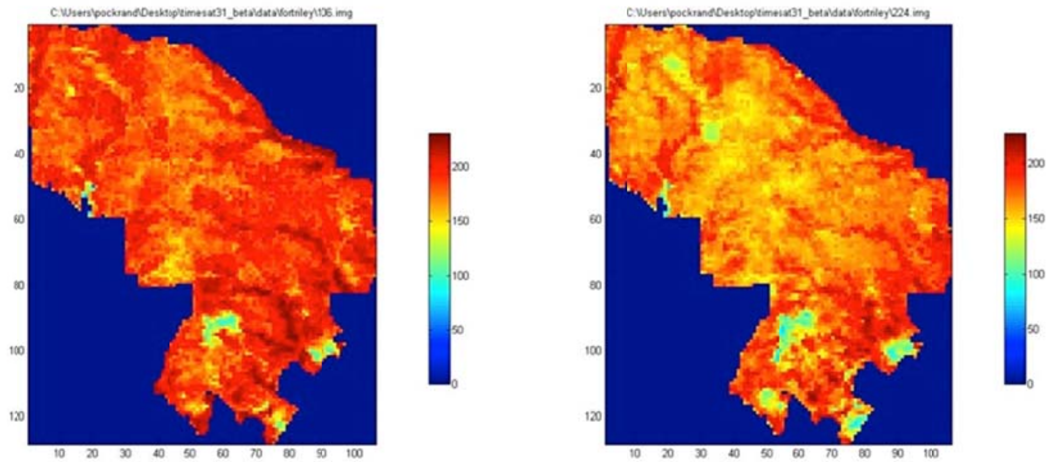

Data Processing in TIMESAT

After data acquisition and preprocessing was complete, unique text files were prepared for Fort Riley and KPBS to serve as input for TIMESAT processing (see Appendix A for the complete text file used for Fort Riley). The first row of the input text file included the number of images to be used in the analysis (*i.e.,* 276) followed in the second row by the full path and filename of the first MOD13Q1 image. Each subsequent row lists the next image, including the full path and filename.

After reading the input file and initial lines for each of the images, TIMESAT reads each image file comprising the time series image (and any optional quality indicators incorporated), preprocesses the images using optional quality indicators, smooth's the time series data using a number of possible filter types and user-defined parameter settings, and extracts seasonality parameters (*i.e.,* phenometrics) to a file based on the selected smoothing function.

The TIMESAT graphical user interface (GUI) presents the controls for selecting the smoothing function and parameter settings, and provides a graphical view of the raw and smoothed curves for one pixel, along with the resulting phenometrics (Figure 5.5). The critical steps of selecting a smoothing function and related parameter settings are organized in three subsections within the TIMESAT interface and include data plotting, common settings, and class-specific settings. A brief discussion of each subsection follows and is summarized in Table 5.1.

Figure 5-5 The TIMESAT graphical user interface showing the raw (blue) and fitted (brown) phenology curves for one MODIS image cell during the study period. The blue line represents the raw NDVI data of one MODIS imagery cell. Brown points on the fitted curve represent the SOS (left) and EOS (right) phenometrics for each season.

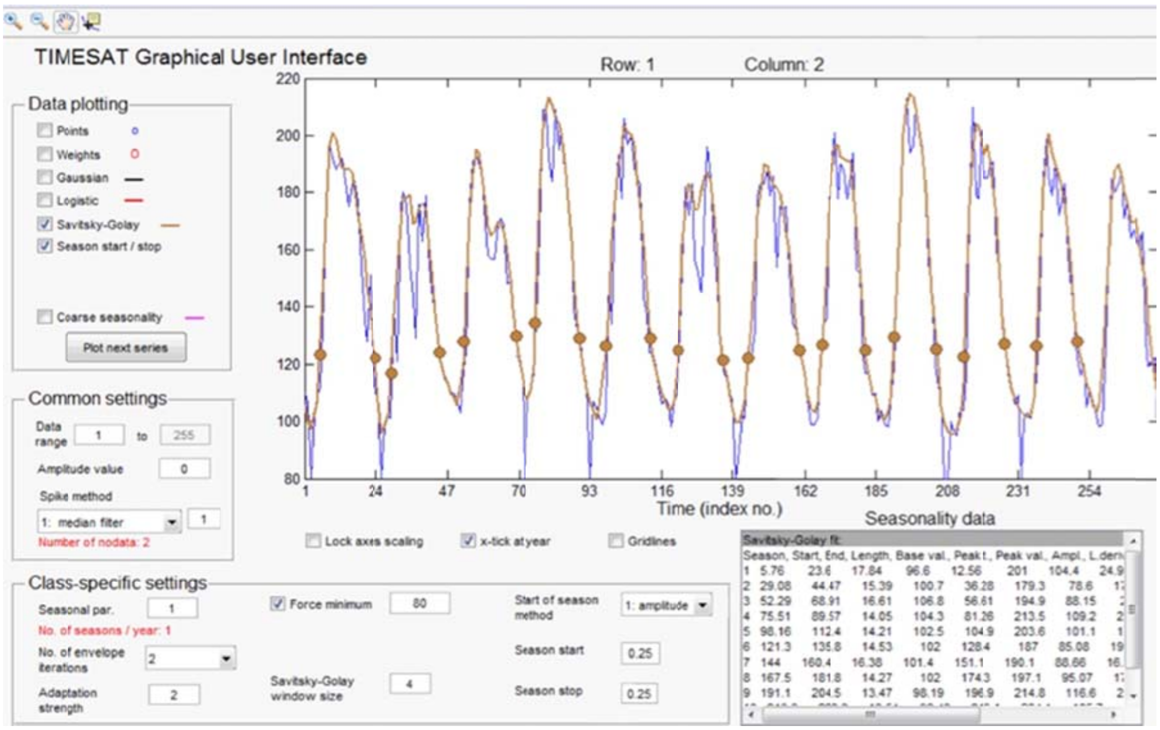

Table 5.1: TIMESAT parameter settings and input values selected for this analysis.

Parameters	Suggested	Source	Used
Data Plotting			
Filters	Gaussian, logistic, Savitsky-Golay	Savitzky and Golay 1964; Jönsson and Eklundh 2002; Hird and McDermid 2009; Jönsson et al., 2010	Savitzky-Golay
Common Settings			
Spike Method	STL original; STL replace spike; median spike	Verbesselt *et al.,* 2009; Eklundh and Jönsson 2010	Median spike
Spike Value	2	Eklundh and Jönsson 2010	2
Class-Specific Settings			
Seasonal Parameter	1	Eklundh and Jönsson 2010	1
Start of Season Method	Amplitude, absolute value	Eklundh and Jönsson 2010	Amplitude
Adaptation Strength	2-3	Eklundh and Jönsson 2010	2
Force Minimum	N/A	N/A	80
Savitzky-Golay Window Size	5	Chapter 4	4
Number of Envelope Iterations	1, 2, 3	Chapter 4	2
SOS/EOS Threshold	10-25%	Chapter 4	25%

Data Plotting

Three different filters, or smoothing functions, are available for selection in TIMESAT, including Gaussian, logistic, and Savitzky-Golay. The Savitzky-Golay filter used in this analysis is a simplified least-squares-fit convolution for extracting derivatives and smoothing a spectrum of consecutive values. It is essentially a weighted moving average filter based on a polynomial where the polynomial order dictates the convolution. When the weight coefficients are applied to a signal, a polynomial least squares fit will be applied to the filter window. Such a procedure is intended to maintain peak times within the data and reduce introduced bias noise from the data (Chen *et al.,* 2004; Eklundh and Jönsson 2010). It is intended to preserve the area and mean position of a seasonal peak, but alter both the width and height. This method is sensitive to local variations in vegetation index values, proving useful when comparing against different regions (Jönsson *et al.,* 2010). The end result is a smoothed curve adapted to the upper envelope (peak values) of the values in a time-series. More information on the mathematics behind this procedure and its coefficients may be found in Steinier *et al.,* (1972), Press *et al.,* (1996), and Savitzky and Golay (1964).

As Figure 5.5 illustrates, Fort Riley experiences growing season transitions during green-up and senescence phases. An optimal smoothing filter for this situation would utilize a narrow moving window approach. The Savitzky-Golay filter has the option of modifying the width of the moving window that is used to filter the raw data. A large window will have a higher degree of filtering, flatten sharp peaks and neglect the ability to detect rapid changes in the data. A smaller window will detect these rapid changes occurring on Fort Riley and preserve sharp peaks in the data.

Common Settings

Common settings in TIMESAT affect all pixels in the image time series. Similar to the data plotting options, TIMESAT make available three different methods in common settings: STL original, STL replace spike method, and median spike method. The median spike method was used in this analysis because, unlike the two STL options, it retains all raw data values. However, any values in the time series that are significantly different from their left- and right neighbors – and from the median in a window – are classified as outliers and are assigned zero weight (Eklundh and Jönsson 2010).

The spike value is used to help determine significant differences in adjacent values in the time series. Data values that differ from the median by more than the product of the spike value and standard deviation of the time series, and that are different from the left- and right neighbors, are removed. The TIMESAT manual suggests that a normal setting for the spike value is 2 and warns that a lower value will remove more data values from the analysis (Eklundh and Jönsson 2010). Based on this recommendation, a spike value of 2 was used in this analysis.

Class-Specific Settings

A total of eight different class-specific settings may be used in TIMESAT and applied to individual land classes (*i.e.,* different landuse/landcover categories). The *seasonal* parameter defines the number of growing seasons per year. A parameter value of 1, like that applied to the Fort Riley data, indicates a single season per year. For areas that experience dual seasons, a parameter value of 0 should be used.

A second parameter, *start of season* method, offers two choices: Amplitude and absolute value. This parameter works with the season start and season stop values. When choosing amplitude as the method, the season start and stop values are entered as percentages of the growing season maximum value. For example, a season start value of 0.20 will identify the time when 20% of the maximum growing season amplitude is reached. Conversely, setting an absolute value for start of season method finds the time each season when that specific digital number value is reached.

Further fine-tuning of the impact of the *number of envelope iterations* (explained in the following section) can be made through adjustments to the third setting adaptation strength. Ranging from a minimum of 1 to a maximum of 10, normal adaptation values are typically 2 or 3 (Eklundh and Jönsson 2010). After reviewing the Fort Riley time series data in the TIMESAT GUI, and visually comparing differences in curve fits using typical adaptation strength values, a final setting of 2 was selected as the curve fit tended to honor the raw data values best.

The *force minimum* option (setting number 4), if active, essentially removes extremely low values in the time series (e.g., outliers) and replaces them with the new value entered. Using this option is helpful in eliminating unusually low NDVI values such as those recorded during the winter when snow covers the land surface. Forcing these low values into something approaching the mean winter minima helps preserve the true seasonal curves generated by the fitted function. These study areas experience extended winter periods with snow on the ground, so this study implements a force minimum value of 80.

The remainder of the settings included in this analysis is the Savitzky-Golay *window size*, *number of envelope iterations*, *start of season* (SOS) and *end of season* (EOS). The *window size* represents the width, or half-window, of the moving window used by the Savitzky-Golay filter during smoothing. The width of the moving window helps to determine the amount of smoothing that takes place and impacts the ability to capture rapid changes in the NDVI time series. Implementing a large window size may neglect important variations and flatten out sharp peaks in the data (Chen *et al.,* 2004). It has been determined that a *window size* of 4 is the optimal setting for providing the best-fitting effect (Chen *et al*., 2004; Chapter 4).

The Savitzky-Golay filter is generally sensitive to the *number of envelope iterations* because it is sensitive to the upper envelope of the smoothing function. The fit of the smoothing function previously selected can be made to approach the upper envelope of a time series using an iterative and multi-step procedure that can be repeated twice. Specifying a value of 1 results in only one “fit” to the data and no adaptation. With values of 2 or 3, one or two additional fits are applied to force the fitted function towards the upper envelope (Eklundh and Jönsson 2010). Selecting too large of a value may introduce error into the estimated beginning of season and end of season dates by over-fitting the curve. Values which are too small may cause errors by including in the fitted curve data related to atmospheric or calibration noise. For Fort Riley, a value of 2 for the *number of envelope iterations* was found to perform satisfactorily (Chapter 4).

The final two class-specific settings are *SOS* and *EOS*, represented in the TIMESAT GUI as season start and season end, respectively. Assuming *amplitude* as the start of season method, values for *SOS* and *EOS* will range between 0 and 1. These values represent a proportion of the seasonal amplitude reached each season. Though two separate settings, *SOS* and *EOS* are typically assigned the same values and will be treated as one setting in this study. Selecting low values for this setting may place *SOS/EOS* too early/late in the season in portions of the fitted curve dominated by atmospheric and calibration noise. High values may mistakenly label as the *SOS/EOS* date periods well inside the actual growing season instead of its true beginning/end. For the Fort Riley study area, a SOS/EOS value of 0.25 was found to be optimal (Chapter 4).

Phenometric Extraction

The TIMESAT seasonality files contain 11 different phenometrics estimated for each pixel in every NDVI image in the 11 season time series (Table 5.2). The study area including all of Fort Riley training areas had 5,188 pixels, Fort Riley High intensity training areas had 1,213, Fort Riley Low intensity training areas had 1,558, and KPBS had 621 pixels. Five of these 11 phenometrics were selected for comparison, including *start of season*, *length of season*, *end of season*, *maximum value*, and *small season integral*. A graphic depiction of these 5 phenometrics is shown in Figure 5.6.

Table 5.2 List, definition, and biological significance of the phenometrics extracted by TIMESAT (Eklundh and Jönsson 2010). Rows highlighted in gray indicate the phenometrics used in later analyses.

Phenometric	Definition	Biological Significance
Start of Season	Time at which the left edge has increased to a user-defined level measured from the left minimum value.	Time of initial vegetation green up
End of Season	Time at which the right edge has decreased to a user-defined level measured from the right minimum value	Time of initial vegetation senescence
Season Length	Time from start to end of season	Length of growing season from green up to senescence
Base Level	Average of the left and right minimum values	Baseline for the seasonal phenology curve
Middle of Season	Mean value of the times at which the left edge has increased to the 80% level and the right edge has decreased to the 80% level.	Time of the middle of the growing season.
Maximum Value	Largest data value for the fitted function during the season.	The highest NDVI value of the season.
Seasonal Amplitude	Difference between the maximum value and base level.	Used for referencing Start and End of Season thresholds.
Rate of Increase at Beginning of Season	Ratio of the difference between the left 20% and 80% levels and the corresponding time difference.	Rate of vegetation green up.
Rate of Decrease at End of Season	Absolute value of the ratio of the difference between the right 20% and 80% levels and the corresponding time difference.	Rate of vegetation senescence.
Large Seasonal Integral	Integral of the function describing the season from season start to season end.	Proxy for the relative amount of vegetation biomass without regarding minimum values.
Small Seasonal Integral	Integral of the difference between the function describing the season and the base level from season start to season end.	Proxy for the relative amount of vegetation biomass while regarding minimum values.

Figure 5-6 Graphic depiction of selected phenometrics used in the sensitivity analysis: Start of season (a), end of season (b), maximum value (e), season length (g), small seasonal integral (h) (from Eklundh and Jönsson 2010).

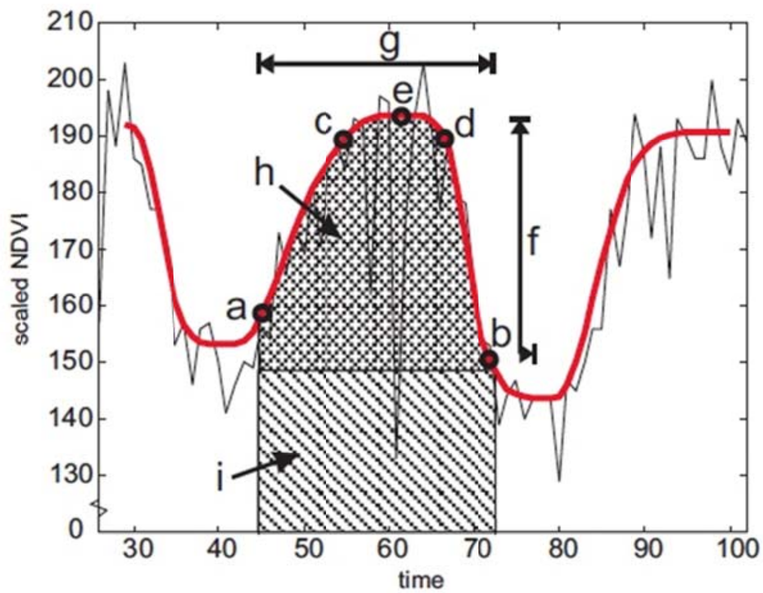

Statistical Analysis

The output generated from the phenometric data files by *TSM_printseasons* were organized by sorting the phenometric data first by season, then row, and then by column which allowed later statistical analysis on the phenometric to be performed uniformly across the different parameter settings files (Figure 5.7).

Phenometric data files were extracted from TIMESAT for KPBS and three different spatial configurations of Fort Riley, including (1) all installation training areas, (2) high intensity training areas only, and (3) low intensity training areas only. A map of Fort Riley training intensity (Figure 5.8) was created using a combination of expert knowledge and information from related literature (P. Denker, pers. comm.; J.M.S. Hutchinson, pers. comm.; Johnson *et al.,* 2011).

Figure 5-7 Example of a portion of one phenometric data file created from a parameter settings file. Columns include the row and column of each image pixel, the season, and the 11 different phenometrics estimated by TIMESAT.

Row	Col.	Seas.	Beg.	End.	Length	Base	Mid-x	Max.	Amp.	L-der.	R-der.	L-integ.	S-integ.
1	1	1	5.2	24.3	19	105.5	9.9	196.7	91.2	26.8	3.9	3459.3	1243.8
1	1	2	28.9	45.5	16.6	108.4	33.4	177.2	68.8	13.9	4.3	2798.3	739.6
1	1	3	52.2	67.3	15	102.4	59.3	188.9	86.5	23.2	15.2	2788.3	1048.3
1	1	4	75.3	91	15.7	103.9	83.6	213.6	109.7	10.3	11	2878.3	1111.6
1	1	5	96.6	112.4	15.8	102.5	104.5	185.6	83.1	13.7	12.9	2877.9	1033.5
1	1	6	121.4	135.9	14.5	98.8	130.3	198.6	99.8	9	18.5	2621.8	1040.4
1	1	7	144.6	161.9	17.3	103.1	150.8	188.5	85.4	17.7	5.7	3001	1042.4
1	1	8	166.5	181.7	15.3	105.4	173.5	190.6	85.2	16.2	12.1	2800.3	1008.1
1	1	9	191.3	204.5	13.3	97.9	197.5	207.4	109.5	18.3	15	2530.4	1061.7
1	1	10	213.5	226.6	13.1	96.6	220.7	211	114.4	15.7	22.7	2574.4	1125
1	1	11	235.6	249.6	13.9	100.7	240.8	195.5	94.8	19.9	8.2	2577.9	966.8
1	2	1	5.8	23.6	17.8	96.6	12.6	201	104.4	25	9.1	3317.7	1385.6
1	2	2	29.1	44.5	15.4	100.7	36.3	179.3	78.6	17.9	10.8	2676	964.4
1	2	3	52.3	68.9	16.6	106.8	56.6	194.9	88.2	23.7	4.9	2957.7	1036
1	2	4	75.5	89.6	14.1	104.3	81.3	213.5	109.2	28.8	13.1	2838	1168.5
1	2	5	98.2	112.4	14.2	102.5	104.9	203.6	101.1	16.4	12.9	2716.5	1076.1
1	2	6	121.3	135.8	14.5	102	128.4	187	85.1	19.5	14.6	2624.5	993.1
1	2	7	144	160.4	16.4	101.4	151.1	190.1	88.7	16.4	8.8	2907.8	1082.8
1	2	8	167.5	181.8	14.3	102	174.3	197.1	95.1	17.9	14.2	2687.9	1055.9
1	2	9	191.1	204.5	13.5	98.2	196.9	214.8	116.6	24.1	14.9	2642.7	1169.8
1	2	10	213.3	226.8	13.5	98.4	219.1	204.1	105.7	29.2	13.6	2587.5	1111.1
1	2	11	237	250	13	102.4	242.1	200.7	98.3	27	10.4	2370	936.1
1	3	1	5.6	21.6	16.1	100.7	12.8	195	94.3	21.3	12	3023.7	1211
1	3	2	29.7	44.5	14.8	105.5	33.9	193.8	88.2	23.3	5.6	2744.4	950.4
1	3	3	52.4	68.8	16.4	109.5	56.7	203.8	94.3	23.9	5.3	3033.9	1062.8
1	3	4	75.3	89.1	13.9	107.2	81.7	205.9	98.8	21.1	13.9	2798.2	1083.4
1	3	5	98.3	112	13.7	104.4	105.1	204.2	99.7	15.6	14.5	2587.6	1021
1	3	6	121.3	136	14.7	103	127.9	190.4	87.3	21.1	12.8	2651.2	1002.4
1	3	7	143.9	160.5	16.6	100.8	151	194.1	93.4	16.3	9.2	3057.8	1143.5
1	3	8	168.1	181	12.9	102.9	174	208	105.1	24	15.9	2604.9	1062.1
1	3	9	190.9	204.4	13.5	100.4	196.5	206.5	106	23.3	13	2678	1070.9
1	3	10	213.3	227.1	13.8	99.3	219.2	206.7	107.4	22.7	12.4	2709.5	1121.2
1	3	11	237.1	250	12.9	102.1	242.8	198.7	96.6	24.8	12.8	2408.8	980
1	4	1	5.6	22	16.4	98.9	12.6	201.4	102.5	26.5	11	3060.1	1279.8
1	4	2	29.3	44.2	14.9	109.2	36.6	182.9	73.8	18.7	12.6	2738.3	882.2

Figure 5-8 Fort Riley training areas highlighted as low and high training intensity study areas based on a collaborative expert opinion.

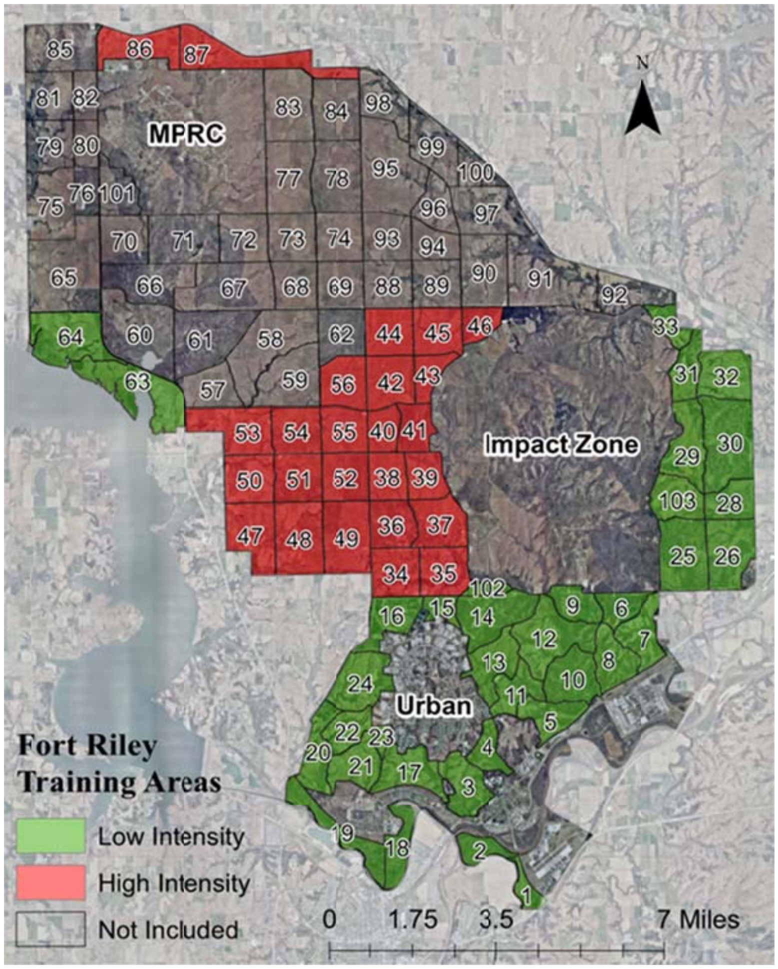

Phenometrics for KPBS and the three different configurations of Fort Riley (all training areas, high intensity training areas, and low intensity training areas) were compared to determine whether the dominant landuse and relative training intensity of each study area contributed to significant differences in beginning/end of season dates, season length, maximum NDVI value attained, and small seasonal integral. A Kolmogorov-Smirnov (K-S) test was applied to ordered pairs of phenometric data from the different study areas to determine if significant differences existed. A K-S test is a nonparametric test that determines equality of continuous, onedimensional probability distributions (McGrew and Monroe 2000). The K-S test statistic measures the maximum distance of the *empirical distribution function* of one study area against the *empirical distribution function* from another study area, and can be used to compare two different datasets.

Output from each K-S test includes an empirical distribution graph, also known as a cumulative fraction function, of a phenometric, across each growing season, for every study area comparison (Figure 5.9). The empirical distribution graph shows the proportion of the data (y-axis) that is strictly smaller than the values on the x-axis. Depending on the phenometric considered, the x-axis represents dates (*e.g.,* beginning of season phenometric) or NDVI value (*e.g.,* maximum value phenometric). A two-sample K-S test statistic (D) was also computed with the *p-value* representing the probability that D is greater than the observed value (d), assuming the null hypothesis that there is no difference in the phenometric between the study areas.

The alpha level to reject or accept the null hypothesis was originally set at 0.05. However, because the analysis was to be completed for each of 11 seasons, a substantial Type 1 error would be introduced due to the number of tests conducted (4 study areas × 5 phenometrics × 11 seasons = 220 tests; standard α of 0.05 / 220 tests = 0.00023). To reduce the possibility of a Type 1 error, the number of seasons was limited to 3 with three growing seasons selected to represent a normal temperature and precipitation year (2002), cool and wet conditions (2008), and a hot and dry season (2011).

Figure 5-9 Example of an empirical distribution graph of the start of season phenometric for KPBS and Fort Riley high intensity training areas.

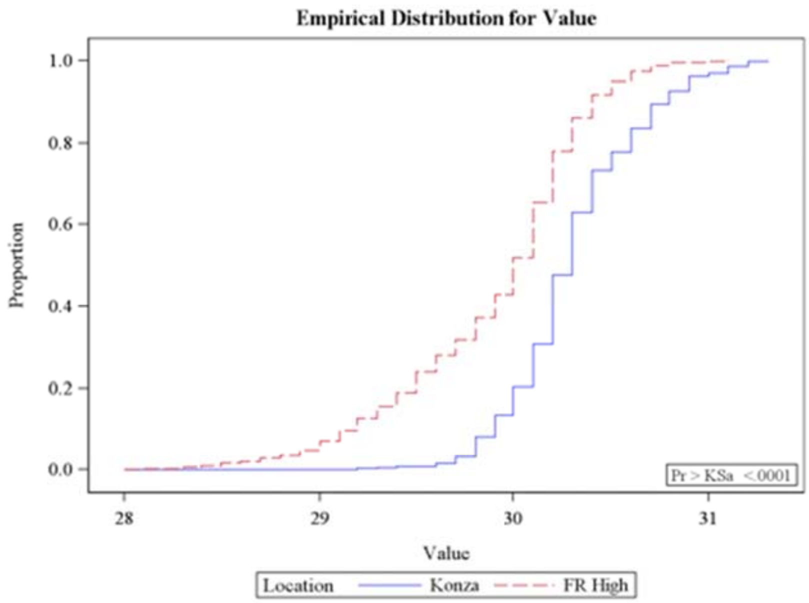

Weather data from the KSU North Agonomy Farm in Manhattan, Kansas was downloaded from the Kansas State University Weather Data Library for the years 2001-2012 and the three representative seasons selected (Figure 5.10). The reduction in the number of evaluated seasons increases the alpha level and decreases the chances of a Type I error (4 study areas × 5 phenometrics × 2 seasons = 60 tests; standard α of 0.05 / 60 tests = 0.00083).

Figure 5-10 Weather data from the KSU North Agronomy Farm for a normal (2002), cool and wet (2008), and hot and dry season (2011). Weather summary graphs provide current and normal daily temperature and monthly precipitation data. Growing degree day (GDD) graphs, a measure of available energy for plant growth, provide the current and normal daily GDD and deviations from normal.

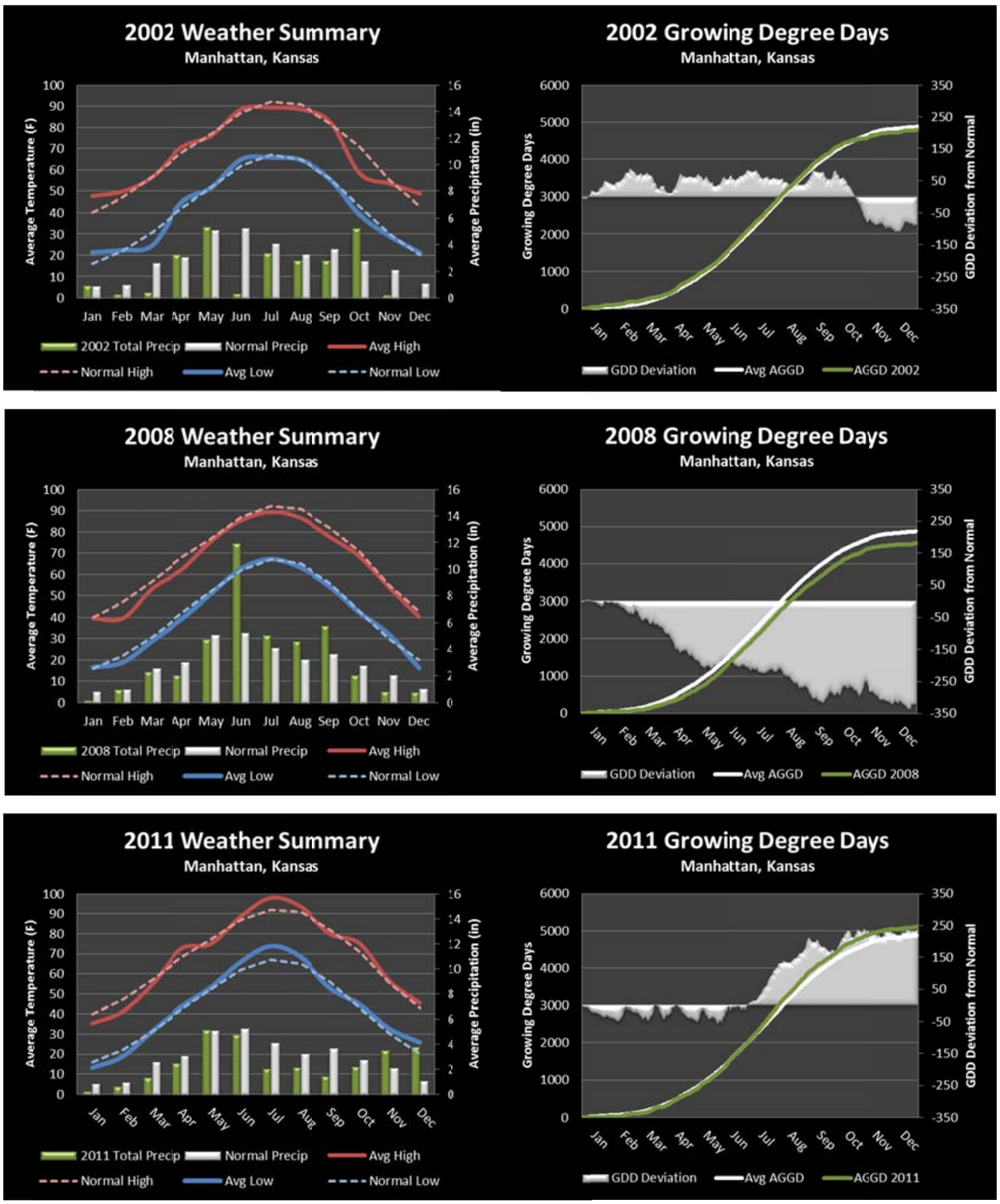

Results

The phenometrics *start of season*, *end of season*, *length of season*, *maximum value*, and *small seasonal integral* were compared between each of the four study sites and three seasons based on annual temperature and precipitation characteristics. Results from the two-sample K-S tests showed that for 58 of 60 (97%) of all possible comparisons made, the underlying null hypotheses that no seasonal differences existed between the phenometric and compared study sites could safely be rejected. The null hypothesis could not be rejected for only two phenometrics – *end of season* in a normal year and *length of season* in a cool, wet year – in the comparison between high- and low-intensity training areas and KPBS, respectively. Though the p-values for these two phenometrics never exceeded 0.003, the risk of a Type 1 error prevented rejection of the null hypothesis.

It is important to point out that when comparing any portion of Fort Riley to KPBS, the empirical distributions will look fairly different. This is because Fort Riley has a larger distribution, or range of values. Fort Riley will have both lower values and higher values than KPBS, indicating higher variability and a more heterogeneous NDVI landscape. This may be due to a number of factors including sample size, plant species composition, vegetation type response to climatic variables, or military training. When comparing the different training intensity areas of Fort Riley, the empirical distributions look fairly similar, indicating a more homogenous NDVI relationship.

In the following subsections, a general description of the results is presented for each of the four paired study area comparisons. All graphs presented within the results section are from the normal season unless otherwise noted. A complete collection of empirical distribution graphs for each phenometric by season and paired comparison can be found in Appendix F.

Fort Riley Training Areas vs. KPBS

Significant differences existed for all phenometrics examined in the comparison for all Fort Riley training areas and KPBS (Table 5.3). In general, and for each of the three season types assessed, Fort Riley training areas have an earlier *start of growing season (SOS)* and *end of season (EOS)* date, shorter *growing season lengths*, and lower *maximum NDVI values* and *small seasonal integrals* than KPBS.

Table 5.3 Summary of K-S test results for all phenometrics between Fort Riley and KPBS.

Season	Phenometric	KS	D	Pr > D
Normal	Start of Season	0.1193	0.3860	< 0.0001
Cool/Wet		0.0627	0.2034	< 0.0001
Hot/Dry		0.0546	0.1773	< 0.0001
Normal	End of Season	0.0384	0.1242	< 0.0001
Cool/Wet		0.0869	0.2820	< 0.0001
Hot/Dry		0.0469	0.1520	< 0.0001
Normal	Length of Season	0.0903	0.2920	< 0.0001
Cool/Wet		0.0353	0.1145	< 0.0001
Hot/Dry		0.0438	0.1414	< 0.0001
Normal	Maximum Value	0.0928	0.3011	< 0.0001
Cool/Wet		0.0752	0.2442	< 0.0001
Hot/Dry		0.0579	0.1880	< 0.0001
Normal	Small Integral	0.1217	0.3938	< 0.0001
Cool/Wet		0.1122	0.3640	< 0.0001
Hot/Dry		0.0738	0.2396	< 0.0001

For both Fort Riley and KPBS, the *SOS* takes place within a very narrow time window. In normal years, the season start at Fort Riley is consistently ahead of that for KPBS (Figure 5.11), though in cool/wet and hot/dry seasons the difference is less pronounced (though still significant).

Figure 5-11 Empirical distribution function for the phenometric beginning of season and Fort Riley versus KPBS.

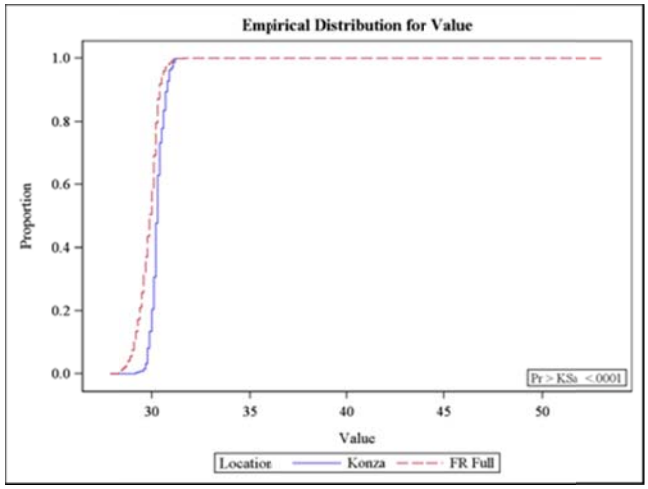

Much more variation in *EOS* dates exist among the two sites, though the growing season at KPBS ends within a much narrower date range than Fort Riley. In normal and hot/dry years, the *EOS* is earlier for between 50-80% of Fort Riley (Figure 5.12). In cool/wet years, a larger proportion of KPBS has a later *EOS* date. However, there is always a small proportion of Fort Riley that experiences both an earlier and later end of season.

Figure 5-12 Empirical distribution function for the phenometric end of season and Fort Riley versus KPBS.

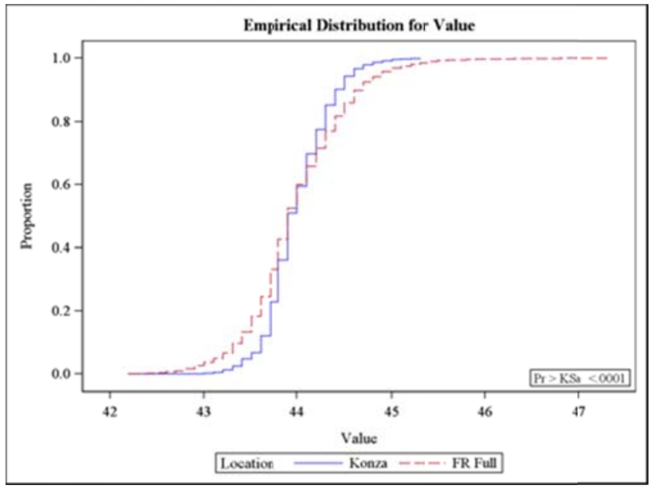

In normal years, the *growing season length* at Fort Riley is consistently longer than KPBS which typically experiences a more compressed growing season (Figure 5.13). In cool/wet and hot/dry seasons, larger proportions of Fort Riley experience shorter growing season lengths, though the KPBS growing season remains shorter than that at Fort Riley.

Figure 5-13 Empirical distribution function for the phenometric length of season and Fort Riley versus KPBS.

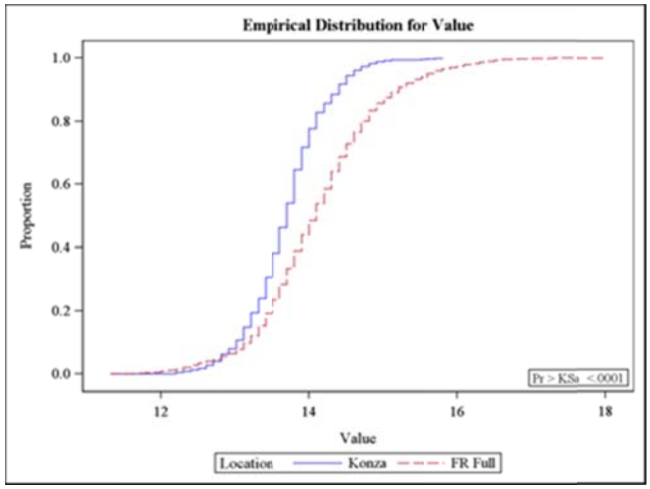

The trend in *maximum NDVI value* recorded is consistent across all seasons, with areas of Fort Riley having a wider range of maximum NDVI values, and a larger proportion of the installation with lower NDVI values, than KPBS (Figure 5.14). Fort Riley also consistently experiences both lower minimum and higher *maximum NDVI values*. Results for the *small seasonal integral* is similar to that of maximum NDVI, with Fort Riley having a wider integral range and a larger proportion of the installation with lower integral values than KPBS across all seasons (Figure 5.15).

Figure 5-14 Empirical distribution function for the phenometric maximum value and Fort Riley versus KPBS.

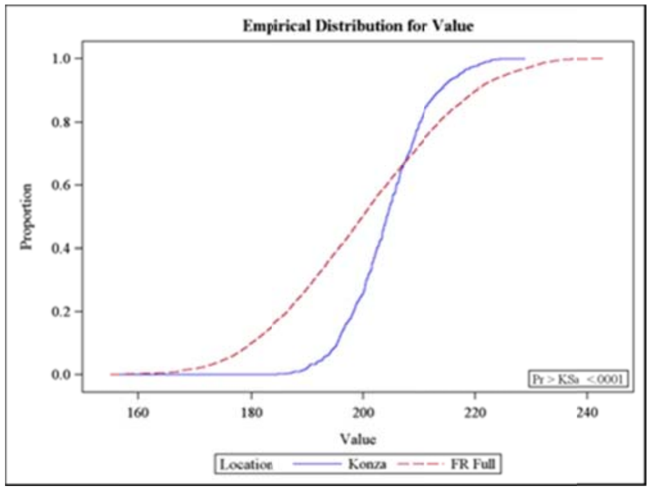

Figure 5-15 Empirical distribution function for the phenometric small seasonal integral and Fort Riley versus KPBS.

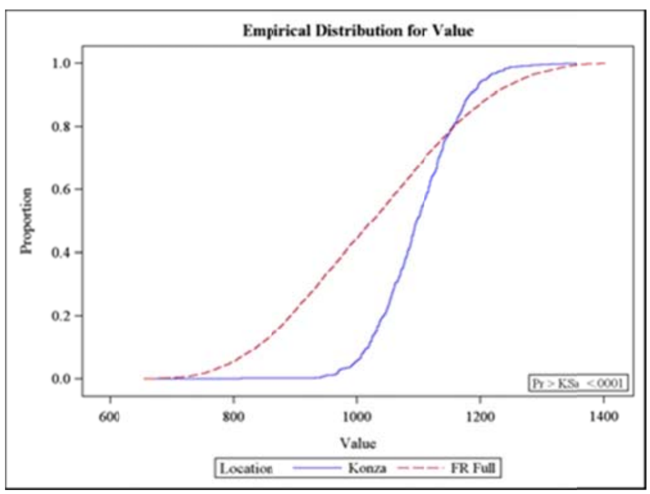

High Intensity Training Areas vs. Low Intensity Training Areas

Significant differences existed for all phenometrics examined in the comparison of Fort Riley's low versus high intensity training areas (Table 5.4). In general, and in most season types assessed, Fort Riley's high intensity training areas have an earlier *SOS* and *EOS* date, shorter *growing season lengths*, and lower *maximum NDVI values* and *small seasonal integral* than Fort Riley's low intensity training areas.

Table 5.4 Summary of K-S test results for all phenometrics between high and low intensity training areas at Fort Riley.

Season	Phenometric	KS	D	Pr > D
Normal	Start of Season	0.0986	0.1988	< 0.0001
Cool/Wet		0.0734	0.1477	< 0.0001
Hot/Dry		0.0849	0.1709	< 0.0001
Normal	End of Season	0.0518	0.1043	< 0.0001
Cool/Wet		0.1207	0.2430	< 0.0001
Hot/Dry		0.0824	0.1660	< 0.0001
Normal	Length of Season	0.0515	0.1037	< 0.0001
Cool/Wet		0.0405	0.0815	0.0002
Hot/Dry		0.0966	0.1948	< 0.0001
Normal	Maximum Value	0.1866	0.3757	< 0.0001
Cool/Wet		0.1918	0.3862	< 0.0001
Hot/Dry		0.1442	0.2904	< 0.0001
Normal	Small Integral	0.1817	0.3663	< 0.0001
Cool/Wet		0.1197	0.2410	< 0.0001
Hot/Dry		0.1283	0.2583	< 0.0001

For all training areas, the *SOS* takes place within a very narrow time window. In cool/wet years, the *SOS* at high intensity training areas is consistently ahead of that for the low intensity training areas (Figure 5.16). In a normal season, about 50% of the area associated with the high intensity training areas experiences a significantly earlier *SOS*, and the other half experiences nearly an identical *SOS* to the low intensity training areas. Hot/dry season differences are less pronounced, and could show slightly later *SOS* times for the high intensity training areas.

Figure 5-16 Empirical distribution function for the phenometric beginning of season and Fort Riley high versus Fort Riley low training intensity areas.

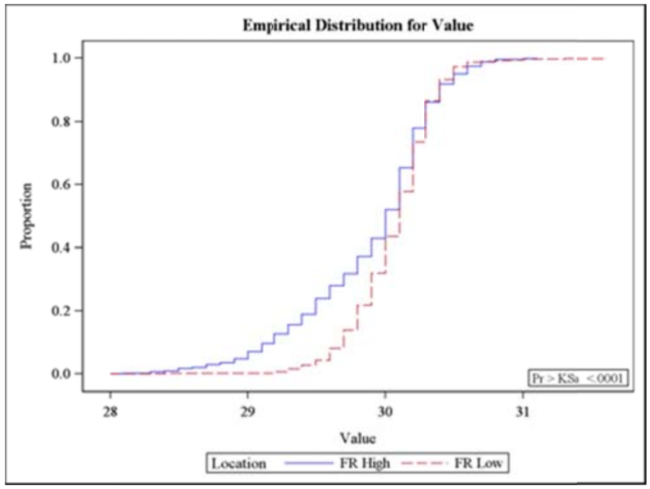

The *EOS* dates are fairly similar across all seasons, and closely resemble that of a normal season. In hot/dry years and cool/wet years, the *EOS* is earlier for about 80% of Fort Riley's high intensity training areas (Figure 5.17). Typically, small portions of the high intensity training areas always experience a later end of season.

Figure 5-17 Empirical distribution function for the phenometric end of season and Fort Riley high versus Fort Riley low training intensity areas.

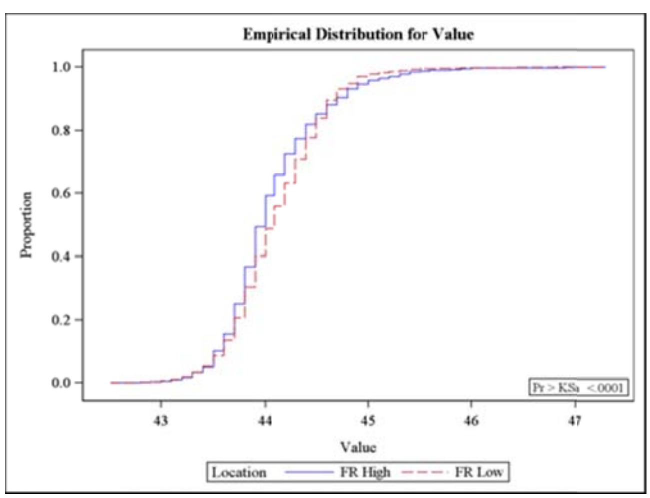

Generally, the *growing season length* for both high and low training intensity areas are fairly similar (Figure 5.18). In a normal season, about 60% of the areas associated with high training intensities have a slightly shorter growing season length. In cool/wet and hot/dry seasons, the majority of this area experience slightly shorter growing season lengths than the low intensity training areas.

Figure 5-18 Empirical distribution function for the phenometric growing season length and Fort Riley high versus Fort Riley low training intensity areas.

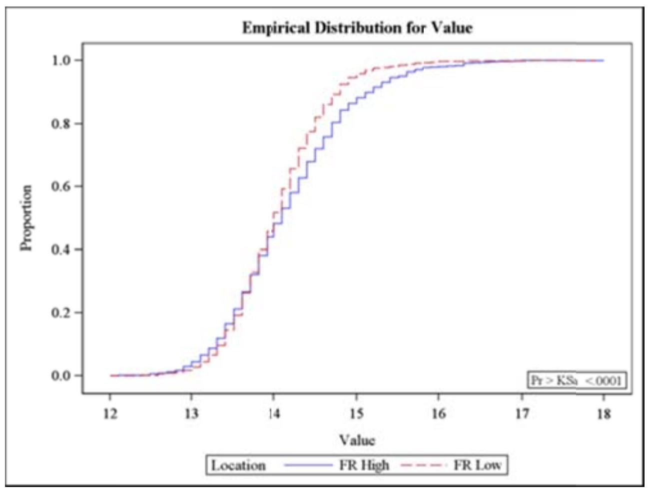

The trend in *maximum NDVI value* recorded is consistent across all seasons, with areas of Fort Riley's high intensity training areas having lower maximum NDVI values (Figure 5.19). Fort Riley's low intensity training areas consistently experience a slightly wider maximum NDVI range and a larger proportion of the installation with higher maximum NDVI values than the high intensity training areas, across all seasons. Results for the *small seasonal integral* is similar to that of *maximum NDVI value* (Figure 5.20), illustrating the same relationship between the training intensity areas.

Figure 5-19 Empirical distribution function for the phenometric maximum value and Fort Riley high versus Fort Riley low training intensity areas.

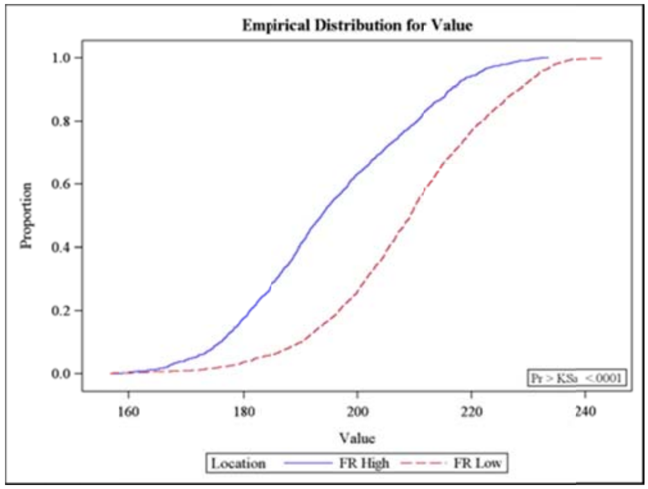

Figure 5-20 Empirical distribution function for the phenometric small seasonal integral and Fort Riley high versus Fort Riley low training intensity areas.

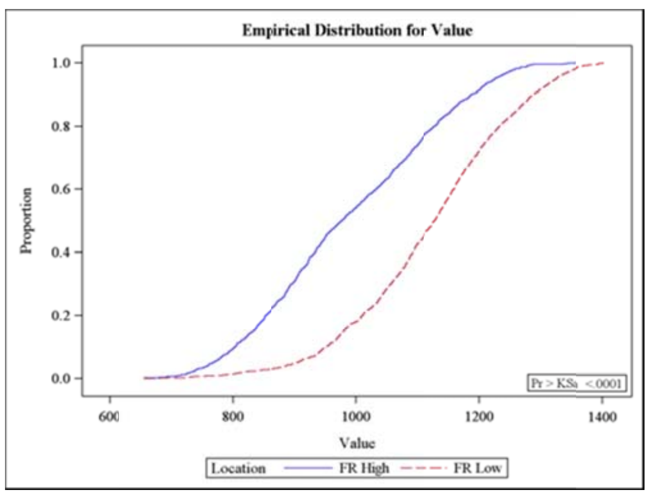

High Intensity Training Areas vs. KPBS

Significant differences existed for all phenometrics examined in the comparison of Fort Riley's high intensity training areas and KPBS, with one exception (Table 5.5). In general, and for the majority of the season types assessed, Fort Riley's high intensity training areas have an earlier *SOS* and *EOS* date, shorter *growing season lengths*, and lower *maximum NDVI values* and *small seasonal integral* than KPBS. The one exception was seen with the *EOS* phenometric in a normal season.

Table 5.5 Summary of K-S test results for all phenometrics between high intensity training areas at Fort Riley and KPBS (bold text indicates no significant difference exists).

Season	Phenometric	KS	D	Pr > D
Normal	Start of Season	0.1630	0.3454	< 0.0001
Cool/Wet		0.1215	0.2575	< 0.0001
Hot/Dry		0.0865	0.1834	< 0.0001
Normal	**End of Season**	**0.0421**	**0.0889**	**0.003**
Cool/Wet		0.1793	0.3801	< 0.0001
Hot/Dry		0.1182	0.2502	< 0.0001
Normal	Length of Season	0.1409	0.2975	< 0.0001
Cool/Wet		0.0720	0.1525	< 0.0001
Hot/Dry		0.0796	0.1680	< 0.0001
Normal	Maximum Value	0.2099	0.4450	< 0.0001
Cool/Wet		0.1602	0.3396	< 0.0001
Hot/Dry		0.1181	0.2503	< 0.0001
Normal	Small Integral	0.2310	0.4881	< 0.0001
Cool/Wet		0.1970	0.4177	< 0.0001
Hot/Dry		0.1338	0.2837	< 0.0001

In normal years, the *SOS* at Fort Riley's high intensity training areas is consistently ahead of that for KPBS (Figure 5.21), though in cool/wet and hot/dry seasons the difference is less pronounced (though still significant).

Figure 5-21 Empirical distribution function for the phenometric beginning of season and Fort Riley's high intensity training areas versus KPBS.

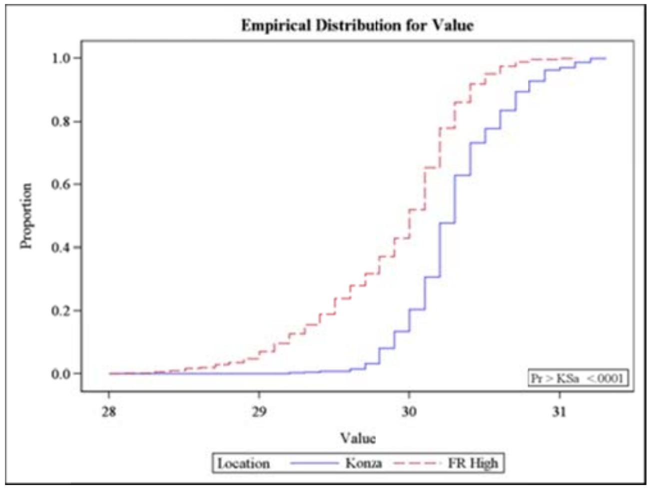

Much more variation in *EOS* dates exist among the two sites, though the growing season at KPBS ends within a much narrower date range than Fort Riley's high intensity training areas. These study areas were not significantly different from one another in a normal season, where the *EOS* is essentially identical for both study areas (Figure 5.22). In cool/wet and hot/dry years, the majority of KPBS has a later *EOS* date, however, there is always a small proportion of Fort Riley that experiences a later *EOS*.

Figure 5-22 The empirical distribution function for the phenometric end of season and Fort Riley's high intensity training areas versus KPBS during a normal (top) and cool/wet season (bottom).

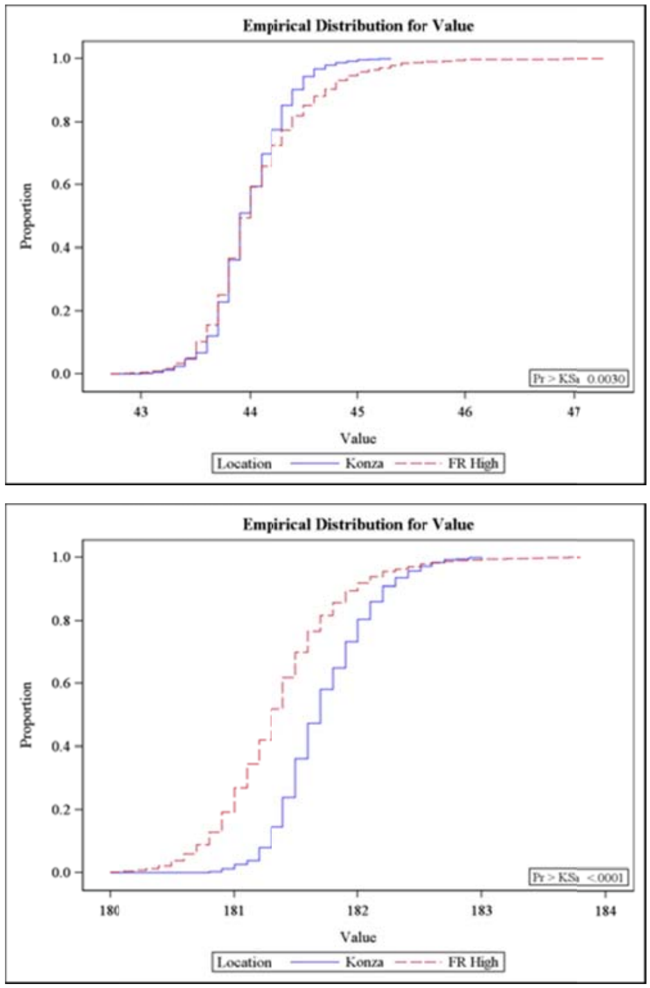

The *growing season length* between the different sites is dependent on type of season (Figure 5.23). In a normal season, KPBS consistently has a shorter growing season length. In cool/wet and hot/dry seasons the majority of the areas associated with high intensity training have a shorter growing season than KPBS. Across all seasons, Fort Riley's high intensity training areas consistently experience a wider range of season lengths with a larger proportion of the installation having higher season length values than KPBS.

Figure 5-23 The empirical distribution function for the phenometric growing season length and the Fort Riley's high intensity training areas vs. KPBS for all season types.

Normal

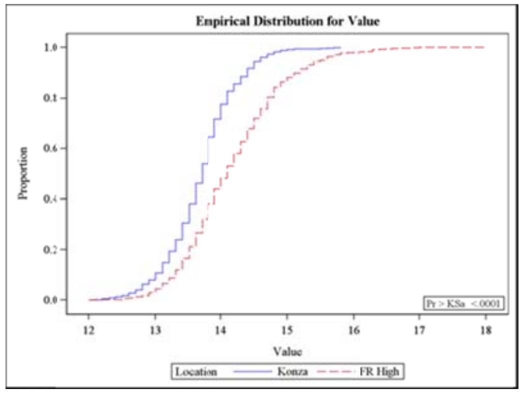

Cool/Wet

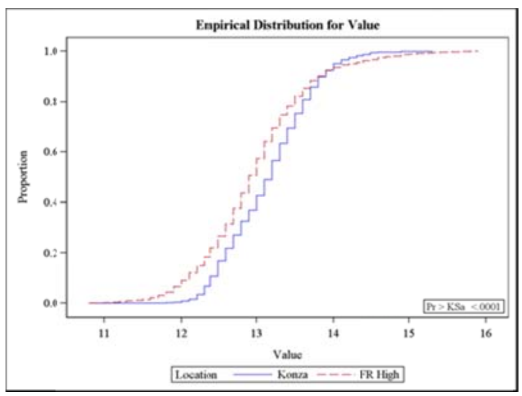

Hot/Dry

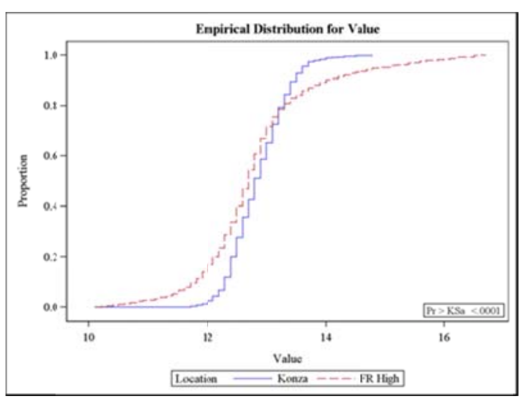

The trend in *maximum NDVI value* recorded is consistent across all seasons, with the majority of Fort Riley's high intensity training areas having lower *maximum NDVI values*

(Figure 5.24). In a normal and cool/wet season, Fort Riley's high intensity training areas experience a slightly wider maximum NDVI range and a slightly larger proportion of the area with higher integral values than KPBS. Results for the *small seasonal integral* are similar to that of *maximum NDVI value* (Figure 5.25) with slight differences. In a cool/wet season, Fort Riley's high intensity training areas never experience larger *small integral values* than KPBS. In addition, these training areas experience a wider range of *small integral values* despite season type.

Figure 5-24 Empirical distribution function for the phenometric maximum value and Fort Riley's high intensity training areas versus KPBS.

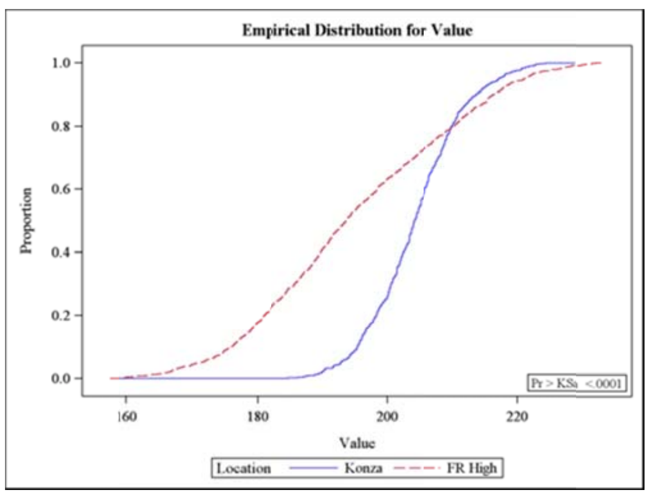

Figure 5-25 Empirical distribution function for the phenometric small seasonal integral and Fort Riley's high intensity training areas versus KPBS for a normal (top) and cool/wet season (bottom).

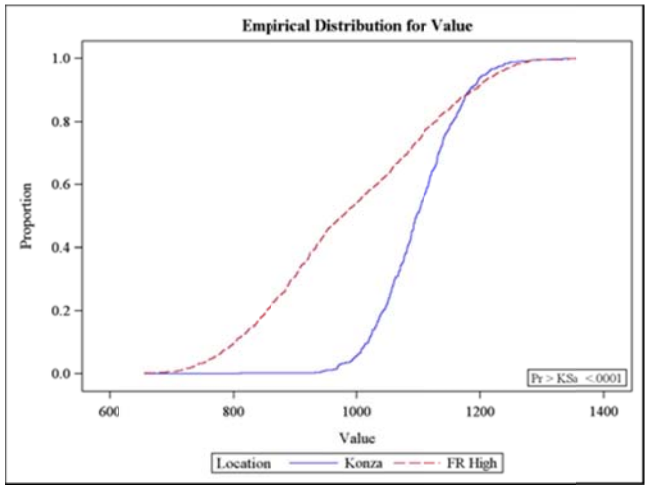

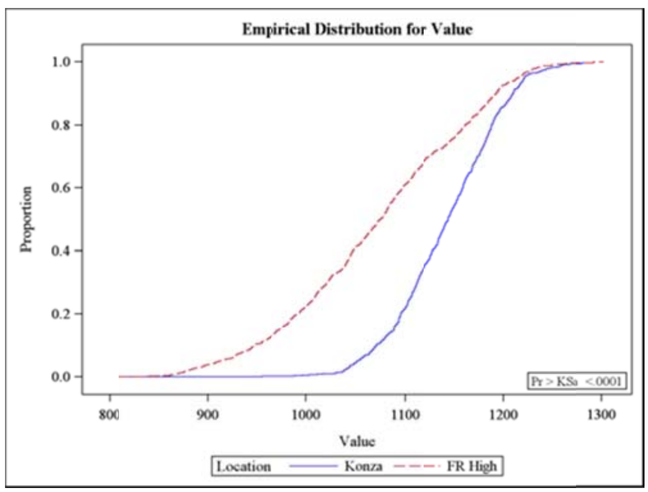

Low Intensity Training Areas vs. KPBS

Significant differences existed for all phenometrics examined in the comparison of Fort Riley low training intensity areas and KPBS, with one exception (Table 5.6). In general, and in most of the season types assessed, Fort Riley's low intensity training areas have an earlier *SOS* and *EOS* date, longer *growing season lengths*, higher *maximum NDVI values*, and a similar *small* *seasonal integral* compared to KPBS. The one exception was seen within the *growing season length* phenometric in a cool/wet season.

Table 5.6 Summary of K-S test results for all phenometrics between low intensity training areas at Fort Riley and KPBS (bold text indicates no significant difference exists).

Season	Phenometric	KS	D	Pr > D
Normal	Start of Season	0.1216	0.2695	< 0.0001
Cool/Wet		0.0496	0.1098	< 0.0001
Hot/Dry		0.1489	0.3298	< 0.0001
Normal	End of Season	0.1649	0.1438	< 0.0001
Cool/Wet		0.0686	0.1519	< 0.0001
Hot/Dry		0.0471	0.1043	< 0.0001
Normal	Length of Season	0.1173	0.2597	< 0.0001
Cool/Wet		**0.0402**	**0.0890**	**0.0018**
Hot/Dry		0.0461	0.1021	0.0002
Normal	Maximum Value	0.1277	0.2828	< 0.0001
Cool/Wet		0.1660	0.3681	< 0.0001
Hot/Dry		0.1093	0.2424	0.0002
Normal	Small Integral	0.1030	0.2281	< 0.0001
Cool/Wet		0.0934	0.2067	< 0.0001
Hot/Dry		0.0797	0.1765	< 0.0001

Much variation in the *SOS* dates exist among the two sites, though the growing season at KPBS begins within a much narrower date range than Fort Riley's low intensity training areas. In normal and hot/dry years, the *SOS* at Fort Riley's low intensity training areas is consistently ahead of that for KPBS (Figure 5.26), though in a cool/wet season the difference is less pronounced (though still significant).

Figure 5-26 Empirical distribution function for the phenometric beginning of season and Fort Riley low intensity training areas versus KPBS.

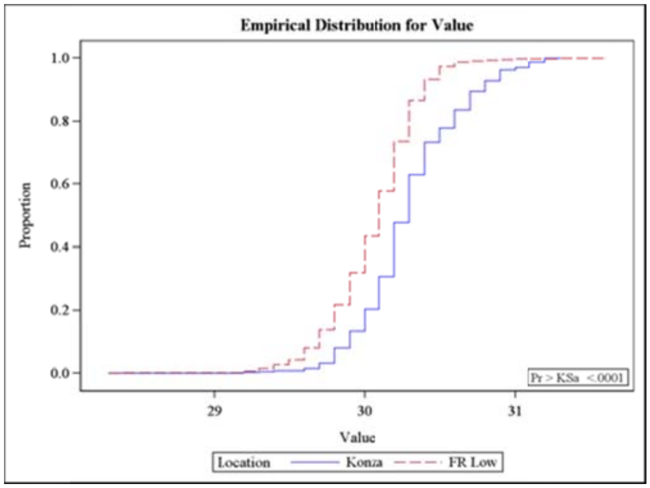

Like *SOS*, *EOS* dates have much variation between the two sites, and the growing season at KPBS ends within a narrower range of dates than Fort Riley's low intensity training areas. In cool/wet and hot/dry years, Fort Riley's low intensity training areas consistently experience an earlier *EOS* (Figure 5.27). In a normal year, the majority of KPBS has an earlier *EOS* date. However, there is always a proportion of Fort Riley that experiences a later *EOS*.

The *growing season length* between the different sites is dependent on type of season (Figure 5.28). In a normal season, KPBS consistently has a shorter *growing season length*, and in a hot/dry season a small portion of Fort Riley's low intensity training areas has a shorter growing season than KPBS. These study areas were not significantly different from one another in a cool/wet season, where the *growing season length* is essentially identical for both study areas (Figure 5.22). Across all seasons, Fort Riley's low intensity training areas consistently experience a wider range of *growing season lengths* and a larger proportion of the installation has a longer season length than KPBS.

Figure 5-27 Empirical distribution function for the phenometric end of season and Fort Riley low intensity training areas versus KPBS for a normal (top) and cool/wet season (bottom).

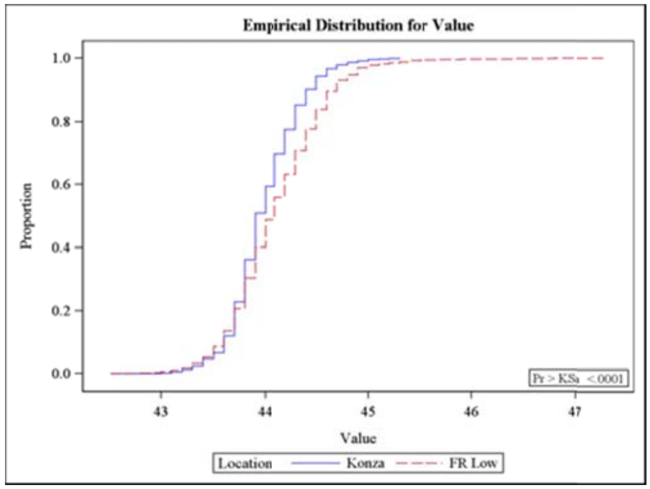

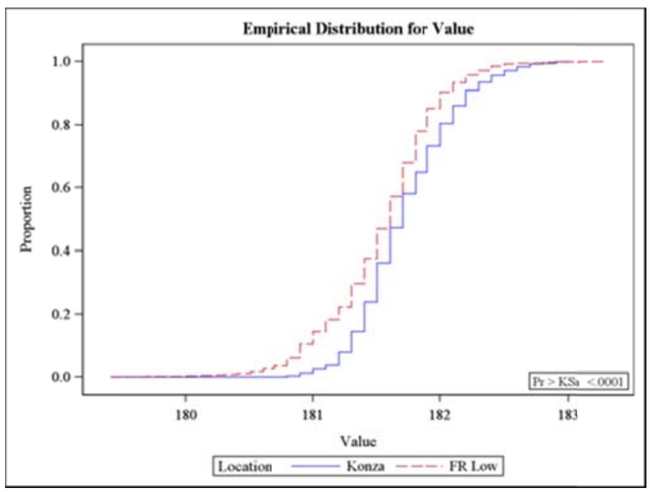

Figure 5-28 Empirical distribution function for the phenometric growing season length and Fort Riley low intensity training areas versus KPBS for all season types.

Normal

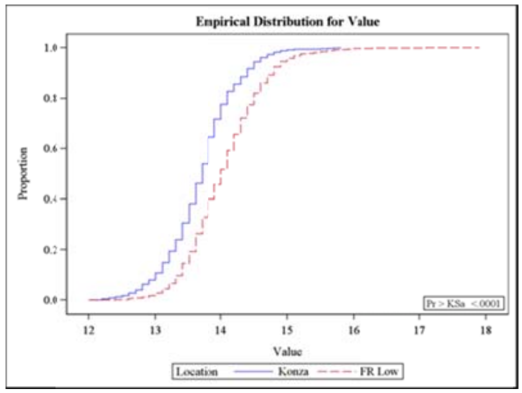

Cool/Wet

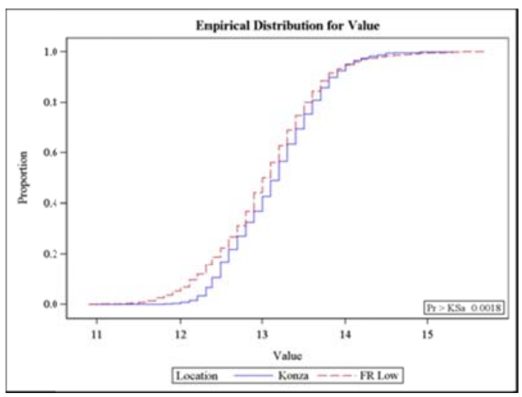

Hot/Dry

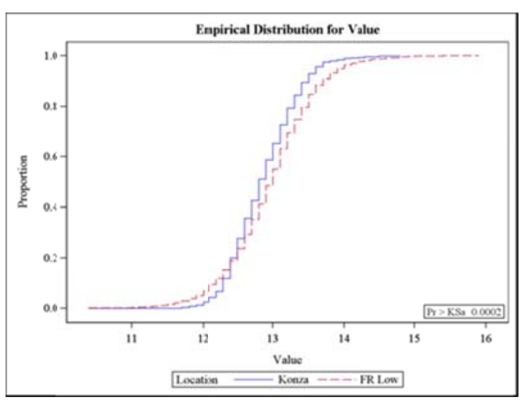

The trend in *maximum NDVI value* is consistent across all seasons, with areas of Fort Riley's low intensity training areas having a wider range of *maximum NDVI values*, and a larger proportion of the installation with higher NDVI values, than KPBS (Figure 5.29). These training areas also consistently experience both lower minimum and higher maximum NDVI values.

Figure 5-29 Empirical distribution function for the phenometric maximum value and Fort Riley low intensity training areas versus KPBS.

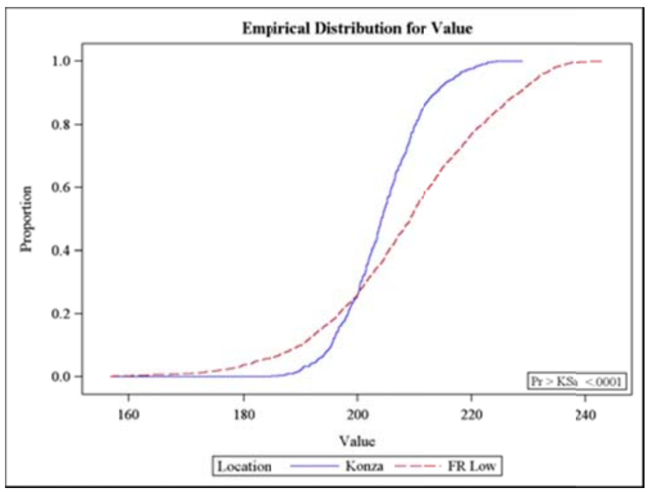

Fort Riley's low intensity training areas have a wider range of *small seasonal integral* values across all seasons. In a normal or hot/dry season, approximately 65% of Fort Riley's low intensity training areas have higher *small seasonal integral* values, but this percentage drops to about 50% in a wet/cool season (Figure 5.30).

Figure 5-30 Empirical distribution function for the phenometric small seasonal integral and Fort Riley low intensity training areas versus KPBS.

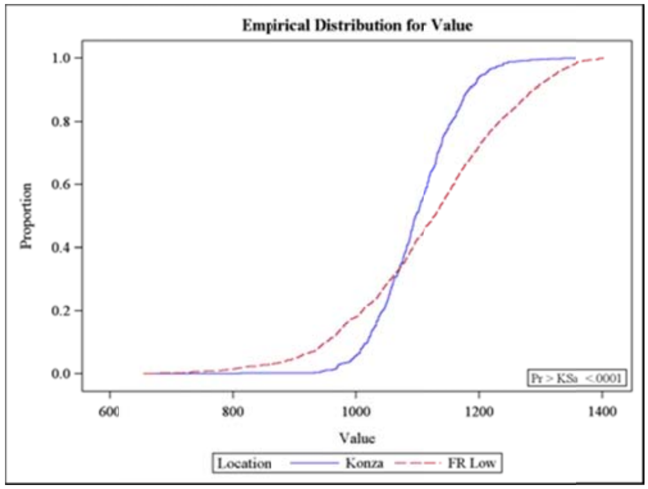

Conclusions and Discussion

The earlier *start of season* may be due to a number of variables related to vegetation species composition, climatic variables, military training, or a cumulative effect of these variables. An additional contributing factor may be due to the MODIS NDVI image composites used in the analysis. According to O'Connor *et al*., (2012), there are two important factors regarding vegetation composites in identifying *start of season* dates. The number of days in each composite image must be within the time taken for significant vegetation change to occur, and there also must be a sufficient number of cloud-free days in the interval (Pinty *et al.,* 2002). In the early spring, Kansas will often experience significant cloud cover. If every day (of 16 in this case) included in the composite processing had significant cloud cover, the composite image would contain inaccurate NDVI values for the areas experiencing cloud cover. It is possible that Konza Prairie could experience more cloud cover than Fort Riley during the early spring.

This analysis shows how inconsistent the *end of season* dates are compared to the beginning of season dates. Again, these values may be due to vegetation species composition, soil characteristics, climatic variables, military training, or a cumulative effect of these variables. The *growing season length* phenometric is dependent upon both the *start* and *end of season* date. Whatever impacts those phenometrics, will affect the *growing season length*. The reasoning behind these differences may be related to the same issues previously discussed, but it is interesting to see that under non-normal season conditions, Fort Riley's *growing season length* were consistently shorter than KPBS's, suggesting that the climate plays a significant role in governing this phenometric.

The amount of variation within the *maximum NDVI value* and *small seasonal integral* values is apparent between Fort Riley and KPBS. With the comparison of the intensity levels against each other, we gain a clear picture of what military training does to vegetation on the installation, which can easily be seen in the average NDVI graphs (Figures 5.31 - 5.34). Compared to low intensity training areas, there is more vegetation loss, and more bare ground associated within those areas experiencing a high intensities of training. Through the Kolmogorov-Smirnov analysis, it is clear that Fort Riley has a greater range and more variability associated with key phenometrics.

Figure 5-31 Raw average NDVI phenology data of KPBS (top) and fitted (bottom) average NDVI phenology data of KPBS after application of the Savitzky-Golay filter.

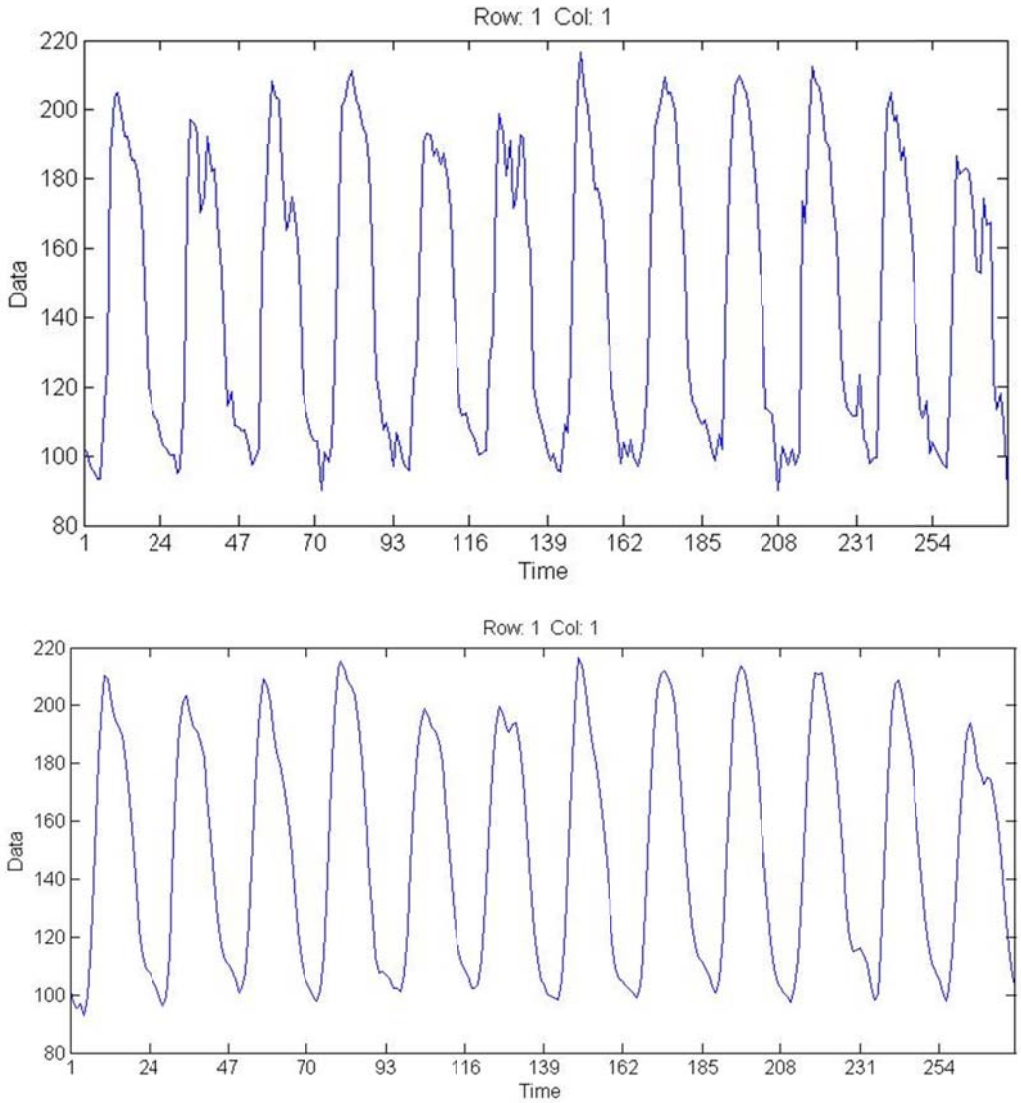

Figure 5-32 Raw average NDVI phenology data (top) and fitted (bottom) average NDVI phenology data for all training areas of Fort Riley after application of the Savitzky-Golay filter.

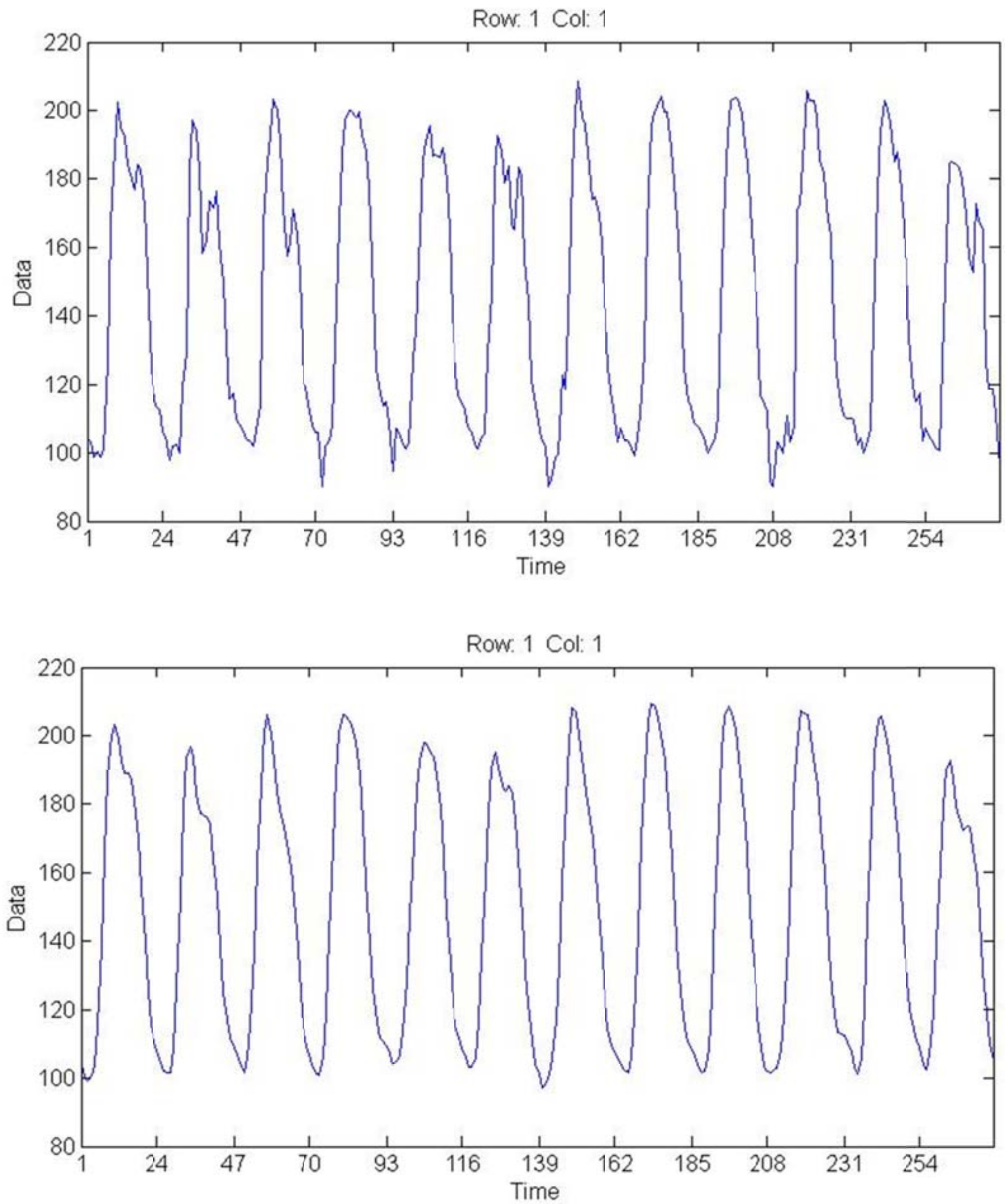

Figure 5-33 Raw average NDVI phenology data (top) and fitted (bottom) average NDVI phenology data for high intensity training areas at Fort Riley after application of the Savitzky-Golay filter.

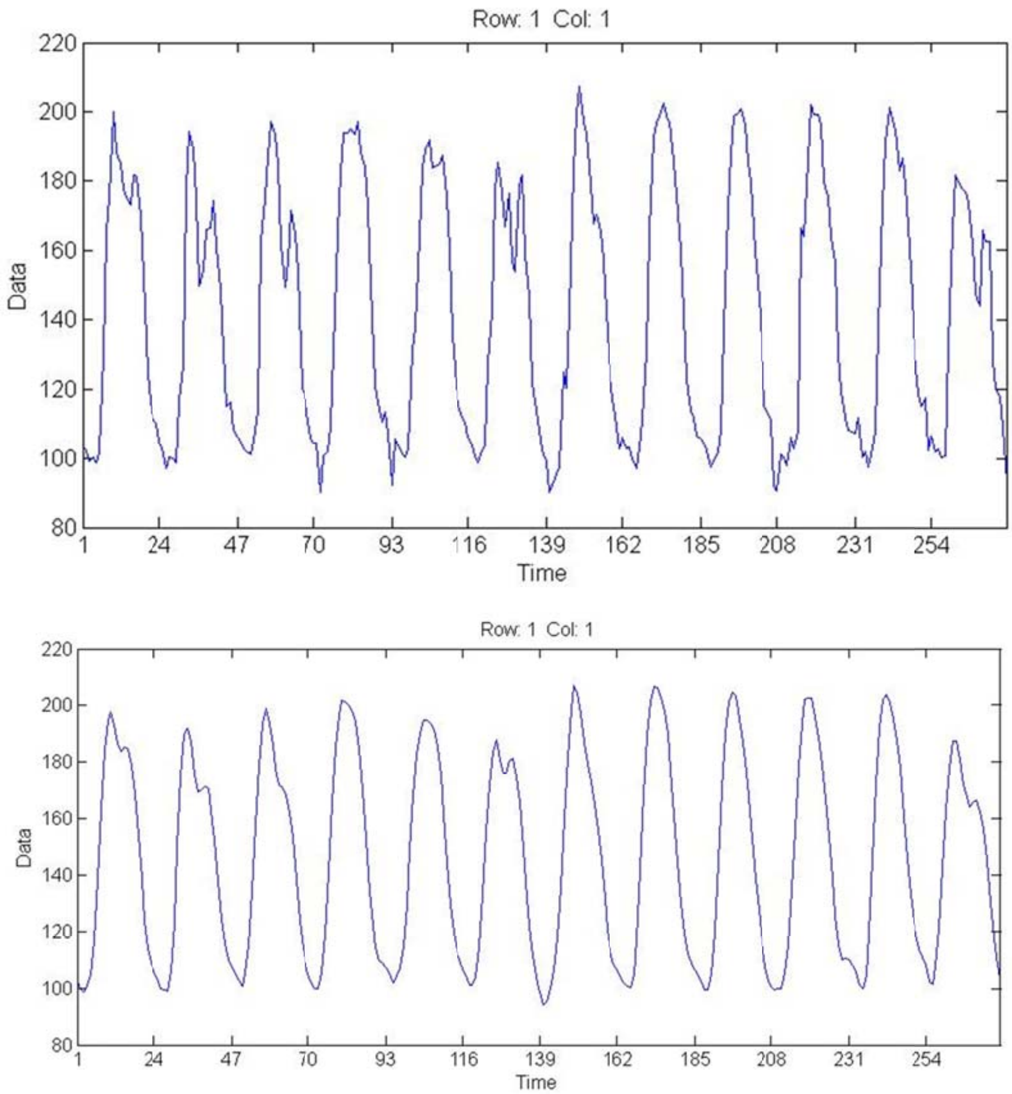

Figure 5-34 Raw average NDVI phenology data (top) and fitted (bottom) average NDVI phenology data for low intensity training at Fort Riley after application of the Savitzky-Golay filter.

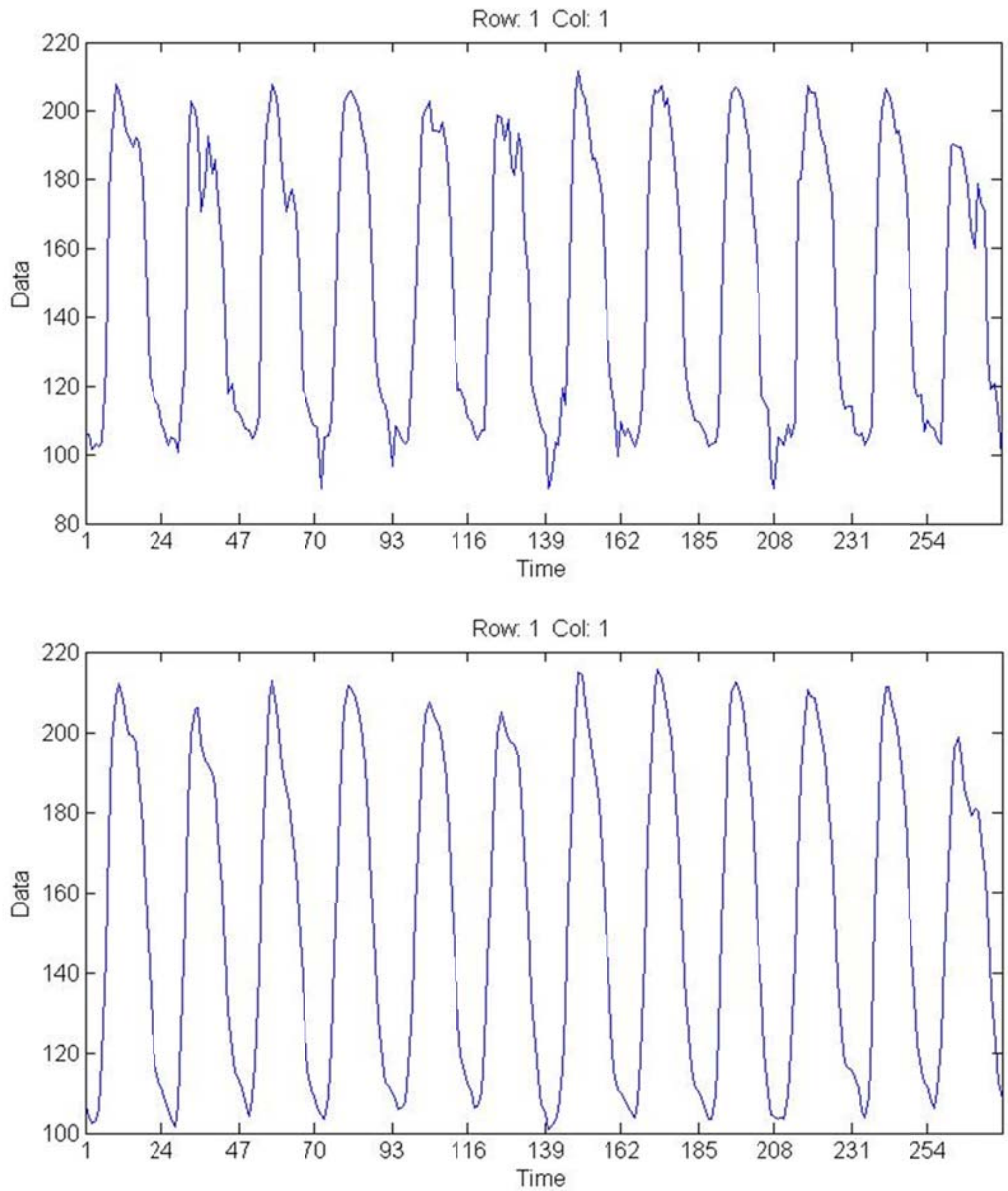

It appears that as the training intensity increases, the number of seasons possibly experiencing two annual seasons per year also increases. These are depicted as seasons with two peaks instead of one, and can be easily seen on the raw average NDVI data (see season 2 in Figure 5.33). For example, it seems that KPBS could potentially have four seasons with a dual season possibility, and Fort Riley training areas could have up to 6 seasons with the bimodal characteristic.

These bimodal peaks could be related to soil differences between the study areas. Fort Riley experiences extensive military training with heavy artillery and mechanized units and it is likely that the soil compaction plays a role in the determining vegetation health and biomass production, which would particularly influence the *maximum NDVI value* and *small seasonal integral*. If the soil is significantly compacted, the soil cannot infiltrate water, restricting vegetation from taking root and fully developing, particularly in seasons with low rainfall. Satellite imagery would detect these areas as low NDVI values, causing the extracted phenometric data to be considerably lower than areas that do not experience such anthropogenic impacts. Even though Fort Riley and Konza Prairie experience similar climate, if their soil characteristics are different, they will experience different vegetation cover and perhaps different vegetation composition.

The bimodal peaks could also suggest that there are vegetation community differences between the study sites. A direction for future work would be to incorporate vegetation community differences between the study sites, while varying the training intensity. In order to do this, an extensive vegetation community inventory is needed. However, since we now know that there is a significant difference between these study areas, of which is partly related to the vegetation communities present, this analysis could be minimized by selecting specific plots based on vegetation community of both study areas. This would give further insight into mitigation processes for military training lands.

In addition to incorporating land cover classes into the analysis, an alternative control study area that future work may integrate would be the Tallgrass Prairie Preserve located in

Kansas, north of Strong City. It is part of the same Flint Hills region shared with Fort Riley and the Konza Prairie Biological Station. The 11,000 acres of tallgrass prairie in the preserve is protected by the United States National Park Service and the Nature Conservancy (http://www.nature.org).

Though NDVI has been proven to be very useful, there are a few key issues that limit the applicability of NDVI for biophysical calculations and vegetation monitoring. Though it may be a poor discriminator of stress when stress occurs at high values of green cover, NDVI proves useful in sparse vegetation plots (Jackson *et al*., 1983). NDVI is more sensitive to early rain seasons and to canopy background noise such as soil or plant litter, which also introduces non-vegetation-related variations in the NDVI data (Huete 1988).

Any analysis including remote sensing must acknowledge the possibility of errors. As with most spectral reflectance combinations, atmospheric path radiance decreases the normalized difference value. A number of other variables may impact NDVI values, including satellite drift and volcanic eruption, calibration uncertainties, inter-satellite sensor differences, and bidirectional and atmospheric effects (Zhou *et al*., 2001). Since the reflectance in the visible and NIR bands cannot penetrate through cloud cover, some MODIS scenes that contain clouds may result in a lower NDVI composite image, which could affect the ability to accurately detect certain phenometrics. Luckily, a composited vegetation index product, such as NDVI, uses a constrained-view angle in order to limit residual cloud and atmospheric effects (Verbesselt *et al*., 2009).

Each vegetation index has its advantages and disadvantages. Though NDVI has proven successful in detecting phenology differences, using other vegetation indices, such as the Enhanced Vegetation Index (EVI) may provide similar, and perhaps even better results. NDVI can easily be computed without requiring statements on land cover classes, soil type or climatic conditions. This proved useful for this specific analysis, as land cover classes and soil type were not accounted for in these results. In addition, NDVI has the ability to conduct long time series (more than 20 years), whereas the EVI is limited to sensor systems designating the blue band of the electromagnetic spectrum. EVI is more responsive to canopy structural variations, such as leaf area index (LAI) (Boegh *et al.,* 2002), and is less sensitive to residual aerosol contamination (Miura *et al.,* 1998; Xiao *et al.,* 2003). EVI is less prone to vegetation index saturation (Xiao *et al.,* 2004; Huete *et al.,* 2006), but to compensate this, EVI usually offers lower vegetation index values across all biomes.

It is important to note that these results are understated. There is a significant lack in the ability to statistically test large data, such as MODIS NDVI data. Such data is based on a pixel count, and when combined with 5 different phenometric data values, as well as 3 seasons of data, anywhere from 1,834 to 5,844 values are being evaluated. These large sample sizes will affect the statistical conclusions by making the results susceptible to a Type 1 error. The large number of tests performed will also cause a higher probability of conducting a Type 1 error. A direction for future work would be to incorporate a more appropriate statistical method for large data comparisons. In addition, all study areas in this analysis contained a different number of observations, because the goal was to see if the study areas were significantly different from one another (Fort Riley Full: 5188; Fort Riley High: 1213; Fort Riley Low: 1558; KPBS: 621). However, a future study may further this work by conducting a similar analysis on these study areas with equal number of observations. This work could result in a lower Type 1 error and could give additional insight into any differences between the study areas.

Chapter 6 - Conclusions

The utility and applicability of vegetation index time-series analysis continues to increase in a number of academic fields. Such analyses give substantial insight into the causes of changing vegetation health conditions. There are a number of filtering, fitting, and smoothing methods that may be implemented to extract phenometric data from satellite-derived vegetation indices. The difficulty lies in selecting the most appropriate technique specific to a study area, tailored for obtaining particular desirable output results. Within each smoothing technique, a number of user-defined input settings must be determined prior to application. Selecting the most appropriate input settings proves as an even more daunting task, as certain phenometric output data may be extremely sensitive to the selected parameter settings.

This thesis presents the first documented sensitivity analysis of specific user-defined input settings for the Savitzky-Golay filter within the TIMESAT program. This thesis contributes to work focused on extraction of phenometrics by illustrating the importance of user-defined input settings when creating and applying a filter to raw vegetation index data and how sensitive particular phenometrics are to input settings. Generally, slightly modified input values do not have a significant impact on the phenometric results. However, there are certain input values to the filter settings that yield statistically different values for select phenometrics. Fort Riley's *end of season* and *growing season length* phenometrics were highly sensitive to user-defined input settings for the Savitzky-Golay filer, but the *start of season*, *maximum NDVI value*, and the *small seasonal integral* were generally insensitive to the input settings analyzed.

Additionally, this thesis presents an optimal settings file for the Savitzky-Golay filter option in the TIMESAT application when used for Fort Riley, Kansas and, possibly, the entire Flint Hills ecoregion. Ideally, the parameter settings file presented here would be applicable to regions experiencing similar climate, latitude, and vegetation composition. Such settings may be used in future work related to time-series analysis of vegetation index data, using this filter option. The optimal settings file reported in this research may not be the optimal settings file for all study areas. However, the methods applied here present a template for future analyses seeking to determine an optimal settings file for their study areas. Once an appropriate filter method and specific input settings has been determined for a study area, multiple study areas may then be compared.

This thesis also presents a time-series comparison analysis between an anthropogenically impacted study area (Fort Riley) and a natural tallgrass prairie preserve (KPBS). Due to the proximity between Fort Riley KPBS (Figure 6.1), the optimal filter settings report for Fort Riley in Chapter 4 were also used to extract phenometric data for KPBS using TIMESAT. Phenometric data was extracted from a total of three Fort Riley study areas, which included all Fort Riley training areas, low intensity training areas only, and high intensity training areas only. The extracted phenometric data was then paired and compared against each study area by using a Kolmogorov-Smirnov test.

This is the first known comparison of extracted phenometric data from a time series of a vegetation index in order to investigate differences in key phenometrics that might be caused by military training activities. Such work is beneficial to Range and Training Land Assessment function of installation ITAM programs for evaluating the sustainability of military training lands. Results confirmed that events occurring on Fort Riley significantly impact its vegetation phenology, especially in areas experiencing high intensity training.

According to this model, Fort Riley generally experiences earlier *SOS* and *EOS* dates compared to KPBS. As training intensity increases, the *SOS/EOS* arrives earlier and earlier.

Earlier dates may be related to vegetation species composition, soil characteristics, climatic variables, military training, or a cumulative effect of these variables.

Figure 6-1 Study area maps illustrating the proximity between Fort Riley and KPBS.

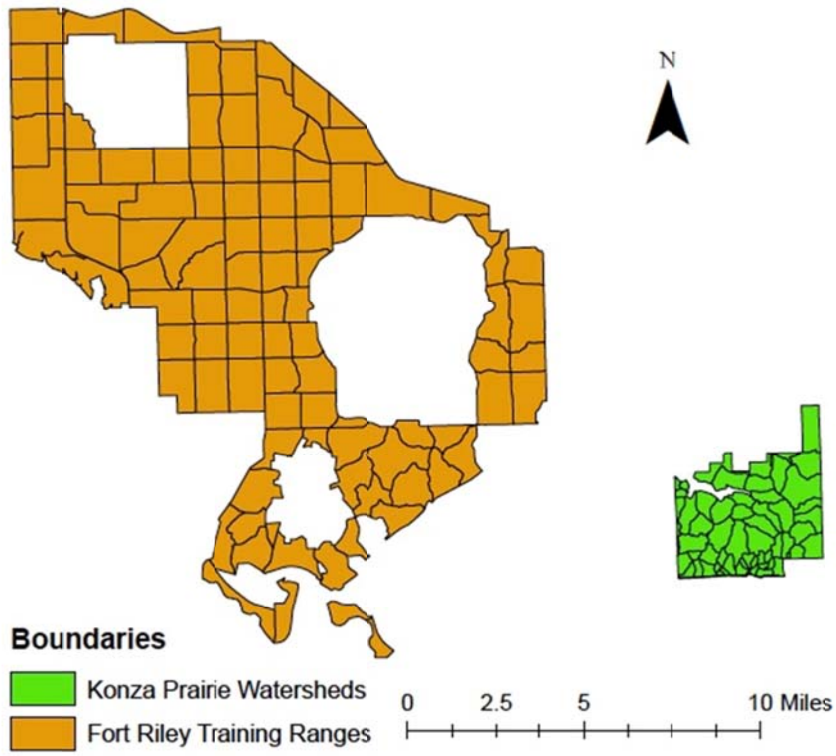

However, Fort Riley experiences a variable *growing season length*. In some seasons, the base will have a shorter length of season compared to KPBS, and in other seasons it will have a longer season length. Fort Riley generally experiences the same season length throughout the different training intensities. Because the length of season parameter is dependent upon both the start and end of season date, whatever impacts those phenometrics will also affect the length of season. Interestingly, under non-normal season conditions, Fort Riley's *growing season lengths* were consistently shorter than those of KPBS. This would suggest that the climate plays a significant role for this phenometric.

There is a substantial amount of variation in the *maximum NDVI values* and *small seasonal integral* between Fort Riley and KPBS. Fort Riley experiences a larger range of values for maximum NDVI values and small seasonal integral, and lower minimum and higher maximum values, than KPBS. As training intensity increases on Fort Riley, the *maximum NDVI* and *small seasonal integral* values decrease. It is apparent that military training has a negative impact on these phenometrics given the decrease in vegetation cover and increase in bare ground associated with more frequent military training and higher training intensities.

This thesis characterizes preliminary results of comparisons between Fort Riley training areas and a natural preserve serving as a type of control. This work could be further expanded by adding moderate intensity training areas to the paired comparisons, finding and incorporating a more appropriate statistical method to test for significance, conducting a similar analysis with equal number of observations per study area, and by incorporating vegetation community differences in a highly detailed comparison. Additional control work on this topic is needed in order to gain a better perspective on the contributing factors upon which Fort Riley's phenology is dependent.

References

Ahas, R., Aasa, A., Menzel, A., Fedotova, V. G., and Scheifinger, H. 2002. Changes in European spring phenology. *International Journal of Climatology* 22: 1727-1738.

Ahl, D.E., Gower, S.T., Burrows, S.N., Shabanov, N.V., Myneni, R.B., and Knyazikhin, Y. 2006. Monitoring spring canopy phenology of a deciduous broadleaf forest using MODIS. *Remote Sensing of Environment* 104: 88-95.

Althoff, D.P., Gipson, P.S., Pontius, J.S., and Woodford, P.B. 2006. Plant community and bare ground trends on Fort Riley, Kansas: Implications for monitoring of a highly distributed landscape. *Transactions of the Kansas Academy of Science* 109 (3/4): 101-119.

An, N. 2009. Estimating Annual Net Primary Productivity of the Tallgrass Prairie Ecosystem of the Central Great Plains using AVHRR NDVI. *University of Kansas*.

Anyamba, A., and Eastman, J.R. 1996. Interannual variability of NDVI over Africa and its relation to El Nino Southern Oscillation. *International Journal of Remote Sensing* 17 (13): 2533–2548.

Asrar, G., Myneni, R.B., and Kanemasu, E.T. 1989. Estimation of plant canopy attributes from spectral reflectance measurements. In *Theory and Applications of Optical Remote Sensing*, Chapter 7: 252-296.

Australian Bureau of Statistics. 2005. Time Series Analysis: The Basics. *Commonwealth of Australia*. http://www.abs.gov.au/websitedbs/D3310114.nsf/home (last accessed September 1, 2012).

Azzali, S., and Menenti, M. 2000. Mapping vegetation–soil–climate complexes in southern Africa using temporal Fourier analysis of NOAA-AVHRR NDVI data. *International Journal of Remote Sensing* 21 (5): 973–996.

Bailey, R.G., Avers, P.E., King, T., and McNab, W.H., eds. 1994. Ecoregions and subregions of the United States (map) (supplementary table of map unit descriptions compiled and edited by McNab, W.H. and Bailey, R.G.): Washington, D.C., U.S. Department of Agriculture–Forest Service, scale 1:7,500,000.

Baret F., Guyot G., Major D.J. 1989. Crop biomass evaluation using radiometric measurements. *Photogrammetria* 43: 241–256.

Baret, F., and Guyot, G. 1991. Potentials and limits to vegetation indices for LAI and APAR assessments. *Remote Sensing of Environment* 35: 161-173.

Beck, P. S. A., Jönsson, P., Högda, K. A., Karlsen, S. R., Eklundh, L. and Skidmore, A.K. 2007. A ground-validated NDVI dataset for monitoring vegetation dynamics and mapping phenology in Fennoscandia and the Kola peninsula. *International Journal of Remote Sensing* 28: 4311-4330.

de Beurs, K. M. and Henebry, G. M. 2004. Trend analysis of the Pathfinder AVHRR Land (PAL) NDVI data for the deserts of Central Asia. *Geoscience and Remote Sensing Letters*. 1: 282–286.

de Beurs, K. M. and Henebry, G. M. 2005. A statistical framework for the analysis of long image time series. *International Journal of Remote Sensing* 26: 1551–1573.

de Beurs, K. M., Wright, C. K., and Henebry, G. M. 2009. Dual scale trend analysis for evaluating climatic and anthropogenic effects on the vegetated land surface in Russia and Kazakhstan. *Environmental Research Letters*. 4: 045012.

Biondo, B. 1997. In Defense of the Longleaf Pine: Military Base as Ecosystems Lab. *Nature Conservancy* September/October: 10-17.

Blair, J. M. 1997. Fire, N Availability, and Plant Response in Grasslands: A Test of the Transient Maxima Hypothesis. *Ecology,* 78: 2359-2368.

Boegh, E., Soegaard, H., Broge, N., Hasager, C. B., Jensen, N. O., Schelde, K., andThomsen, A.2002. Airborne multispectral data for quantifying leaf area index, nitrogen concentration, and photosynthetic efficiency in agriculture. *Remote Sensing of Environment*, 81: 179−193.

Briggs, J. 2012. Konza Prairie LTER KN: Konza Prairie Biological Station - Primary. Long Term Ecological Research Network. http://www.lternet.edu/sites/knz/research (last accessed November 15, 2013).

Chen, J., Jönsson, P., Tamura, M., Gu, Z., Matsushita, B., and Eklundh, L. 2004. A simple method for reconstructing a high-quality NDVI time-series data set based on the Savitzky–Golay filter. *Remote Sensing of the Environment* 91: 332–344.

Cihlar, J., St.-Laurent, L., and Dyer, J.A. 1991. Relation Between the Normalized Difference Vegetation Index and Ecological Variables. *Remote Sensing of Environment*. 35: 279-298.

Cleland, E. E., Chuine, I., Menzel, A., Mooney, H.A., and Schwartz, M.D. 2007. Shifting plant phenology in response to global change. *Trends in Ecology & Evolution* 22: 357–365.

Cleveland, R.B., Cleveland, W.S., McRae, J.E., and Terpenning, I. 1990. STL: A Seasonal-Trend Decomposition Procedure Based on Loess. *Journal of Official Statistics* Vol. 6(1): 3-73.

Colwell, J.E. 1973. Bidirectional spectral reflectance of grass canopies for determination of above ground standing biomass. University of Michigan, Ann Arbor, Michigan.

Colwell, J.E. 1974. Vegetation canopy reflectance. *Remote Sensing of Environment*. 3:175-183.

Crist, E.P., and Cicone, R.C. 1984. A physically-based transformation of thematic mapper data—The TM tasseled cap. *IEEE Transactions on Geoscience and Remote Sensing* 22(3): 256–263.

Department of the Army. 1988. Environmental Effects of Army Actions (Army Regulation 200-2). Headquarters, Department of the Army, Washington, D.C.

Department of the Army. 2005. The Army Sustainable Range Program (Army Regulation 350-19). Headquarters, Department of the Army, Washington, D.C.

Dickson, T. L., Wilsey, B. J., Busby, R. R., and Gebhart, D. L. 2008. Grassland plant composition alters vehicular disturbance effects in Kansas, USA. *Environmental Management 41*(5): 676-84.

Doxford, D., and Hill, T. 1998. Land use for Military Training in the UK: The Current Situation, Likely Developments and Possible Alternatives. *Journal of Environmental Planning and Management* 41 (3): 279-297.

Dragoni, D., and Rahman, A. F. 2012. Trends in fall phenology across the deciduous forests of the Eastern USA. *Agricultural and Forest Meteorology* 157: 96-105.

Earth Observing System Data and Information System (EOSDIS). 2009. Earth Observing System ClearingHOuse (ECHO) / Reverb, Version 10.X [online application]. Greenbelt, MD: EOSDIS, Goddard Space Flight Center (GSFC) National Aeronautics and Space Administration (NASA). http://reverb.earthdata.nasa.gov (last accessed November 15, 2013).

Eklundh, L., and Jönsson, P. 2003. Extracting Information about Vegetation Seasons in Africa from Pathfinder AVHRR NDVI Imagery using Temporal Filtering and Least-Squares

Fits to Asymmetric Gaussian Functions. *In Image and Signal Processing for Remote Sensing VIII: Proceedings of Society of Photo-Optical Instrumentation Engineers,* S.S. Serpico Ed. 4885: 215-225.

Eklundh, L., and Jönsson, P. 2010. Timesat 3.0 Software Manual. *Lund University, Sweden.*

Eklundh, L., and Olsson, L. 2003. Vegetation index trends for the African Sahel 1982-1999. *Geophysical Research Letters* 30: 1430-1433.

Eidenshink, J. C., and Faundeen, J. L. 1994. The 1-km AVHRR global land data set: first stages in implementation. *International Journal of Remote Sensing* 15: 3443–3462.

ENVI Online Help. 2005. Vegetation Indices. *ENVI User's Guide*. http://geol.hu/data/online_help/Vegetation_Indices.html (last accessed September 1, 2012).

Freeman, C.C. and L.C. Hulbert. 1985. An annotated list of the vascular flora of Konza Prairie Research Natural Area, Kansas. *Transactions of the Kansas Academy of Science* 88:84-115.

Freeman, C. C. 1998. The flora of Konza Prairie: a historical review and contemporary patterns. In *Grassland Dynamics: Long-term Ecological Research in Tallgrass Prairie*, ed. A. K. Knapp, J. M. Briggs, D. C. Hartnett, and S. L. Collins, 69-80. New York: Oxford University Press.

Geyer, W. A., Carlisle, J., Fick, W. H., and Barbur J. 2000. Weed management on military artillery ranges. *Transactions of the Kansas Academy of Science* 103(1–2): 58–63.

Guretzky, J. A., Anderson, A.B., and Fehmi, J. S. 2006. Grazing and military vehicle effects on grassland soils and vegetation. *Great Plains Research, 16*(1): 51-61.

Hayden, B. P. 1998. Regional climate and the distribution of tallgrass. In *Grassland dynamics: long-term ecological research in tallgrass prairie,* 19-34. Oxford University Press, New York, NY.

Heumann, B.W., Seaquist, J. W., Eklundh, L., and Jönsson, P. 2007. AVHRR Derived Phenological Change in the Sahel and Soudan, Africa, 1982 - 2005. *Remote Sensing of Environment* 108: 385-392.

Hickler, T., Eklundh, L., Seaquist, J., Smith, B., Ardö, J., Olsson, L., Sykes, M., and Sjöström, M. 2005. Precipitation controls Sahel greening trend. *Geophysical Research Letters* 32: L21415.

Hird, J. N., and McDermid, G. J. 2009. Noise reduction of NDVI time series: An empirical comparison of selected techniques. *Remote Sensing of Environment* 113: 248−258.

Hirsch, R. M., and Slack, J. R. 1984. A nonparametric trend test for seasonal data with serial dependence. *Water Resources Research.* 20: 727–32.

Huete, J. R. 1988. A soil adjusted vegetation index (SAVI). *Remote Sensing of Environment* 25: 295–309.

Huete, A., Didan, K., Miura, T., Rodriguez, E.P., Gao, X., and Ferreira, L.G. 2002. Overview of the radiometric and biophysical performance of the MODIS vegetation indices. *Remote Sensing of Environment* 83:195-213.

Huete, A. R., Didan, K., Shimabukuro, Y. E., Ratana, P., Saleska, C. R., Hutyra, L. R., Yang, W., Nemani, R.R., and Myneni, R. 2006. Amazon rainforests green-up with sunlight in dry season. *Geophysical Research Letters*, 33, L06405.

Huete, A., Justice, C., and van Leeuwen, W. 1999. MODIS Vegetation Index (MOD 13): Algorithm Theoretical Basis Document, Ed. 3. University of Arizona, Tuscan, Arizona.

Jackson, R. D., Slater, P. N., and Pinter, P. 1983. Discrimination of growth and water stress in wheat by various vegetation indices through clear and turbid atmospheres. *Remote Sensing of Environment* 13(3): 187-208.

Jacquin, A., Sheeren, D., and Jean-Paul, L. 2009. Vegetation cover degradation assessment in Madagascar savanna based on trend analysis of MODIS NDVI time series. *International Journal of Applied Earth Observations and Geoinformation*. 12S: S3-S10.

Jensen, A. R. 1983. Biophysical Remote Sensing. Annals of the Association of American Geographers, 73(1): 111–132.

Johnson, S., Wang, G., Howard, H., and Anderson, A. 2011. Identification of superfluous roads in terms of sustainable military land carrying capacity and environment. *Journal of Terramechanics* 48: 97-104.

Jones, J., Kimball, J., Lucas, J., and McDonald, K. 2012. Satellite passive microwave detection of North America start of season. *Remote Sensing of Environment* 123: 324-333.

Jönsson, P., and Eklundh, L. 2002. Seasonality extraction by function fitting to time-series of satellite sensor data. *IEEE Transactions on Geoscience and Remote Sensing* 40(8): 1824–1832.

Jönsson, A.M., Eklundh, L., Hellström, M., Bärring, L., and Jönsson, P. 2010. Annual changes in MODIS vegetation indices of Swedish coniferous forests in relation to snow dynamics and tree phenology. *Remote Sensing of Environment* 114: 2719–2730.

Justice, C., and Townshend, J. 2002. Special issue on the moderate resolution imaging spectroradiometer (MODIS): a new generation of land surface monitoring. *Remote Sensing of Environment* 83(1-2): 1-2.

Justice, C.O., Vermote, E., Townshend, J.R.G., DeFries, R., Roy, D.P., Hall, D.K., Salomonson, V.V., Privette, J., Riggs, G., Strahler, A., Lucht, W., Myneni, R., Knjazihhin, Y., Running, S., Nemani, R., Wan, Z., Huete, A., VanLeeuwen, W., Wolfe, R., Giglio, L., Muller, J.- P., Lewis, P., and Barnesley M. 1998. The Moderate Resolution Imaging Spectroradiometer (MODIS): land remote sensing for global change research. *IEEE Transactions on Geoscience and Remote Sensing* 36(4): 1228-1249.

Kansas State University Data Library. 2013. Kansas State University Research and Extension. http://www.ksre.ksu.edu/wdl/ (last accessed November 1, 2013).

Kauth, R.J., and Thomas, G.S. 1976. The Tasseled cap- graphic description of the spectral temporal development of agricultural crops as seen by LANDSAT. *Proceedings of the Symposium Machine Processing of Remote Sensing Data*. LARS, Purdue.

Knapp, A. K., Briggs, J. M., Blair, J. M., and Turner, C. L. 1998. Patterns and controls of aboveground net primary production in tallgrass prairie. In *Grassland dynamics: long-term ecological research in tallgrass prairie,* ed. A. K. Knapp, J. M. Briggs, D. C. Hartnett, and S. L. Collins, 193–221. New York: Oxford University Press.

Kuchler, A.W. 1974. A new vegetation map of Kansas. *Ecology* 55:586-604.

Lambin, E.F., and Strahler, A.H. 1994. Change-Vector Analysis in multitemporal space—A tool to detect and categorize land-cover change processes using high temporal-resolution satellite data. *Remote Sensing of Environment* 48(2): 231–244.

Le Page, Y., Oom, D., Silva, J. M. N., Jönsson, P., and Pereira, J. M. C. 2009. Fire season: climatic driving and human footprint. *Global Ecology and Biogeography* (in press).

Lin, Lawrence I-Kuei. 1989. A Concordance Correlation Coefficient to Evaluate Reproducibility. *Biometrics* 45(1): 255-268.

Linderholm H.W. 2006. Growing season changes in the last century. *Agricultural and Forest Meteorology*. 137:1-14

McGrew, Jr., J.C., and Monroe, C.B. 2000. An Introduction to Statistical Problem Solving in Geography, Second Edition, McGraw-Hill, New York.

Milchunas, D. G., Shulz, K. A., and Shaw, R. B. 1999. Plant community responses to disturbance by mechanized military maneuvers. *Journal of Environmental Quality* 28: 1533-1547.

Milchunas, D. G., Shulz, K. A., and Shaw, R. B. 2000. Plant community structure in relation to long-term disturbance by mechanized military maneuvers in a semiarid region. *Environmental Management* 25: 525-539.

Miura, T., Huete, A. R., & van Leeuwen, W. J. D. 1998. Vegetation detection through smoke-filled AVHRIS images: An assessment using MODIS band passes. Journal of Geophysical Research, 103(D24): 32,001−32,011.

Moser, L. E., and Hoveland, C. S. 1996. Cool-season grass overview. In *Cool-Season Forage Grasses*, L. E. Moser, D. R. Buxton, and M. D. Casler, eds. Pp 1-14. Madison, WI: American Society of Agronomy.

National Resources Conservation Service (NRCS). 2007. Kansas Annual Precipitation. United States Department of Agriculture. KS-08-22. Salina, KS: Resource Conservation Staff. http://www.nrcs.usda.gov/Internet/FSE_DOCUMENTS/nrcs142p2_032018.pdf (last accessed March 1, 2014).

The Nature Conservancy. Tallgrass Prairie Natural Preserve. http://www.nature.org/ourinitiatives/regions/northamerica/unitedstates/kansas/placesweprotect/tallgrass-prairie-national-preserve.xml (last accessed January 30, 2014).

Nellis, M. D., Price, K. P., Rundquist, D. 2009. Remote Sensing of Cropland Agriculture. In *The SAGE Handbook of Remote Sensing*, C-26, 368-380. SAGE Publications.

NIST/SEMATECH. 2003. Introduction to Time Series Analysis. *e-Handbook of Statistical Methods*. http://www.itl.nist.gov/div898/handbook/pmc/section4/pmc4.htm last accessed (September 1, 2012).

O'Connor, B., Dwyer, E., Cawkwell, F., Eklundh, L. 2012. Spatio-temporal patterns in vegetation start of season across the island of Ireland using the MERIS Global Vegetation Index. *ISPRS Journal of Photogrammetry and Remote Sensing*, 68: 79–94.

Ohlenbush, P. D., Bidwell, T., Fick, W. H., Kilgore, G., Scott, W., Davidson, J., Clubine, S., Mayo, J., and Coffin, M. 2001. Sericea lespedeza: history, characteristics, and identification. Publication No. MF-2408. Kansas State University Agricultural Experiment Station and Cooperative Extension Service Manhattan. 6 p.

Olsson, L., Eklundh, L., and Ardö, J. 2005. A recent greening of the Sahel - trends, patterns and potential causes. *Journal of Arid Environments* 63: 556-566.

Omernik, J.M. 1987. Ecoregions of the conterminous United States. Map (scale 1:7,500,000). *Annals of the Association of American Geographers* 77(1):118-125.

Parmesan, C. 2006. Ecological and Evolutionary Responses to Recent Climate Change. *Annual Review of Ecology, Evolution, and Systematics* 37: 637-669.

Pinty, B., Gobron, N., Mélin, F., Verstraete, M. 2002. A Time Composite Algorithm for FAPAR products, Theoretical Basis Document, Institute for Environment and Sustainability. Joint Research Centre, Ispra, Italy, p. 8.

PRISM Climate Group. 2012. US Maximum Temperature 30-arcsec (800m) Normals. http://prism.oregonstate.edu (last accessed, created February 27, 2013).

Prosser, C. W., Sedivec, K. K., and Barker, W. T. 2000. Tracked vehicle effects on vegetation and soil characteristics. *Journal of Range Management* 53(6): 666-670.

Press, W. H., Teukolsky, S. A., Vetterling, W. T., and Flannery, B. P. 1996. Numerical Recipes in Fortran 90: The Art of Parallel Scientific Computing, In *ed. 2 of Fortran Numerical Recipes*, Ed. 2. New York: Cambridge University Press.

Price, K. P., Yu, F., Lee, R., and Ellis, J. E. 2004. Characterizing Ecosystem Variability Using the Onset of Green-Up Derived from Time-Series AVHRR NDVI Data. *GIScience and Remote Sensing* 41: 45-61.

Quist, M. C., Fay, P. A., Guy, C. S., Knapp, A. K., and Rubenstein, B. N. 2003. Military training effects on terrestrial and aquatic communities on a grassland military installation. *Ecological Applications 13*(2): 432-442.

Reed, B. C., Brown, J. F., VanderZee, D., Loveland, T. R., Merchant, J. W., and Ohlen, D. O. 1994. Measuring phenological variability from satellite imagery. *Journal of Vegetation Science* 5: 703-714.

Richardson, A.J., and Wiegand, C.L. 1977. Distinguishing vegetation from soil background information. *Photogrammetric Engineering & Remote Sensing*. 43:1541-1552.

Rouse, J. W., Haas, Jr., R.H., Schell J.A., and Deering, D.W. 1973. Monitoring the vernal advancement and retrogradation (green wave effect) of natural vegetation. *Prog. Rep. RSC* 1978-1, Remote Sensing Center, Texas A&M Univ., College Station, 93p.

Savitzky, A., and Golay, M. J. E. 1964. Smoothing and differentiation of data by simplified least squares procedures. *Analytical Chemistry* 36: 1627– 1639.

Schwarts, M.D. 1998. Green-wave phenology. *Nature* 394: 839-840.

Sellers, P.J. 1985. Canopy reflectance, photosynthesis and transpiration. *International Journal of Remote Sensing* 6:1335-1372.

Seaquist, J. W., Hickler, T., Eklundh, L., Ardö, J., and Heumann, B. 2009. Disentangling the effects of climate and people on Sahel vegetation dynamics. *Biogeosciences* 6: 469-477.

Seaquist, J. W., Olsson, L., Ardö, J., and Eklundh, L. 2006. Broad-scale increase in NPP Quantified for the African Sahel, 1982-1999. *International Journal of Remote Sensing* 27: 5115-5122.

Shaw, R.B., and Diersing, V.E. 1990. Tracked vehicle impacts on vegetation at the Piñon Canyon Maneuver Site, Colorado. *Journal of Environmental Quality* 19: 234-243.

Slater, P. N. 1980. Remote Sensing, Optics and Optical Systems, Addison-Wesley, London.

Solano, R., Didan, K., Jacobson, A., and Huete, A. 2010. MODIS Vegetation Indices (MOD13) C5 User's Guide. Terrestrial Biophysics and Remote Sensing Lab, University of Arizona, Tuscan, Arizona.

Steinier, J., Termonia, Y., and Deltour, J. 1972. Comments on smoothing and differentiation of data by simplified least square procedure. *Analytical Chemistry*. 44: 1906-1909.

Suits, G. H. 1975. The nature of electromagnetic radiation: In *Manual of Remote Sensing*, American Society of Photogrammetry: 51 -73.

Tazik, D. J., Warren, S. D., Diersing, V. E., Shaw, R. B., Brozka, R. J., Bagley, C. F. and Whitworth, W. R. 1992. U.S. Army Land Condition-Trend Analysis (LCTA) Plot inventory field methods. *USACERL Technical Report* N-92/03: 67.

Townshend, J. R. G., and Justice, C. O. 1988. Selecting the spatial resolution of sensors required for global monitoring of land transformations. *International Journal of Remote Sensing* 9: 187-236.

Trumbell, V. L., Dubois, P. C., Brozka, R. J., and Guyette, R. 1994. Military camping impacts on vegetation and soils of the Ozark Plateau. *Journal of Environmental Management*. 40: 329-339.

Tucker, C. J. 1979. Red and photographic infrared linear combinations for monitoring vegetation. *Remote Sensing of Environment*. 8: 127–150.

Tucker, C. J., Dregne, H. E., and Newcomb, W.W. 1991. Expansion and contraction of the Sahara Desert from 1980 to 1990. *Science* 253: 299-301.

U.S. Department of Agriculture, Soil Conservation Service. 1975. Soil Survey of Riley County and Part of Geary County, Kansas. Washington, D.C.: U.S. Government Printing Office.

U.S. Department of Agriculture, National Resources Conservation Service. 2012. Web Soil Survey. http://websoilsurvey.nrcs.usda.gov/ (last accessed May 3, 2013).

U.S. Army. 1994. Integrated natural resource management plan for Fort Riley, Kansas. *Directorate of Engineering and Housing, Environmental and Natural Resources Division*. Berger and Associates, Chicago, Illinois, USA.

Verbesselt, J., Hyndman, R., Newnham, G., Culvenor, D. 2009. Detecting trend and seasonal changes in satellite image time series. *International Journal of Remote Sensing*. 114: 106-115.

Verbesselt, J., Jönsson, P., Lhermitte, S., van Aardt, J., and Coppin, P. 2006. Evaluating satellite and climate data derived indices as fire risk indicators in savanna ecosystems. *IEEE transactions of Geoscience and Remote Sensing* 44: 1622.

Walther, G. R., Post, E., Convey, P., Menze, A., Parmesan, C., Beebee, T. J. C., Fromentin, J. M., Hoegh-Guldberg, O., and Bairlein, F. 2002. Ecological responses to recent climate change. *Nature* 416: 389–395.

Wardlow, B. D. 2005. An Evaluation of Time-Series MODIS 250-Meter Vegetation Index Data for Crop Mapping in the U.S. Central Great Plains. PhD Dissertation, Department of Geography, University of Kansas, Lawrence, Kansas.

White, M. A., Thornton, P. E., and Running, S. W. 1997. A continental phenology model for monitoring vegetation responses to interannual climatic variability. *Global Biogeochemical Cycles* 11: 217–234.

Whitecotton, R. C. A., David, M.B., Darmondy, R.G., and Price, D.L. 2000. Impact of foot traffic from military training on soil and vegetation properties. *Environmental Management.* 26: 697-706.

Wilson, S. D. 1988. The effects of military tank traffic on prairie: A management model. *Environmental Management* 12: 397-403.

Wolfe, R. E., Nishihama, M., Fleig, A. J., Kuyper, J. A., Roy, D. P., Storey, J. C., and Patt, F. S., 2002. Achieving sub-pixel geolocation accuracy in support of MODIS land science. *Remote Sensing of Environment* 83(1-2): 31-49.

Wright, C. K., de Beurs, K. M., Henebry, G. M., 2012. Combined analysis of land cover change and NDVI trends in the Northern Eurasian wheat belt. *Frontier of Earth Science*, 6(2):177–187.

Xiao, X., Braswell, B., Zhang, Q., Boles, S., Frolking, S., & Moore, B., 2003. Sensitivity of vegetation indices to atmospheric aerosols: Continental-scale observations in Northern Asia. *Remote Sensing of Environment*, 84: 385−392.

Xiao, X., Hollinger, D., Aber, J., Goltz, M., Davidson, E. A., Zhang, Q., et al., 2004. Satellite based modeling of gross primary production in an evergreen needle leaf forest. *Remote Sensing of Environment*, 89: 519−534.

Yu, F., Price, K. P., Ellis, J. E., and Kastens, D., 2004. Satellite Observations of the Seasonal Vegetation Growth in Central Asia:1982–1990. *Photogrammetric Engineering & Remote Sensing* 70: 461-469.

Zhang, X., Friedl, M. A., Schaaf, C.B., Strahler, A.H., Hodges, J. C. F., Gao, F., Reed, B. C., and Huete, A., 2003. Monitoring vegetation phenology using MODIS. *Remote Sensing of Environment* 84: 471-475.

Zhang, X., Friedl, M., Schaaf, C., 2009. Sensitivity of vegetation phenology detection to the temporal resolution of satellite data. *International Journal of Remote Sensing* 30 (8): 2061–2074.

Zhou, L., Tucker, C. J., Kaufmann, R. K., Slayback, D., Shabanov, N. V., Myneni, R. B., 2001. Variations in northern vegetation activity inferred from satellite data of vegetation index during 1981–1999. *Journal of Geophysical Research*. 106: 20069–20083.

Appendix A - TIMESAT Input Text File

276
C:\Users\pockrand\Desktop\timesat31_beta\data\fortriley\1.img
C:\Users\pockrand\Desktop\timesat31_beta\data\fortriley\2.img
C:\Users\pockrand\Desktop\timesat31_beta\data\fortriley\3.img
C:\Users\pockrand\Desktop\timesat31_beta\data\fortriley\4.img
C:\Users\pockrand\Desktop\timesat31_beta\data\fortriley\5.img
C:\Users\pockrand\Desktop\timesat31_beta\data\fortriley\6.img
C:\Users\pockrand\Desktop\timesat31_beta\data\fortriley\7.img
C:\Users\pockrand\Desktop\timesat31_beta\data\fortriley\8.img
C:\Users\pockrand\Desktop\timesat31_beta\data\fortriley\9.img
C:\Users\pockrand\Desktop\timesat31_beta\data\fortriley\10.img
C:\Users\pockrand\Desktop\timesat31_beta\data\fortriley\11.img
C:\Users\pockrand\Desktop\timesat31_beta\data\fortriley\12.img
C:\Users\pockrand\Desktop\timesat31_beta\data\fortriley\13.img
C:\Users\pockrand\Desktop\timesat31_beta\data\fortriley\14.img
C:\Users\pockrand\Desktop\timesat31_beta\data\fortriley\15.img
C:\Users\pockrand\Desktop\timesat31_beta\data\fortriley\16.img
C:\Users\pockrand\Desktop\timesat31_beta\data\fortriley\17.img
C:\Users\pockrand\Desktop\timesat31_beta\data\fortriley\18.img
C:\Users\pockrand\Desktop\timesat31_beta\data\fortriley\19.img
C:\Users\pockrand\Desktop\timesat31_beta\data\fortriley\20.img
C:\Users\pockrand\Desktop\timesat31_beta\data\fortriley\21.img
C:\Users\pockrand\Desktop\timesat31_beta\data\fortriley\22.img
C:\Users\pockrand\Desktop\timesat31_beta\data\fortriley\23.img
C:\Users\pockrand\Desktop\timesat31_beta\data\fortriley\24.img
C:\Users\pockrand\Desktop\timesat31_beta\data\fortriley\25.img
C:\Users\pockrand\Desktop\timesat31_beta\data\fortriley\26.img
C:\Users\pockrand\Desktop\timesat31_beta\data\fortriley\27.img
C:\Users\pockrand\Desktop\timesat31_beta\data\fortriley\28.img
C:\Users\pockrand\Desktop\timesat31_beta\data\fortriley\29.img
C:\Users\pockrand\Desktop\timesat31_beta\data\fortriley\30.img
C:\Users\pockrand\Desktop\timesat31_beta\data\fortriley\31.img
C:\Users\pockrand\Desktop\timesat31_beta\data\fortriley\32.img
C:\Users\pockrand\Desktop\timesat31_beta\data\fortriley\33.img
C:\Users\pockrand\Desktop\timesat31_beta\data\fortriley\34.img
C:\Users\pockrand\Desktop\timesat31_beta\data\fortriley\35.img
C:\Users\pockrand\Desktop\timesat31_beta\data\fortriley\36.img
C:\Users\pockrand\Desktop\timesat31_beta\data\fortriley\37.img
C:\Users\pockrand\Desktop\timesat31_beta\data\fortriley\38.img
C:\Users\pockrand\Desktop\timesat31_beta\data\fortriley\39.img
C:\Users\pockrand\Desktop\timesat31_beta\data\fortriley\40.img
C:\Users\pockrand\Desktop\timesat31_beta\data\fortriley\41.img
C:\Users\pockrand\Desktop\timesat31_beta\data\fortriley\42.img
C:\Users\pockrand\Desktop\timesat31_beta\data\fortriley\43.img
C:\Users\pockrand\Desktop\timesat31_beta\data\fortriley\44.img
C:\Users\pockrand\Desktop\timesat31_beta\data\fortriley\45.img
C:\Users\pockrand\Desktop\timesat31_beta\data\fortriley\46.img
C:\Users\pockrand\Desktop\timesat31_beta\data\fortriley\47.img
C:\Users\pockrand\Desktop\timesat31_beta\data\fortriley\48.img
C:\Users\pockrand\Desktop\timesat31_beta\data\fortriley\49.img
C:\Users\pockrand\Desktop\timesat31_beta\data\fortriley\50.img
C:\Users\pockrand\Desktop\timesat31_beta\data\fortriley\51.img
C:\Users\pockrand\Desktop\timesat31_beta\data\fortriley\52.img
C:\Users\pockrand\Desktop\timesat31_beta\data\fortriley\53.img
C:\Users\pockrand\Desktop\timesat31_beta\data\fortriley\54.img
C:\Users\pockrand\Desktop\timesat31_beta\data\fortriley\55.img
C:\Users\pockrand\Desktop\timesat31_beta\data\fortriley\56.img
C:\Users\pockrand\Desktop\timesat31_beta\data\fortriley\57.img
C:\Users\pockrand\Desktop\timesat31_beta\data\fortriley\58.img
C:\Users\pockrand\Desktop\timesat31_beta\data\fortriley\59.img
C:\Users\pockrand\Desktop\timesat31_beta\data\fortriley\60.img
C:\Users\pockrand\Desktop\timesat31_beta\data\fortriley\61.img
C:\Users\pockrand\Desktop\timesat31_beta\data\fortriley\62.img
C:\Users\pockrand\Desktop\timesat31_beta\data\fortriley\63.img
C:\Users\pockrand\Desktop\timesat31_beta\data\fortriley\64.img
C:\Users\pockrand\Desktop\timesat31_beta\data\fortriley\65.img

C:\Users\pockrand\Desktop\timesat31_beta\data\fortriley\66.img
C:\Users\pockrand\Desktop\timesat31_beta\data\fortriley\67.img
C:\Users\pockrand\Desktop\timesat31_beta\data\fortriley\68.img
C:\Users\pockrand\Desktop\timesat31_beta\data\fortriley\69.img
C:\Users\pockrand\Desktop\timesat31_beta\data\fortriley\70.img
C:\Users\pockrand\Desktop\timesat31_beta\data\fortriley\71.img
C:\Users\pockrand\Desktop\timesat31_beta\data\fortriley\72.img
C:\Users\pockrand\Desktop\timesat31_beta\data\fortriley\73.img
C:\Users\pockrand\Desktop\timesat31_beta\data\fortriley\74.img
C:\Users\pockrand\Desktop\timesat31_beta\data\fortriley\75.img
C:\Users\pockrand\Desktop\timesat31_beta\data\fortriley\76.img
C:\Users\pockrand\Desktop\timesat31_beta\data\fortriley\77.img
C:\Users\pockrand\Desktop\timesat31_beta\data\fortriley\78.img
C:\Users\pockrand\Desktop\timesat31_beta\data\fortriley\79.img
C:\Users\pockrand\Desktop\timesat31_beta\data\fortriley\80.img
C:\Users\pockrand\Desktop\timesat31_beta\data\fortriley\81.img
C:\Users\pockrand\Desktop\timesat31_beta\data\fortriley\82.img
C:\Users\pockrand\Desktop\timesat31_beta\data\fortriley\83.img
C:\Users\pockrand\Desktop\timesat31_beta\data\fortriley\84.img
C:\Users\pockrand\Desktop\timesat31_beta\data\fortriley\85.img
C:\Users\pockrand\Desktop\timesat31_beta\data\fortriley\86.img
C:\Users\pockrand\Desktop\timesat31_beta\data\fortriley\87.img
C:\Users\pockrand\Desktop\timesat31_beta\data\fortriley\88.img
C:\Users\pockrand\Desktop\timesat31_beta\data\fortriley\89.img
C:\Users\pockrand\Desktop\timesat31_beta\data\fortriley\90.img
C:\Users\pockrand\Desktop\timesat31_beta\data\fortriley\91.img
C:\Users\pockrand\Desktop\timesat31_beta\data\fortriley\92.img
C:\Users\pockrand\Desktop\timesat31_beta\data\fortriley\93.img
C:\Users\pockrand\Desktop\timesat31_beta\data\fortriley\94.img
C:\Users\pockrand\Desktop\timesat31_beta\data\fortriley\95.img
C:\Users\pockrand\Desktop\timesat31_beta\data\fortriley\96.img
C:\Users\pockrand\Desktop\timesat31_beta\data\fortriley\97.img
C:\Users\pockrand\Desktop\timesat31_beta\data\fortriley\98.img
C:\Users\pockrand\Desktop\timesat31_beta\data\fortriley\99.img
C:\Users\pockrand\Desktop\timesat31_beta\data\fortriley\100.img
C:\Users\pockrand\Desktop\timesat31_beta\data\fortriley\101.img
C:\Users\pockrand\Desktop\timesat31_beta\data\fortriley\102.img
C:\Users\pockrand\Desktop\timesat31_beta\data\fortriley\103.img
C:\Users\pockrand\Desktop\timesat31_beta\data\fortriley\104.img
C:\Users\pockrand\Desktop\timesat31_beta\data\fortriley\105.img
C:\Users\pockrand\Desktop\timesat31_beta\data\fortriley\106.img
C:\Users\pockrand\Desktop\timesat31_beta\data\fortriley\107.img
C:\Users\pockrand\Desktop\timesat31_beta\data\fortriley\108.img
C:\Users\pockrand\Desktop\timesat31_beta\data\fortriley\109.img
C:\Users\pockrand\Desktop\timesat31_beta\data\fortriley\110.img
C:\Users\pockrand\Desktop\timesat31_beta\data\fortriley\111.img
C:\Users\pockrand\Desktop\timesat31_beta\data\fortriley\112.img
C:\Users\pockrand\Desktop\timesat31_beta\data\fortriley\113.img
C:\Users\pockrand\Desktop\timesat31_beta\data\fortriley\114.img
C:\Users\pockrand\Desktop\timesat31_beta\data\fortriley\115.img
C:\Users\pockrand\Desktop\timesat31_beta\data\fortriley\116.img
C:\Users\pockrand\Desktop\timesat31_beta\data\fortriley\117.img
C:\Users\pockrand\Desktop\timesat31_beta\data\fortriley\118.img
C:\Users\pockrand\Desktop\timesat31_beta\data\fortriley\119.img
C:\Users\pockrand\Desktop\timesat31_beta\data\fortriley\120.img
C:\Users\pockrand\Desktop\timesat31_beta\data\fortriley\121.img
C:\Users\pockrand\Desktop\timesat31_beta\data\fortriley\122.img
C:\Users\pockrand\Desktop\timesat31_beta\data\fortriley\123.img
C:\Users\pockrand\Desktop\timesat31_beta\data\fortriley\124.img
C:\Users\pockrand\Desktop\timesat31_beta\data\fortriley\125.img
C:\Users\pockrand\Desktop\timesat31_beta\data\fortriley\126.img
C:\Users\pockrand\Desktop\timesat31_beta\data\fortriley\127.img
C:\Users\pockrand\Desktop\timesat31_beta\data\fortriley\128.img
C:\Users\pockrand\Desktop\timesat31_beta\data\fortriley\129.img
C:\Users\pockrand\Desktop\timesat31_beta\data\fortriley\130.img
C:\Users\pockrand\Desktop\timesat31_beta\data\fortriley\131.img
C:\Users\pockrand\Desktop\timesat31_beta\data\fortriley\132.img
C:\Users\pockrand\Desktop\timesat31_beta\data\fortriley\133.img
C:\Users\pockrand\Desktop\timesat31_beta\data\fortriley\134.img
C:\Users\pockrand\Desktop\timesat31_beta\data\fortriley\135.img

C:\Users\pockrand\Desktop\timesat31_beta\data\fortriley\136.img
C:\Users\pockrand\Desktop\timesat31_beta\data\fortriley\137.img
C:\Users\pockrand\Desktop\timesat31_beta\data\fortriley\138.img
C:\Users\pockrand\Desktop\timesat31_beta\data\fortriley\139.img
C:\Users\pockrand\Desktop\timesat31_beta\data\fortriley\140.img
C:\Users\pockrand\Desktop\timesat31_beta\data\fortriley\141.img
C:\Users\pockrand\Desktop\timesat31_beta\data\fortriley\142.img
C:\Users\pockrand\Desktop\timesat31_beta\data\fortriley\143.img
C:\Users\pockrand\Desktop\timesat31_beta\data\fortriley\144.img
C:\Users\pockrand\Desktop\timesat31_beta\data\fortriley\145.img
C:\Users\pockrand\Desktop\timesat31_beta\data\fortriley\146.img
C:\Users\pockrand\Desktop\timesat31_beta\data\fortriley\147.img
C:\Users\pockrand\Desktop\timesat31_beta\data\fortriley\148.img
C:\Users\pockrand\Desktop\timesat31_beta\data\fortriley\149.img
C:\Users\pockrand\Desktop\timesat31_beta\data\fortriley\150.img
C:\Users\pockrand\Desktop\timesat31_beta\data\fortriley\151.img
C:\Users\pockrand\Desktop\timesat31_beta\data\fortriley\152.img
C:\Users\pockrand\Desktop\timesat31_beta\data\fortriley\153.img
C:\Users\pockrand\Desktop\timesat31_beta\data\fortriley\154.img
C:\Users\pockrand\Desktop\timesat31_beta\data\fortriley\155.img
C:\Users\pockrand\Desktop\timesat31_beta\data\fortriley\156.img
C:\Users\pockrand\Desktop\timesat31_beta\data\fortriley\157.img
C:\Users\pockrand\Desktop\timesat31_beta\data\fortriley\158.img
C:\Users\pockrand\Desktop\timesat31_beta\data\fortriley\159.img
C:\Users\pockrand\Desktop\timesat31_beta\data\fortriley\160.img
C:\Users\pockrand\Desktop\timesat31_beta\data\fortriley\161.img
C:\Users\pockrand\Desktop\timesat31_beta\data\fortriley\162.img
C:\Users\pockrand\Desktop\timesat31_beta\data\fortriley\163.img
C:\Users\pockrand\Desktop\timesat31_beta\data\fortriley\164.img
C:\Users\pockrand\Desktop\timesat31_beta\data\fortriley\165.img
C:\Users\pockrand\Desktop\timesat31_beta\data\fortriley\166.img
C:\Users\pockrand\Desktop\timesat31_beta\data\fortriley\167.img
C:\Users\pockrand\Desktop\timesat31_beta\data\fortriley\168.img
C:\Users\pockrand\Desktop\timesat31_beta\data\fortriley\169.img
C:\Users\pockrand\Desktop\timesat31_beta\data\fortriley\170.img
C:\Users\pockrand\Desktop\timesat31_beta\data\fortriley\171.img
C:\Users\pockrand\Desktop\timesat31_beta\data\fortriley\172.img
C:\Users\pockrand\Desktop\timesat31_beta\data\fortriley\173.img
C:\Users\pockrand\Desktop\timesat31_beta\data\fortriley\174.img
C:\Users\pockrand\Desktop\timesat31_beta\data\fortriley\175.img
C:\Users\pockrand\Desktop\timesat31_beta\data\fortriley\176.img
C:\Users\pockrand\Desktop\timesat31_beta\data\fortriley\177.img
C:\Users\pockrand\Desktop\timesat31_beta\data\fortriley\178.img
C:\Users\pockrand\Desktop\timesat31_beta\data\fortriley\179.img
C:\Users\pockrand\Desktop\timesat31_beta\data\fortriley\180.img
C:\Users\pockrand\Desktop\timesat31_beta\data\fortriley\181.img
C:\Users\pockrand\Desktop\timesat31_beta\data\fortriley\182.img
C:\Users\pockrand\Desktop\timesat31_beta\data\fortriley\183.img
C:\Users\pockrand\Desktop\timesat31_beta\data\fortriley\184.img
C:\Users\pockrand\Desktop\timesat31_beta\data\fortriley\185.img
C:\Users\pockrand\Desktop\timesat31_beta\data\fortriley\186.img
C:\Users\pockrand\Desktop\timesat31_beta\data\fortriley\187.img
C:\Users\pockrand\Desktop\timesat31_beta\data\fortriley\188.img
C:\Users\pockrand\Desktop\timesat31_beta\data\fortriley\189.img
C:\Users\pockrand\Desktop\timesat31_beta\data\fortriley\190.img
C:\Users\pockrand\Desktop\timesat31_beta\data\fortriley\191.img
C:\Users\pockrand\Desktop\timesat31_beta\data\fortriley\192.img
C:\Users\pockrand\Desktop\timesat31_beta\data\fortriley\193.img
C:\Users\pockrand\Desktop\timesat31_beta\data\fortriley\194.img
C:\Users\pockrand\Desktop\timesat31_beta\data\fortriley\195.img
C:\Users\pockrand\Desktop\timesat31_beta\data\fortriley\196.img
C:\Users\pockrand\Desktop\timesat31_beta\data\fortriley\197.img
C:\Users\pockrand\Desktop\timesat31_beta\data\fortriley\198.img
C:\Users\pockrand\Desktop\timesat31_beta\data\fortriley\199.img
C:\Users\pockrand\Desktop\timesat31_beta\data\fortriley\200.img
C:\Users\pockrand\Desktop\timesat31_beta\data\fortriley\201.img
C:\Users\pockrand\Desktop\timesat31_beta\data\fortriley\202.img
C:\Users\pockrand\Desktop\timesat31_beta\data\fortriley\203.img
C:\Users\pockrand\Desktop\timesat31_beta\data\fortriley\204.img
C:\Users\pockrand\Desktop\timesat31_beta\data\fortriley\205.img

C:\Users\pockrand\Desktop\timesat31_beta\data\fortriley\206.img
C:\Users\pockrand\Desktop\timesat31_beta\data\fortriley\207.img
C:\Users\pockrand\Desktop\timesat31_beta\data\fortriley\208.img
C:\Users\pockrand\Desktop\timesat31_beta\data\fortriley\209.img
C:\Users\pockrand\Desktop\timesat31_beta\data\fortriley\210.img
C:\Users\pockrand\Desktop\timesat31_beta\data\fortriley\211.img
C:\Users\pockrand\Desktop\timesat31_beta\data\fortriley\212.img
C:\Users\pockrand\Desktop\timesat31_beta\data\fortriley\213.img
C:\Users\pockrand\Desktop\timesat31_beta\data\fortriley\214.img
C:\Users\pockrand\Desktop\timesat31_beta\data\fortriley\215.img
C:\Users\pockrand\Desktop\timesat31_beta\data\fortriley\216.img
C:\Users\pockrand\Desktop\timesat31_beta\data\fortriley\217.img
C:\Users\pockrand\Desktop\timesat31_beta\data\fortriley\218.img
C:\Users\pockrand\Desktop\timesat31_beta\data\fortriley\219.img
C:\Users\pockrand\Desktop\timesat31_beta\data\fortriley\220.img
C:\Users\pockrand\Desktop\timesat31_beta\data\fortriley\221.img
C:\Users\pockrand\Desktop\timesat31_beta\data\fortriley\222.img
C:\Users\pockrand\Desktop\timesat31_beta\data\fortriley\223.img
C:\Users\pockrand\Desktop\timesat31_beta\data\fortriley\224.img
C:\Users\pockrand\Desktop\timesat31_beta\data\fortriley\225.img
C:\Users\pockrand\Desktop\timesat31_beta\data\fortriley\226.img
C:\Users\pockrand\Desktop\timesat31_beta\data\fortriley\227.img
C:\Users\pockrand\Desktop\timesat31_beta\data\fortriley\228.img
C:\Users\pockrand\Desktop\timesat31_beta\data\fortriley\229.img
C:\Users\pockrand\Desktop\timesat31_beta\data\fortriley\230.img
C:\Users\pockrand\Desktop\timesat31_beta\data\fortriley\231.img
C:\Users\pockrand\Desktop\timesat31_beta\data\fortriley\232.img
C:\Users\pockrand\Desktop\timesat31_beta\data\fortriley\233.img
C:\Users\pockrand\Desktop\timesat31_beta\data\fortriley\234.img
C:\Users\pockrand\Desktop\timesat31_beta\data\fortriley\235.img
C:\Users\pockrand\Desktop\timesat31_beta\data\fortriley\236.img
C:\Users\pockrand\Desktop\timesat31_beta\data\fortriley\237.img
C:\Users\pockrand\Desktop\timesat31_beta\data\fortriley\238.img
C:\Users\pockrand\Desktop\timesat31_beta\data\fortriley\239.img
C:\Users\pockrand\Desktop\timesat31_beta\data\fortriley\240.img
C:\Users\pockrand\Desktop\timesat31_beta\data\fortriley\241.img
C:\Users\pockrand\Desktop\timesat31_beta\data\fortriley\242.img
C:\Users\pockrand\Desktop\timesat31_beta\data\fortriley\243.img
C:\Users\pockrand\Desktop\timesat31_beta\data\fortriley\244.img
C:\Users\pockrand\Desktop\timesat31_beta\data\fortriley\245.img
C:\Users\pockrand\Desktop\timesat31_beta\data\fortriley\246.img
C:\Users\pockrand\Desktop\timesat31_beta\data\fortriley\247.img
C:\Users\pockrand\Desktop\timesat31_beta\data\fortriley\248.img
C:\Users\pockrand\Desktop\timesat31_beta\data\fortriley\249.img
C:\Users\pockrand\Desktop\timesat31_beta\data\fortriley\250.img
C:\Users\pockrand\Desktop\timesat31_beta\data\fortriley\251.img
C:\Users\pockrand\Desktop\timesat31_beta\data\fortriley\252.img
C:\Users\pockrand\Desktop\timesat31_beta\data\fortriley\253.img
C:\Users\pockrand\Desktop\timesat31_beta\data\fortriley\254.img
C:\Users\pockrand\Desktop\timesat31_beta\data\fortriley\255.img
C:\Users\pockrand\Desktop\timesat31_beta\data\fortriley\256.img
C:\Users\pockrand\Desktop\timesat31_beta\data\fortriley\257.img
C:\Users\pockrand\Desktop\timesat31_beta\data\fortriley\258.img
C:\Users\pockrand\Desktop\timesat31_beta\data\fortriley\259.img
C:\Users\pockrand\Desktop\timesat31_beta\data\fortriley\260.img
C:\Users\pockrand\Desktop\timesat31_beta\data\fortriley\261.img
C:\Users\pockrand\Desktop\timesat31_beta\data\fortriley\262.img
C:\Users\pockrand\Desktop\timesat31_beta\data\fortriley\263.img
C:\Users\pockrand\Desktop\timesat31_beta\data\fortriley\264.img
C:\Users\pockrand\Desktop\timesat31_beta\data\fortriley\265.img
C:\Users\pockrand\Desktop\timesat31_beta\data\fortriley\266.img
C:\Users\pockrand\Desktop\timesat31_beta\data\fortriley\267.img
C:\Users\pockrand\Desktop\timesat31_beta\data\fortriley\268.img
C:\Users\pockrand\Desktop\timesat31_beta\data\fortriley\269.img
C:\Users\pockrand\Desktop\timesat31_beta\data\fortriley\270.img
C:\Users\pockrand\Desktop\timesat31_beta\data\fortriley\271.img
C:\Users\pockrand\Desktop\timesat31_beta\data\fortriley\272.img
C:\Users\pockrand\Desktop\timesat31_beta\data\fortriley\273.img
C:\Users\pockrand\Desktop\timesat31_beta\data\fortriley\274.img
C:\Users\pockrand\Desktop\timesat31_beta\data\fortriley\275.img

C:\Users\pockrand\Desktop\timesat31_beta\data\fortriley\276.img

Appendix B - SAS Code for Sensitivity Analysis

```
************************************************************************;
* Bryanna Pockrandt Project: Systematic Phenometric Sensitivity Analysis *;
************************************************************************;


*Importing the Beg_Fort Data from Excel to SAS;
 proc import out=Beg_Fort
   datafile='C:\Desktop\FINAL.xlsx'
   dbms=xlsx
   replace;
   sheet="Beg";
   getnames=yes;
 run;


*Importing the End_Fort Data from Excel to SAS;
 proc import out=End_Fort
   datafile='C:\Desktop\FINAL.xlsx'
   dbms=xlsx
   replace;
   sheet="End";
   getnames=yes;
 run;


*Importing the Length_Fort Data from Excel to SAS;
 proc import out=Length_Fort
   datafile='C:\Desktop\FINAL.xlsx'
   dbms=xlsx
   replace;
   sheet="Length";
   getnames=yes;
 run;


*Importing the Max_Fort Data from Excel to SAS;
 proc import out=Max_Fort
   datafile='C:\Desktop\FINAL.xlsx'
   dbms=xlsx
   replace;
   sheet="Max";
   getnames=yes;
 run;
```

```
*Importing the Sint_Fort Data from Excel to SAS;
 proc import out=Sint_Fort
   datafile='C:\Desktop\FINAL.xlsx'
   dbms=xlsx
   replace;
   sheet="Sint";
   getnames=yes;
 run;


******************************************;
* Macro for Lin's Concordance Coefficient ;
******************************************;
*NOTE: The following macro calculates Lin's concordance coefficent (rc) and lower and upper CI
       for ONE pair of the above variables in the PROC CORR VAR statement;
*NOTE: run the macro to get Lin's rc for each pair of variables;
%macro concorr(x, y, yname, title);

 data Model;
   set pstats;
   keep _TYPE_ _NAME_ &x &y;
 run;

 data ModelM; set Model;
   if _TYPE_ ='MEAN';
   *getting xbar-ybar for the two variables in the corr;
   xbar=&x;
   ybar=&y;
   diffmean=&x - &y;
   keep xbar ybar diffmean;
 run;

 data ModelS; set Model;
   if _TYPE_='STD';
   *getting the ratio of SDs for the two variables in the corr;
   sdx=&x;
   sdy=&y;
   keep sdy sdx;
 run;

 data ModelN; set Model;
   if _TYPE_='N';
   n=min(&x,&y);
 run;

 data ModelC; set Model;
```

```
  if _TYPE_='CORR' and _NAME_=&yname;
  r=&x;
run;

data all;
  merge modelM modelS modelN modelC;
run;

data all; set all;
  keep n xbar ybar diffmean sdx sdy r;
run;

data all2; set all;
  u=diffmean/sqrt(sdy*sdx);
  usq=u**2;
  v=sdy/sdx;
  cb=2*(1/(v+(1/v)+usq));
  rc=r*cb;
  z=.5*log((1+rc)/(1-rc));
  sig2z=(1/(n-2))*
        ( ( (1-r**2)*(rc**2))/((1-rc**2)*(r**2)       )
         +( (4*(rc**3)*(1-rc)*usq)/(r*((1-rc**2)**2)) )
                              -( (2*(rc**4)*(u**4))/((r**2)*((1-rc**2)**2))  )  );
  lz=z - 1.96*sqrt(sig2z);
  uz=z + 1.96*sqrt(sig2z);
  lrc=(exp(2*lz)-1)/(exp(2*lz)+1);
  urc=(exp(2*uz)-1)/(exp(2*uz)+1);
  if (r>=.9 & rc>=.9) then thres_90='*'; else thres_90='.';
  if (r>=.9 & rc>=.9) then Threshold='>= 0.90'; else Threshold='< 0.90';
  if abs(r-rc)<.05 then rdiff_05='+'; else rdiff_05='.';
  if .05 <= abs(r-rc)<.10 then rdiff_05_10='#'; else rdiff_05_10='.';
  if abs(r-rc)<.05 then Difference='Below'; else if (.05<=abs(r-rc)<.10) then Difference='Between'; else Difference='Over';
run;

proc print data=all2;
  var n xbar ybar diffmean sdx sdy u v r cb lrc rc urc;
  title3 'Concordance Coefficient: Print-out of all pieces for the calculation';
  title4 &title;
run;

proc print data=all2;
  var r rc thres_90 rdiff_05 rdiff_05_10;
  title3 'Comparison between Pearson & Lin Concordance Correlation Coefficient';
  title4 &title;
run;

proc freq data=all2;
```

```
   tables Threshold*Difference / norow nocol nopercent;;
 run;


%mend concorr;


%macro sensitivity(data);

 proc corr data=&data /*cov*/ outp=pstats noprint;
   *NOTE: Give the list of variables to be correlated in the VAR statement;
   var E1_WS4_SOS20
       E2_WS3_SOS20 E2_WS4_SOS10 E2_WS4_SOS20 E2_WS4_SOS25 E2_WS4_SOS30 E2_WS5_SOS20
       E3_WS4_SOS20;
   by Season;
   title3 'CORR Results' ;
 run;

 *Preliminary Comparisons for Sensity Analysis;
   /* Adjusts Filter Settings 1 Parameter at a time */
       /* Treats E2_WS4_SOS20 as Gold Standard */
  %concorr(E2_WS4_SOS20, E2_WS4_SOS10, 'E2_WS4_SOS10','E2_WS4_SOS20 and E2_WS4_SOS10');
  %concorr(E2_WS4_SOS20, E2_WS4_SOS25, 'E2_WS4_SOS25','E2_WS4_SOS20 and E2_WS4_SOS25');
  %concorr(E2_WS4_SOS20, E2_WS4_SOS30, 'E2_WS4_SOS30','E2_WS4_SOS20 and E2_WS4_SOS30');
  %concorr(E2_WS4_SOS20, E2_WS3_SOS20, 'E2_WS3_SOS20','E2_WS4_SOS20 and E2_WS3_SOS20');
  %concorr(E2_WS4_SOS20, E2_WS5_SOS20, 'E2_WS5_SOS20','E2_WS4_SOS20 and E2_WS5_SOS20');
  %concorr(E2_WS4_SOS20, E1_WS4_SOS20, 'E1_WS4_SOS20','E2_WS4_SOS20 and E1_WS4_SOS20');
  %concorr(E2_WS4_SOS20, E3_WS4_SOS20, 'E3_WS4_SOS20','E2_WS4_SOS20 and E3_WS4_SOS20');


%mend sensitivity;


ods rtf file = "C:\Desktop\Systematic Statistical Analysis on Phenometric Sensitivity Analysis (Bryanna Pockrandt).doc";

title 'Systematic Phenometric Sensitivity Analysis (Bryanna Pockrandt)';


title2 'Beginning of the Season for Fort Riley';
%sensitivity(Beg_Fort);

title2 'End of the Season for Fort Riley';
%sensitivity(End_Fort);

title2 'Length of the Season for Fort Riley';
%sensitivity(Length_Fort);
```

```
title2 'Maximum Value of the Season for Fort Riley';
%sensitivity(Max_Fort);

title2 'Small Integral of the Season for Fort Riley';
%sensitivity(Sint_Fort);


ods rtf close;



%macro season_plot(var,x,y,seas);

  data diag;
    set &var;
    where Season=&seas;
    z1=&x;
    z2=&x;
  run;

 *Specifies conditions for symbols used in the plots;
  symbol1 value=circle  height=0.75 cv=blue width=1;
  symbol2 value=diamond height=0.25 cv=red  width=1 interpol=join;

 *Generates a Lins Concordance Correlation Plot;
  proc gplot data=diag;
    plot &y*&x z2*z1 / overlay ;
  run;

%mend season_plot;


%macro settings_plot(var,x,y);

 title4 'Season 1';
 %season_plot(&var,&x,&y,1);

 title4 'Season 2';
 %season_plot(&var,&x,&y,2);

 title4 'Season 3';
 %season_plot(&var,&x,&y,3);

 title4 'Season 4';
 %season_plot(&var,&x,&y,4);

 title4 'Season 5';
```

```
 %season_plot(&var,&x,&y,5);

 title4 'Season 6';
 %season_plot(&var,&x,&y,6);

 title4 'Season 7';
 %season_plot(&var,&x,&y,7);

 title4 'Season 8';
 %season_plot(&var,&x,&y,8);

 title4 'Season 9';
 %season_plot(&var,&x,&y,9);

 title4 'Season 10';
 %season_plot(&var,&x,&y,10);

 title4 'Season 11';
 %season_plot(&var,&x,&y,11);

%mend settings_plot;


%macro var_plot(var);

 title3 'E2_WS4_SOS20 and E2_WS4_SOS10';
 %settings_plot(&var,E2_WS4_SOS20,E2_WS4_SOS10);

 title3 'E2_WS4_SOS20 and E2_WS4_SOS25';
 %settings_plot(&var,E2_WS4_SOS20,E2_WS4_SOS25);

 title3 'E2_WS4_SOS20 and E2_WS4_SOS30';
 %settings_plot(&var,E2_WS4_SOS20,E2_WS4_SOS30);

 title3 'E2_WS4_SOS20 and E2_WS3_SOS20';
 %settings_plot(&var,E2_WS4_SOS20,E2_WS3_SOS20);

 title3 'E2_WS4_SOS20 and E2_WS5_SOS20';
 %settings_plot(&var,E2_WS4_SOS20,E2_WS5_SOS20);

 title3 'E2_WS4_SOS20 and E1_WS4_SOS20';
 %settings_plot(&var,E2_WS4_SOS20,E1_WS4_SOS20);

 title3 'E2_WS4_SOS20 and E3_WS4_SOS20';
 %settings_plot(&var,E2_WS4_SOS20,E3_WS4_SOS20);

%mend var_plot;
```

```
ods rtf file = "C:\Desktop\Plots for Phenometric Sensitivity Analysis (Beg_Fort).doc";

 title 'Plots for Phenometric Sensitivity Analysis (Bryanna Pockrandt)';

 title2 'Beginning of the Season for Fort Riley';
 %var_plot(Beg_Fort);

ods rtf close;


ods rtf file = "C:\Desktop\Plots for Phenometric Sensitivity Analysis (End_Fort).doc";

 title 'Plots for Phenometric Sensitivity Analysis (Bryanna Pockrandt)';

 title2 'End of the Season for Fort Riley';
 %var_plot(End_Fort);

ods rtf close;


ods rtf file = "C:\Desktop\Plots for Phenometric Sensitivity Analysis (Length_Fort).doc";

 title 'Plots for Phenometric Sensitivity Analysis (Bryanna Pockrandt)';

 title2 'Length of the Season for Fort Riley';
 %var_plot(Length_Fort);

ods rtf close;



ods rtf file = "C:\Desktop\Plots for Phenometric Sensitivity Analysis (Max_Fort).doc";

 title 'Plots for Phenometric Sensitivity Analysis (Bryanna Pockrandt)';

 title2 'Maximum Value of the Season for Fort Riley';
 %var_plot(Max_Fort);

ods rtf close;



ods rtf file = "C:\Desktop\Plots for Phenometric Sensitivity Analysis (Sint_Fort).doc";

 title 'Plots for Phenometric Sensitivity Analysis (Bryanna Pockrandt)';
```

```
 title2 'Small Integral of the Season for Fort Riley';
 %var_plot(Sint_Fort);

ods rtf close;


***********************************************;
* Previous Comparisons for Sensitivity Analysis ;
***********************************************;

 *Combinations for Envelope Iteration = 1;
 %concorr(E1_WS3_SOS10, E1_WS3_SOS30, 'E1_WS3_SOS30','E1_WS3_SOS10 and E1_WS3_SOS30');
 %concorr(E1_WS3_SOS10, E1_WS4_SOS10, 'E1_WS4_SOS10','E1_WS3_SOS10 and E1_WS4_SOS10');
 %concorr(E1_WS3_SOS10, E1_WS4_SOS20, 'E1_WS4_SOS20','E1_WS3_SOS10 and E1_WS4_SOS20');
 %concorr(E1_WS3_SOS10, E1_WS4_SOS25, 'E1_WS4_SOS25','E1_WS3_SOS10 and E1_WS4_SOS25');
 %concorr(E1_WS3_SOS10, E1_WS4_SOS30, 'E1_WS4_SOS30','E1_WS3_SOS10 and E1_WS4_SOS30');
 %concorr(E1_WS3_SOS10, E1_WS5_SOS10, 'E1_WS5_SOS10','E1_WS3_SOS10 and E1_WS5_SOS10');
 %concorr(E1_WS3_SOS10, E1_WS5_SOS30, 'E1_WS5_SOS30','E1_WS3_SOS10 and E1_WS5_SOS30');

 %concorr(E1_WS3_SOS30, E1_WS4_SOS10, 'E1_WS4_SOS10','E1_WS3_SOS30 and E1_WS4_SOS10');
 %concorr(E1_WS3_SOS30, E1_WS4_SOS20, 'E1_WS4_SOS20','E1_WS3_SOS30 and E1_WS4_SOS20');
 %concorr(E1_WS3_SOS30, E1_WS4_SOS25, 'E1_WS4_SOS25','E1_WS3_SOS30 and E1_WS4_SOS25');
 %concorr(E1_WS3_SOS30, E1_WS4_SOS30, 'E1_WS4_SOS30','E1_WS3_SOS30 and E1_WS4_SOS30');
 %concorr(E1_WS3_SOS30, E1_WS5_SOS10, 'E1_WS5_SOS10','E1_WS3_SOS30 and E1_WS5_SOS10');
 %concorr(E1_WS3_SOS30, E1_WS5_SOS30, 'E1_WS5_SOS30','E1_WS3_SOS30 and E1_WS5_SOS30');

 %concorr(E1_WS4_SOS10, E1_WS4_SOS20, 'E1_WS4_SOS20','E1_WS4_SOS10 and E1_WS4_SOS20');
 %concorr(E1_WS4_SOS10, E1_WS4_SOS25, 'E1_WS4_SOS25','E1_WS4_SOS10 and E1_WS4_SOS25');
 %concorr(E1_WS4_SOS10, E1_WS4_SOS30, 'E1_WS4_SOS30','E1_WS4_SOS10 and E1_WS4_SOS30');
 %concorr(E1_WS4_SOS10, E1_WS5_SOS10, 'E1_WS5_SOS10','E1_WS4_SOS10 and E1_WS5_SOS10');
 %concorr(E1_WS4_SOS10, E1_WS5_SOS30, 'E1_WS5_SOS30','E1_WS4_SOS10 and E1_WS5_SOS30');

 %concorr(E1_WS4_SOS20, E1_WS4_SOS25, 'E1_WS4_SOS25','E1_WS4_SOS20 and E1_WS4_SOS25');
 %concorr(E1_WS4_SOS20, E1_WS4_SOS30, 'E1_WS4_SOS30','E1_WS4_SOS20 and E1_WS4_SOS30');
 %concorr(E1_WS4_SOS20, E1_WS5_SOS10, 'E1_WS5_SOS10','E1_WS4_SOS20 and E1_WS5_SOS10');
 %concorr(E1_WS4_SOS20, E1_WS5_SOS30, 'E1_WS5_SOS30','E1_WS4_SOS20 and E1_WS5_SOS30');

 %concorr(E1_WS4_SOS25, E1_WS4_SOS30, 'E1_WS4_SOS30','E1_WS4_SOS25 and E1_WS4_SOS30');
 %concorr(E1_WS4_SOS25, E1_WS5_SOS10, 'E1_WS5_SOS10','E1_WS4_SOS25 and E1_WS5_SOS10');
 %concorr(E1_WS4_SOS25, E1_WS5_SOS30, 'E1_WS5_SOS30','E1_WS4_SOS25 and E1_WS5_SOS30');

 %concorr(E1_WS4_SOS30, E1_WS5_SOS10, 'E1_WS5_SOS10','E1_WS4_SOS30 and E1_WS5_SOS10');
 %concorr(E1_WS4_SOS30, E1_WS5_SOS30, 'E1_WS5_SOS30','E1_WS4_SOS30 and E1_WS5_SOS30');

 %concorr(E1_WS5_SOS10, E1_WS5_SOS30, 'E1_WS5_SOS30','E1_WS5_SOS10 and E1_WS5_SOS30');
```

```
*Combinations for Envelope Iteration = 2;
%concorr(E2_WS3_SOS10, E2_WS3_SOS30, 'E2_WS3_SOS30','E2_WS3_SOS10 and E2_WS3_SOS30');
%concorr(E2_WS3_SOS10, E2_WS4_SOS10, 'E2_WS4_SOS10','E2_WS3_SOS10 and E2_WS4_SOS10');
%concorr(E2_WS3_SOS10, E2_WS4_SOS20, 'E2_WS4_SOS20','E2_WS3_SOS10 and E2_WS4_SOS20');
%concorr(E2_WS3_SOS10, E2_WS4_SOS25, 'E2_WS4_SOS25','E2_WS3_SOS10 and E2_WS4_SOS25');
%concorr(E2_WS3_SOS10, E2_WS4_SOS30, 'E2_WS4_SOS30','E2_WS3_SOS10 and E2_WS4_SOS30');
%concorr(E2_WS3_SOS10, E2_WS5_SOS10, 'E2_WS5_SOS10','E2_WS3_SOS10 and E2_WS5_SOS10');
%concorr(E2_WS3_SOS10, E2_WS5_SOS30, 'E2_WS5_SOS30','E2_WS3_SOS10 and E2_WS5_SOS30');

%concorr(E2_WS3_SOS30, E2_WS4_SOS10, 'E2_WS4_SOS10','E2_WS3_SOS30 and E2_WS4_SOS10');
%concorr(E2_WS3_SOS30, E2_WS4_SOS20, 'E2_WS4_SOS20','E2_WS3_SOS30 and E2_WS4_SOS20');
%concorr(E2_WS3_SOS30, E2_WS4_SOS25, 'E2_WS4_SOS25','E2_WS3_SOS30 and E2_WS4_SOS25');
%concorr(E2_WS3_SOS30, E2_WS4_SOS30, 'E2_WS4_SOS30','E2_WS3_SOS30 and E2_WS4_SOS30');
%concorr(E2_WS3_SOS30, E2_WS5_SOS10, 'E2_WS5_SOS10','E2_WS3_SOS30 and E2_WS5_SOS10');
%concorr(E2_WS3_SOS30, E2_WS5_SOS30, 'E2_WS5_SOS30','E2_WS3_SOS30 and E2_WS5_SOS30');

%concorr(E2_WS4_SOS10, E2_WS4_SOS20, 'E2_WS4_SOS20','E2_WS4_SOS10 and E2_WS4_SOS20');
%concorr(E2_WS4_SOS10, E2_WS4_SOS25, 'E2_WS4_SOS25','E2_WS4_SOS10 and E2_WS4_SOS25');
%concorr(E2_WS4_SOS10, E2_WS4_SOS30, 'E2_WS4_SOS30','E2_WS4_SOS10 and E2_WS4_SOS30');
%concorr(E2_WS4_SOS10, E2_WS5_SOS10, 'E2_WS5_SOS10','E2_WS4_SOS10 and E2_WS5_SOS10');
%concorr(E2_WS4_SOS10, E2_WS5_SOS30, 'E2_WS5_SOS30','E2_WS4_SOS10 and E2_WS5_SOS30');

%concorr(E2_WS4_SOS20, E2_WS4_SOS25, 'E2_WS4_SOS25','E2_WS4_SOS20 and E2_WS4_SOS25');
%concorr(E2_WS4_SOS20, E2_WS4_SOS30, 'E2_WS4_SOS30','E2_WS4_SOS20 and E2_WS4_SOS30');
%concorr(E2_WS4_SOS20, E2_WS5_SOS10, 'E2_WS5_SOS10','E2_WS4_SOS20 and E2_WS5_SOS10');
%concorr(E2_WS4_SOS20, E2_WS5_SOS30, 'E2_WS5_SOS30','E2_WS4_SOS20 and E2_WS5_SOS30');

%concorr(E2_WS4_SOS25, E2_WS4_SOS30, 'E2_WS4_SOS30','E2_WS4_SOS25 and E2_WS4_SOS30');
%concorr(E2_WS4_SOS25, E2_WS5_SOS10, 'E2_WS5_SOS10','E2_WS4_SOS25 and E2_WS5_SOS10');
%concorr(E2_WS4_SOS25, E2_WS5_SOS30, 'E2_WS5_SOS30','E2_WS4_SOS25 and E2_WS5_SOS30');

%concorr(E2_WS4_SOS30, E2_WS5_SOS10, 'E2_WS5_SOS10','E2_WS4_SOS30 and E2_WS5_SOS10');
%concorr(E2_WS4_SOS30, E2_WS5_SOS30, 'E2_WS5_SOS30','E2_WS4_SOS30 and E2_WS5_SOS30');

%concorr(E2_WS5_SOS10, E2_WS5_SOS30, 'E2_WS5_SOS30','E2_WS5_SOS10 and E2_WS5_SOS30');


*Combinations for Envelope Iteration = 3;
%concorr(E3_WS3_SOS10, E3_WS3_SOS30, 'E3_WS3_SOS30','E3_WS3_SOS10 and E3_WS3_SOS30');
%concorr(E3_WS3_SOS10, E3_WS4_SOS10, 'E3_WS4_SOS10','E3_WS3_SOS10 and E3_WS4_SOS10');
%concorr(E3_WS3_SOS10, E3_WS4_SOS20, 'E3_WS4_SOS20','E3_WS3_SOS10 and E3_WS4_SOS20');
%concorr(E3_WS3_SOS10, E3_WS4_SOS25, 'E3_WS4_SOS25','E3_WS3_SOS10 and E3_WS4_SOS25');
%concorr(E3_WS3_SOS10, E3_WS4_SOS30, 'E3_WS4_SOS30','E3_WS3_SOS10 and E3_WS4_SOS30');
%concorr(E3_WS3_SOS10, E3_WS5_SOS10, 'E3_WS5_SOS10','E3_WS3_SOS10 and E3_WS5_SOS10');
%concorr(E3_WS3_SOS10, E3_WS5_SOS30, 'E3_WS5_SOS30','E3_WS3_SOS10 and E3_WS5_SOS30');
```

```
%concorr(E3_WS3_SOS30, E3_WS4_SOS10, 'E3_WS4_SOS10','E3_WS3_SOS30 and E3_WS4_SOS10');
%concorr(E3_WS3_SOS30, E3_WS4_SOS20, 'E3_WS4_SOS20','E3_WS3_SOS30 and E3_WS4_SOS20');
%concorr(E3_WS3_SOS30, E3_WS4_SOS25, 'E3_WS4_SOS25','E3_WS3_SOS30 and E3_WS4_SOS25');
%concorr(E3_WS3_SOS30, E3_WS4_SOS30, 'E3_WS4_SOS30','E3_WS3_SOS30 and E3_WS4_SOS30');
%concorr(E3_WS3_SOS30, E3_WS5_SOS10, 'E3_WS5_SOS10','E3_WS3_SOS30 and E3_WS5_SOS10');
%concorr(E3_WS3_SOS30, E3_WS5_SOS30, 'E3_WS5_SOS30','E3_WS3_SOS30 and E3_WS5_SOS30');

%concorr(E3_WS4_SOS10, E3_WS4_SOS20, 'E3_WS4_SOS20','E3_WS4_SOS10 and E3_WS4_SOS20');
%concorr(E3_WS4_SOS10, E3_WS4_SOS25, 'E3_WS4_SOS25','E3_WS4_SOS10 and E3_WS4_SOS25');
%concorr(E3_WS4_SOS10, E3_WS4_SOS30, 'E3_WS4_SOS30','E3_WS4_SOS10 and E3_WS4_SOS30');
%concorr(E3_WS4_SOS10, E3_WS5_SOS10, 'E3_WS5_SOS10','E3_WS4_SOS10 and E3_WS5_SOS10');
%concorr(E3_WS4_SOS10, E3_WS5_SOS30, 'E3_WS5_SOS30','E3_WS4_SOS10 and E3_WS5_SOS30');

%concorr(E3_WS4_SOS20, E3_WS4_SOS25, 'E3_WS4_SOS25','E3_WS4_SOS20 and E3_WS4_SOS25');
%concorr(E3_WS4_SOS20, E3_WS4_SOS30, 'E3_WS4_SOS30','E3_WS4_SOS20 and E3_WS4_SOS30');
%concorr(E3_WS4_SOS20, E3_WS5_SOS10, 'E3_WS5_SOS10','E3_WS4_SOS20 and E3_WS5_SOS10');
%concorr(E3_WS4_SOS20, E3_WS5_SOS30, 'E3_WS5_SOS30','E3_WS4_SOS20 and E3_WS5_SOS30');

%concorr(E3_WS4_SOS25, E3_WS4_SOS30, 'E3_WS4_SOS30','E3_WS4_SOS25 and E3_WS4_SOS30');
%concorr(E3_WS4_SOS25, E3_WS5_SOS10, 'E3_WS5_SOS10','E3_WS4_SOS25 and E3_WS5_SOS10');
%concorr(E3_WS4_SOS25, E3_WS5_SOS30, 'E3_WS5_SOS30','E3_WS4_SOS25 and E3_WS5_SOS30');

%concorr(E3_WS4_SOS30, E3_WS5_SOS10, 'E3_WS5_SOS10','E3_WS4_SOS30 and E3_WS5_SOS10');
%concorr(E3_WS4_SOS30, E3_WS5_SOS30, 'E3_WS5_SOS30','E3_WS4_SOS30 and E3_WS5_SOS30');

%concorr(E3_WS5_SOS10, E3_WS5_SOS30, 'E3_WS5_SOS30','E3_WS5_SOS10 and E3_WS5_SOS30');


*Comparisons between Envelope Iterations;
%concorr(E1_WS4_SOS20, E1_WS4_SOS25, 'E1_WS4_SOS25','E1_WS4_SOS20 and E1_WS4_SOS25');
%concorr(E1_WS4_SOS20, E2_WS4_SOS20, 'E2_WS4_SOS20','E1_WS4_SOS20 and E2_WS4_SOS20');
%concorr(E1_WS4_SOS20, E2_WS4_SOS25, 'E2_WS4_SOS25','E1_WS4_SOS20 and E2_WS4_SOS25');
%concorr(E1_WS4_SOS20, E3_WS4_SOS20, 'E3_WS4_SOS20','E1_WS4_SOS20 and E3_WS4_SOS20');
%concorr(E1_WS4_SOS20, E3_WS4_SOS25, 'E3_WS4_SOS25','E1_WS4_SOS20 and E3_WS4_SOS25');

%concorr(E1_WS4_SOS25, E2_WS4_SOS20, 'E2_WS4_SOS20','E1_WS4_SOS25 and E2_WS4_SOS20');
%concorr(E1_WS4_SOS25, E2_WS4_SOS25, 'E2_WS4_SOS25','E1_WS4_SOS25 and E2_WS4_SOS25');
%concorr(E1_WS4_SOS25, E3_WS4_SOS20, 'E3_WS4_SOS20','E1_WS4_SOS25 and E3_WS4_SOS20');
%concorr(E1_WS4_SOS25, E3_WS4_SOS25, 'E3_WS4_SOS25','E1_WS4_SOS25 and E3_WS4_SOS25');

%concorr(E2_WS4_SOS20, E2_WS4_SOS25, 'E2_WS4_SOS25','E2_WS4_SOS20 and E2_WS4_SOS25');
%concorr(E2_WS4_SOS20, E3_WS4_SOS20, 'E3_WS4_SOS20','E2_WS4_SOS20 and E3_WS4_SOS20');
%concorr(E2_WS4_SOS20, E3_WS4_SOS25, 'E3_WS4_SOS25','E2_WS4_SOS20 and E3_WS4_SOS25');

%concorr(E2_WS4_SOS25, E3_WS4_SOS20, 'E3_WS4_SOS20','E2_WS4_SOS25 and E3_WS4_SOS20');
%concorr(E2_WS4_SOS25, E3_WS4_SOS25, 'E3_WS4_SOS25','E2_WS4_SOS25 and E3_WS4_SOS25');
```

```
 %concorr(E3_WS4_SOS20, E3_WS4_SOS25, 'E3_WS4_SOS25','E3_WS4_SOS20 and E3_WS4_SOS25');



*ods rtf file = "E:\GRA (Consulting)\Bryanna Pockrandt\Lins Concordance Plots on Phenometric Sensitivity Analysis (Bryanna Pockrandt).doc";

*title 'Lins Concordance Plots on Phenometric Sensitivity Analysis (Bryanna Pockrandt)';


%macro concord_plot(var,x,y,seas);

 data diag;
   set &var;
   where Season=&seas;
   z1=&x;
   z2=&x;
 run;

 *Specifies conditions for symbols used in the plots;
  symbol1 value=circle  height=0.75 cv=blue width=1;
  symbol2 value=diamond height=0.25 cv=red  width=1 interpol=join;

 *Generates a Lins Concordance Correlation Plot;
  proc gplot data=diag;
    plot &y*&x z2*z1 / overlay ;
                title3 'Lins Concordance Correlation Plot';
  run;

%mend concord_plot;

title2 'Beginning of the Season for E2_WS3_SOS30 and E2_WS5_SOS30 (Season 2)';
%concord_plot(Beg_Fort,E2_WS3_SOS30,E2_WS5_SOS30,2);

title2 'Beginning of the Season for E2_WS3_SOS30 and E2_WS5_SOS30 (Season 4)';
%concord_plot(Beg_Fort,E2_WS3_SOS30,E2_WS5_SOS30,4);

title2 'Beginning of the Season for E2_WS3_SOS30 and E2_WS5_SOS30 (Season 5)';
%concord_plot(Beg_Fort,E2_WS3_SOS30,E2_WS5_SOS30,5);

title2 'Beginning of the Season for E2_WS3_SOS30 and E2_WS5_SOS30 (Season 9)';
%concord_plot(Beg_Fort,E2_WS3_SOS30,E2_WS5_SOS30,9);

title2 'Beginning of the Season for E2_WS3_SOS30 and E2_WS5_SOS30 (Season 11)';
%concord_plot(Beg_Fort,E2_WS3_SOS30,E2_WS5_SOS30,11);


*ods rtf close;
```

Appendix C - SAS Results from Sensitivity Analysis

Systematic Phenometric Sensitivity Analysis (Bryanna Pockrandt)

Beginning of the Season for Fort Riley

Concordance Coefficient: Print-out of all pieces for the calculation

E2_WS4_SOS20 and E2_WS4_SOS10

Obs	n	xbar	ybar	diffmean	sdx	sdy	u	v	r	cb	lrc	rc	urc
1	5226	1193.66	1218.04	-24.3842	125.305	128.528	-0.19214	1.02572	0.99420	0.98156	0.97485	0.97587	0.97685
2	5188	1036.42	1056.42	-20.0003	145.557	148.887	-0.13586	1.02288	0.99733	0.99060	0.98745	0.98796	0.98844
3	5211	1087.52	1102.74	-15.2207	107.559	109.350	-0.14035	1.01665	0.99736	0.99011	0.98699	0.98750	0.98799
4	5224	1118.90	1142.33	-23.4235	100.029	102.570	-0.23125	1.02540	0.98339	0.97366	0.95538	0.95749	0.95949
5	5225	1028.06	1048.72	-20.6595	136.809	138.739	-0.14996	1.01411	0.99755	0.98879	0.98585	0.98637	0.98686
6	5228	1079.09	1090.62	-11.5299	139.714	141.649	-0.08196	1.01385	0.99876	0.99656	0.99512	0.99533	0.99553
7	5227	1151.10	1178.07	-26.9643	116.805	117.532	-0.23013	1.00622	0.98988	0.97418	0.96275	0.96433	0.96584
8	5223	1098.55	1124.41	-25.8599	101.660	103.692	-0.25187	1.01999	0.99081	0.96907	0.95855	0.96016	0.96171
9	5225	1087.65	1099.50	-11.8438	121.065	120.005	-0.09826	0.99125	0.99845	0.99516	0.99334	0.99362	0.99388
10	5223	1151.63	1199.46	-47.8308	135.913	143.690	-0.34227	1.05722	0.96319	0.94329	0.90423	0.90857	0.91271
11	5228	1025.80	1047.84	-22.0350	124.914	123.440	-0.17745	0.98819	0.99371	0.98443	0.97725	0.97824	0.97918

Comparison between Pearson & Lin Concordance Correlation Coefficient

E2_WS4_SOS20 and E2_WS4_SOS10

Obs	r	rc	thres_90	rdiff_05	rdiff_05_10
1	0.99420	0.97587	*	+	.
2	0.99733	0.98796	*	+	.
3	0.99736	0.98750	*	+	.
4	0.98339	0.95749	*	+	.
5	0.99755	0.98637	*	+	.
6	0.99876	0.99533	*	+	.
7	0.98988	0.96433	*	+	.
8	0.99081	0.96016	*	+	.
9	0.99845	0.99362	*	+	.
10	0.96319	0.90857	*	.	#
11	0.99371	0.97824	*	+	.

Table of Threshold by Difference			
Threshold	**Difference**		
Frequency	**Below**	**Betwe**	**Total**
>= 0.90	10	1	11
Total	10	1	11

Systematic Phenometric Sensitivity Analysis (Bryanna Pockrandt)

Beginning of the Season for Fort Riley

Concordance Coefficient: Print-out of all pieces for the calculation

E2_WS4_SOS20 and E2_WS4_SOS25

Obs	n	xbar	ybar	diffmean	sdx	sdy	u	v	r	cb	lrc	rc	urc
1	5226	1193.66	1183.38	10.2754	125.305	124.336	0.08232	0.99227	0.99712	0.99659	0.99339	0.99373	0.99405
2	5188	1036.42	1026.77	9.6475	145.557	144.648	0.06649	0.99375	0.99821	0.99778	0.99577	0.99599	0.99619
3	5211	1087.52	1079.11	8.4046	107.559	107.717	0.07808	1.00147	0.99719	0.99696	0.99384	0.99416	0.99447
4	5224	1118.90	1108.93	9.9769	100.029	99.353	0.10008	0.99324	0.99556	0.99499	0.99007	0.99058	0.99107
5	5225	1028.06	1018.43	9.6285	136.809	136.159	0.07055	0.99525	0.99791	0.99751	0.99518	0.99543	0.99566
6	5228	1079.09	1070.47	8.6202	139.714	138.497	0.06197	0.99129	0.99837	0.99805	0.99622	0.99642	0.99660
7	5227	1151.10	1137.87	13.2376	116.805	117.089	0.11319	1.00243	0.99561	0.99363	0.98872	0.98927	0.98980
8	5223	1098.55	1088.44	10.1049	101.660	101.718	0.09937	1.00057	0.99569	0.99509	0.99030	0.99080	0.99128
9	5225	1087.65	1080.79	6.8590	121.065	121.786	0.05649	1.00595	0.99792	0.99839	0.99611	0.99632	0.99652
10	5223	1151.63	1139.28	12.3466	135.913	136.101	0.09078	1.00138	0.99495	0.99590	0.99035	0.99086	0.99135
11	5228	1025.80	1014.70	11.1075	124.914	126.094	0.08850	1.00945	0.99621	0.99605	0.99185	0.99228	0.99268

Comparison between Pearson & Lin Concordance Correlation Coefficient

E2_WS4_SOS20 and E2_WS4_SOS25

Obs	r	rc	thres_90	rdiff_05	rdiff_05_10
1	0.99712	0.99373	*	+	.
2	0.99821	0.99599	*	+	.
3	0.99719	0.99416	*	+	.
4	0.99556	0.99058	*	+	.
5	0.99791	0.99543	*	+	.
6	0.99837	0.99642	*	+	.
7	0.99561	0.98927	*	+	.
8	0.99569	0.99080	*	+	.
9	0.99792	0.99632	*	+	.
10	0.99495	0.99086	*	+	.
11	0.99621	0.99228	*	+	.

Table of Threshold by Difference		
Threshold	Difference	
Frequency	Below	Total
>= 0.90	11	11
Total	11	11

Systematic Phenometric Sensitivity Analysis (Bryanna Pockrandt)

Beginning of the Season for Fort Riley

Concordance Coefficient: Print-out of all pieces for the calculation

E2_WS4_SOS20 and E2_WS4_SOS30

Obs	n	xbar	ybar	diffmean	sdx	sdy	u	v	r	cb	lrc	rc	urc
1	5226	1193.66	1174.09	19.5694	125.305	124.656	0.15658	0.99482	0.99648	0.98788	0.98375	0.98440	0.98501
2	5188	1036.42	1017.74	18.6744	145.557	144.050	0.12897	0.98964	0.99785	0.99170	0.98915	0.98957	0.98997
3	5211	1087.52	1069.21	18.3056	107.559	107.937	0.16989	1.00351	0.99626	0.98577	0.98136	0.98208	0.98276
4	5224	1118.90	1099.98	18.9236	100.029	99.812	0.18939	0.99782	0.99448	0.98238	0.97600	0.97696	0.97789
5	5225	1028.06	1008.33	19.7286	136.809	135.629	0.14483	0.99137	0.99718	0.98958	0.98626	0.98679	0.98731
6	5228	1079.09	1060.58	18.5149	139.714	137.714	0.13348	0.98569	0.99755	0.99107	0.98818	0.98864	0.98909
7	5227	1151.10	1123.69	27.4160	116.805	117.586	0.23394	1.00668	0.99388	0.97334	0.96617	0.96739	0.96856
8	5223	1098.55	1077.63	20.9212	101.660	102.427	0.20502	1.00754	0.99555	0.97939	0.97411	0.97503	0.97592
9	5225	1087.65	1071.23	16.4212	121.065	122.712	0.13473	1.01361	0.99644	0.99092	0.98681	0.98739	0.98794
10	5223	1151.63	1127.48	24.1530	135.913	137.114	0.17693	1.00884	0.99334	0.98455	0.97698	0.97799	0.97896
11	5228	1025.80	1003.28	22.5275	124.914	126.960	0.17889	1.01638	0.99327	0.98412	0.97647	0.97750	0.97849

Comparison between Pearson & Lin Concordance Correlation Coefficient

E2_WS4_SOS20 and E2_WS4_SOS30

Obs	r	rc	thres_90	rdiff_05	rdiff_05_10
1	0.99648	0.98440	*	+	.
2	0.99785	0.98957	*	+	.
3	0.99626	0.98208	*	+	.
4	0.99448	0.97696	*	+	.
5	0.99718	0.98679	*	+	.
6	0.99755	0.98864	*	+	.
7	0.99388	0.96739	*	+	.
8	0.99555	0.97503	*	+	.
9	0.99644	0.98739	*	+	.
10	0.99334	0.97799	*	+	.
11	0.99327	0.97750	*	+	.

Table of Threshold by Difference		
Threshold	Difference	
Frequency	Below	Total
>= 0.90	11	11
Total	11	11

Systematic Phenometric Sensitivity Analysis (Bryanna Pockrandt)

Beginning of the Season for Fort Riley

Concordance Coefficient: Print-out of all pieces for the calculation

E2_WS4_SOS20 and E2_WS3_SOS20

Obs	n	xbar	ybar	diffmean	sdx	sdy	u	v	r	cb	lrc	rc	urc
1	5226	1193.66	1167.69	25.9671	125.305	123.934	0.20837	0.98906	0.97515	0.97869	0.95188	0.95437	0.95673
2	5188	1036.42	1001.62	34.7993	145.557	145.108	0.23945	0.99692	0.97849	0.97213	0.94872	0.95122	0.95360
3	5211	1087.52	1064.41	23.1078	107.559	105.335	0.21709	0.97933	0.97292	0.97677	0.94762	0.95032	0.95288
4	5224	1118.90	1106.26	12.6431	100.029	96.068	0.12897	0.96040	0.96820	0.99095	0.95713	0.95944	0.96162
5	5225	1028.06	1017.18	10.8798	136.809	136.168	0.07971	0.99531	0.98329	0.99682	0.97901	0.98016	0.98125
6	5228	1079.09	1086.12	-7.0239	139.714	150.603	-0.04842	1.07794	0.97908	0.99603	0.97388	0.97519	0.97644
7	5227	1151.10	1154.24	-3.1360	116.805	121.665	-0.02631	1.04160	0.96310	0.99882	0.95990	0.96197	0.96392
8	5223	1098.55	1084.45	14.0986	101.660	99.123	0.14045	0.97505	0.97638	0.98992	0.96462	0.96654	0.96836
9	5225	1087.65	1095.77	-8.1144	121.065	118.006	-0.06789	0.97473	0.98103	0.99737	0.97723	0.97845	0.97961
10	5223	1151.63	1155.46	-3.8354	135.913	129.479	-0.02891	0.95266	0.97400	0.99841	0.97096	0.97245	0.97386
11	5228	1025.80	1013.34	12.4580	124.914	122.666	0.10064	0.98200	0.97345	0.99480	0.96658	0.96839	0.97011

Comparison between Pearson & Lin Concordance Correlation Coefficient

E2_WS4_SOS20 and E2_WS3_SOS20

Obs	r	rc	thres_90	rdiff_05	rdiff_05_10
1	0.97515	0.95437	*	+	.
2	0.97849	0.95122	*	+	.
3	0.97292	0.95032	*	+	.
4	0.96820	0.95944	*	+	.
5	0.98329	0.98016	*	+	.
6	0.97908	0.97519	*	+	.
7	0.96310	0.96197	*	+	.
8	0.97638	0.96654	*	+	.
9	0.98103	0.97845	*	+	.
10	0.97400	0.97245	*	+	.
11	0.97345	0.96839	*	+	.

Table of Threshold by Difference		
Threshold	Difference	
Frequency	Below	Total
>= 0.90	11	11
Total	11	11

Systematic Phenometric Sensitivity Analysis (Bryanna Pockrandt)

Beginning of the Season for Fort Riley

Concordance Coefficient: Print-out of all pieces for the calculation

E2_WS4_SOS20 and E2_WS5_SOS20

Obs	n	xbar	ybar	diffmean	sdx	sdy	u	v	r	cb	lrc	rc	urc
1	5226	1193.66	1228.59	-34.9322	125.305	125.558	-0.27850	1.00202	0.96932	0.96267	0.92974	0.93314	0.93637
2	5188	1036.42	1065.56	-29.1442	145.557	143.738	-0.20149	0.98750	0.97953	0.98003	0.95780	0.95997	0.96202
3	5211	1087.52	1113.88	-26.3577	107.559	108.958	-0.24348	1.01301	0.97434	0.97113	0.94341	0.94621	0.94888
4	5224	1118.90	1135.54	-16.6326	100.029	105.348	-0.16203	1.05317	0.97748	0.98574	0.96150	0.96354	0.96547
5	5225	1028.06	1035.68	-7.6239	136.809	142.230	-0.05465	1.03962	0.98918	0.99776	0.98623	0.98696	0.98765
6	5228	1079.09	1094.56	-15.4624	139.714	143.381	-0.10925	1.02625	0.97563	0.99374	0.96777	0.96952	0.97118
7	5227	1151.10	1163.83	-12.7251	116.805	119.882	-0.10754	1.02634	0.95857	0.99392	0.95008	0.95274	0.95526
8	5223	1098.55	1107.24	-8.6943	101.660	108.182	-0.08290	1.06415	0.97885	0.99466	0.97216	0.97363	0.97501
9	5225	1087.65	1106.41	-18.7541	121.065	127.861	-0.15074	1.05614	0.97847	0.98731	0.96415	0.96606	0.96786
10	5223	1151.63	1171.14	-19.5081	135.913	145.971	-0.13850	1.07400	0.96526	0.98800	0.95110	0.95368	0.95613
11	5228	1025.80	1032.60	-6.7977	124.914	134.241	-0.05249	1.07467	0.97785	0.99604	0.97259	0.97398	0.97530

Comparison between Pearson & Lin Concordance Correlation Coefficient

E2_WS4_SOS20 and E2_WS5_SOS20

Obs	r	rc	thres_90	rdiff_05	rdiff_05_10
1	0.96932	0.93314	*	+	.
2	0.97953	0.95997	*	+	.
3	0.97434	0.94621	*	+	.
4	0.97748	0.96354	*	+	.
5	0.98918	0.98696	*	+	.
6	0.97563	0.96952	*	+	.
7	0.95857	0.95274	*	+	.
8	0.97885	0.97363	*	+	.
9	0.97847	0.96606	*	+	.
10	0.96526	0.95368	*	+	.
11	0.97785	0.97398	*	+	.

Table of Threshold by Difference		
Threshold	Difference	
Frequency	Below	Total
>= 0.90	11	11
Total	11	11

Systematic Phenometric Sensitivity Analysis (Bryanna Pockrandt)

Beginning of the Season for Fort Riley

Concordance Coefficient: Print-out of all pieces for the calculation

E2_WS4_SOS20 and E1_WS4_SOS20

Obs	n	xbar	ybar	diffmean	sdx	sdy	u	v	r	cb	lrc	rc	urc
1	5226	1193.66	1148.60	45.0564	125.305	122.018	0.36438	0.97377	0.96463	0.93743	0.89992	0.90427	0.90845
2	5188	1036.42	979.60	56.8130	145.557	145.434	0.39048	0.99916	0.97991	0.92916	0.90714	0.91050	0.91373
3	5211	1087.52	1066.93	20.5844	107.559	115.656	0.18456	1.07528	0.96648	0.98071	0.94495	0.94784	0.95057
4	5224	1118.90	1131.93	-13.0321	100.029	103.276	-0.12822	1.03246	0.95245	0.99135	0.94107	0.94421	0.94718
5	5225	1028.06	1008.04	20.0202	136.809	138.139	0.14563	1.00972	0.98125	0.98946	0.96925	0.97091	0.97249
6	5228	1079.09	1051.61	27.4789	139.714	152.265	0.18840	1.08983	0.96148	0.97900	0.93808	0.94129	0.94435
7	5227	1151.10	1143.58	7.5245	116.805	120.510	0.06342	1.03171	0.95706	0.99751	0.95218	0.95467	0.95704
8	5223	1098.55	1081.55	16.9992	101.660	98.867	0.16956	0.97253	0.96849	0.98545	0.95181	0.95440	0.95685
9	5225	1087.65	1098.55	-10.9004	121.065	121.980	-0.08970	1.00756	0.97376	0.99597	0.96810	0.96983	0.97147
10	5223	1151.63	1148.95	2.6827	135.913	138.057	0.01958	1.01578	0.95548	0.99969	0.95274	0.95518	0.95750
11	5228	1025.80	1015.72	10.0813	124.914	128.358	0.07962	1.02757	0.97407	0.99647	0.96897	0.97064	0.97221

Comparison between Pearson & Lin Concordance Correlation Coefficient

E2_WS4_SOS20 and E1_WS4_SOS20

Obs	r	rc	thres_90	rdiff_05	rdiff_05_10
1	0.96463	0.90427	*	.	#
2	0.97991	0.91050	*	.	#
3	0.96648	0.94784	*	+	.
4	0.95245	0.94421	*	+	.
5	0.98125	0.97091	*	+	.
6	0.96148	0.94129	*	+	.
7	0.95706	0.95467	*	+	.
8	0.96849	0.95440	*	+	.
9	0.97376	0.96983	*	+	.
10	0.95548	0.95518	*	+	.
11	0.97407	0.97064	*	+	.

Table of Threshold by Difference			
Threshold	Difference		
Frequency	Below	Betwe	Total
>= 0.90	9	2	11
Total	9	2	11

Systematic Phenometric Sensitivity Analysis (Bryanna Pockrandt)

Beginning of the Season for Fort Riley

Concordance Coefficient: Print-out of all pieces for the calculation

E2_WS4_SOS20 and E3_WS4_SOS20

Obs	n	xbar	ybar	diffmean	sdx	sdy	u	v	r	cb	lrc	rc	urc
1	5226	1193.66	1223.24	-29.5783	125.305	123.070	-0.23818	0.98216	0.99164	0.97226	0.96267	0.96413	0.96554
2	5188	1036.42	1069.13	-32.7106	145.557	147.144	-0.22351	1.01091	0.99109	0.97557	0.96543	0.96688	0.96826
3	5211	1087.52	1116.36	-28.8385	107.559	106.290	-0.26971	0.98820	0.98975	0.96484	0.95315	0.95495	0.95668
4	5224	1118.90	1134.94	-16.0353	100.029	100.620	-0.15983	1.00591	0.99390	0.98737	0.98046	0.98135	0.98220
5	5225	1028.06	1042.62	-14.5646	136.809	140.057	-0.10522	1.02374	0.99743	0.99422	0.99127	0.99167	0.99205
6	5228	1079.09	1105.95	-26.8556	139.714	143.254	-0.18983	1.02534	0.99351	0.98200	0.97455	0.97562	0.97665
7	5227	1151.10	1169.14	-18.0350	116.805	118.018	-0.15361	1.01039	0.99444	0.98829	0.98197	0.98279	0.98357
8	5223	1098.55	1109.71	-11.1611	101.660	104.606	-0.10823	1.02898	0.99601	0.99377	0.98928	0.98981	0.99031
9	5225	1087.65	1098.13	-10.4754	121.065	124.428	-0.08535	1.02778	0.99745	0.99600	0.99312	0.99346	0.99378
10	5223	1151.63	1162.01	-10.3791	135.913	139.362	-0.07541	1.02538	0.99672	0.99685	0.99323	0.99358	0.99392
11	5228	1025.80	1038.80	-12.9986	124.914	128.319	-0.10267	1.02726	0.99672	0.99440	0.99068	0.99114	0.99157

Comparison between Pearson & Lin Concordance Correlation Coefficient

E2_WS4_SOS20 and E3_WS4_SOS20

Obs	r	rc	thres_90	rdiff_05	rdiff_05_10
1	0.99164	0.96413	*	+	.
2	0.99109	0.96688	*	+	.
3	0.98975	0.95495	*	+	.
4	0.99390	0.98135	*	+	.
5	0.99743	0.99167	*	+	.
6	0.99351	0.97562	*	+	.
7	0.99444	0.98279	*	+	.
8	0.99601	0.98981	*	+	.
9	0.99745	0.99346	*	+	.
10	0.99672	0.99358	*	+	.
11	0.99672	0.99114	*	+	.

Table of Threshold by Difference		
Threshold	**Difference**	
Frequency	**Below**	**Total**
>= 0.90	11	11
Total	11	11

Systematic Phenometric Sensitivity Analysis (Bryanna Pockrandt)

End of the Season for Fort Riley

Concordance Coefficient: Print-out of all pieces for the calculation

E2_WS4_SOS20 and E2_WS4_SOS10

Obs	n	xbar	ybar	diffmean	sdx	sdy	u	v	r	cb	lrc	rc	urc
1	5219	21.536	23.367	-1.83070	0.66664	1.03501	-2.20393	1.55258	0.70193	0.28353	0.19216	0.19902	0.20585
2	5184	44.501	46.271	-1.77025	0.59969	0.92998	-2.37048	1.55076	0.70359	0.25593	0.17392	0.18007	0.18620
3	5214	67.369	68.769	-1.39941	0.70863	0.86927	-1.78302	1.22668	0.87580	0.38307	0.32878	0.33549	0.34217
4	5222	89.227	91.019	-1.79113	0.51183	1.28337	-2.20998	2.50741	0.63872	0.25673	0.15699	0.16398	0.17095
5	5217	113.120	114.953	-1.83237	0.58607	0.87728	-2.55547	1.49690	0.75195	0.23001	0.16780	0.17295	0.17810
6	5223	136.376	137.756	-1.38051	0.72245	0.66204	-1.99614	0.91638	0.86419	0.33377	0.28258	0.28844	0.29427
7	5227	159.102	160.893	-1.79099	0.63784	1.18262	-2.06211	1.85409	0.69398	0.30094	0.20123	0.20885	0.21644
8	5221	181.954	183.925	-1.97129	0.50009	1.00920	-2.77482	2.01803	0.61463	0.19582	0.11532	0.12036	0.12540
9	5217	204.708	205.814	-1.10571	0.46685	0.54215	-2.19782	1.16128	0.80454	0.29185	0.22890	0.23480	0.24069
10	5198	227.709	230.564	-2.85552	0.62303	2.01435	-2.54897	3.23317	0.39409	0.19921	0.07293	0.07851	0.08408
11	5206	250.672	252.497	-1.82511	0.75990	1.07744	-2.01703	1.41787	0.71737	0.32302	0.22406	0.23172	0.23936

Comparison between Pearson & Lin Concordance Correlation Coefficient

E2_WS4_SOS20 and E2_WS4_SOS10

Obs	r	rc	thres_90	rdiff_05	rdiff_05_10
1	0.70193	0.19902	.	.	.
2	0.70359	0.18007	.	.	.
3	0.87580	0.33549	.	.	.
4	0.63872	0.16398	.	.	.
5	0.75195	0.17295	.	.	.
6	0.86419	0.28844	.	.	.
7	0.69398	0.20885	.	.	.
8	0.61463	0.12036	.	.	.
9	0.80454	0.23480	.	.	.
10	0.39409	0.07851	.	.	.
11	0.71737	0.23172	.	.	.

Table of Threshold by Difference		
Threshold	**Difference**	
Frequency	**Over**	**Total**
< 0.90	11	11
Total	11	11

Systematic Phenometric Sensitivity Analysis (Bryanna Pockrandt)

End of the Season for Fort Riley

Concordance Coefficient: Print-out of all pieces for the calculation

E2_WS4_SOS20 and E2_WS4_SOS25

Obs	n	xbar	ybar	diffmean	sdx	sdy	u	v	r	cb	lrc	rc	urc
1	5219	21.536	21.035	0.50144	0.66664	0.61354	0.78406	0.92034	0.97913	0.76288	0.74222	0.74696	0.75162
2	5184	44.501	43.986	0.51537	0.59969	0.54497	0.90151	0.90875	0.96594	0.70874	0.67863	0.68461	0.69049
3	5214	67.369	66.888	0.48120	0.70863	0.67525	0.69564	0.95289	0.98560	0.80442	0.78906	0.79284	0.79657
4	5222	89.227	88.748	0.47951	0.51183	0.45048	0.99861	0.88013	0.95360	0.66367	0.62605	0.63287	0.63960
5	5217	113.120	112.602	0.51783	0.58607	0.52045	0.93761	0.88804	0.96514	0.69127	0.66109	0.66717	0.67317
6	5223	136.376	135.838	0.53745	0.72245	0.69188	0.76018	0.95768	0.97262	0.77527	0.74882	0.75404	0.75917
7	5227	159.102	158.567	0.53539	0.63784	0.59359	0.87011	0.93062	0.96417	0.72405	0.69207	0.69810	0.70403
8	5221	181.954	181.425	0.52829	0.50009	0.47025	1.08939	0.94033	0.96333	0.62685	0.59813	0.60386	0.60954
9	5217	204.708	204.275	0.43306	0.46685	0.49945	0.89685	1.06981	0.96551	0.71202	0.68157	0.68746	0.69327
10	5198	227.709	227.200	0.50839	0.62303	0.50565	0.90577	0.81161	0.89832	0.69829	0.61720	0.62729	0.63717
11	5206	250.672	250.087	0.58500	0.75990	0.68425	0.81128	0.90044	0.93855	0.74929	0.69535	0.70325	0.71098

Comparison between Pearson & Lin Concordance Correlation Coefficient

E2_WS4_SOS20 and E2_WS4_SOS25

Obs	r	rc	thres_90	rdiff_05	rdiff_05_10
1	0.97913	0.74696	.	.	.
2	0.96594	0.68461	.	.	.
3	0.98560	0.79284	.	.	.
4	0.95360	0.63287	.	.	.
5	0.96514	0.66717	.	.	.
6	0.97262	0.75404	.	.	.
7	0.96417	0.69810	.	.	.
8	0.96333	0.60386	.	.	.
9	0.96551	0.68746	.	.	.
10	0.89832	0.62729	.	.	.
11	0.93855	0.70325	.	.	.

Table of Threshold by Difference		
Threshold	Difference	
Frequency	Over	Total
< 0.90	11	11
Total	11	11

Systematic Phenometric Sensitivity Analysis (Bryanna Pockrandt)

End of the Season for Fort Riley

Concordance Coefficient: Print-out of all pieces for the calculation

E2_WS4_SOS20 and E2_WS4_SOS30

Obs	n	xbar	ybar	diffmean	sdx	sdy	u	v	r	cb	lrc	rc	urc
1	5219	21.536	20.619	0.91694	0.66664	0.58158	1.47262	0.87240	0.94679	0.47764	0.44650	0.45222	0.45790
2	5184	44.501	43.565	0.93571	0.59969	0.51807	1.67873	0.86390	0.91789	0.41326	0.37330	0.37933	0.38532
3	5214	67.369	66.461	0.90830	0.70863	0.65462	1.33360	0.92377	0.96117	0.52843	0.50265	0.50791	0.51314
4	5222	89.227	88.340	0.88734	0.51183	0.41736	1.91988	0.81542	0.89238	0.34918	0.30584	0.31160	0.31733
5	5217	113.120	112.184	0.93667	0.58607	0.48657	1.75404	0.83024	0.92120	0.39129	0.35477	0.36045	0.36611
6	5223	136.376	135.395	0.98047	0.72245	0.65207	1.42851	0.90258	0.93937	0.49369	0.45762	0.46375	0.46984
7	5227	159.102	158.102	1.00040	0.63784	0.59215	1.62780	0.92836	0.89412	0.42962	0.37731	0.38413	0.39091
8	5221	181.954	180.979	0.97437	0.50009	0.46638	2.01758	0.93258	0.90631	0.32919	0.29343	0.29835	0.30325
9	5217	204.708	203.837	0.87138	0.46685	0.55486	1.71209	1.18851	0.90641	0.40313	0.35915	0.36540	0.37162
10	5198	227.709	226.781	0.92747	0.62303	0.49714	1.66652	0.79794	0.84380	0.41421	0.34152	0.34951	0.35744
11	5206	250.672	249.588	1.08438	0.75990	0.63208	1.56465	0.83180	0.80344	0.44622	0.34926	0.35851	0.36769

Comparison between Pearson & Lin Concordance Correlation Coefficient

E2_WS4_SOS20 and E2_WS4_SOS30

Obs	r	rc	thres_90	rdiff_05	rdiff_05_10
1	0.94679	0.45222	.	.	.
2	0.91789	0.37933	.	.	.
3	0.96117	0.50791	.	.	.
4	0.89238	0.31160	.	.	.
5	0.92120	0.36045	.	.	.
6	0.93937	0.46375	.	.	.
7	0.89412	0.38413	.	.	.
8	0.90631	0.29835	.	.	.
9	0.90641	0.36540	.	.	.
10	0.84380	0.34951	.	.	.
11	0.80344	0.35851	.	.	.

Table of Threshold by Difference		
Threshold	**Difference**	
Frequency	**Over**	**Total**
< 0.90	11	11
Total	11	11

Systematic Phenometric Sensitivity Analysis (Bryanna Pockrandt)

End of the Season for Fort Riley

Concordance Coefficient: Print-out of all pieces for the calculation

E2_WS4_SOS20 and E2_WS3_SOS20

Obs	n	xbar	ybar	diffmean	sdx	sdy	u	v	r	cb	lrc	rc	urc
1	5219	21.536	21.271	0.26563	0.66664	0.80397	0.36283	1.20601	0.94104	0.92300	0.86239	0.86858	0.87451
2	5184	44.501	44.345	0.15635	0.59969	0.65153	0.25012	1.08645	0.90049	0.96644	0.86338	0.87027	0.87684
3	5214	67.369	67.130	0.23926	0.70863	0.81293	0.31523	1.14718	0.95792	0.94417	0.89978	0.90445	0.90891
4	5222	89.227	89.099	0.12811	0.51183	0.59266	0.23261	1.15792	0.86080	0.96356	0.82085	0.82943	0.83764
5	5217	113.120	112.934	0.18647	0.58607	0.72269	0.28652	1.23312	0.90469	0.94066	0.84372	0.85101	0.85798
6	5223	136.376	136.519	-0.14279	0.72245	0.89989	-0.17709	1.24560	0.90697	0.96164	0.86600	0.87218	0.87809
7	5227	159.102	158.903	0.19918	0.63784	0.66548	0.30571	1.04333	0.93300	0.95454	0.88484	0.89059	0.89606
8	5221	181.954	181.831	0.12289	0.50009	0.51804	0.24144	1.03589	0.90252	0.97109	0.86978	0.87643	0.88276
9	5217	204.708	204.885	-0.17671	0.46685	0.49530	-0.36748	1.06094	0.89518	0.93522	0.82898	0.83718	0.84502
10	5198	227.709	227.496	0.21285	0.62303	0.55871	0.36077	0.89676	0.84570	0.93369	0.77927	0.78962	0.79953
11	5206	250.672	250.552	0.12032	0.75990	0.89534	0.14587	1.17823	0.91162	0.97645	0.88458	0.89015	0.89545

Comparison between Pearson & Lin Concordance Correlation Coefficient

E2_WS4_SOS20 and E2_WS3_SOS20

Obs	r	rc	thres_90	rdiff_05	rdiff_05_10
1	0.94104	0.86858	.	.	#
2	0.90049	0.87027	.	+	.
3	0.95792	0.90445	*	.	#
4	0.86080	0.82943	.	+	.
5	0.90469	0.85101	.	.	#
6	0.90697	0.87218	.	+	.
7	0.93300	0.89059	.	+	.
8	0.90252	0.87643	.	+	.
9	0.89518	0.83718	.	.	#
10	0.84570	0.78962	.	.	#
11	0.91162	0.89015	.	+	.

Table of Threshold by Difference			
Threshold	**Difference**		
Frequency	**Below**	**Betwe**	**Total**
< 0.90	6	4	10
>= 0.90	0	1	1
Total	6	5	11

Systematic Phenometric Sensitivity Analysis (Bryanna Pockrandt)

End of the Season for Fort Riley

Concordance Coefficient: Print-out of all pieces for the calculation

E2_WS4_SOS20 and E2_WS5_SOS20

Obs	n	xbar	ybar	diffmean	sdx	sdy	u	v	r	cb	lrc	rc	urc
1	5219	21.536	21.739	-0.20326	0.66664	0.56864	-0.33013	0.85300	0.92681	0.93707	0.86196	0.86848	0.87472
2	5184	44.501	44.712	-0.21128	0.59969	0.52439	-0.37677	0.87444	0.91436	0.92593	0.83913	0.84664	0.85383
3	5214	67.369	67.643	-0.27378	0.70863	0.61568	-0.41449	0.86882	0.94705	0.91257	0.85815	0.86425	0.87012
4	5222	89.227	89.331	-0.10304	0.51183	0.45780	-0.21288	0.89443	0.90086	0.97192	0.86903	0.87557	0.88180
5	5217	113.120	113.265	-0.14468	0.58607	0.51337	-0.26377	0.87596	0.90521	0.95825	0.86056	0.86742	0.87396
6	5223	136.376	136.410	-0.03391	0.72245	0.59751	-0.05161	0.82705	0.89865	0.98095	0.87583	0.88153	0.88698
7	5227	159.102	159.317	-0.21492	0.63784	0.63975	-0.33645	1.00299	0.94162	0.94643	0.88565	0.89118	0.89645
8	5221	181.954	182.022	-0.06799	0.50009	0.50695	-0.13504	1.01372	0.91421	0.99087	0.90074	0.90587	0.91075
9	5217	204.708	204.787	-0.07903	0.46685	0.47176	-0.16840	1.01051	0.88994	0.98597	0.87087	0.87745	0.88371
10	5198	227.709	228.041	-0.33238	0.62303	0.92838	-0.43703	1.49011	0.66226	0.85027	0.54679	0.56310	0.57898
11	5206	250.672	250.706	-0.03362	0.75990	0.62005	-0.04897	0.81596	0.88832	0.97852	0.86301	0.86924	0.87520

End of the Season for Fort Riley

Comparison between Pearson & Lin Concordance Correlation Coefficient

E2_WS4_SOS20 and E2_WS5_SOS20

Obs	r	rc	thres_90	rdiff_05	rdiff_05_10
1	0.92681	0.86848	.	.	#
2	0.91436	0.84664	.	.	#
3	0.94705	0.86425	.	.	#
4	0.90086	0.87557	.	+	.
5	0.90521	0.86742	.	+	.
6	0.89865	0.88153	.	+	.
7	0.94162	0.89118	.	.	#
8	0.91421	0.90587	*	+	.
9	0.88994	0.87745	.	+	.
10	0.66226	0.56310	.	.	#
11	0.88832	0.86924	.	+	.

Table of Threshold by Difference			
Threshold	Difference		
Frequency	Below	Betwe	Total
< 0.90	5	5	10
>= 0.90	1	0	1
Total	6	5	11

Systematic Phenometric Sensitivity Analysis (Bryanna Pockrandt)

End of the Season for Fort Riley

Concordance Coefficient: Print-out of all pieces for the calculation

E2_WS4_SOS20 and E1_WS4_SOS20

Obs	n	xbar	ybar	diffmean	sdx	sdy	u	v	r	cb	lrc	rc	urc
1	5219	21.536	21.529	0.00772	0.66664	0.71083	0.01122	1.06629	0.93453	0.99788	0.92897	0.93255	0.93594
2	5184	44.501	44.613	-0.11171	0.59969	0.62425	-0.18258	1.04095	0.92095	0.98283	0.89991	0.90513	0.91009
3	5214	67.369	67.581	-0.21208	0.70863	0.78044	-0.28518	1.10132	0.95044	0.95664	0.90452	0.90923	0.91372
4	5222	89.227	89.240	-0.01250	0.51183	0.51270	-0.02441	1.00169	0.79652	0.99970	0.78613	0.79628	0.80600
5	5217	113.120	113.089	0.03088	0.58607	0.61361	0.05149	1.04700	0.92452	0.99763	0.91817	0.92233	0.92628
6	5223	136.376	136.753	-0.37748	0.72245	0.64330	-0.55372	0.89043	0.86692	0.86204	0.73653	0.74732	0.75773
7	5227	159.102	159.089	0.01303	0.63784	0.64411	0.02033	1.00982	0.94592	0.99975	0.94274	0.94568	0.94848
8	5221	181.954	181.939	0.01467	0.50009	0.47987	0.02995	0.95956	0.91869	0.99870	0.91311	0.91749	0.92167
9	5217	204.708	204.805	-0.09674	0.46685	0.42362	-0.21754	0.90740	0.91050	0.97240	0.87926	0.88537	0.89118
10	5198	227.709	227.793	-0.08471	0.62303	0.61737	-0.13658	0.99092	0.87328	0.99072	0.85805	0.86518	0.87197
11	5206	250.672	250.645	0.02755	0.75990	0.72168	0.03720	0.94970	0.93377	0.99798	0.92824	0.93188	0.93535

Comparison between Pearson & Lin Concordance Correlation Coefficient

E2_WS4_SOS20 and E1_WS4_SOS20

Obs	r	rc	thres_90	rdiff_05	rdiff_05_10
1	0.93453	0.93255	*	+	.
2	0.92095	0.90513	*	+	.
3	0.95044	0.90923	*	+	.
4	0.79652	0.79628	.	+	.
5	0.92452	0.92233	*	+	.
6	0.86692	0.74732	.	.	.
7	0.94592	0.94568	*	+	.
8	0.91869	0.91749	*	+	.
9	0.91050	0.88537	.	+	.
10	0.87328	0.86518	.	+	.
11	0.93377	0.93188	*	+	.

Table of Threshold by Difference			
Threshold	**Difference**		
Frequency	**Below**	**Over**	**Total**
< 0.90	3	1	4
>= 0.90	7	0	7
Total	10	1	11

Systematic Phenometric Sensitivity Analysis (Bryanna Pockrandt)

End of the Season for Fort Riley

Concordance Coefficient: Print-out of all pieces for the calculation

E2_WS4_SOS20 and E3_WS4_SOS20

Obs	n	xbar	ybar	diffmean	sdx	sdy	u	v	r	cb	lrc	rc	urc
1	5219	21.536	21.409	0.12748	0.66664	0.65917	0.19230	0.98880	0.98676	0.98178	0.96718	0.96878	0.97031
2	5184	44.501	44.311	0.19034	0.59969	0.60218	0.31673	1.00415	0.97353	0.95223	0.92362	0.92703	0.93028
3	5214	67.369	67.310	0.05965	0.70863	0.70899	0.08415	1.00051	0.99517	0.99647	0.99118	0.99166	0.99211
4	5222	89.227	89.149	0.07897	0.51183	0.48114	0.15914	0.94005	0.96843	0.98563	0.95196	0.95451	0.95693
5	5217	113.120	112.987	0.13372	0.58607	0.56644	0.23208	0.96650	0.98404	0.97323	0.95562	0.95769	0.95967
6	5223	136.376	136.272	0.10423	0.72245	0.70913	0.14562	0.98156	0.98139	0.98934	0.96927	0.97092	0.97249
7	5227	159.102	158.996	0.10561	0.63784	0.63193	0.16634	0.99073	0.99112	0.98631	0.97642	0.97756	0.97864
8	5221	181.954	181.853	0.10013	0.50009	0.49787	0.20068	0.99556	0.98584	0.98025	0.96465	0.96637	0.96801
9	5217	204.708	204.637	0.07178	0.46685	0.45533	0.15570	0.97533	0.98192	0.98772	0.96816	0.96986	0.97147
10	5198	227.709	227.628	0.08055	0.62303	0.61317	0.13032	0.98418	0.98889	0.99145	0.97933	0.98044	0.98148
11	5206	250.672	250.551	0.12165	0.75990	0.75255	0.16086	0.99033	0.98988	0.98718	0.97599	0.97719	0.97834

Comparison between Pearson & Lin Concordance Correlation Coefficient

E2_WS4_SOS20 and E3_WS4_SOS20

Obs	r	rc	thres_90	rdiff_05	rdiff_05_10
1	0.98676	0.96878	*	+	.
2	0.97353	0.92703	*	+	.
3	0.99517	0.99166	*	+	.
4	0.96843	0.95451	*	+	.
5	0.98404	0.95769	*	+	.
6	0.98139	0.97092	*	+	.
7	0.99112	0.97756	*	+	.
8	0.98584	0.96637	*	+	.
9	0.98192	0.96986	*	+	.
10	0.98889	0.98044	*	+	.
11	0.98988	0.97719	*	+	.

Table of Threshold by Difference		
Threshold	Difference	
Frequency	Below	Total
>= 0.90	11	11
Total	11	11

Systematic Phenometric Sensitivity Analysis (Bryanna Pockrandt)

Length of the Season for Fort Riley

Concordance Coefficient: Print-out of all pieces for the calculation

E2_WS4_SOS20 and E2_WS4_SOS10

Obs	n	xbar	ybar	diffmean	sdx	sdy	u	v	r	cb	lrc	rc	urc
1	5201	15.3632	17.9450	-2.58177	0.91546	1.21432	-2.44868	1.32646	0.76183	0.24764	0.18326	0.18866	0.19405
2	5180	14.8770	17.2614	-2.38436	0.91271	1.14814	-2.32921	1.25794	0.81512	0.26745	0.21265	0.21800	0.22334
3	5214	15.0240	17.0925	-2.06845	0.94565	1.09867	-2.02930	1.16182	0.91084	0.32570	0.29181	0.29666	0.30151
4	5203	14.1149	16.5941	-2.47919	0.65494	1.35368	-2.63300	2.06689	0.66683	0.21090	0.13526	0.14063	0.14600
5	5200	14.5043	17.0885	-2.58415	0.90806	1.10309	-2.58199	1.21477	0.84517	0.22976	0.18999	0.19419	0.19837
6	5199	15.1219	17.1517	-2.02989	0.92776	0.87408	-2.25414	0.94214	0.91244	0.28230	0.25354	0.25758	0.26161
7	5216	15.0626	17.7280	-2.66539	1.17538	1.55253	-1.97311	1.32087	0.82234	0.33495	0.26865	0.27544	0.28220
8	5200	13.7895	16.4440	-2.65454	0.70979	1.12416	-2.97173	1.58379	0.69248	0.18105	0.12113	0.12538	0.12962
9	5198	13.8148	15.5870	-1.77226	0.72799	0.77367	-2.36150	1.06275	0.90563	0.26384	0.23506	0.23894	0.24281
10	5133	14.6410	18.4376	-3.79667	0.87474	2.16437	-2.75930	2.47430	0.49559	0.19062	0.08924	0.09447	0.09969
11	5157	13.6425	16.0871	-2.44462	0.87511	1.13435	-2.45361	1.29623	0.74416	0.24728	0.17850	0.18402	0.18953

Comparison between Pearson & Lin Concordance Correlation Coefficient

E2_WS4_SOS20 and E2_WS4_SOS10

Obs	r	rc	thres_90	rdiff_05	rdiff_05_10
1	0.76183	0.18866	.	.	.
2	0.81512	0.21800	.	.	.
3	0.91084	0.29666	.	.	.
4	0.66683	0.14063	.	.	.
5	0.84517	0.19419	.	.	.
6	0.91244	0.25758	.	.	.
7	0.82234	0.27544	.	.	.
8	0.69248	0.12538	.	.	.
9	0.90563	0.23894	.	.	.
10	0.49559	0.09447	.	.	.
11	0.74416	0.18402	.	.	.

Table of Threshold by Difference		
Threshold	**Difference**	
Frequency	**Over**	**Total**
< 0.90	11	11
Total	11	11

Systematic Phenometric Sensitivity Analysis (Bryanna Pockrandt)

Length of the Season for Fort Riley

Concordance Coefficient: Print-out of all pieces for the calculation

E2_WS4_SOS20 and E2_WS4_SOS25

Obs	n	xbar	ybar	diffmean	sdx	sdy	u	v	r	cb	lrc	rc	urc
1	5201	15.3632	14.6114	0.75186	0.91546	0.87001	0.84247	0.95035	0.98761	0.73737	0.72462	0.72823	0.73181
2	5180	14.8770	14.1246	0.75237	0.91271	0.85174	0.85332	0.93320	0.98371	0.73181	0.71569	0.71989	0.72403
3	5214	15.0240	14.2862	0.73788	0.94565	0.92119	0.79058	0.97413	0.99141	0.76170	0.75221	0.75516	0.75807
4	5203	14.1149	13.3729	0.74196	0.65494	0.61172	1.17220	0.93401	0.97319	0.59194	0.57127	0.57607	0.58084
5	5200	14.5043	13.6889	0.81542	0.90806	0.84585	0.93042	0.93149	0.98345	0.69669	0.68097	0.68516	0.68931
6	5199	15.1219	14.3226	0.79929	0.92776	0.90881	0.87046	0.97958	0.98313	0.72513	0.70879	0.71290	0.71695
7	5216	15.0626	14.1852	0.87740	1.17538	1.11410	0.76673	0.94786	0.98758	0.77198	0.75878	0.76239	0.76595
8	5200	13.7895	13.0130	0.77650	0.70979	0.67968	1.11795	0.95758	0.97937	0.61506	0.59809	0.60238	0.60663
9	5198	13.8148	13.1357	0.67909	0.72799	0.75432	0.91640	1.03618	0.98355	0.70396	0.68832	0.69238	0.69640
10	5133	14.6410	13.8057	0.83526	0.87474	0.79909	0.99904	0.91352	0.95954	0.66527	0.63202	0.63835	0.64460
11	5157	13.6425	12.8341	0.80840	0.87511	0.81974	0.95445	0.93673	0.96047	0.68605	0.65267	0.65893	0.66509

Comparison between Pearson & Lin Concordance Correlation Coefficient

E2_WS4_SOS20 and E2_WS4_SOS25

Obs	r	rc	thres_90	rdiff_05	rdiff_05_10
1	0.98761	0.72823	.	.	.
2	0.98371	0.71989	.	.	.
3	0.99141	0.75516	.	.	.
4	0.97319	0.57607	.	.	.
5	0.98345	0.68516	.	.	.
6	0.98313	0.71290	.	.	.
7	0.98758	0.76239	.	.	.
8	0.97937	0.60238	.	.	.
9	0.98355	0.69238	.	.	.
10	0.95954	0.63835	.	.	.
11	0.96047	0.65893	.	.	.

Table of Threshold by Difference		
Threshold	Difference	
Frequency	Over	Total
< 0.90	11	11
Total	11	11

Systematic Phenometric Sensitivity Analysis (Bryanna Pockrandt)

Length of the Season for Fort Riley

Concordance Coefficient: Print-out of all pieces for the calculation

E2_WS4_SOS20 and E2_WS4_SOS30

Obs	n	xbar	ybar	diffmean	sdx	sdy	u	v	r	cb	lrc	rc	urc
1	5201	15.3632	13.9706	1.39260	0.91546	0.84438	1.58393	0.92236	0.97118	0.44293	0.42624	0.43017	0.43408
2	5180	14.8770	13.4917	1.38529	0.91271	0.81683	1.60439	0.89495	0.96119	0.43607	0.41463	0.41915	0.42365
3	5214	15.0240	13.6241	1.39992	0.94565	0.90094	1.51667	0.95272	0.97734	0.46483	0.45070	0.45430	0.45788
4	5203	14.1149	12.7223	1.39260	0.65494	0.59514	2.23057	0.90870	0.93430	0.28634	0.26389	0.26753	0.27116
5	5200	14.5043	12.9982	1.50613	0.90806	0.80921	1.75701	0.89113	0.96076	0.39213	0.37265	0.37674	0.38081
6	5199	15.1219	13.6380	1.48388	0.92776	0.87833	1.64381	0.94673	0.96136	0.42507	0.40438	0.40864	0.41289
7	5216	15.0626	13.4136	1.64898	1.17538	1.06812	1.47169	0.90874	0.96059	0.47904	0.45525	0.46016	0.46504
8	5200	13.7895	12.3413	1.44821	0.70979	0.67337	2.09478	0.94870	0.94838	0.31295	0.29324	0.29679	0.30033
9	5198	13.8148	12.4718	1.34298	0.72799	0.80275	1.75678	1.10270	0.95279	0.39248	0.36955	0.37395	0.37833
10	5133	14.6410	13.0903	1.55071	0.87474	0.77946	1.87800	0.89107	0.89448	0.36100	0.31710	0.32290	0.32869
11	5157	13.6425	12.1323	1.51016	0.87511	0.78600	1.82087	0.89817	0.88450	0.37544	0.32582	0.33207	0.33830

Comparison between Pearson & Lin Concordance Correlation Coefficient

E2_WS4_SOS20 and E2_WS4_SOS30

Obs	r	rc	thres_90	rdiff_05	rdiff_05_10
1	0.97118	0.43017	.	.	.
2	0.96119	0.41915	.	.	.
3	0.97734	0.45430	.	.	.
4	0.93430	0.26753	.	.	.
5	0.96076	0.37674	.	.	.
6	0.96136	0.40864	.	.	.
7	0.96059	0.46016	.	.	.
8	0.94838	0.29679	.	.	.
9	0.95279	0.37395	.	.	.
10	0.89448	0.32290	.	.	.
11	0.88450	0.33207	.	.	.

Table of Threshold by Difference		
Threshold	**Difference**	
Frequency	**Over**	**Total**
< 0.90	11	11
Total	11	11

Systematic Phenometric Sensitivity Analysis (Bryanna Pockrandt)

Length of the Season for Fort Riley

Concordance Coefficient: Print-out of all pieces for the calculation

E2_WS4_SOS20 and E2_WS3_SOS20

Obs	n	xbar	ybar	diffmean	sdx	sdy	u	v	r	cb	lrc	rc	urc
1	5201	15.3632	14.9209	0.44232	0.91546	1.03758	0.45384	1.13340	0.94838	0.90022	0.84749	0.85375	0.85977
2	5180	14.8770	14.4203	0.45668	0.91271	0.99130	0.48011	1.08611	0.93391	0.89392	0.82767	0.83484	0.84173
3	5214	15.0240	14.5907	0.43331	0.94565	1.06558	0.43166	1.12682	0.96450	0.90884	0.87151	0.87657	0.88145
4	5203	14.1149	13.8373	0.27757	0.65494	0.76913	0.39109	1.17435	0.89103	0.91792	0.80914	0.81790	0.82629
5	5200	14.5043	14.2128	0.29158	0.90806	1.07023	0.29577	1.17858	0.94228	0.94583	0.88579	0.89124	0.89644
6	5199	15.1219	15.0228	0.09908	0.92776	1.16497	0.09530	1.25568	0.93446	0.97033	0.90245	0.90673	0.91084
7	5216	15.0626	14.9142	0.14839	1.17538	1.34694	0.11793	1.14595	0.95892	0.98401	0.94067	0.94358	0.94636
8	5200	13.7895	13.4909	0.29860	0.70979	0.77651	0.40220	1.09399	0.93144	0.92173	0.85178	0.85853	0.86499
9	5198	13.8148	13.8340	-0.01922	0.72799	0.75716	-0.02589	1.04008	0.94160	0.99889	0.93735	0.94056	0.94360
10	5133	14.6410	14.3920	0.24900	0.87474	1.04392	0.26057	1.19341	0.88872	0.95273	0.83897	0.84671	0.85410
11	5157	13.6425	13.3394	0.30308	0.87511	1.00922	0.32251	1.15324	0.92179	0.94145	0.86113	0.86782	0.87422

Comparison between Pearson & Lin Concordance Correlation Coefficient

E2_WS4_SOS20 and E2_WS3_SOS20

Obs	r	rc	thres_90	rdiff_05	rdiff_05_10
1	0.94838	0.85375	.	.	#
2	0.93391	0.83484	.	.	#
3	0.96450	0.87657	.	.	#
4	0.89103	0.81790	.	.	#
5	0.94228	0.89124	.	.	#
6	0.93446	0.90673	*	+	.
7	0.95892	0.94358	*	+	.
8	0.93144	0.85853	.	.	#
9	0.94160	0.94056	*	+	.
10	0.88872	0.84671	.	+	.
11	0.92179	0.86782	.	.	#

Table of Threshold by Difference			
Threshold	Difference		
Frequency	Below	Betwe	Total
< 0.90	1	7	8
>= 0.90	3	0	3
Total	4	7	11

Systematic Phenometric Sensitivity Analysis (Bryanna Pockrandt)

Length of the Season for Fort Riley

Concordance Coefficient: Print-out of all pieces for the calculation

E2_WS4_SOS20 and E2_WS5_SOS20

Obs	n	xbar	ybar	diffmean	sdx	sdy	u	v	r	cb	lrc	rc	urc
1	5201	15.3632	15.8723	-0.50906	0.91546	0.81119	-0.59072	0.88611	0.94101	0.84617	0.78884	0.79625	0.80343
2	5180	14.8770	15.5033	-0.62627	0.91271	0.78380	-0.74045	0.85876	0.91852	0.77776	0.70526	0.71438	0.72327
3	5214	15.0240	15.5934	-0.56935	0.94565	0.85286	-0.63398	0.90188	0.95744	0.82898	0.78727	0.79370	0.79995
4	5203	14.1149	14.3978	-0.28297	0.65494	0.59399	-0.45368	0.90695	0.91549	0.90278	0.81851	0.82648	0.83414
5	5200	14.5043	14.8302	-0.32587	0.90806	0.81611	-0.37854	0.89873	0.94202	0.92820	0.86837	0.87439	0.88015
6	5199	15.1219	15.4688	-0.34699	0.92776	0.79698	-0.40353	0.85904	0.91670	0.91493	0.83105	0.83871	0.84605
7	5216	15.0626	15.3689	-0.30631	1.17538	1.01969	-0.27979	0.86753	0.95797	0.95306	0.90862	0.91300	0.91717
8	5200	13.7895	14.1077	-0.31825	0.70979	0.71855	-0.44563	1.01235	0.93281	0.90961	0.84160	0.84850	0.85513
9	5198	13.8148	14.1200	-0.30521	0.72799	0.69971	-0.42764	0.96116	0.93790	0.91556	0.85220	0.85871	0.86495
10	5133	14.6410	15.1694	-0.52838	0.87474	1.01924	-0.55959	1.16520	0.76726	0.85596	0.64234	0.65674	0.67068
11	5157	13.6425	13.9744	-0.33194	0.87511	0.77729	-0.40247	0.88821	0.90286	0.91910	0.82155	0.82982	0.83774

Comparison between Pearson & Lin Concordance Correlation Coefficient

E2_WS4_SOS20 and E2_WS5_SOS20

Obs	r	rc	thres_90	rdiff_05	rdiff_05_10
1	0.94101	0.79625	.	.	.
2	0.91852	0.71438	.	.	.
3	0.95744	0.79370	.	.	.
4	0.91549	0.82648	.	.	#
5	0.94202	0.87439	.	.	#
6	0.91670	0.83871	.	.	#
7	0.95797	0.91300	*	+	.
8	0.93281	0.84850	.	.	#
9	0.93790	0.85871	.	.	#
10	0.76726	0.65674	.	.	.
11	0.90286	0.82982	.	.	#

Table of Threshold by Difference				
Threshold	Difference			
Frequency	Below	Betwe	Over	Total
< 0.90	0	6	4	10
>= 0.90	1	0	0	1
Total	1	6	4	11

Systematic Phenometric Sensitivity Analysis (Bryanna Pockrandt)

Length of the Season for Fort Riley

Concordance Coefficient: Print-out of all pieces for the calculation

E2_WS4_SOS20 and E1_WS4_SOS20

Obs	n	xbar	ybar	diffmean	sdx	sdy	u	v	r	cb	lrc	rc	urc
1	5201	15.3632	15.1945	0.16878	0.91546	0.95462	0.18054	1.04278	0.94419	0.98312	0.92423	0.92825	0.93205
2	5180	14.8770	14.7667	0.11029	0.91271	0.93613	0.11932	1.02566	0.94576	0.99262	0.93535	0.93878	0.94203
3	5214	15.0240	15.0563	-0.03228	0.94565	1.05417	-0.03233	1.11476	0.96210	0.99361	0.95371	0.95595	0.95809
4	5203	14.1149	14.2138	-0.09890	0.65494	0.70285	-0.14578	1.07316	0.85605	0.98705	0.83694	0.84496	0.85262
5	5200	14.5043	14.4272	0.07719	0.90806	0.98536	0.08161	1.08512	0.95103	0.99338	0.94176	0.94473	0.94756
6	5199	15.1219	15.3479	-0.22608	0.92776	0.91240	-0.24573	0.98345	0.91022	0.97056	0.87710	0.88343	0.88944
7	5216	15.0626	15.0151	0.04745	1.17538	1.23169	0.03944	1.04791	0.96590	0.99813	0.96215	0.96410	0.96595
8	5200	13.7895	13.7186	0.07088	0.70979	0.71396	0.09957	1.00588	0.94303	0.99505	0.93494	0.93836	0.94161
9	5198	13.8148	13.8111	0.00364	0.72799	0.72438	0.00501	0.99505	0.95349	0.99998	0.95093	0.95347	0.95587
10	5133	14.6410	14.4873	0.15363	0.87474	0.88626	0.17449	1.01317	0.84192	0.98492	0.82032	0.82922	0.83772
11	5157	13.6425	13.5685	0.07402	0.87511	0.88587	0.08406	1.01229	0.93430	0.99641	0.92714	0.93094	0.93455

Comparison between Pearson & Lin Concordance Correlation Coefficient

E2_WS4_SOS20 and E1_WS4_SOS20

Obs	r	rc	thres_90	rdiff_05	rdiff_05_10
1	0.94419	0.92825	*	+	.
2	0.94576	0.93878	*	+	.
3	0.96210	0.95595	*	+	.
4	0.85605	0.84496	.	+	.
5	0.95103	0.94473	*	+	.
6	0.91022	0.88343	.	+	.
7	0.96590	0.96410	*	+	.
8	0.94303	0.93836	*	+	.
9	0.95349	0.95347	*	+	.
10	0.84192	0.82922	.	+	.
11	0.93430	0.93094	*	+	.

Table of Threshold by Difference		
Threshold	**Difference**	
Frequency	**Below**	**Total**
< 0.90	3	3
>= 0.90	8	8
Total	11	11

Systematic Phenometric Sensitivity Analysis (Bryanna Pockrandt)

Length of the Season for Fort Riley

Concordance Coefficient: Print-out of all pieces for the calculation

E2_WS4_SOS20 and E3_WS4_SOS20

Obs	n	xbar	ybar	diffmean	sdx	sdy	u	v	r	cb	lrc	rc	urc
1	5201	15.3632	15.1619	0.20138	0.91546	0.92591	0.21874	1.01141	0.98676	0.97657	0.96188	0.96365	0.96534
2	5180	14.8770	14.5342	0.34280	0.91271	0.95247	0.36766	1.04356	0.96632	0.93589	0.90007	0.90437	0.90850
3	5214	15.0240	14.9128	0.11122	0.94565	0.93971	0.11798	0.99372	0.99260	0.99307	0.98492	0.98572	0.98647
4	5203	14.1149	13.9774	0.13748	0.65494	0.63548	0.21310	0.97029	0.97024	0.97736	0.94543	0.94827	0.95097
5	5200	14.5043	14.2666	0.23773	0.90806	0.90050	0.26290	0.99167	0.98676	0.96656	0.95174	0.95377	0.95571
6	5199	15.1219	14.8822	0.23962	0.92776	0.95275	0.25487	1.02695	0.97943	0.96821	0.94574	0.94829	0.95073
7	5216	15.0626	14.8963	0.16624	1.17538	1.19315	0.14038	1.01511	0.99397	0.99013	0.98336	0.98416	0.98492
8	5200	13.7895	13.6265	0.16296	0.70979	0.70206	0.23085	0.98911	0.98535	0.97399	0.95777	0.95972	0.96158
9	5198	13.8148	13.6962	0.11855	0.72799	0.71841	0.16392	0.98684	0.98770	0.98666	0.97315	0.97452	0.97583
10	5133	14.6410	14.4898	0.15118	0.87474	0.85155	0.17516	0.97349	0.98622	0.98454	0.96940	0.97097	0.97246
11	5157	13.6425	13.4629	0.17964	0.87511	0.86940	0.20595	0.99347	0.99068	0.97921	0.96870	0.97009	0.97142

Comparison between Pearson & Lin Concordance Correlation Coefficient

E2_WS4_SOS20 and E3_WS4_SOS20

Obs	r	rc	thres_90	rdiff_05	rdiff_05_10
1	0.98676	0.96365	*	+	.
2	0.96632	0.90437	*	.	#
3	0.99260	0.98572	*	+	.
4	0.97024	0.94827	*	+	.
5	0.98676	0.95377	*	+	.
6	0.97943	0.94829	*	+	.
7	0.99397	0.98416	*	+	.
8	0.98535	0.95972	*	+	.
9	0.98770	0.97452	*	+	.
10	0.98622	0.97097	*	+	.
11	0.99068	0.97009	*	+	.

Table of Threshold by Difference			
Threshold	Difference		
Frequency	Below	Betwe	Total
>= 0.90	10	1	11
Total	10	1	11

Systematic Phenometric Sensitivity Analysis (Bryanna Pockrandt)

Maximum Value of the Season for Fort Riley

Concordance Coefficient: Print-out of all pieces for the calculation

E2_WS4_SOS20 and E2_WS4_SOS10

Obs	n	xbar	ybar	diffmean	sdx	sdy	u	v	r	cb	lrc	rc	urc
1	5227	205.033	205.033	0	12.4303	12.4303	0	1	1	1	.	1	.
2	5229	200.095	200.095	0	15.2525	15.2525	0	1	1	1	1	1	1
3	5222	207.156	207.156	0	12.5454	12.5454	0	1	1	1	.	1	.
4	5221	209.121	209.121	0	11.1342	11.1342	0	1	1	1	.	1	.
5	5227	200.191	200.191	0	14.1475	14.1475	0	1	1	1	.	1	.
6	5228	197.462	197.462	0	14.8426	14.8426	0	1	1	1	.	1	.
7	5225	209.855	209.855	0	11.9124	11.9124	0	1	1	1	1	1	1
8	5227	211.179	211.179	0	10.5940	10.5940	0	1	1	1	1	1	1
9	5228	209.977	209.977	0	10.5576	10.5576	0	1	1	1	.	1	.
10	5227	210.033	210.033	0	10.8602	10.8602	0	1	1	1	1	1	1
11	5226	207.910	207.910	0	11.5955	11.5955	0	1	1	1	.	1	.

Comparison between Pearson & Lin Concordance Correlation Coefficient

E2_WS4_SOS20 and E2_WS4_SOS10

Obs	r	rc	thres_90	rdiff_05	rdiff_05_10
1	1	1	*	+	.
2	1	1	*	+	.
3	1	1	*	+	.
4	1	1	*	+	.
5	1	1	*	+	.
6	1	1	*	+	.
7	1	1	*	+	.
8	1	1	*	+	.
9	1	1	*	+	.
10	1	1	*	+	.
11	1	1	*	+	.

Table of Threshold by Difference		
Threshold	**Difference**	
Frequency	**Below**	**Total**
>= 0.90	11	11
Total	11	11

Systematic Phenometric Sensitivity Analysis (Bryanna Pockrandt)

Maximum Value of the Season for Fort Riley

Concordance Coefficient: Print-out of all pieces for the calculation

E2_WS4_SOS20 and E2_WS4_SOS25

Obs	n	xbar	ybar	diffmean	sdx	sdy	u	v	r	cb	lrc	rc	urc
1	5227	205.033	205.033	0	12.4303	12.4303	0	1	1	1	.	1	.
2	5229	200.095	200.095	0	15.2525	15.2525	0	1	1	1	1	1	1
3	5222	207.156	207.156	0	12.5454	12.5454	0	1	1	1	.	1	.
4	5221	209.121	209.121	0	11.1342	11.1342	0	1	1	1	.	1	.
5	5227	200.191	200.191	0	14.1475	14.1475	0	1	1	1	.	1	.
6	5228	197.462	197.462	0	14.8426	14.8426	0	1	1	1	.	1	.
7	5225	209.855	209.855	0	11.9124	11.9124	0	1	1	1	1	1	1
8	5227	211.179	211.179	0	10.5940	10.5940	0	1	1	1	1	1	1
9	5228	209.977	209.977	0	10.5576	10.5576	0	1	1	1	.	1	.
10	5227	210.033	210.033	0	10.8602	10.8602	0	1	1	1	1	1	1
11	5226	207.910	207.910	0	11.5955	11.5955	0	1	1	1	.	1	.

Comparison between Pearson & Lin Concordance Correlation Coefficient

E2_WS4_SOS20 and E2_WS4_SOS25

Obs	r	rc	thres_90	rdiff_05	rdiff_05_10
1	1	1	*	+	.
2	1	1	*	+	.
3	1	1	*	+	.
4	1	1	*	+	.
5	1	1	*	+	.
6	1	1	*	+	.
7	1	1	*	+	.
8	1	1	*	+	.
9	1	1	*	+	.
10	1	1	*	+	.
11	1	1	*	+	.

Table of Threshold by Difference		
Threshold	**Difference**	
Frequency	**Below**	**Total**
>= 0.90	11	11
Total	11	11

Systematic Phenometric Sensitivity Analysis (Bryanna Pockrandt)

Maximum Value of the Season for Fort Riley

Concordance Coefficient: Print-out of all pieces for the calculation

E2_WS4_SOS20 and E2_WS4_SOS30

Obs	n	xbar	ybar	diffmean	sdx	sdy	u	v	r	cb	lrc	rc	urc
1	5227	205.033	205.033	0	12.4303	12.4303	0	1	1	1	.	1	.
2	5229	200.095	200.095	0	15.2525	15.2525	0	1	1	1	1	1	1
3	5222	207.156	207.156	0	12.5454	12.5454	0	1	1	1	.	1	.
4	5221	209.121	209.121	0	11.1342	11.1342	0	1	1	1	.	1	.
5	5227	200.191	200.191	0	14.1475	14.1475	0	1	1	1	.	1	.
6	5228	197.462	197.462	0	14.8426	14.8426	0	1	1	1	.	1	.
7	5225	209.855	209.855	0	11.9124	11.9124	0	1	1	1	1	1	1
8	5227	211.179	211.179	0	10.5940	10.5940	0	1	1	1	1	1	1
9	5228	209.977	209.977	0	10.5576	10.5576	0	1	1	1	.	1	.
10	5227	210.033	210.033	0	10.8602	10.8602	0	1	1	1	1	1	1
11	5226	207.910	207.910	0	11.5955	11.5955	0	1	1	1	.	1	.

Comparison between Pearson & Lin Concordance Correlation Coefficient

E2_WS4_SOS20 and E2_WS4_SOS30

Obs	r	rc	thres_90	rdiff_05	rdiff_05_10
1	1	1	*	+	.
2	1	1	*	+	.
3	1	1	*	+	.
4	1	1	*	+	.
5	1	1	*	+	.
6	1	1	*	+	.
7	1	1	*	+	.
8	1	1	*	+	.
9	1	1	*	+	.
10	1	1	*	+	.
11	1	1	*	+	.

Table of Threshold by Difference		
Threshold	**Difference**	
Frequency	**Below**	**Total**
>= 0.90	11	11
Total	11	11

Systematic Phenometric Sensitivity Analysis (Bryanna Pockrandt)

Maximum Value of the Season for Fort Riley

Concordance Coefficient: Print-out of all pieces for the calculation

E2_WS4_SOS20 and E2_WS3_SOS20

Obs	n	xbar	ybar	diffmean	sdx	sdy	u	v	r	cb	lrc	rc	urc
1	5227	205.033	205.294	-0.26097	12.4303	11.8167	-0.02153	0.95064	0.98165	0.99849	0.97910	0.98016	0.98117
2	5229	200.095	201.714	-1.61933	15.2525	14.2890	-0.10969	0.93683	0.97104	0.99192	0.96114	0.96319	0.96514
3	5222	207.156	207.323	-0.16762	12.5454	11.7959	-0.01378	0.94026	0.98225	0.99801	0.97926	0.98030	0.98128
4	5221	209.121	208.352	0.76853	11.1342	10.9726	0.06953	0.98549	0.98032	0.99748	0.97659	0.97786	0.97905
5	5227	200.191	199.683	0.50809	14.1475	14.1084	0.03596	0.99724	0.99149	0.99935	0.99032	0.99085	0.99134
6	5228	197.462	198.927	-1.46417	14.8426	14.2318	-0.10074	0.95885	0.98372	0.99408	0.97663	0.97789	0.97909
7	5225	209.855	211.273	-1.41742	11.9124	11.6464	-0.12034	0.97767	0.98387	0.99256	0.97520	0.97655	0.97783
8	5227	211.179	209.891	1.28799	10.5940	10.1577	0.12416	0.95881	0.97869	0.99148	0.96866	0.97036	0.97196
9	5228	209.977	209.261	0.71609	10.5576	10.1767	0.06908	0.96392	0.98402	0.99695	0.97994	0.98102	0.98204
10	5227	210.033	211.016	-0.98288	10.8602	9.9231	-0.09468	0.91371	0.96179	0.99152	0.95113	0.95363	0.95600
11	5226	207.910	207.441	0.46961	11.5955	11.0073	0.04157	0.94927	0.97880	0.99779	0.97537	0.97664	0.97784

Comparison between Pearson & Lin Concordance Correlation Coefficient

E2_WS4_SOS20 and E2_WS3_SOS20

Obs	r	rc	thres_90	rdiff_05	rdiff_05_10
1	0.98165	0.98016	*	+	.
2	0.97104	0.96319	*	+	.
3	0.98225	0.98030	*	+	.
4	0.98032	0.97786	*	+	.
5	0.99149	0.99085	*	+	.
6	0.98372	0.97789	*	+	.
7	0.98387	0.97655	*	+	.
8	0.97869	0.97036	*	+	.
9	0.98402	0.98102	*	+	.
10	0.96179	0.95363	*	+	.
11	0.97880	0.97664	*	+	.

Table of Threshold by Difference		
Threshold	**Difference**	
Frequency	**Below**	**Total**
>= 0.90	11	11
Total	11	11

Systematic Phenometric Sensitivity Analysis (Bryanna Pockrandt)

Maximum Value of the Season for Fort Riley

Concordance Coefficient: Print-out of all pieces for the calculation

E2_WS4_SOS20 and E2_WS5_SOS20

Obs	n	xbar	ybar	diffmean	sdx	sdy	u	v	r	cb	lrc	rc	urc
1	5227	205.033	204.780	0.25357	12.4303	13.1637	0.01982	1.05900	0.98261	0.99816	0.97979	0.98081	0.98177
2	5229	200.095	198.964	1.13092	15.2525	16.2398	0.07186	1.06473	0.97819	0.99547	0.97232	0.97376	0.97512
3	5222	207.156	204.887	2.26886	12.5454	12.8720	0.17854	1.02603	0.98420	0.98399	0.96674	0.96844	0.97006
4	5221	209.121	209.899	-0.77862	11.1342	11.1780	-0.06979	1.00393	0.98492	0.99756	0.98151	0.98252	0.98348
5	5227	200.191	201.436	-1.24494	14.1475	14.1944	-0.08785	1.00332	0.99116	0.99615	0.98660	0.98734	0.98804
6	5228	197.462	196.570	0.89250	14.8426	15.3882	0.05906	1.03676	0.98004	0.99761	0.97645	0.97770	0.97888
7	5225	209.855	208.592	1.26270	11.9124	12.8007	0.10225	1.07457	0.98109	0.99225	0.97202	0.97349	0.97487
8	5227	211.179	211.715	-0.53629	10.5940	10.6352	-0.05052	1.00389	0.98356	0.99872	0.98129	0.98230	0.98325
9	5228	209.977	210.623	-0.64635	10.5576	11.0989	-0.05971	1.05127	0.98195	0.99698	0.97782	0.97898	0.98008
10	5227	210.033	209.823	0.20995	10.8602	11.2779	0.01897	1.03846	0.98161	0.99911	0.97969	0.98074	0.98173
11	5226	207.910	208.141	-0.23104	11.5955	11.8599	-0.01970	1.02280	0.98122	0.99955	0.97972	0.98078	0.98178

Comparison between Pearson & Lin Concordance Correlation Coefficient

E2_WS4_SOS20 and E2_WS5_SOS20

Obs	r	rc	thres_90	rdiff_05	rdiff_05_10
1	0.98261	0.98081	*	+	.
2	0.97819	0.97376	*	+	.
3	0.98420	0.96844	*	+	.
4	0.98492	0.98252	*	+	.
5	0.99116	0.98734	*	+	.
6	0.98004	0.97770	*	+	.
7	0.98109	0.97349	*	+	.
8	0.98356	0.98230	*	+	.
9	0.98195	0.97898	*	+	.
10	0.98161	0.98074	*	+	.
11	0.98122	0.98078	*	+	.

Table of Threshold by Difference		
Threshold	Difference	
Frequency	Below	Total
>= 0.90	11	11
Total	11	11

Systematic Phenometric Sensitivity Analysis (Bryanna Pockrandt)

Maximum Value of the Season for Fort Riley

Concordance Coefficient: Print-out of all pieces for the calculation

E2_WS4_SOS20 and E1_WS4_SOS20

Obs	n	xbar	ybar	diffmean	sdx	sdy	u	v	r	cb	lrc	rc	urc
1	5227	205.033	200.172	4.86086	12.4303	13.0269	0.38199	1.04799	0.97754	0.93105	0.90659	0.91013	0.91355
2	5229	200.095	193.647	6.44777	15.2525	14.7667	0.42963	0.96815	0.96547	0.91507	0.87874	0.88347	0.88803
3	5222	207.156	204.034	3.12139	12.5454	12.5975	0.24829	1.00415	0.98377	0.97009	0.95217	0.95434	0.95642
4	5221	209.121	204.893	4.22775	11.1342	11.6396	0.37137	1.04539	0.97800	0.93463	0.91062	0.91406	0.91738
5	5227	200.191	195.051	5.14006	14.1475	14.4543	0.35944	1.02168	0.98715	0.93912	0.92454	0.92705	0.92948
6	5228	197.462	190.987	6.47565	14.8426	15.4160	0.42810	1.03863	0.98043	0.91546	0.89402	0.89754	0.90095
7	5225	209.855	205.912	3.94323	11.9124	12.1757	0.32742	1.02210	0.97937	0.94891	0.92631	0.92934	0.93224
8	5227	211.179	207.543	3.63623	10.5940	10.1613	0.35047	0.95915	0.97855	0.94137	0.91791	0.92117	0.92431
9	5228	209.977	206.976	3.00143	10.5576	10.2432	0.28862	0.97022	0.98346	0.95959	0.94125	0.94372	0.94609
10	5227	210.033	206.884	3.14901	10.8602	11.1908	0.28564	1.03044	0.97895	0.96039	0.93737	0.94017	0.94285
11	5226	207.910	203.909	4.00151	11.5955	11.3533	0.34875	0.97911	0.98145	0.94247	0.92201	0.92499	0.92787

Comparison between Pearson & Lin Concordance Correlation Coefficient

E2_WS4_SOS20 and E1_WS4_SOS20

Obs	r	rc	thres_90	rdiff_05	rdiff_05_10
1	0.97754	0.91013	*	.	#
2	0.96547	0.88347	.	.	#
3	0.98377	0.95434	*	+	.
4	0.97800	0.91406	*	.	#
5	0.98715	0.92705	*	.	#
6	0.98043	0.89754	.	.	#
7	0.97937	0.92934	*	.	#
8	0.97855	0.92117	*	.	#
9	0.98346	0.94372	*	+	.
10	0.97895	0.94017	*	+	.
11	0.98145	0.92499	*	.	#

Table of Threshold by Difference			
Threshold	**Difference**		
Frequency	**Below**	**Betwe**	**Total**
< 0.90	0	2	2
>= 0.90	3	6	9
Total	3	8	11

Systematic Phenometric Sensitivity Analysis (Bryanna Pockrandt)

Maximum Value of the Season for Fort Riley

Concordance Coefficient: Print-out of all pieces for the calculation

E2_WS4_SOS20 and E3_WS4_SOS20

Obs	n	xbar	ybar	diffmean	sdx	sdy	u	v	r	cb	lrc	rc	urc
1	5227	205.033	210.867	-5.83417	12.4303	12.5261	-0.46755	1.00771	0.96442	0.90144	0.86436	0.86937	0.87421
2	5229	200.095	208.294	-8.19935	15.2525	17.2486	-0.50551	1.13087	0.95833	0.88079	0.83817	0.84409	0.84980
3	5222	207.156	210.087	-2.93123	12.5454	13.4631	-0.22555	1.07315	0.98816	0.97283	0.95951	0.96132	0.96304
4	5221	209.121	214.236	-5.11559	11.1342	11.2903	-0.45626	1.01402	0.96598	0.90565	0.87000	0.87484	0.87951
5	5227	200.191	205.786	-5.59460	14.1475	14.9917	-0.38415	1.05967	0.98377	0.92983	0.91169	0.91474	0.91768
6	5228	197.462	203.062	-5.59962	14.8426	15.0292	-0.37492	1.01257	0.97411	0.93427	0.90635	0.91008	0.91367
7	5225	209.855	214.764	-4.90926	11.9124	12.4907	-0.40246	1.04854	0.97707	0.92412	0.89923	0.90293	0.90650
8	5227	211.179	215.966	-4.78756	10.5940	11.9232	-0.42598	1.12547	0.97685	0.91098	0.88576	0.88988	0.89386
9	5228	209.977	213.827	-3.85050	10.5576	11.6218	-0.34761	1.10080	0.97833	0.93894	0.91516	0.91859	0.92188
10	5227	210.033	213.856	-3.82298	10.8602	12.0348	-0.33440	1.10816	0.97367	0.94234	0.91383	0.91753	0.92108
11	5226	207.910	212.888	-4.97788	11.5955	12.6471	-0.41106	1.09069	0.98059	0.91890	0.89749	0.90107	0.90453

Comparison between Pearson & Lin Concordance Correlation Coefficient

E2_WS4_SOS20 and E3_WS4_SOS20

Obs	r	rc	thres_90	rdiff_05	rdiff_05_10
1	0.96442	0.86937	.	.	#
2	0.95833	0.84409	.	.	.
3	0.98816	0.96132	*	+	.
4	0.96598	0.87484	.	.	#
5	0.98377	0.91474	*	.	#
6	0.97411	0.91008	*	.	#
7	0.97707	0.90293	*	.	#
8	0.97685	0.88988	.	.	#
9	0.97833	0.91859	*	.	#
10	0.97367	0.91753	*	.	#
11	0.98059	0.90107	*	.	#

Table of Threshold by Difference				
Threshold	Difference			
Frequency	Below	Betwe	Over	Total
< 0.90	0	3	1	4
>= 0.90	1	6	0	7
Total	1	9	1	11

Systematic Phenometric Sensitivity Analysis (Bryanna Pockrandt)

Small Integral of the Season for Fort Riley

Concordance Coefficient: Print-out of all pieces for the calculation

E2_WS4_SOS20 and E2_WS4_SOS10

Obs	n	xbar	ybar	diffmean	sdx	sdy	u	v	r	cb	lrc	rc	urc
1	5226	1193.66	1218.04	-24.3842	125.305	128.528	-0.19214	1.02572	0.99420	0.98156	0.97485	0.97587	0.97685
2	5188	1036.42	1056.42	-20.0003	145.557	148.887	-0.13586	1.02288	0.99733	0.99060	0.98745	0.98796	0.98844
3	5211	1087.52	1102.74	-15.2207	107.559	109.350	-0.14035	1.01665	0.99736	0.99011	0.98699	0.98750	0.98799
4	5224	1118.90	1142.33	-23.4235	100.029	102.570	-0.23125	1.02540	0.98339	0.97366	0.95538	0.95749	0.95949
5	5225	1028.06	1048.72	-20.6595	136.809	138.739	-0.14996	1.01411	0.99755	0.98879	0.98585	0.98637	0.98686
6	5228	1079.09	1090.62	-11.5299	139.714	141.649	-0.08196	1.01385	0.99876	0.99656	0.99512	0.99533	0.99553
7	5227	1151.10	1178.07	-26.9643	116.805	117.532	-0.23013	1.00622	0.98988	0.97418	0.96275	0.96433	0.96584
8	5223	1098.55	1124.41	-25.8599	101.660	103.692	-0.25187	1.01999	0.99081	0.96907	0.95855	0.96016	0.96171
9	5225	1087.65	1099.50	-11.8438	121.065	120.005	-0.09826	0.99125	0.99845	0.99516	0.99334	0.99362	0.99388
10	5223	1151.63	1199.46	-47.8308	135.913	143.690	-0.34227	1.05722	0.96319	0.94329	0.90423	0.90857	0.91271
11	5228	1025.80	1047.84	-22.0350	124.914	123.440	-0.17745	0.98819	0.99371	0.98443	0.97725	0.97824	0.97918

Comparison between Pearson & Lin Concordance Correlation Coefficient

E2_WS4_SOS20 and E2_WS4_SOS10

Obs	r	rc	thres_90	rdiff_05	rdiff_05_10
1	0.99420	0.97587	*	+	.
2	0.99733	0.98796	*	+	.
3	0.99736	0.98750	*	+	.
4	0.98339	0.95749	*	+	.
5	0.99755	0.98637	*	+	.
6	0.99876	0.99533	*	+	.
7	0.98988	0.96433	*	+	.
8	0.99081	0.96016	*	+	.
9	0.99845	0.99362	*	+	.
10	0.96319	0.90857	*	.	#
11	0.99371	0.97824	*	+	.

Table of Threshold by Difference			
Threshold	Difference		
Frequency	Below	Betwe	Total
>= 0.90	10	1	11
Total	10	1	11

Systematic Phenometric Sensitivity Analysis (Bryanna Pockrandt)

Small Integral of the Season for Fort Riley

Concordance Coefficient: Print-out of all pieces for the calculation

E2_WS4_SOS20 and E2_WS4_SOS25

Obs	n	xbar	ybar	diffmean	sdx	sdy	u	v	r	cb	lrc	rc	urc
1	5226	1193.66	1183.38	10.2754	125.305	124.336	0.08232	0.99227	0.99712	0.99659	0.99339	0.99373	0.99405
2	5188	1036.42	1026.77	9.6475	145.557	144.648	0.06649	0.99375	0.99821	0.99778	0.99577	0.99599	0.99619
3	5211	1087.52	1079.11	8.4046	107.559	107.717	0.07808	1.00147	0.99719	0.99696	0.99384	0.99416	0.99447
4	5224	1118.90	1108.93	9.9769	100.029	99.353	0.10008	0.99324	0.99556	0.99499	0.99007	0.99058	0.99107
5	5225	1028.06	1018.43	9.6285	136.809	136.159	0.07055	0.99525	0.99791	0.99751	0.99518	0.99543	0.99566
6	5228	1079.09	1070.47	8.6202	139.714	138.497	0.06197	0.99129	0.99837	0.99805	0.99622	0.99642	0.99660
7	5227	1151.10	1137.87	13.2376	116.805	117.089	0.11319	1.00243	0.99561	0.99363	0.98872	0.98927	0.98980
8	5223	1098.55	1088.44	10.1049	101.660	101.718	0.09937	1.00057	0.99569	0.99509	0.99030	0.99080	0.99128
9	5225	1087.65	1080.79	6.8590	121.065	121.786	0.05649	1.00595	0.99792	0.99839	0.99611	0.99632	0.99652
10	5223	1151.63	1139.28	12.3466	135.913	136.101	0.09078	1.00138	0.99495	0.99590	0.99035	0.99086	0.99135
11	5228	1025.80	1014.70	11.1075	124.914	126.094	0.08850	1.00945	0.99621	0.99605	0.99185	0.99228	0.99268

Comparison between Pearson & Lin Concordance Correlation Coefficient

E2_WS4_SOS20 and E2_WS4_SOS25

Obs	r	rc	thres_90	rdiff_05	rdiff_05_10
1	0.99712	0.99373	*	+	.
2	0.99821	0.99599	*	+	.
3	0.99719	0.99416	*	+	.
4	0.99556	0.99058	*	+	.
5	0.99791	0.99543	*	+	.
6	0.99837	0.99642	*	+	.
7	0.99561	0.98927	*	+	.
8	0.99569	0.99080	*	+	.
9	0.99792	0.99632	*	+	.
10	0.99495	0.99086	*	+	.
11	0.99621	0.99228	*	+	.

Table of Threshold by Difference		
Threshold	Difference	
Frequency	Below	Total
>= 0.90	11	11
Total	11	11

Systematic Phenometric Sensitivity Analysis (Bryanna Pockrandt)

Small Integral of the Season for Fort Riley

Concordance Coefficient: Print-out of all pieces for the calculation

E2_WS4_SOS20 and E2_WS4_SOS30

Obs	n	xbar	ybar	diffmean	sdx	sdy	u	v	r	cb	lrc	rc	urc
1	5226	1193.66	1174.09	19.5694	125.305	124.656	0.15658	0.99482	0.99648	0.98788	0.98375	0.98440	0.98501
2	5188	1036.42	1017.74	18.6744	145.557	144.050	0.12897	0.98964	0.99785	0.99170	0.98915	0.98957	0.98997
3	5211	1087.52	1069.21	18.3056	107.559	107.937	0.16989	1.00351	0.99626	0.98577	0.98136	0.98208	0.98276
4	5224	1118.90	1099.98	18.9236	100.029	99.812	0.18939	0.99782	0.99448	0.98238	0.97600	0.97696	0.97789
5	5225	1028.06	1008.33	19.7286	136.809	135.629	0.14483	0.99137	0.99718	0.98958	0.98626	0.98679	0.98731
6	5228	1079.09	1060.58	18.5149	139.714	137.714	0.13348	0.98569	0.99755	0.99107	0.98818	0.98864	0.98909
7	5227	1151.10	1123.69	27.4160	116.805	117.586	0.23394	1.00668	0.99388	0.97334	0.96617	0.96739	0.96856
8	5223	1098.55	1077.63	20.9212	101.660	102.427	0.20502	1.00754	0.99555	0.97939	0.97411	0.97503	0.97592
9	5225	1087.65	1071.23	16.4212	121.065	122.712	0.13473	1.01361	0.99644	0.99092	0.98681	0.98739	0.98794
10	5223	1151.63	1127.48	24.1530	135.913	137.114	0.17693	1.00884	0.99334	0.98455	0.97698	0.97799	0.97896
11	5228	1025.80	1003.28	22.5275	124.914	126.960	0.17889	1.01638	0.99327	0.98412	0.97647	0.97750	0.97849

Comparison between Pearson & Lin Concordance Correlation Coefficient

E2_WS4_SOS20 and E2_WS4_SOS30

Obs	r	rc	thres_90	rdiff_05	rdiff_05_10
1	0.99648	0.98440	*	+	.
2	0.99785	0.98957	*	+	.
3	0.99626	0.98208	*	+	.
4	0.99448	0.97696	*	+	.
5	0.99718	0.98679	*	+	.
6	0.99755	0.98864	*	+	.
7	0.99388	0.96739	*	+	.
8	0.99555	0.97503	*	+	.
9	0.99644	0.98739	*	+	.
10	0.99334	0.97799	*	+	.
11	0.99327	0.97750	*	+	.

Table of Threshold by Difference		
Threshold	Difference	
Frequency	Below	Total
>= 0.90	11	11
Total	11	11

Systematic Phenometric Sensitivity Analysis (Bryanna Pockrandt)

Small Integral of the Season for Fort Riley

Concordance Coefficient: Print-out of all pieces for the calculation

E2_WS4_SOS20 and E2_WS3_SOS20

Obs	n	xbar	ybar	diffmean	sdx	sdy	u	v	r	cb	lrc	rc	urc
1	5226	1193.66	1167.69	25.9671	125.305	123.934	0.20837	0.98906	0.97515	0.97869	0.95188	0.95437	0.95673
2	5188	1036.42	1001.62	34.7993	145.557	145.108	0.23945	0.99692	0.97849	0.97213	0.94872	0.95122	0.95360
3	5211	1087.52	1064.41	23.1078	107.559	105.335	0.21709	0.97933	0.97292	0.97677	0.94762	0.95032	0.95288
4	5224	1118.90	1106.26	12.6431	100.029	96.068	0.12897	0.96040	0.96820	0.99095	0.95713	0.95944	0.96162
5	5225	1028.06	1017.18	10.8798	136.809	136.168	0.07971	0.99531	0.98329	0.99682	0.97901	0.98016	0.98125
6	5228	1079.09	1086.12	-7.0239	139.714	150.603	-0.04842	1.07794	0.97908	0.99603	0.97388	0.97519	0.97644
7	5227	1151.10	1154.24	-3.1360	116.805	121.665	-0.02631	1.04160	0.96310	0.99882	0.95990	0.96197	0.96392
8	5223	1098.55	1084.45	14.0986	101.660	99.123	0.14045	0.97505	0.97638	0.98992	0.96462	0.96654	0.96836
9	5225	1087.65	1095.77	-8.1144	121.065	118.006	-0.06789	0.97473	0.98103	0.99737	0.97723	0.97845	0.97961
10	5223	1151.63	1155.46	-3.8354	135.913	129.479	-0.02891	0.95266	0.97400	0.99841	0.97096	0.97245	0.97386
11	5228	1025.80	1013.34	12.4580	124.914	122.666	0.10064	0.98200	0.97345	0.99480	0.96658	0.96839	0.97011

Comparison between Pearson & Lin Concordance Correlation Coefficient

E2_WS4_SOS20 and E2_WS3_SOS20

Obs	r	rc	thres_90	rdiff_05	rdiff_05_10
1	0.97515	0.95437	*	+	.
2	0.97849	0.95122	*	+	.
3	0.97292	0.95032	*	+	.
4	0.96820	0.95944	*	+	.
5	0.98329	0.98016	*	+	.
6	0.97908	0.97519	*	+	.
7	0.96310	0.96197	*	+	.
8	0.97638	0.96654	*	+	.
9	0.98103	0.97845	*	+	.
10	0.97400	0.97245	*	+	.
11	0.97345	0.96839	*	+	.

Table of Threshold by Difference		
Threshold	Difference	
Frequency	Below	Total
>= 0.90	11	11
Total	11	11

Systematic Phenometric Sensitivity Analysis (Bryanna Pockrandt)

Small Integral of the Season for Fort Riley

Concordance Coefficient: Print-out of all pieces for the calculation

E2_WS4_SOS20 and E2_WS5_SOS20

Obs	n	xbar	ybar	diffmean	sdx	sdy	u	v	r	cb	lrc	rc	urc
1	5226	1193.66	1228.59	-34.9322	125.305	125.558	-0.27850	1.00202	0.96932	0.96267	0.92974	0.93314	0.93637
2	5188	1036.42	1065.56	-29.1442	145.557	143.738	-0.20149	0.98750	0.97953	0.98003	0.95780	0.95997	0.96202
3	5211	1087.52	1113.88	-26.3577	107.559	108.958	-0.24348	1.01301	0.97434	0.97113	0.94341	0.94621	0.94888
4	5224	1118.90	1135.54	-16.6326	100.029	105.348	-0.16203	1.05317	0.97748	0.98574	0.96150	0.96354	0.96547
5	5225	1028.06	1035.68	-7.6239	136.809	142.230	-0.05465	1.03962	0.98918	0.99776	0.98623	0.98696	0.98765
6	5228	1079.09	1094.56	-15.4624	139.714	143.381	-0.10925	1.02625	0.97563	0.99374	0.96777	0.96952	0.97118
7	5227	1151.10	1163.83	-12.7251	116.805	119.882	-0.10754	1.02634	0.95857	0.99392	0.95008	0.95274	0.95526
8	5223	1098.55	1107.24	-8.6943	101.660	108.182	-0.08290	1.06415	0.97885	0.99466	0.97216	0.97363	0.97501
9	5225	1087.65	1106.41	-18.7541	121.065	127.861	-0.15074	1.05614	0.97847	0.98731	0.96415	0.96606	0.96786
10	5223	1151.63	1171.14	-19.5081	135.913	145.971	-0.13850	1.07400	0.96526	0.98800	0.95110	0.95368	0.95613
11	5228	1025.80	1032.60	-6.7977	124.914	134.241	-0.05249	1.07467	0.97785	0.99604	0.97259	0.97398	0.97530

Comparison between Pearson & Lin Concordance Correlation Coefficient

E2_WS4_SOS20 and E2_WS5_SOS20

Obs	r	rc	thres_90	rdiff_05	rdiff_05_10
1	0.96932	0.93314	*	+	.
2	0.97953	0.95997	*	+	.
3	0.97434	0.94621	*	+	.
4	0.97748	0.96354	*	+	.
5	0.98918	0.98696	*	+	.
6	0.97563	0.96952	*	+	.
7	0.95857	0.95274	*	+	.
8	0.97885	0.97363	*	+	.
9	0.97847	0.96606	*	+	.
10	0.96526	0.95368	*	+	.
11	0.97785	0.97398	*	+	.

Table of Threshold by Difference		
Threshold	Difference	
Frequency	Below	Total
>= 0.90	11	11
Total	11	11

Systematic Phenometric Sensitivity Analysis (Bryanna Pockrandt)

Small Integral of the Season for Fort Riley

Concordance Coefficient: Print-out of all pieces for the calculation

E2_WS4_SOS20 and E1_WS4_SOS20

Obs	n	xbar	ybar	diffmean	sdx	sdy	u	v	r	cb	lrc	rc	urc
1	5226	1193.66	1148.60	45.0564	125.305	122.018	0.36438	0.97377	0.96463	0.93743	0.89992	0.90427	0.90845
2	5188	1036.42	979.60	56.8130	145.557	145.434	0.39048	0.99916	0.97991	0.92916	0.90714	0.91050	0.91373
3	5211	1087.52	1066.93	20.5844	107.559	115.656	0.18456	1.07528	0.96648	0.98071	0.94495	0.94784	0.95057
4	5224	1118.90	1131.93	-13.0321	100.029	103.276	-0.12822	1.03246	0.95245	0.99135	0.94107	0.94421	0.94718
5	5225	1028.06	1008.04	20.0202	136.809	138.139	0.14563	1.00972	0.98125	0.98946	0.96925	0.97091	0.97249
6	5228	1079.09	1051.61	27.4789	139.714	152.265	0.18840	1.08983	0.96148	0.97900	0.93808	0.94129	0.94435
7	5227	1151.10	1143.58	7.5245	116.805	120.510	0.06342	1.03171	0.95706	0.99751	0.95218	0.95467	0.95704
8	5223	1098.55	1081.55	16.9992	101.660	98.867	0.16956	0.97253	0.96849	0.98545	0.95181	0.95440	0.95685
9	5225	1087.65	1098.55	-10.9004	121.065	121.980	-0.08970	1.00756	0.97376	0.99597	0.96810	0.96983	0.97147
10	5223	1151.63	1148.95	2.6827	135.913	138.057	0.01958	1.01578	0.95548	0.99969	0.95274	0.95518	0.95750
11	5228	1025.80	1015.72	10.0813	124.914	128.358	0.07962	1.02757	0.97407	0.99647	0.96897	0.97064	0.97221

Comparison between Pearson & Lin Concordance Correlation Coefficient

E2_WS4_SOS20 and E1_WS4_SOS20

Obs	r	rc	thres_90	rdiff_05	rdiff_05_10
1	0.96463	0.90427	*	.	#
2	0.97991	0.91050	*	.	#
3	0.96648	0.94784	*	+	.
4	0.95245	0.94421	*	+	.
5	0.98125	0.97091	*	+	.
6	0.96148	0.94129	*	+	.
7	0.95706	0.95467	*	+	.
8	0.96849	0.95440	*	+	.
9	0.97376	0.96983	*	+	.
10	0.95548	0.95518	*	+	.
11	0.97407	0.97064	*	+	.

Table of Threshold by Difference			
Threshold	Difference		
Frequency	Below	Betwe	Total
>= 0.90	9	2	11
Total	9	2	11

Systematic Phenometric Sensitivity Analysis (Bryanna Pockrandt)

Small Integral of the Season for Fort Riley

Concordance Coefficient: Print-out of all pieces for the calculation

E2_WS4_SOS20 and E3_WS4_SOS20

Obs	n	xbar	ybar	diffmean	sdx	sdy	u	v	r	cb	lrc	rc	urc
1	5226	1193.66	1223.24	-29.5783	125.305	123.070	-0.23818	0.98216	0.99164	0.97226	0.96267	0.96413	0.96554
2	5188	1036.42	1069.13	-32.7106	145.557	147.144	-0.22351	1.01091	0.99109	0.97557	0.96543	0.96688	0.96826
3	5211	1087.52	1116.36	-28.8385	107.559	106.290	-0.26971	0.98820	0.98975	0.96484	0.95315	0.95495	0.95668
4	5224	1118.90	1134.94	-16.0353	100.029	100.620	-0.15983	1.00591	0.99390	0.98737	0.98046	0.98135	0.98220
5	5225	1028.06	1042.62	-14.5646	136.809	140.057	-0.10522	1.02374	0.99743	0.99422	0.99127	0.99167	0.99205
6	5228	1079.09	1105.95	-26.8556	139.714	143.254	-0.18983	1.02534	0.99351	0.98200	0.97455	0.97562	0.97665
7	5227	1151.10	1169.14	-18.0350	116.805	118.018	-0.15361	1.01039	0.99444	0.98829	0.98197	0.98279	0.98357
8	5223	1098.55	1109.71	-11.1611	101.660	104.606	-0.10823	1.02898	0.99601	0.99377	0.98928	0.98981	0.99031
9	5225	1087.65	1098.13	-10.4754	121.065	124.428	-0.08535	1.02778	0.99745	0.99600	0.99312	0.99346	0.99378
10	5223	1151.63	1162.01	-10.3791	135.913	139.362	-0.07541	1.02538	0.99672	0.99685	0.99323	0.99358	0.99392
11	5228	1025.80	1038.80	-12.9986	124.914	128.319	-0.10267	1.02726	0.99672	0.99440	0.99068	0.99114	0.99157

Comparison between Pearson & Lin Concordance Correlation Coefficient

E2_WS4_SOS20 and E3_WS4_SOS20

Obs	r	rc	thres_90	rdiff_05	rdiff_05_10
1	0.99164	0.96413	*	+	.
2	0.99109	0.96688	*	+	.
3	0.98975	0.95495	*	+	.
4	0.99390	0.98135	*	+	.
5	0.99743	0.99167	*	+	.
6	0.99351	0.97562	*	+	.
7	0.99444	0.98279	*	+	.
8	0.99601	0.98981	*	+	.
9	0.99745	0.99346	*	+	.
10	0.99672	0.99358	*	+	.
11	0.99672	0.99114	*	+	.

Table of Threshold by Difference		
Threshold	**Difference**	
Frequency	**Below**	**Total**
>= 0.90	11	11
Total	11	11

Appendix D - SAS Code for Time Series Analysis

```
*********************************************************************;
* Bryanna Pockrandt Project: Systematic Kolmogorov-Smirnov Analysis  *;
*********************************************************************;

*Importing the Beg Data from Excel to SAS;
 proc import out=Beg
   datafile='F:\GRA (Consulting)\Bryanna Pockrandt\Data\Kolmogorov-Smirnov
Analysis\Composite KS Data.xlsx'
   dbms=xlsx
   replace;
   sheet="Beg";
   getnames=yes;
 run;

*Importing the End Data from Excel to SAS;
 proc import out=End
   datafile='F:\GRA (Consulting)\Bryanna Pockrandt\Data\Kolmogorov-Smirnov
Analysis\Composite KS Data.xlsx'
   dbms=xlsx
   replace;
   sheet="End";
   getnames=yes;
 run;

*Importing the Length Data from Excel to SAS;
 proc import out=Length
   datafile='F:\GRA (Consulting)\Bryanna Pockrandt\Data\Kolmogorov-Smirnov
Analysis\Composite KS Data.xlsx'
   dbms=xlsx
   replace;
   sheet="Length";
   getnames=yes;
 run;
```

```
*Importing the Max Data from Excel to SAS;
 proc import out=Max
   datafile='F:\GRA (Consulting)\Bryanna Pockrandt\Data\Kolmogorov-Smirnov
Analysis\Composite KS Data.xlsx'
   dbms=xlsx
   replace;
   sheet="Max";
   getnames=yes;
 run;

*Importing the Sint Data from Excel to SAS;
 proc import out=Sint
   datafile='F:\GRA (Consulting)\Bryanna Pockrandt\Data\Kolmogorov-Smirnov
Analysis\Composite KS Data.xlsx'
   dbms=xlsx
   replace;
   sheet="Sint";
   getnames=yes;
 run;

/* Performs Kolmogorov-Smirnov Test for Comparisons between Locations during
a Particular Season & Specified Phenometric */
 %macro kstest(pheno,loc1,loc2,season);

   ods graphics on;
   proc npar1way data=&pheno edf plots=edfplot;
      where ( Location in(&loc1,&loc2) & Season=&season );
      var Value;
      class Location;
   run;
   ods graphics off;

 %mend kstest;

/* Performs Kolmogorov-Smirnov Test for all Comparisons within a Particular
Season */
 %macro ks_season(pheno,season);
```

```
  *Comparison of Konza vs. Fort Riley Full;
    title4 'Comparison of Konza vs. Fort Riley Full';
    %kstest(&pheno,'Konza','FR Full',&season);

  *Comparison of Fort Riley High vs. Fort Riley Low;
      title4 'Comparison of Fort Riley High vs. Fort Riley Low';
    %kstest(&pheno,'FR High','FR Low',&season);

  *Comparison of Konza vs. Fort Riley High;
      title4 'Comparison of Konza vs. Fort Riley High';
    %kstest(&pheno,'Konza','FR High',&season);

  *Comparison of Konza vs. Fort Riley Low;
    title4 'Comparison of Konza vs. Fort Riley Low';
    %kstest(&pheno,'Konza','FR Low',&season);

 %mend ks_season;

/* Performs Kolmogorov-Smirnov Test for all Comparisons within a Particular
Phenometric */
 %macro ks_pheno(pheno);

  *Analysis of the Normal Season;
    title3 'Season 2 (Normal)';
    %ks_season(&pheno,2);

  *Analysis of the Cool, Wet Season;
      title3 'Season 8 (Cool, Wet)';
    %ks_season(&pheno,8);

  *Analysis of the Hot, Dry Season;
    title3 'Season 11 (Hot, Dry)';
    %ks_season(&pheno,11);

 %mend ks_pheno;
```

```
ods rtf file = "F:\GRA (Consulting)\Bryanna Pockrandt\Systematic Statistical
Analysis on Kolmogorov-Smirnov Analysis (Bryanna Pockrandt).doc";

title 'Systematic Kolmogorov-Smirnov Analysis (Bryanna Pockrandt)';

  title2 'Phenometric: Beginning of the Season';
  %ks_pheno(Beg);

  title2 'Phenometric: End of the Season';
  %ks_pheno(End);

  title2 'Phenometric: Length of the Season';
  %ks_pheno(Length);

  title2 'Phenometric: Maximum Value of the Season';
  %ks_pheno(Max);

  title2 'Phenometric: Small Integral of the Season';
  %ks_pheno(Sint);

ods rtf close;

  %kstest(Beg,'Konza','FR Full',11);



  %kstest(Beg,'Konza','FR High',2);
  %kstest(Beg,'Konza','FR Low',2);

  %kstest(Beg,'FR High','FR Low',2);



  %kstest(Beg,'Konza','FR Full',11);

  %kstest(Beg,'Konza','FR Full',11);
```

Appendix E - SAS Results for Time Series Analysis

Systematic Kolmogorov-Smirnov Analysis (Bryanna Pockrandt)
Phenometric: Beginning of the Season
Season 2 (Normal)
Comparison of Konza vs. Fort Riley Full

The NPAR1WAY Procedure

Kolmogorov-Smirnov Test for Variable Value Classified by Variable Location			
Location	**N**	**EDF at Maximum**	**Deviation from Mean at Maximum**
Konza	621	0.307568	-8.589762
FR Full	5188	0.693524	2.971851
Total	5809	0.652264	
Maximum Deviation Occurred at Observation 2913			
Value of Value at Maximum = 30.10			

Kolmogorov-Smirnov Two-Sample Test (Asymptotic)			
KS	0.119256	**D**	0.385955
KSa	9.089330	**Pr > KSa**	<.0001

Cramer-von Mises Test for Variable Value Classified by Variable Location		
Location	**N**	**Summed Deviation from Mean**
Konza	621	39.933521
FR Full	5188	4.780015

Cramer-von Mises Statistics (Asymptotic)			
CM	0.007697	**CMa**	44.713536

Kuiper Test for Variable Value Classified by Variable Location		
Location	**N**	**Deviation from Mean**
Konza	621	0.001157
FR Full	5188	0.385955

Kuiper Two-Sample Test (Asymptotic)					
K	0.387112	**Ka**	9.116566	**Pr > Ka**	<.0001

Systematic Kolmogorov-Smirnov Analysis (Bryanna Pockrandt)
Phenometric: Beginning of the Season
Season 2 (Normal)
Comparison of Fort Riley High vs. Fort Riley Low

The NPAR1WAY Procedure

Kolmogorov-Smirnov Test for Variable Value Classified by Variable Location			
Location	N	EDF at Maximum	Deviation from Mean at Maximum
FR High	1213	0.280297	3.892588
FR Low	1558	0.081515	-3.434671
Total	2771	0.168531	
Maximum Deviation Occurred at Observation 1388			
Value of Value at Maximum = 29.60			

Kolmogorov-Smirnov Two-Sample Test (Asymptotic)			
KS	0.098618	D	0.198782
KSa	5.191262	Pr > KSa	<.0001

Cramer-von Mises Test for Variable Value Classified by Variable Location		
Location	N	Summed Deviation from Mean
FR High	1213	3.859020
FR Low	1558	3.004487

Cramer-von Mises Statistics (Asymptotic)			
CM	0.002477	CMa	6.863507

Kuiper Test for Variable Value Classified by Variable Location		
Location	**N**	**Deviation from Mean**
FR High	1213	0.198782
FR Low	1558	0.023331

Kuiper Two-Sample Test (Asymptotic)					
K	0.222113	**Ka**	5.800557	**Pr > Ka**	<.0001

Systematic Kolmogorov-Smirnov Analysis (Bryanna Pockrandt)
Phenometric: Beginning of the Season
Season 2 (Normal)
Comparison of Konza vs. Fort Riley High

The NPAR1WAY Procedure

Kolmogorov-Smirnov Test for Variable Value Classified by Variable Location			
Location	N	EDF at Maximum	Deviation from Mean at Maximum
Konza	621	0.307568	-5.692159
FR High	1213	0.652927	4.072794
Total	1834	0.535987	
Maximum Deviation Occurred at Observation 939			
Value of Value at Maximum = 30.10			

Kolmogorov-Smirnov Two-Sample Test (Asymptotic)			
KS	0.163436	D	0.345358
KSa	6.999166	Pr > KSa	<.0001

Cramer-von Mises Test for Variable Value Classified by Variable Location		
Location	N	Summed Deviation from Mean
Konza	621	17.293772
FR High	1213	8.853613

Cramer-von Mises Statistics (Asymptotic)			
CM	0.014257	CMa	26.147385

Kuiper Test for Variable Value Classified by Variable Location		
Location	**N**	**Deviation from Mean**
Konza	621	0.000000
FR High	1213	0.345358

Kuiper Two-Sample Test (Asymptotic)					
K	0.345358	**Ka**	6.999166	**Pr > Ka**	<.0001

Systematic Kolmogorov-Smirnov Analysis (Bryanna Pockrandt)
Phenometric: Beginning of the Season
Season 2 (Normal)
Comparison of Konza vs. Fort Riley Low

The NPAR1WAY Procedure

Kolmogorov-Smirnov Test for Variable Value Classified by Variable Location			
Location	N	EDF at Maximum	Deviation from Mean at Maximum
Konza	621	0.307568	-4.801088
FR Low	1558	0.577022	3.031110
Total	2179	0.500229	
Maximum Deviation Occurred at Observation 1109			
Value of Value at Maximum = 30.10			

Kolmogorov-Smirnov Two-Sample Test (Asymptotic)			
KS	0.121634	D	0.269453
KSa	5.677858	Pr > KSa	<.0001

Cramer-von Mises Test for Variable Value Classified by Variable Location		
Location	N	Summed Deviation from Mean
Konza	621	13.924339
FR Low	1558	5.550073

Cramer-von Mises Statistics (Asymptotic)			
CM	0.008937	**CMa**	19.474412

Kuiper Test for Variable Value Classified by Variable Location		
Location	**N**	**Deviation from Mean**
Konza	621	0.001926
FR Low	1558	0.269453

Kuiper Two-Sample Test (Asymptotic)					
K	0.271379	**Ka**	5.718433	**Pr > Ka**	<.0001

Systematic Kolmogorov-Smirnov Analysis (Bryanna Pockrandt)
Phenometric: Beginning of the Season
Season 8 (Cool, Wet)
Comparison of Konza vs. Fort Riley Full

The NPAR1WAY Procedure

Kolmogorov-Smirnov Test for Variable Value Classified by Variable Location			
Location	**N**	**EDF at Maximum**	**Deviation from Mean at Maximum**
Konza	621	0.202899	-4.529672
FR Full	5223	0.406280	1.561898
Total	5844	0.384668	
Maximum Deviation Occurred at Observation 2977			
Value of Value at Maximum = 168.30			

Kolmogorov-Smirnov Two-Sample Test (Asymptotic)			
KS	0.062677	**D**	0.203381
KSa	4.791394	**Pr > KSa**	<.0001

Cramer-von Mises Test for Variable Value Classified by Variable Location		
Location	**N**	**Summed Deviation from Mean**
Konza	621	8.365952
FR Full	5223	0.994688

Cramer-von Mises Statistics (Asymptotic)			
CM	0.001602	**CMa**	9.360641

Kuiper Test for Variable Value Classified by Variable Location		
Location	**N**	**Deviation from Mean**
Konza	621	0.001610
FR Full	5223	0.203381

Kuiper Two-Sample Test (Asymptotic)					
K	0.204992	**Ka**	4.829330	**Pr > Ka**	<.0001

Systematic Kolmogorov-Smirnov Analysis (Bryanna Pockrandt)
Phenometric: Beginning of the Season
Season 8 (Cool, Wet)
Comparison of Fort Riley High vs. Fort Riley Low

The NPAR1WAY Procedure

Kolmogorov-Smirnov Test for Variable Value Classified by Variable Location			
Location	**N**	**EDF at Maximum**	**Deviation from Mean at Maximum**
FR High	1237	0.362167	2.892401
FR Low	1553	0.214424	-2.581414
Total	2790	0.279928	
Maximum Deviation Occurred at Observation 1403			
Value of Value at Maximum = 168.20			

Kolmogorov-Smirnov Two-Sample Test (Asymptotic)			
KS	0.073396	**D**	0.147743
KSa	3.876813	**Pr > KSa**	<.0001

Cramer-von Mises Test for Variable Value Classified by Variable Location		
Location	**N**	**Summed Deviation from Mean**
FR High	1237	4.525396
FR Low	1553	3.604581

Cramer-von Mises Statistics (Asymptotic)			
CM	0.002914	**CMa**	8.129976

Kuiper Test for Variable Value Classified by Variable Location		
Location	**N**	**Deviation from Mean**
FR High	1237	0.147743
FR Low	1553	0.000000

Kuiper Two-Sample Test (Asymptotic)					
K	0.147743	**Ka**	3.876813	**Pr > Ka**	<.0001

Systematic Kolmogorov-Smirnov Analysis (Bryanna Pockrandt)
Phenometric: Beginning of the Season
Season 8 (Cool, Wet)
Comparison of Konza vs. Fort Riley High

The NPAR1WAY Procedure

Kolmogorov-Smirnov Test for Variable Value Classified by Variable Location			
Location	N	EDF at Maximum	Deviation from Mean at Maximum
Konza	621	0.104670	-4.272100
FR High	1237	0.362167	3.026930
Total	1858	0.276103	
Maximum Deviation Occurred at Observation 972			
Value of Value at Maximum = 168.20			

Kolmogorov-Smirnov Two-Sample Test (Asymptotic)			
KS	0.121466	D	0.257497
KSa	5.235756	Pr > KSa	<.0001

Cramer-von Mises Test for Variable Value Classified by Variable Location		
Location	N	Summed Deviation from Mean
Konza	621	6.941662
FR High	1237	3.484860

Cramer-von Mises Statistics (Asymptotic)			
CM	0.005612	CMa	10.426522

Kuiper Test for Variable Value Classified by Variable Location		
Location	**N**	**Deviation from Mean**
Konza	621	0.001610
FR High	1237	0.257497

Kuiper Two-Sample Test (Asymptotic)					
K	0.259107	**Ka**	5.268498	**Pr > Ka**	<.0001

Systematic Kolmogorov-Smirnov Analysis (Bryanna Pockrandt)
Phenometric: Beginning of the Season
Season 8 (Cool, Wet)
Comparison of Konza vs. Fort Riley Low

The NPAR1WAY Procedure

Kolmogorov-Smirnov Test for Variable Value Classified by Variable Location			
Location	**N**	**EDF at Maximum**	**Deviation from Mean at Maximum**
Konza	621	0.104670	-1.953787
FR Low	1553	0.214424	1.235485
Total	2174	0.183073	
Maximum Deviation Occurred at Observation 1110			
Value of Value at Maximum = 168.20			

Kolmogorov-Smirnov Two-Sample Test (Asymptotic)			
KS	0.049578	**D**	0.109754
KSa	2.311646	**Pr > KSa**	<.0001

Cramer-von Mises Test for Variable Value Classified by Variable Location		
Location	**N**	**Summed Deviation from Mean**
Konza	621	0.903923
FR Low	1553	0.361453

Cramer-von Mises Statistics (Asymptotic)			
CM	0.000582	**CMa**	1.265376

Kuiper Test for Variable Value Classified by Variable Location		
Location	**N**	**Deviation from Mean**
Konza	621	0.017951
FR Low	1553	0.109754

Kuiper Two-Sample Test (Asymptotic)					
K	0.127705	**Ka**	2.689728	**Pr > Ka**	<.0001

Systematic Kolmogorov-Smirnov Analysis (Bryanna Pockrandt)
Phenometric: Beginning of the Season
Season 11 (Hot, Dry)
Comparison of Konza vs. Fort Riley Full

The NPAR1WAY Procedure

Kolmogorov-Smirnov Test for Variable Value Classified by Variable Location			
Location	**N**	**EDF at Maximum**	**Deviation from Mean at Maximum**
Konza	621	0.162641	-3.948295
FR Full	5228	0.339901	1.360779
Total	5849	0.321081	
Maximum Deviation Occurred at Observation 2948			
Value of Value at Maximum = 237.10			

Kolmogorov-Smirnov Two-Sample Test (Asymptotic)			
KS	0.054606	**D**	0.177260
KSa	4.176213	**Pr > KSa**	<.0001

Cramer-von Mises Test for Variable Value Classified by Variable Location		
Location	**N**	**Summed Deviation from Mean**
Konza	621	5.677255
FR Full	5228	0.674364

Cramer-von Mises Statistics (Asymptotic)			
CM	0.001086	**CMa**	6.351619

Kuiper Test for Variable Value Classified by Variable Location		
Location	**N**	**Deviation from Mean**
Konza	621	0.047579
FR Full	5228	0.177260

Kuiper Two-Sample Test (Asymptotic)					
K	0.224838	**Ka**	5.297157	**Pr > Ka**	<.0001

Systematic Kolmogorov-Smirnov Analysis (Bryanna Pockrandt)
Phenometric: Beginning of the Season
Season 11 (Hot, Dry)
Comparison of Fort Riley High vs. Fort Riley Low

The NPAR1WAY Procedure

Kolmogorov-Smirnov Test for Variable Value Classified by Variable Location			
Location	**N**	**EDF at Maximum**	**Deviation from Mean at Maximum**
FR High	1237	0.466451	-3.350611
FR Low	1558	0.637356	2.985555
Total	2795	0.561717	
Maximum Deviation Occurred at Observation 1386			
Value of Value at Maximum = 237.20			

Kolmogorov-Smirnov Two-Sample Test (Asymptotic)			
KS	0.084887	**D**	0.170904
KSa	4.487776	**Pr > KSa**	<.0001

Cramer-von Mises Test for Variable Value Classified by Variable Location		
Location	**N**	**Summed Deviation from Mean**
FR High	1237	4.225889
FR Low	1558	3.355215

Cramer-von Mises Statistics (Asymptotic)			
CM	0.002712	**CMa**	7.581103

Kuiper Test for Variable Value Classified by Variable Location		
Location	**N**	**Deviation from Mean**
FR High	1237	0.015080
FR Low	1558	0.170904

Kuiper Two-Sample Test (Asymptotic)					
K	0.185984	**Ka**	4.883749	**Pr > Ka**	<.0001

Systematic Kolmogorov-Smirnov Analysis (Bryanna Pockrandt)
Phenometric: Beginning of the Season
Season 11 (Hot, Dry)
Comparison of Konza vs. Fort Riley High

The NPAR1WAY Procedure

Kolmogorov-Smirnov Test for Variable Value Classified by Variable Location

Location	N	EDF at Maximum	Deviation from Mean at Maximum
Konza	621	0.162641	-3.042065
FR High	1237	0.345998	2.155407
Total	1858	0.284715	
Maximum Deviation Occurred at Observation 935			
Value of Value at Maximum = 237.10			

Kolmogorov-Smirnov Two-Sample Test (Asymptotic)			
KS	0.086494	**D**	0.183357
KSa	3.728262	**Pr > KSa**	<.0001

Cramer-von Mises Test for Variable Value Classified by Variable Location

Location	N	Summed Deviation from Mean
Konza	621	3.674826
FR High	1237	1.844840

Cramer-von Mises Statistics (Asymptotic)			
CM	0.002971	**CMa**	5.519667

Kuiper Test for Variable Value Classified by Variable Location

Location	N	Deviation from Mean
Konza	621	0.004876
FR High	1237	0.183357

Kuiper Two-Sample Test (Asymptotic)					
K	0.188234	**Ka**	3.827417	**Pr > Ka**	<.0001

Systematic Kolmogorov-Smirnov Analysis (Bryanna Pockrandt)
Phenometric: Beginning of the Season
Season 11 (Hot, Dry)
Comparison of Konza vs. Fort Riley Low

The NPAR1WAY Procedure

Kolmogorov-Smirnov Test for Variable Value Classified by Variable Location			
Location	**N**	**EDF at Maximum**	**Deviation from Mean at Maximum**
Konza	621	0.307568	-5.876108
FR Low	1558	0.637356	3.709811
Total	2179	0.543369	
Maximum Deviation Occurred at Observation 1139			
Value of Value at Maximum = 237.20			

Kolmogorov-Smirnov Two-Sample Test (Asymptotic)			
KS	0.148870	**D**	0.329787
KSa	6.949197	**Pr > KSa**	<.0001

Cramer-von Mises Test for Variable Value Classified by Variable Location		
Location	**N**	**Summed Deviation from Mean**
Konza	621	16.484817
FR Low	1558	6.570649

Cramer-von Mises Statistics (Asymptotic)			
CM	0.010581	**CMa**	23.055465

Kuiper Test for Variable Value Classified by Variable Location		
Location	**N**	**Deviation from Mean**
Konza	621	0.002567
FR Low	1558	0.329787

Kuiper Two-Sample Test (Asymptotic)					
K	0.332355	**Ka**	7.003297	**Pr > Ka**	<.0001

Systematic Kolmogorov-Smirnov Analysis (Bryanna Pockrandt)
Phenometric: End of the Season
Season 2 (Normal)
Comparison of Konza vs. Fort Riley Full

The NPAR1WAY Procedure

Kolmogorov-Smirnov Test for Variable Value Classified by Variable Location			
Location	**N**	**EDF at Maximum**	**Deviation from Mean at Maximum**
Konza	621	0.120773	-2.764209
FR Full	5184	0.244985	0.956718
Total	5805	0.231697	
Maximum Deviation Occurred at Observation 2849			
Value of Value at Maximum = 43.60			

Kolmogorov-Smirnov Two-Sample Test (Asymptotic)			
KS	0.038392	**D**	0.124212
KSa	2.925091	**Pr > KSa**	<.0001

Cramer-von Mises Test for Variable Value Classified by Variable Location		
Location	**N**	**Summed Deviation from Mean**
Konza	621	2.486717
FR Full	5184	0.297888

Cramer-von Mises Statistics (Asymptotic)			
CM	0.000480	**CMa**	2.784605

Kuiper Test for Variable Value Classified by Variable Location		
Location	**N**	**Deviation from Mean**
Konza	621	0.085288
FR Full	5184	0.124212

Kuiper Two-Sample Test (Asymptotic)					
K	0.209499	**Ka**	4.933549	**Pr > Ka**	<.0001

Systematic Kolmogorov-Smirnov Analysis (Bryanna Pockrandt)
Phenometric: End of the Season
Season 2 (Normal)
Comparison of Fort Riley High vs. Fort Riley Low

The NPAR1WAY Procedure

Kolmogorov-Smirnov Test for Variable Value Classified by Variable Location			
Location	**N**	**EDF at Maximum**	**Deviation from Mean at Maximum**
FR High	1212	0.592409	2.040719
FR Low	1555	0.488103	-1.801646
Total	2767	0.533791	
Maximum Deviation Occurred at Observation 1377			
Value of Value at Maximum = 44.0			

Kolmogorov-Smirnov Two-Sample Test (Asymptotic)			
KS	0.051751	**D**	0.104306
KSa	2.722217	**Pr > KSa**	<.0001

Cramer-von Mises Test for Variable Value Classified by Variable Location		
Location	**N**	**Summed Deviation from Mean**
FR High	1212	1.626095
FR Low	1555	1.267413

Cramer-von Mises Statistics (Asymptotic)			
CM	0.001046	**CMa**	2.893508

Kuiper Test for Variable Value Classified by Variable Location		
Location	**N**	**Deviation from Mean**
FR High	1212	0.104306
FR Low	1555	0.025795

Kuiper Two-Sample Test (Asymptotic)					
K	0.130101	**Ka**	3.395424	**Pr > Ka**	<.0001

Systematic Kolmogorov-Smirnov Analysis (Bryanna Pockrandt)
Phenometric: End of the Season
Season 2 (Normal)
Comparison of Konza vs. Fort Riley High

The NPAR1WAY Procedure

Kolmogorov-Smirnov Test for Variable Value Classified by Variable Location			
Location	**N**	**EDF at Maximum**	**Deviation from Mean at Maximum**
Konza	621	0.942029	1.464727
FR High	1212	0.853135	-1.048459
Total	1833	0.883252	
Maximum Deviation Occurred at Observation 905			
Value of Value at Maximum = 44.50			

Kolmogorov-Smirnov Two-Sample Test (Asymptotic)			
KS	0.042073	**D**	0.088894
KSa	1.801303	**Pr > KSa**	0.0030

Cramer-von Mises Test for Variable Value Classified by Variable Location		
Location	**N**	**Summed Deviation from Mean**
Konza	621	0.512714
FR High	1212	0.262703

Cramer-von Mises Statistics (Asymptotic)			
CM	0.000423	**CMa**	0.775417

Kuiper Test for Variable Value Classified by Variable Location		
Location	**N**	**Deviation from Mean**
Konza	621	0.088894
FR High	1212	0.035168

Kuiper Two-Sample Test (Asymptotic)					
K	0.124061	**Ka**	2.513925	**Pr > Ka**	0.0002

Systematic Kolmogorov-Smirnov Analysis (Bryanna Pockrandt)
Phenometric: End of the Season
Season 2 (Normal)
Comparison of Konza vs. Fort Riley Low

The NPAR1WAY Procedure

Kolmogorov-Smirnov Test for Variable Value Classified by Variable Location			
Location	**N**	**EDF at Maximum**	**Deviation from Mean at Maximum**
Konza	621	0.851852	2.561039
FR Low	1555	0.708039	-1.618441
Total	2176	0.749081	
Maximum Deviation Occurred at Observation 1072			
Value of Value at Maximum = 44.30			

Kolmogorov-Smirnov Two-Sample Test (Asymptotic)			
KS	0.064946	**D**	0.143813
KSa	3.029567	**Pr > KSa**	<.0001

Cramer-von Mises Test for Variable Value Classified by Variable Location		
Location	**N**	**Summed Deviation from Mean**
Konza	621	2.923523
FR Low	1555	1.167529

Cramer-von Mises Statistics (Asymptotic)			
CM	0.001880	**CMa**	4.091052

Kuiper Test for Variable Value Classified by Variable Location		
Location	**N**	**Deviation from Mean**
Konza	621	0.143813
FR Low	1555	0.018541

Kuiper Two-Sample Test (Asymptotic)					
K	0.162354	**Ka**	3.420146	**Pr > Ka**	<.0001

Systematic Kolmogorov-Smirnov Analysis (Bryanna Pockrandt)
Phenometric: End of the Season
Season 8 (Cool, Wet)
Comparison of Konza vs. Fort Riley Full

The NPAR1WAY Procedure

Kolmogorov-Smirnov Test for Variable Value Classified by Variable Location			
Location	**N**	**EDF at Maximum**	**Deviation from Mean at Maximum**
Konza	621	0.144928	-6.280445
FR Full	5221	0.426930	2.166004
Total	5842	0.396953	
Maximum Deviation Occurred at Observation 2924			
Value of Value at Maximum = 181.30			

Kolmogorov-Smirnov Two-Sample Test (Asymptotic)			
KS	0.086919	**D**	0.282002
KSa	6.643460	**Pr > KSa**	<.0001

Cramer-von Mises Test for Variable Value Classified by Variable Location		
Location	**N**	**Summed Deviation from Mean**
Konza	621	20.278663
FR Full	5221	2.412000

Cramer-von Mises Statistics (Asymptotic)			
CM	0.003884	**CMa**	22.690663

Kuiper Test for Variable Value Classified by Variable Location		
Location	**N**	**Deviation from Mean**
Konza	621	0.002873
FR Full	5221	0.282002

Kuiper Two-Sample Test (Asymptotic)					
K	0.284875	**Ka**	6.711143	**Pr > Ka**	<.0001

Systematic Kolmogorov-Smirnov Analysis (Bryanna Pockrandt)
Phenometric: End of the Season
Season 8 (Cool, Wet)
Comparison of Fort Riley High vs. Fort Riley Low

The NPAR1WAY Procedure

Kolmogorov-Smirnov Test for Variable Value Classified by Variable Location			
Location	N	EDF at Maximum	Deviation from Mean at Maximum
FR High	1237	0.618432	4.757849
FR Low	1553	0.375402	-4.246291
Total	2790	0.483154	
Maximum Deviation Occurred at Observation 1390			
Value of Value at Maximum = 181.40			

Kolmogorov-Smirnov Two-Sample Test (Asymptotic)			
KS	0.120733	D	0.243029
KSa	6.377156	Pr > KSa	<.0001

Cramer-von Mises Test for Variable Value Classified by Variable Location		
Location	N	Summed Deviation from Mean
FR High	1237	9.395299
FR Low	1553	7.483570

Cramer-von Mises Statistics (Asymptotic)			
CM	0.006050	CMa	16.878869

Kuiper Test for Variable Value Classified by Variable Location		
Location	N	Deviation from Mean
FR High	1237	0.243029
FR Low	1553	0.014457

Kuiper Two-Sample Test (Asymptotic)					
K	0.257486	Ka	6.756514	Pr > Ka	<.0001

Systematic Kolmogorov-Smirnov Analysis (Bryanna Pockrandt)
Phenometric: End of the Season
Season 8 (Cool, Wet)
Comparison of Konza vs. Fort Riley High

The NPAR1WAY Procedure

Kolmogorov-Smirnov Test for Variable Value Classified by Variable Location

Location	N	EDF at Maximum	Deviation from Mean at Maximum
Konza	621	0.238325	-6.306305
FR High	1237	0.618432	4.468234
Total	1858	0.491389	
Maximum Deviation Occurred at Observation 917			
Value of Value at Maximum = 181.40			

Kolmogorov-Smirnov Two-Sample Test (Asymptotic)

KS	0.179304	**D**	0.380106
KSa	7.728816	**Pr > KSa**	<.0001

Cramer-von Mises Test for Variable Value Classified by Variable Location

Location	N	Summed Deviation from Mean
Konza	621	19.341937
FR High	1237	9.710059

Cramer-von Mises Statistics (Asymptotic)

CM	0.015636	**CMa**	29.051995

Kuiper Test for Variable Value Classified by Variable Location

Location	N	Deviation from Mean
Konza	621	0.007282
FR High	1237	0.380106

Kuiper Two-Sample Test (Asymptotic)

K	0.387389	**Ka**	7.876887	**Pr > Ka**	<.0001

Systematic Kolmogorov-Smirnov Analysis (Bryanna Pockrandt)
Phenometric: End of the Season
Season 8 (Cool, Wet)
Comparison of Konza vs. Fort Riley Low

The NPAR1WAY Procedure

Kolmogorov-Smirnov Test for Variable Value Classified by Variable Location			
Location	**N**	**EDF at Maximum**	**Deviation from Mean at Maximum**
Konza	621	0.144928	-2.704362
FR Low	1553	0.296845	1.710114
Total	2174	0.253450	
Maximum Deviation Occurred at Observation 1113			
Value of Value at Maximum = 181.30			

Kolmogorov-Smirnov Two-Sample Test (Asymptotic)			
KS	0.068624	**D**	0.151917
KSa	3.199698	**Pr > KSa**	<.0001

Cramer-von Mises Test for Variable Value Classified by Variable Location		
Location	**N**	**Summed Deviation from Mean**
Konza	621	3.864416
FR Low	1553	1.545269

Cramer-von Mises Statistics (Asymptotic)			
CM	0.002488	**CMa**	5.409684

Kuiper Test for Variable Value Classified by Variable Location		
Location	**N**	**Deviation from Mean**
Konza	621	0.001932
FR Low	1553	0.151917

Kuiper Two-Sample Test (Asymptotic)					
K	0.153849	**Ka**	3.240384	**Pr > Ka**	<.0001

Systematic Kolmogorov-Smirnov Analysis (Bryanna Pockrandt)
Phenometric: End of the Season
Season 11 (Hot, Dry)
Comparison of Konza vs. Fort Riley Full

The NPAR1WAY Procedure

Kolmogorov-Smirnov Test for Variable Value Classified by Variable Location			
Location	**N**	**EDF at Maximum**	**Deviation from Mean at Maximum**
Konza	621	0.144928	-2.704362
FR Low	1553	0.296845	1.710114
Total	2174	0.253450	
Maximum Deviation Occurred at Observation 1113			
Value of Value at Maximum = 181.30			

Kolmogorov-Smirnov Two-Sample Test (Asymptotic)			
KS	0.068624	**D**	0.151917
KSa	3.199698	**Pr > KSa**	<.0001

Cramer-von Mises Test for Variable Value Classified by Variable Location		
Location	**N**	**Summed Deviation from Mean**
Konza	621	5.451269
FR Full	5206	0.650257

Cramer-von Mises Statistics (Asymptotic)			
CM	0.001047	**CMa**	6.101526

Kuiper Test for Variable Value Classified by Variable Location		
Location	**N**	**Deviation from Mean**
Konza	621	0.044788
FR Full	5206	0.151974

Kuiper Two-Sample Test (Asymptotic)					
K	0.196762	**Ka**	4.634654	**Pr > Ka**	<.0001

Systematic Kolmogorov-Smirnov Analysis (Bryanna Pockrandt)
Phenometric: End of the Season
Season 11 (Hot, Dry)
Comparison of Fort Riley High vs. Fort Riley Low

The NPAR1WAY Procedure

Kolmogorov-Smirnov Test for Variable Value Classified by Variable Location

Location	N	EDF at Maximum	Deviation from Mean at Maximum
FR High	1223	0.380213	3.258133
FR Low	1564	0.214194	-2.881135
Total	2787	0.287047	

Maximum Deviation Occurred at Observation 1377
Value of Value at Maximum = 249.70

Kolmogorov-Smirnov Two-Sample Test (Asymptotic)

KS	0.082385	**D**	0.166018
KSa	4.349295	**Pr > KSa**	<.0001

Cramer-von Mises Test for Variable Value Classified by Variable Location

Location	N	Summed Deviation from Mean
FR High	1223	4.565427
FR Low	1564	3.570024

Cramer-von Mises Statistics (Asymptotic)

CM	0.002919	**CMa**	8.135450

Kuiper Test for Variable Value Classified by Variable Location

Location	N	Deviation from Mean
FR High	1223	0.166018
FR Low	1564	0.096883

Kuiper Two-Sample Test (Asymptotic)

K	0.262902	**Ka**	6.887419	**Pr > Ka**	<.0001

Systematic Kolmogorov-Smirnov Analysis (Bryanna Pockrandt)
Phenometric: End of the Season
Season 11 (Hot, Dry)
Comparison of Konza vs. Fort Riley High

The NPAR1WAY Procedure

Kolmogorov-Smirnov Test for Variable Value Classified by Variable Location			
Location	**N**	**EDF at Maximum**	**Deviation from Mean at Maximum**
Konza	621	0.209340	-4.134989
FR High	1223	0.459526	2.946503
Total	1844	0.375271	
Maximum Deviation Occurred at Observation 935			
Value of Value at Maximum = 249.80			

Kolmogorov-Smirnov Two-Sample Test (Asymptotic)			
KS	0.118239	**D**	0.250186
KSa	5.077402	**Pr > KSa**	<.0001

Cramer-von Mises Test for Variable Value Classified by Variable Location		
Location	**N**	**Summed Deviation from Mean**
Konza	621	7.857872
FR High	1223	3.989974

Cramer-von Mises Statistics (Asymptotic)			
CM	0.006425	**CMa**	11.847846

Kuiper Test for Variable Value Classified by Variable Location		
Location	**N**	**Deviation from Mean**
Konza	621	0.098370
FR High	1223	0.250186

Kuiper Two-Sample Test (Asymptotic)					
K	0.348556	**Ka**	7.073764	**Pr > Ka**	<.0001

Systematic Kolmogorov-Smirnov Analysis (Bryanna Pockrandt)
Phenometric: End of the Season
Season 11 (Hot, Dry)
Comparison of Konza vs. Fort Riley Low

The NPAR1WAY Procedure

Kolmogorov-Smirnov Test for Variable Value Classified by Variable Location			
Location	**N**	**EDF at Maximum**	**Deviation from Mean at Maximum**
Konza	621	0.592593	-1.861123
FR Low	1564	0.696931	1.172742
Total	2185	0.667277	
Maximum Deviation Occurred at Observation 1048			
Value of Value at Maximum = 250.30			

Kolmogorov-Smirnov Two-Sample Test (Asymptotic)			
KS	0.047061	**D**	0.104338
KSa	2.199796	**Pr > KSa**	0.0001

Cramer-von Mises Test for Variable Value Classified by Variable Location		
Location	**N**	**Summed Deviation from Mean**
Konza	621	1.702348
FR Low	1564	0.675932

Cramer-von Mises Statistics (Asymptotic)			
CM	0.001088	**CMa**	2.378280

Kuiper Test for Variable Value Classified by Variable Location		
Location	**N**	**Deviation from Mean**
Konza	621	0.003836
FR Low	1564	0.104338

Kuiper Two-Sample Test (Asymptotic)					
K	0.108175	**Ka**	2.280678	**Pr > Ka**	0.0012

Systematic Kolmogorov-Smirnov Analysis (Bryanna Pockrandt)
Phenometric: Length of the Season
Season 2 (Normal)
Comparison of Konza vs. Fort Riley Full

The NPAR1WAY Procedure

Kolmogorov-Smirnov Test for Variable Value Classified by Variable Location			
Location	**N**	**EDF at Maximum**	**Deviation from Mean at Maximum**
Konza	621	0.776167	6.497585
FR Full	5180	0.484170	-2.249743
Total	5801	0.515428	
Maximum Deviation Occurred at Observation 2929			
Value of Value at Maximum = 14.0			

Kolmogorov-Smirnov Two-Sample Test (Asymptotic)			
KS	0.090279	**D**	0.291998
KSa	6.876042	**Pr > KSa**	<.0001

Cramer-von Mises Test for Variable Value Classified by Variable Location		
Location	**N**	**Summed Deviation from Mean**
Konza	621	18.416415
FR Full	5180	2.207837

Cramer-von Mises Statistics (Asymptotic)			
CM	0.003555	**CMa**	20.624252

Kuiper Test for Variable Value Classified by Variable Location		
Location	**N**	**Deviation from Mean**
Konza	621	0.291998
FR Full	5180	0.015877

Kuiper Two-Sample Test (Asymptotic)					
K	0.307875	**Ka**	7.249927	**Pr > Ka**	<.0001

Systematic Kolmogorov-Smirnov Analysis (Bryanna Pockrandt)
Phenometric: Length of the Season
Season 2 (Normal)
Comparison of Fort Riley High vs. Fort Riley Low

The NPAR1WAY Procedure

Kolmogorov-Smirnov Test for Variable Value Classified by Variable Location			
Location	**N**	**EDF at Maximum**	**Deviation from Mean at Maximum**
FR High	1209	0.758478	-2.027872
FR Low	1553	0.862202	1.789238
Total	2762	0.816799	
Maximum Deviation Occurred at Observation 1384			
Value of Value at Maximum = 14.60			

Kolmogorov-Smirnov Two-Sample Test (Asymptotic)			
KS	0.051458	**D**	0.103724
KSa	2.704374	**Pr > KSa**	<.0001

Cramer-von Mises Test for Variable Value Classified by Variable Location		
Location	**N**	**Summed Deviation from Mean**
FR High	1209	1.344671
FR Low	1553	1.046818

Cramer-von Mises Statistics (Asymptotic)			
CM	0.000866	**CMa**	2.391489

Kuiper Test for Variable Value Classified by Variable Location		
Location	**N**	**Deviation from Mean**
FR High	1209	0.023807
FR Low	1553	0.103724

Kuiper Two-Sample Test (Asymptotic)					
K	0.127531	**Ka**	3.325096	**Pr > Ka**	<.0001

Systematic Kolmogorov-Smirnov Analysis (Bryanna Pockrandt)
Phenometric: Length of the Season
Season 2 (Normal)
Comparison of Konza vs. Fort Riley High

The NPAR1WAY Procedure

Kolmogorov-Smirnov Test for Variable Value Classified by Variable Location			
Location	**N**	**EDF at Maximum**	**Deviation from Mean at Maximum**
Konza	621	0.827697	4.897994
FR High	1209	0.530190	-3.510354
Total	1830	0.631148	
Maximum Deviation Occurred at Observation 921			
Value of Value at Maximum = 14.10			

Kolmogorov-Smirnov Two-Sample Test (Asymptotic)			
KS	0.140866	**D**	0.297507
KSa	6.026021	**Pr > KSa**	<.0001

Cramer-von Mises Test for Variable Value Classified by Variable Location		
Location	**N**	**Summed Deviation from Mean**
Konza	621	11.307076
FR High	1209	5.807853

Cramer-von Mises Statistics (Asymptotic)			
CM	0.009352	**CMa**	17.114928

Kuiper Test for Variable Value Classified by Variable Location		
Location	**N**	**Deviation from Mean**
Konza	621	0.297507
FR High	1209	0.001654

Kuiper Two-Sample Test (Asymptotic)					
K	0.261226	**Ka**	5.504496	**Pr > Ka**	<.0001

Appendix F - Phenometric Empirical Distribution Functions

Beginning of Season: Fort Riley Full Vs. KPBS

Normal Season

KS	0.119256
D	0.385955
Pr > D	<.0001

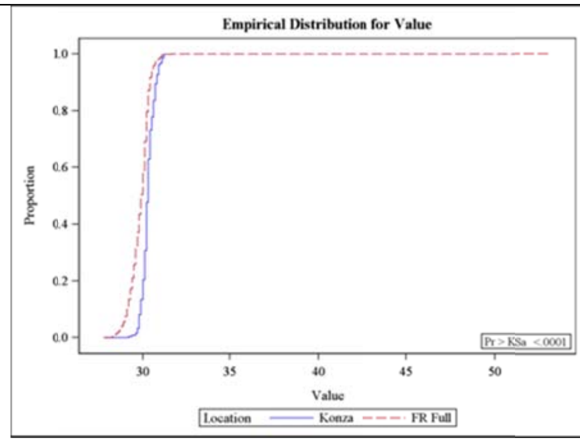

Cool, Wet Season

KS	0.062677
D	0.203381
Pr > D	<.0001

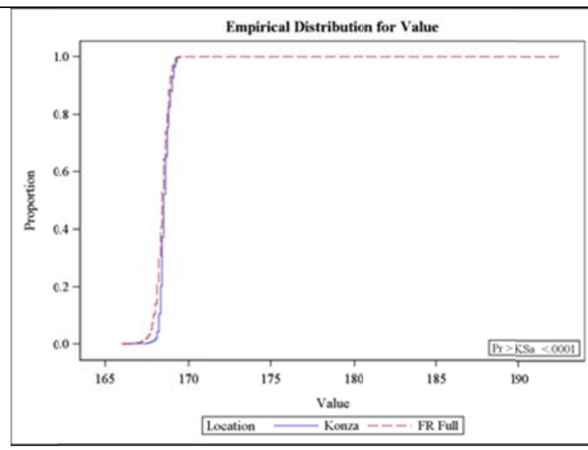

Hot, Dry Season

KS	0.054606
D	0.177260
Pr > D	<.0001

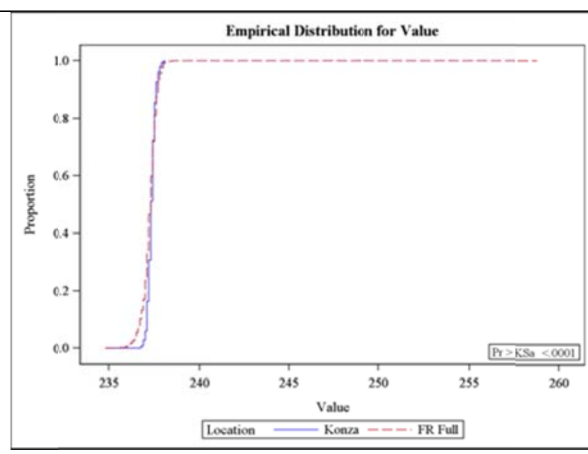

End of Season: Fort Riley Full Vs. KPBS

Normal Season

KS	0.038392
D	0.124212
Pr > D	<.0001

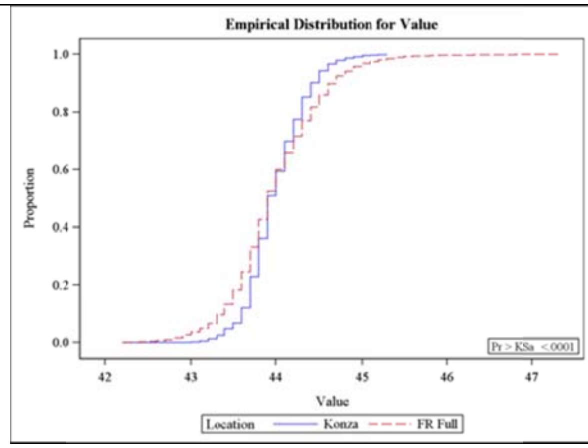

Cool, Wet Season

KS	0.086919
D	0.282002
Pr > D	<.0001

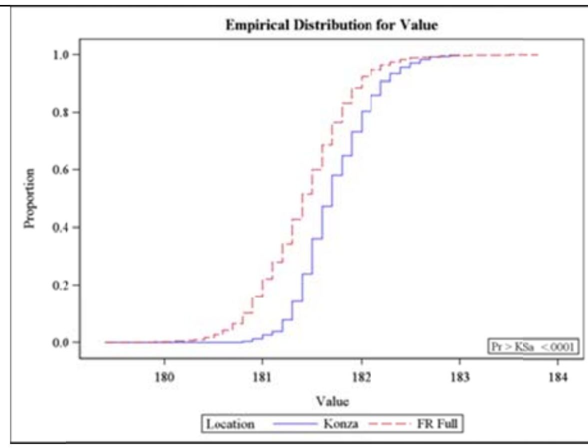

Hot, Dry Season

KS	0.046895
D	0.151974
Pr > D	<.0001

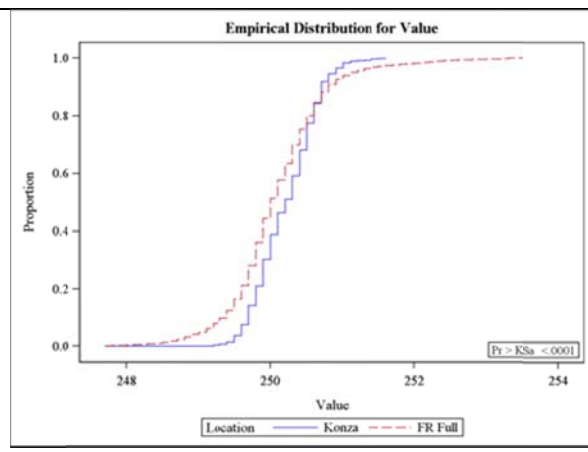

Length of Season: Fort Riley Full Vs. KPBS

Normal Season

KS	0.090279
D	0.291998
Pr > D	<.0001

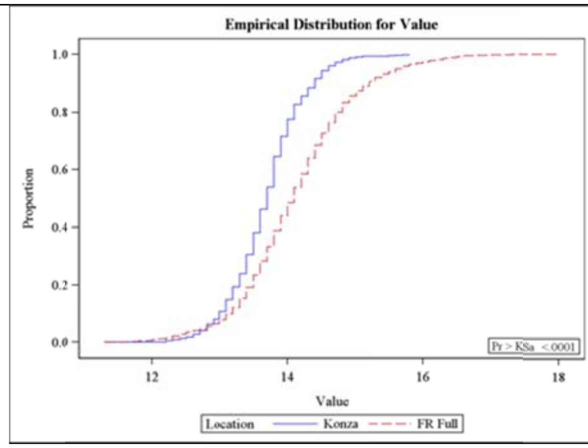

Cool, Wet Season

KS	0.035346
D	0.114495
Pr > D	<.0001

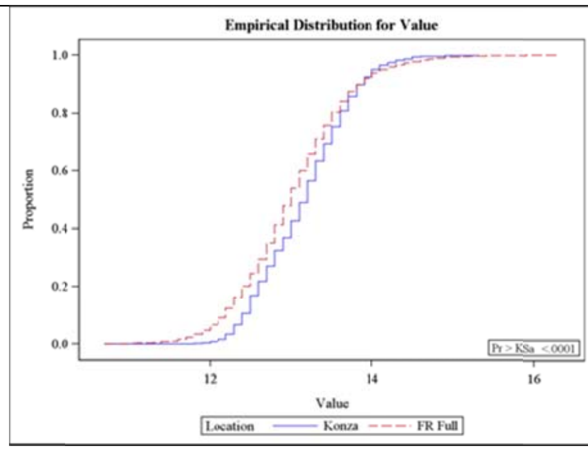

Hot, Dry Season

KS	0.043795
D	0.141403
Pr > D	<.0001

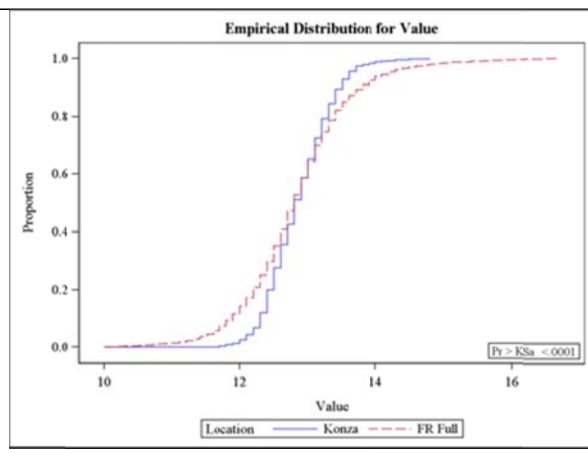

Maximum NDVI Value: Fort Riley Full Vs. KPBS

Normal Season

KS	0.092750
D	0.301102
Pr > D	<.0001

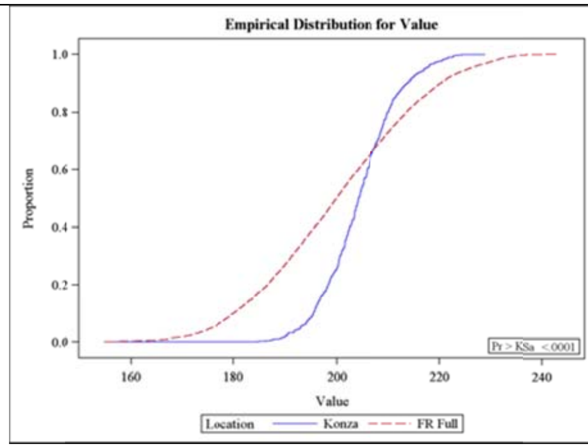

Cool, Wet Season

KS	0.075222
D	0.244162
Pr > D	<.0001

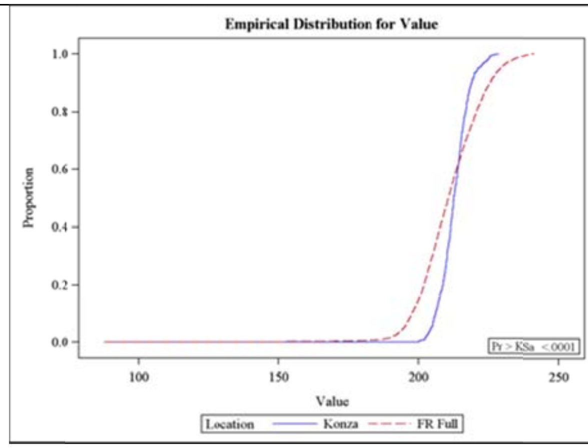

Hot, Dry Season

KS	0.057852
D	0.187950
Pr > D	<.0001

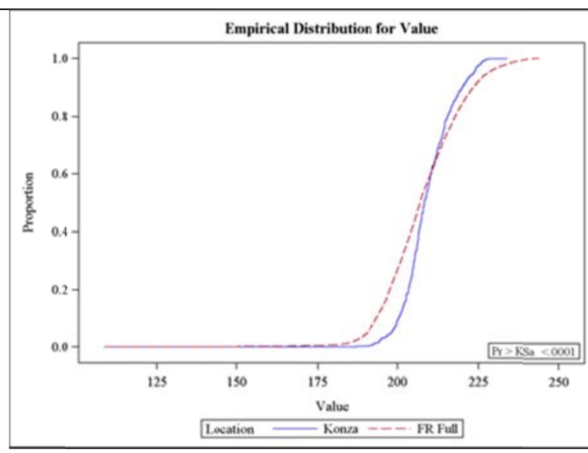

Small Integral: Fort Riley Full Vs. KPBS

Normal Season

KS	0.121689
D	0.393829
Pr > D	<.0001

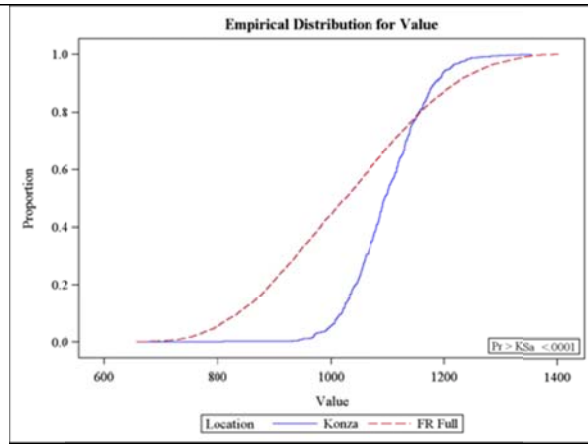

Cool, Wet Season

KS	0.112168
D	0.363975
Pr > D	<.0001

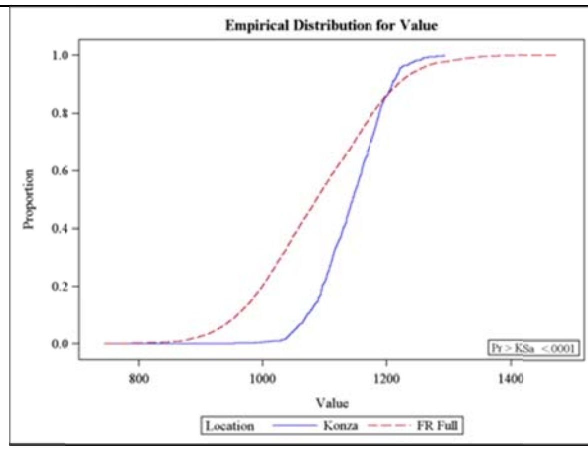

Hot, Dry Season

KS	0.073807
D	0.239590
Pr > D	<.0001

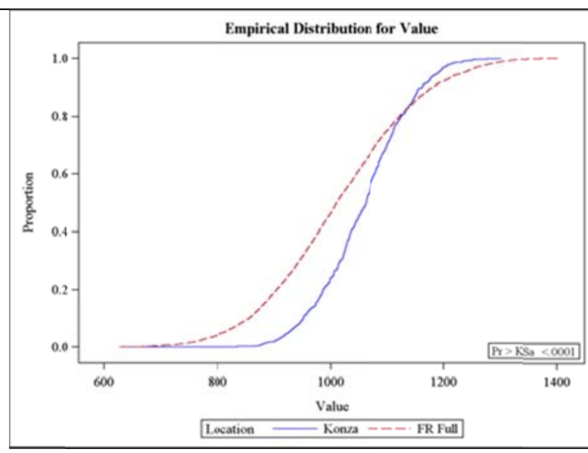

Beginning of Season: Fort Riley High Vs. Fort Riley Low

Normal Season

KS	0.098618
D	0.198782
Pr > D	<.0001

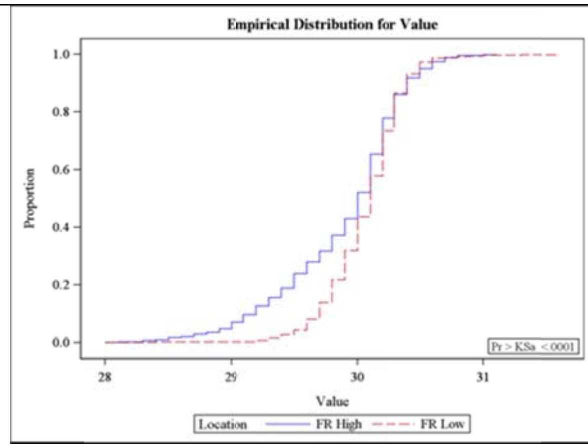

Cool, Wet Season

KS	0.073396
D	0.147743
Pr > D	<.0001

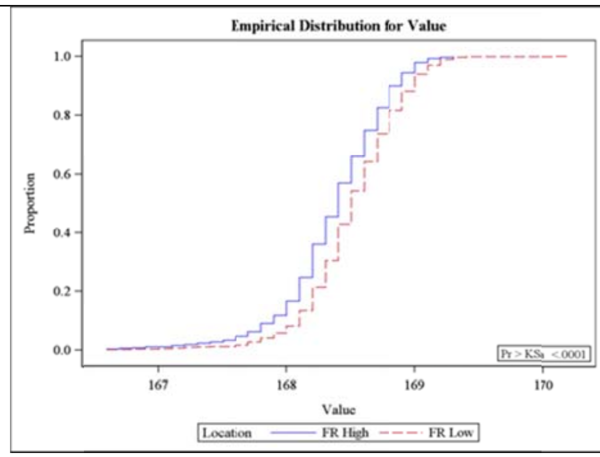

Hot, Dry Season

KS	0.084887
D	0.170904
Pr > D	<.0001

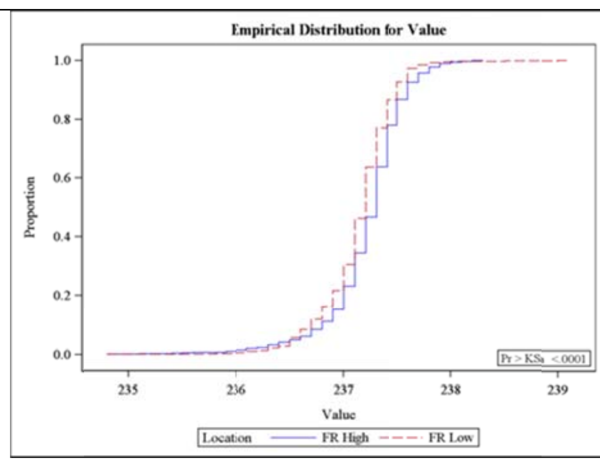

End of Season: Fort Riley High Vs. Fort Riley Low

Normal Season

KS	0.051751
D	0.104306
Pr > D	<.0001

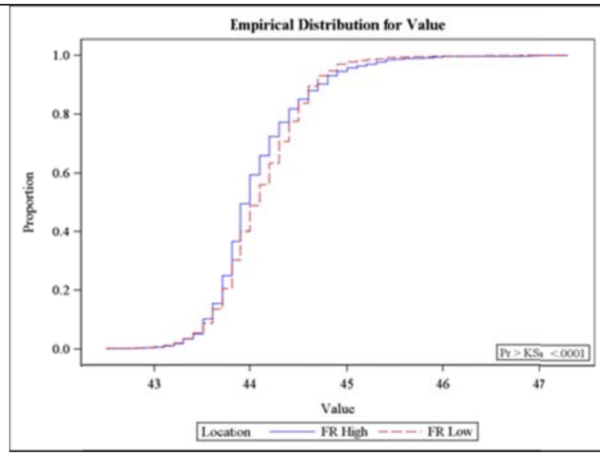

Cool, Wet Season

KS	0.120733
D	0.243029
Pr > D	<.0001

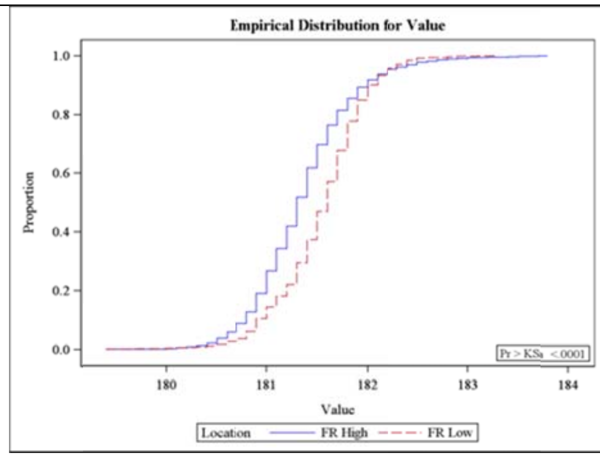

Hot, Dry Season

KS	0.082385
D	0.166018
Pr > D	<.0001

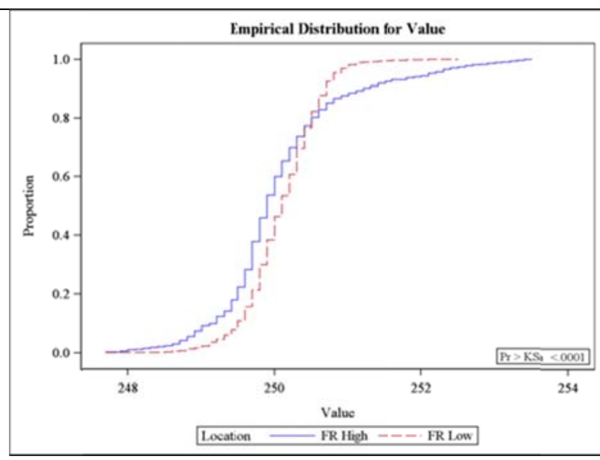

Length of Season: Fort Riley High Vs. Fort Riley Low

Normal Season

KS	0.051458
D	0.103724
Pr > D	<.0001

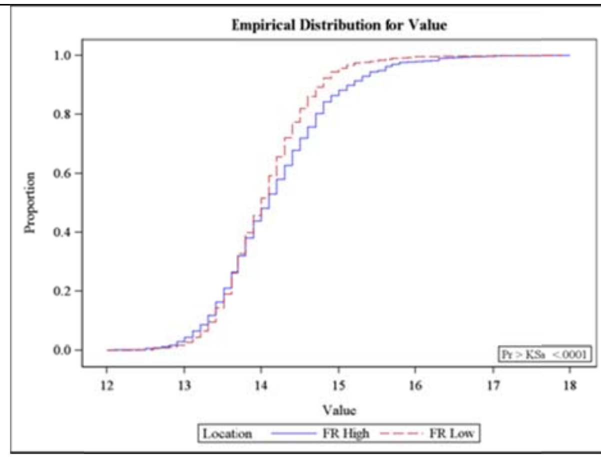

Cool, Wet Season

KS	0.040469
D	0.081468
Pr > D	0.0002

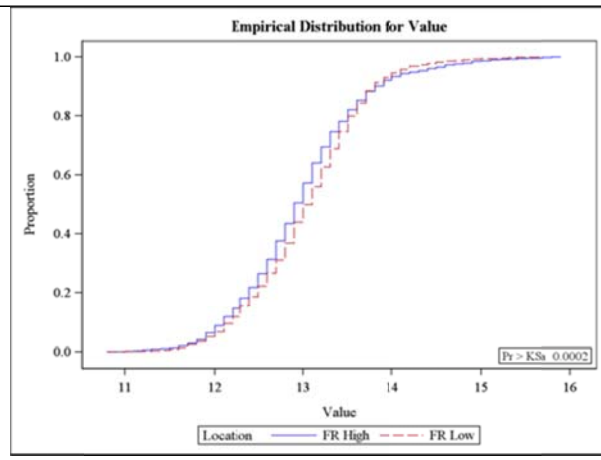

Hot, Dry Season

KS	0.096582
D	0.194760
Pr > D	<.0001

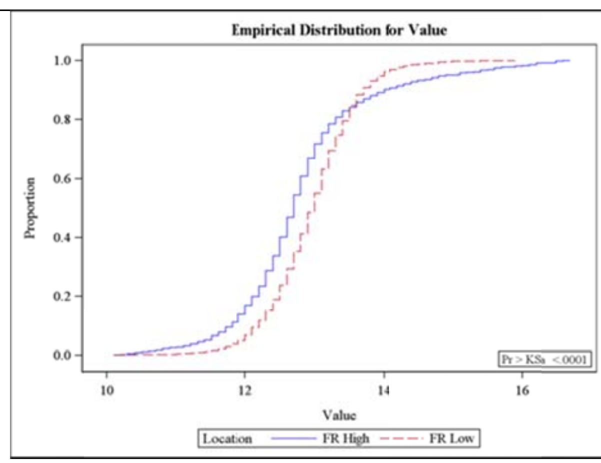

Maximum NDVI Value: Fort Riley High Vs. Fort Riley Low

Normal Season

KS	0.186626
D	0.375724
Pr > D	<.0001

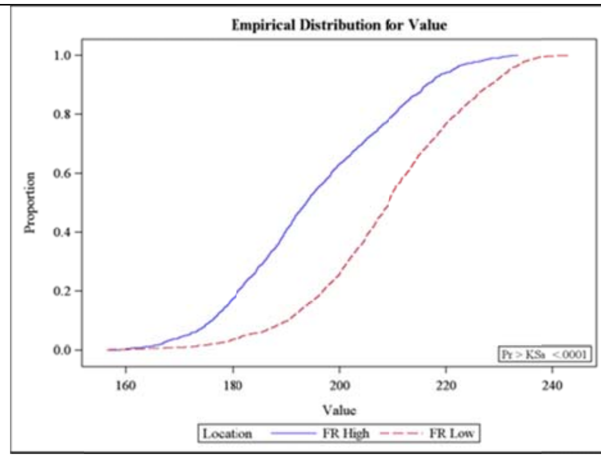

Cool, Wet Season

KS	0.191760
D	0.386212
Pr > D	<.0001

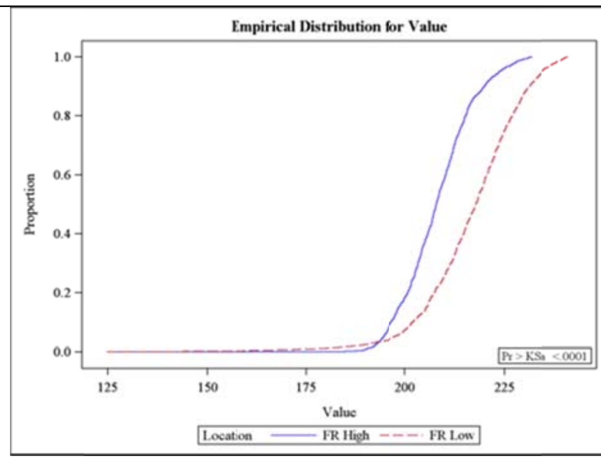

Hot, Dry Season

KS	0.144218
D	0.290434
Pr > D	<.0001

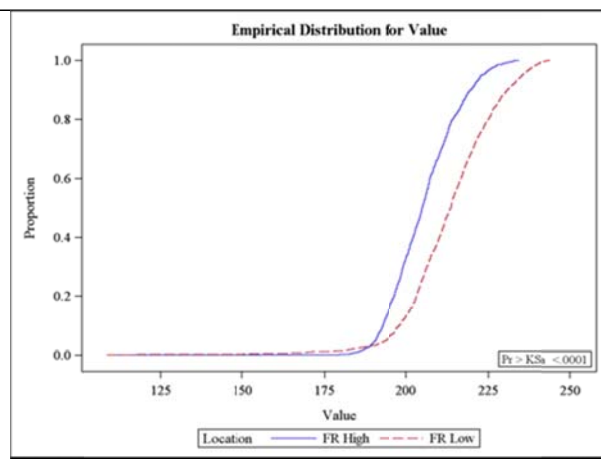

Small Integral: Fort Riley High Vs. Fort Riley Low

Normal Season

KS	0.181729
D	0.366308
Pr > D	<.0001

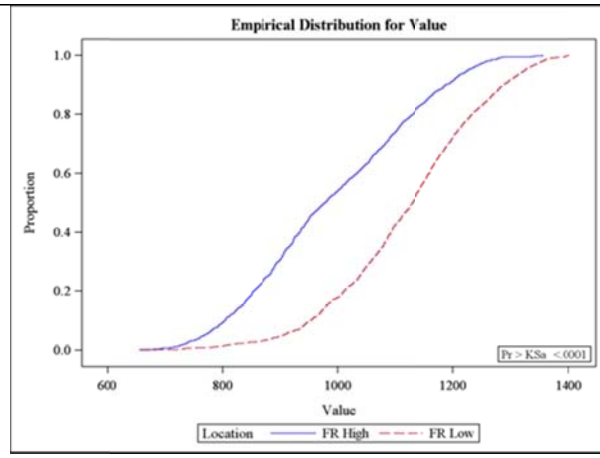

Cool, Wet Season

KS	0.119702
D	0.240955
Pr > D	<.0001

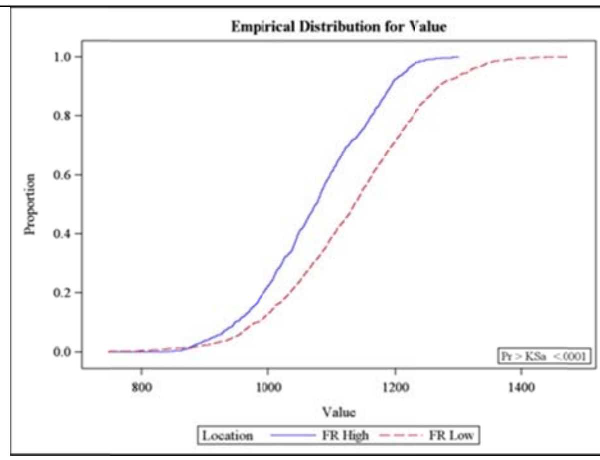

Hot, Dry Season

KS	0.128290
D	0.258290
Pr > D	<.0001

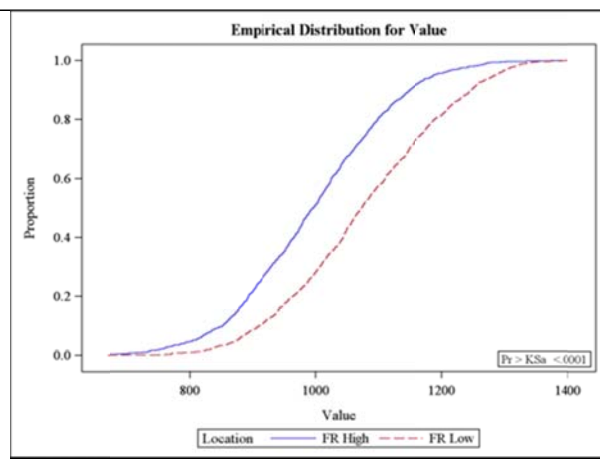

Beginning of Season: Fort Riley High Vs. KPBS

Normal Season

KS	0.163436
D	0.345358
Pr > D	<.0001

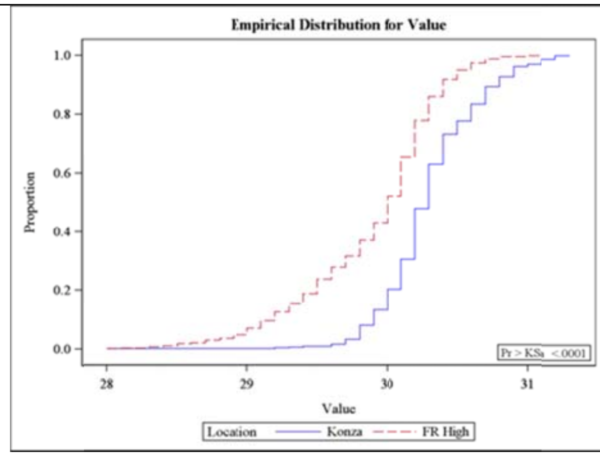

Wet, Cool Season

KS	0.121466
D	0.257497
Pr > D	<.0001

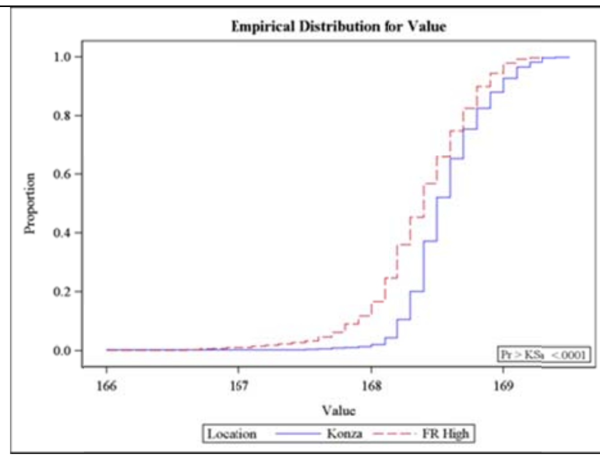

Hot, Dry Season

KS	0.086494
D	0.183357
Pr > D	<.0001

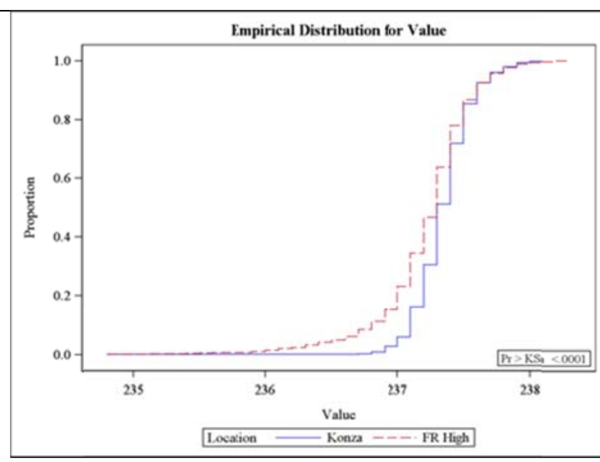

End of Season: Fort Riley High Vs. KPBS

Normal Season

KS	0.042073
D	0.088894
Pr > D	0.0030

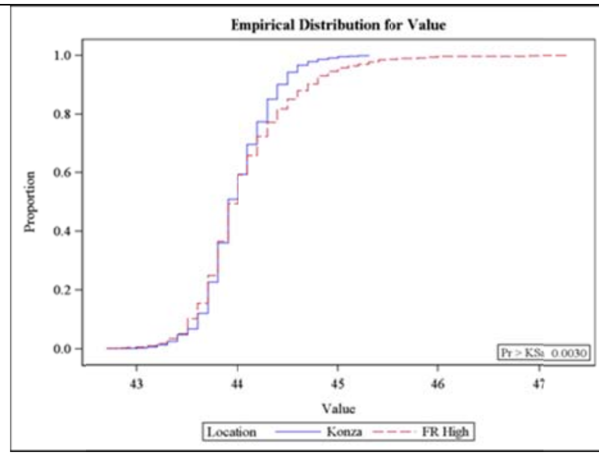

Wet, Cool Season

KS	0.179304
D	0.380106
Pr > D	<.0001

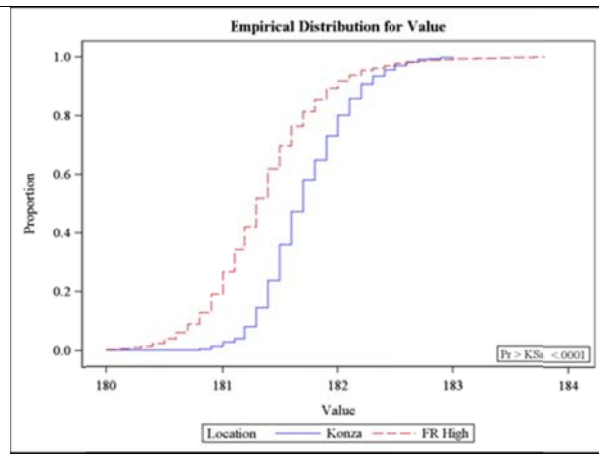

Hot, Dry Season

KS	0.118239
D	0.250186
Pr > D	<.0001

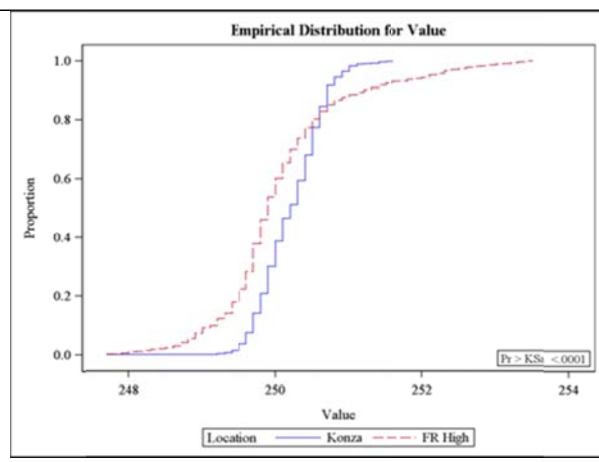

Length of Season: Fort Riley High Vs. KPBS

Normal Season

KS	0.140866
D	0.297507
Pr > D	<.0001

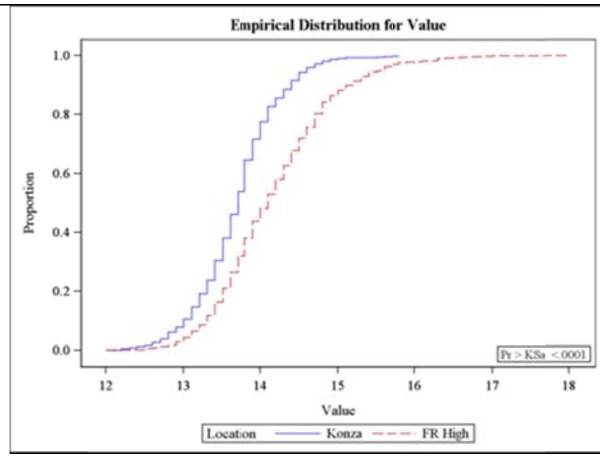

Wet, Cool Season

KS	0.071992
D	0.152452
Pr > D	<.0001

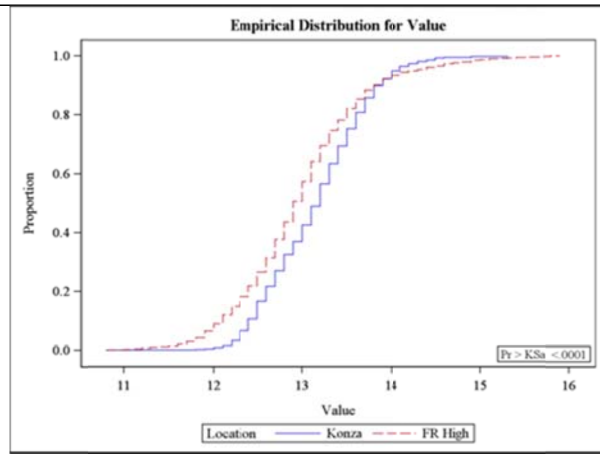

Hot, Dry Season

KS	0.079576
D	0.167974
Pr > D	<.0001

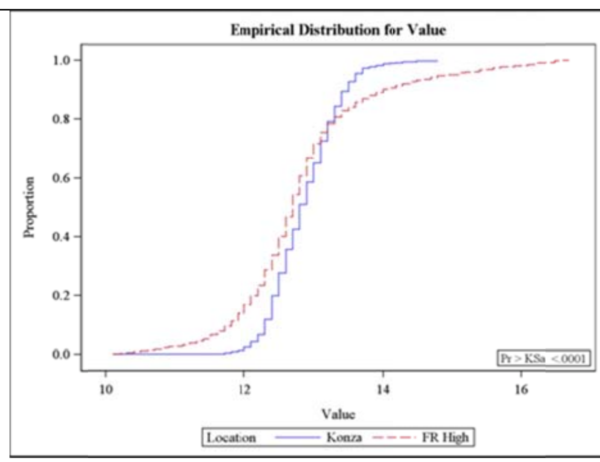

Maximum NDVI Value: Fort Riley High Vs. KPBS

Normal Season

KS	0.209910
D	0.444989
Pr > D	<.0001

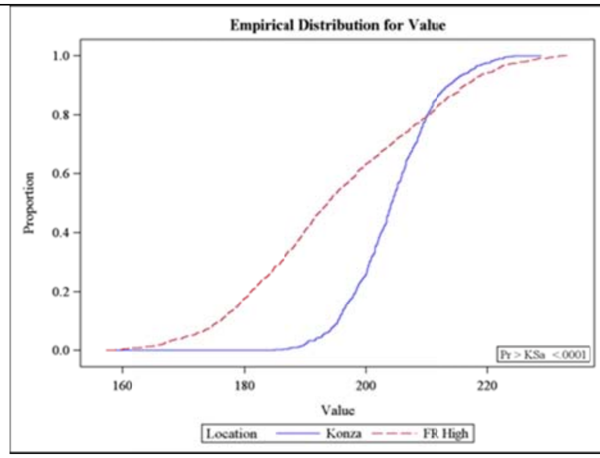

Wet, Cool Season

KS	0.160245
D	0.339612
Pr > D	<.0001

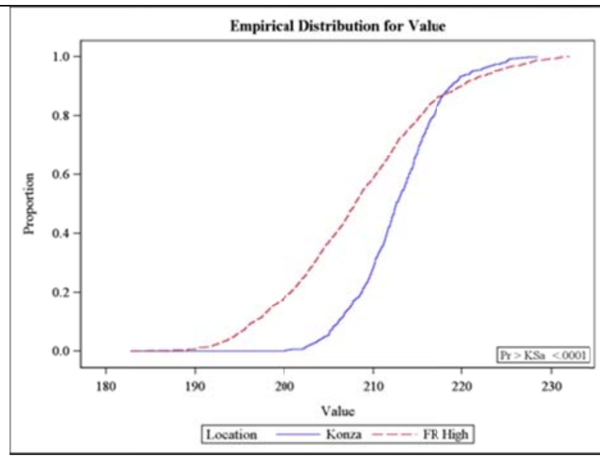

Hot, Dry Season

KS	0.118074
D	0.250306
Pr > D	<.0001

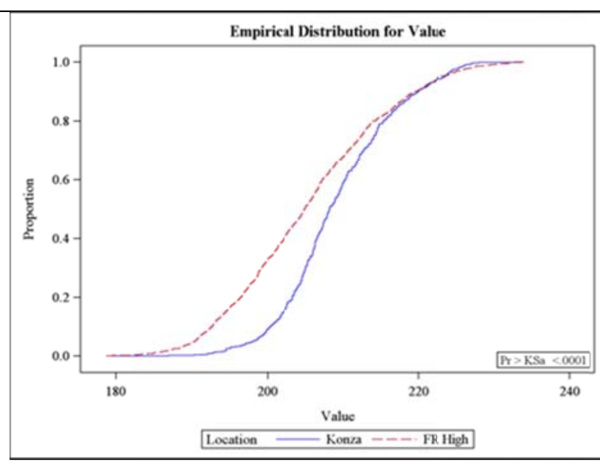

Small Integral: Fort Riley High Vs. KPBS

Normal Season

KS	0.231008
D	0.488146
Pr > D	<.0001

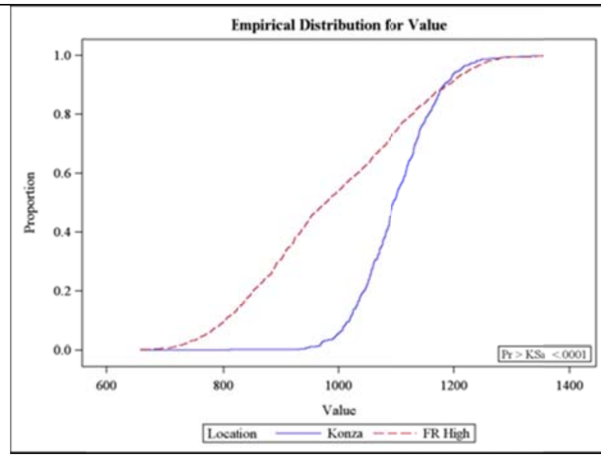

Wet, Cool Season

KS	0.197049
D	0.417724
Pr > D	<.0001

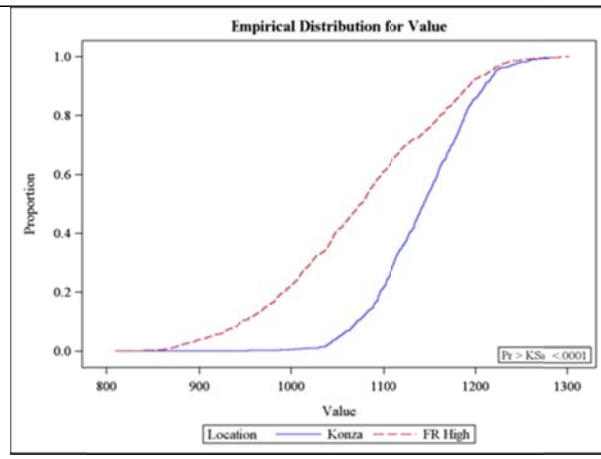

Hot, Dry Season

KS	0.133808
D	0.283659
Pr > D	<.0001

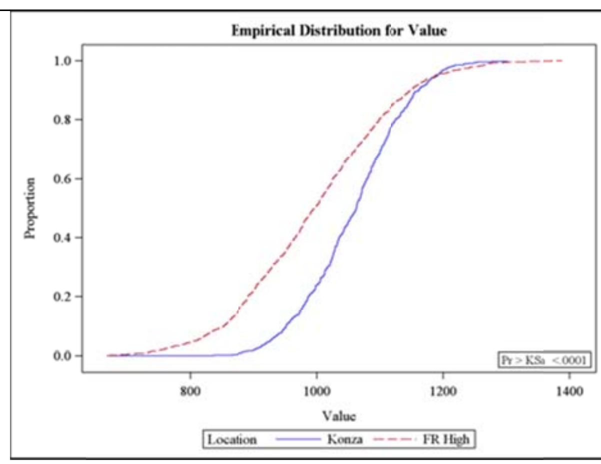

Beginning of Season: Fort Riley Low Vs. KPBS

Normal Season

KS	0.121634
D	0.269453
Pr > D	<.0001

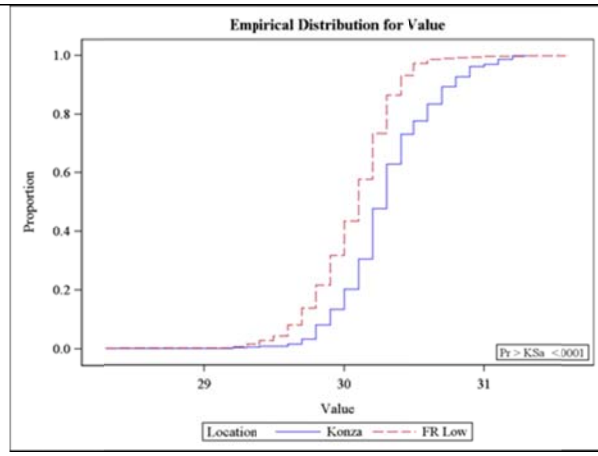

Cool, Wet Season

KS	0.049578
D	0.109754
Pr > D	<.0001

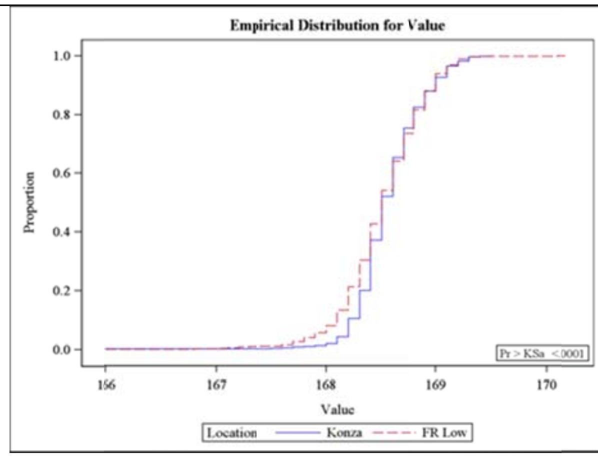

Hot, Dry Season

KS	0.148870
D	0.329787
Pr > D	<.0001

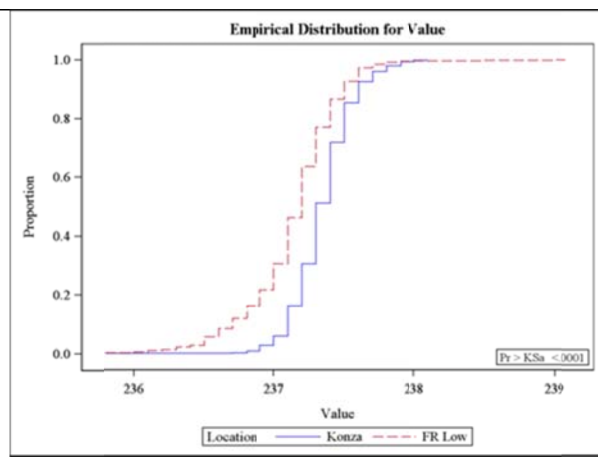

End of Season: Fort Riley Low Vs. KPBS

Normal Season

KS	0.064946
D	0.143813
Pr > D	<.0001

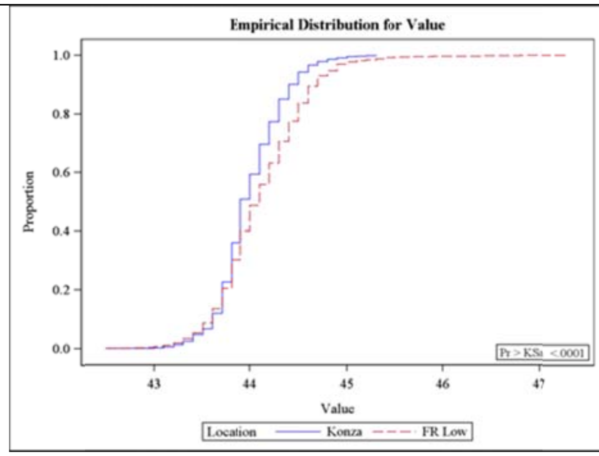

Cool, Wet Season

KS	0.068624
D	0.151917
Pr > D	<.0001

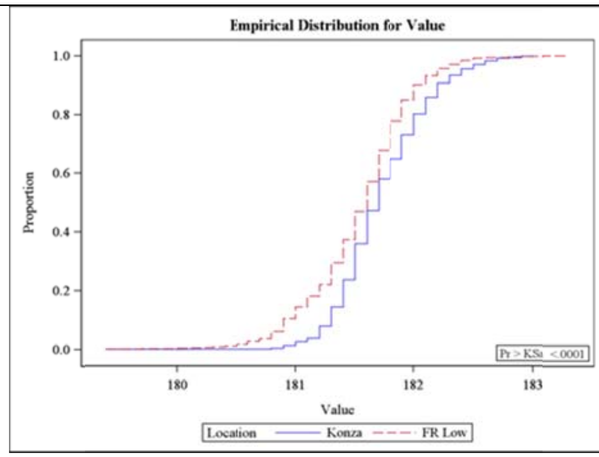

Hot, Dry Season

KS	0.047061
D	0.104338
Pr > D	0.0001

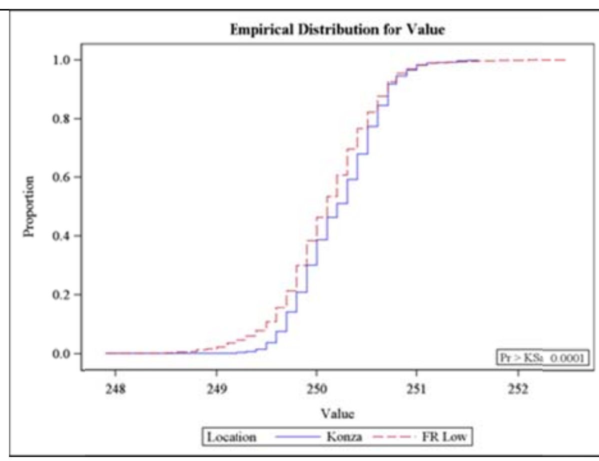

Length of Season: Fort Riley Low Vs. KPBS

Normal Season

KS	0.117334
D	0.259748
Pr > D	<.0001

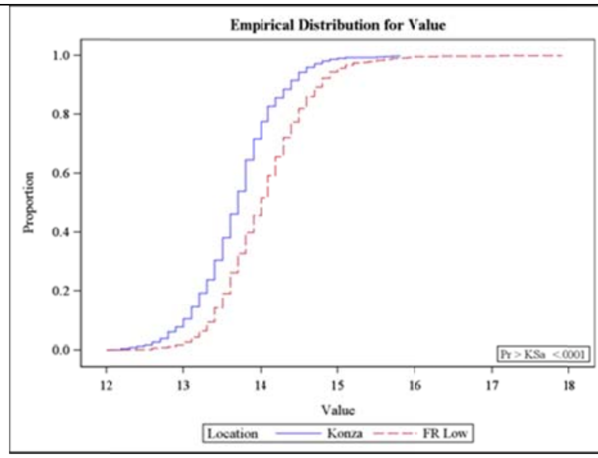

Cool, Wet Season

KS	0.040248
D	0.089001
Pr > D	0.0018

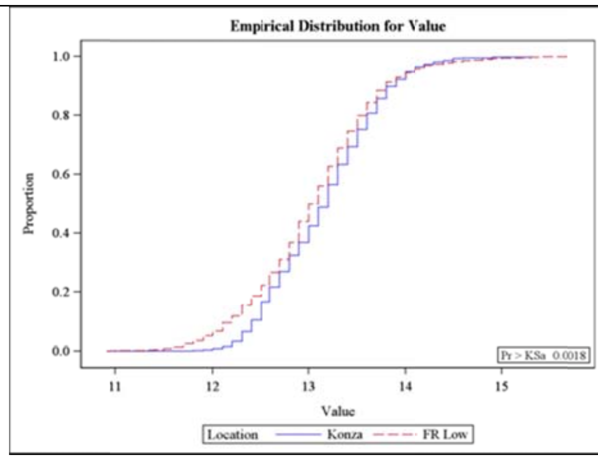

Hot, Dry Season

KS	0.046093
D	0.102110
Pr > D	0.0002

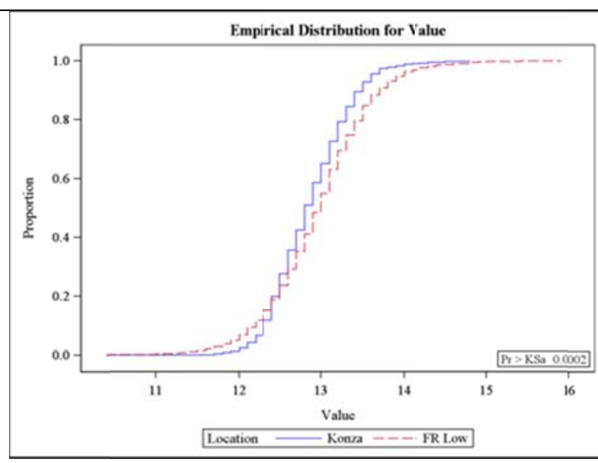

Maximum NDVI Value: Fort Riley Low Vs. KPBS

Normal Season

KS	0.127676
D	0.282800
Pr > D	<.0001

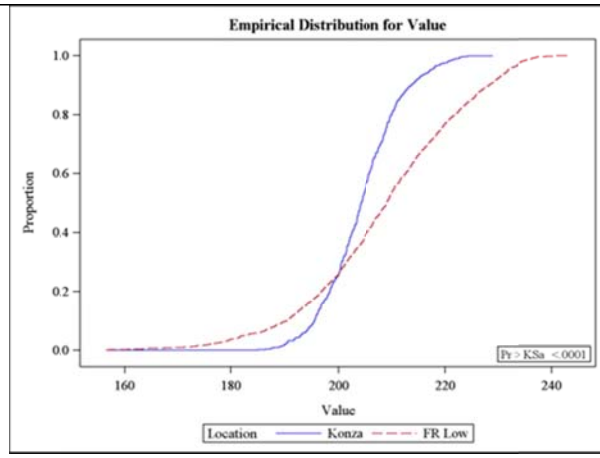

Cool, Wet Season

KS	0.165991
D	0.368071
Pr > D	<.0001

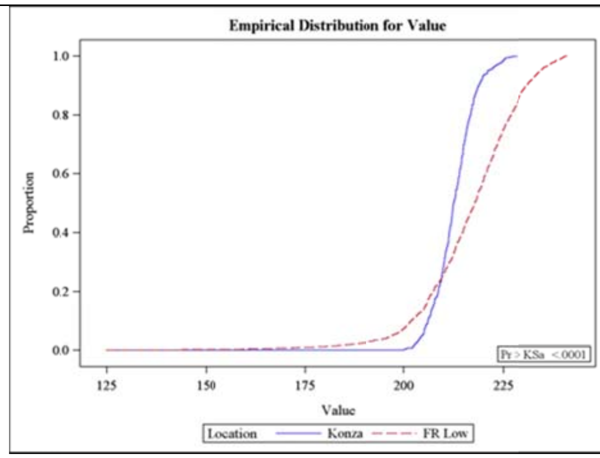

Hot, Dry Season

KS	0.109313
D	0.242392
Pr > D	0.0002

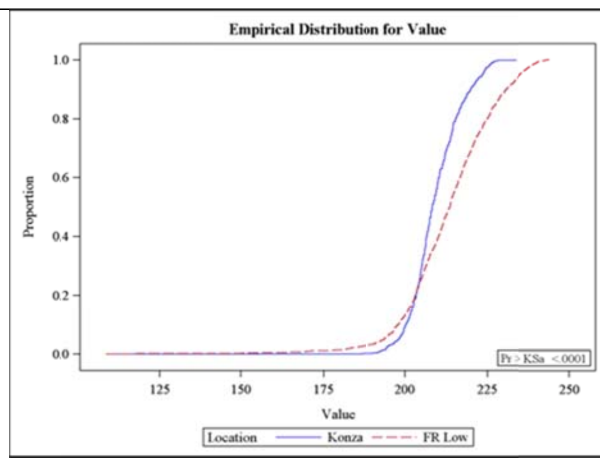

Small Integral: Fort Riley Low Vs. KPBS

Normal Season

KS	0.102987
D	0.228146
Pr > D	<.0001

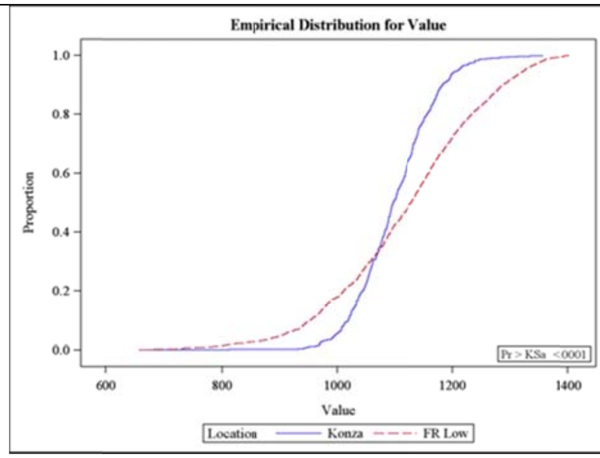

Cool, Wet Season

KS	0.093359
D	0.206674
Pr > D	<.0001

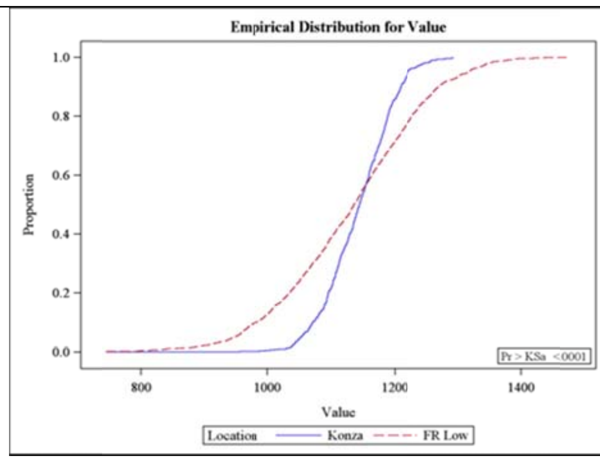

Hot, Dry Season

KS	0.079656
D	0.176460
Pr > D	<.0001